TÉCNICO LISBOA

UNIVERSIDADE DE LISBOA

INSTITUTO SUPERIOR TÉCNICO

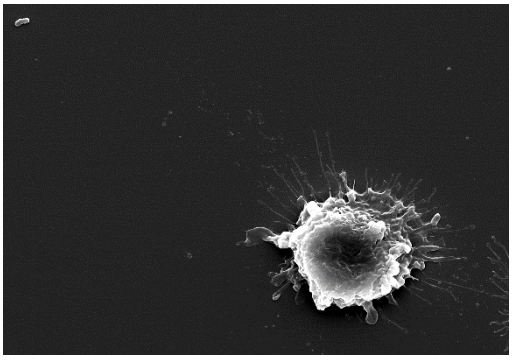

New insights into the interaction of *Burkholderia cenocepacia* with host cells: Trimeric autotransporter adhesins as pathogenicity factors

Andreia Isabel de Melo Pimenta

Supervisor: Doctor Arsénio do Carmo Sales Mendes Fialho

Co-supervisor: Doctor Dalila Madeira Nascimento Mil-Homens

Thesis approved in public session to obtain the PhD Degree in Biotechnology and Biosciences

Jury final classification: Pass with Distinction

2020

UNIVERSIDADE DE LISBOA

INSTITUTO SUPERIOR TÉCNICO

New insights into the interaction of *Burkholderia cenocepacia* with host cells: Trimeric autotransporter adhesins as pathogenicity factors

Andreia Isabel de Melo Pimenta

Supervisor: Doctor Arsénio do Carmo Sales Mendes Fialho

Co-supervisor: Doctor Dalila Madeira Nascimento Mil-Homens

Thesis approved in public session to obtain the PhD Degree in Biotechnology and Biosciences

Jury final classification: Pass with Distinction

Jury:

Chairperson: Doctor Isabel Maria de Sá Correia Leite de Almeida, Instituto Superior Técnico, Universidade de Lisboa

Members of the Committee:

Doctor Lígia Raquel Mendonça Faria Marques Saraiva Teixeira, Instituto de Tecnologia Química e Biológica António Xavier, Universidade Nova de Lisboa

Doctor Isabel Maria de Sá Correia Leite de Almeida, Instituto Superior Técnico, Universidade de Lisboa

Doctor Arsénio do Carmo Sales Mendes Fialho, Instituto Superior Técnico, Universidade de Lisboa

Doctor Leonilde de Fátima Morais Moreira, Instituto Superior Técnico, Universidade de Lisboa

Doctor Michelle Kilcoyne, School of Natural Sciences, National University of Ireland Galway, Ireland

Funding Institution – Fundação para a Ciência e Tecnologia

2020

Cover image was obtained by scanning electron microscopy and represents the adhesion of *Burkholderia cenocepacia* K56-2 to a bronchial epithelial cell (16HBE14o-). (2,500 x)

Abstract

Burkholderia cenocepacia is an opportunistic pathogen capable of establishing infection and causing disease in Cystic Fibrosis (CF) patients and other immunocompromised individuals. The intrinsic resistance to several classes of antibiotics, the large panel of virulence factors and ability to adapt to various environments facilitate *B. cenocepacia* colonization and persistence in their hosts. The *B. cenocepacia* arsenal of virulence factors is wide and diversified and include specialized surface exposed proteins. Among those, Trimeric Autotransporter Adhesins (TAAs) represent a unique class of proteins known to play relevant roles in pathogenicity. The general objective of this thesis is to gain an in-depth knowledge regarding the early steps of *B. cenocepacia*-host interaction, particularly elucidating the roles played by TAAs in that process. The results allowed the functional characterization of two *B. cenocepacia* TAAs – BcaC and BCAM2418. Both were found to be multifunctional proteins and important players during the bacterial adhesion to cells and extracellular matrix components. The expression of those TAA genes proved to be under fine-tuned regulation. *bcaC* was negatively regulated by a neighbor histidine kinase while *BCAM2418* expression increased upon initial contact of bacterium with the host cell. Elimination of O-glycans both from mucins and surface of bronchial epithelial cells was found to turned *BCAM2418* gene expression off and impaired bacterial adherence. The use of an anti-BCAM2418 antibody caused a marked reduction in the adhesion of *B. cenocepacia* to bronchial cells and mucins and an inhibition of *in vivo* virulence. Using glycan microarrays, host glycan epitopes for BCAM2418 were predicted and *Burkholderia* species were found to interact in different ways with distinct classes of CF-associated carbohydrate moieties. Finally, *B. cenocepacia* transcriptional modulation and adaptation to the host upon the initial contacts was assessed using giant plasma membrane vesicles (GPMVs) as a cell-like alternative. RNA-sequencing analysis demonstrated that the early physical interactions between bacteria and GPMVs caused a shift in the transcription of genes related to central metabolism, transport systems, and virulence traits, including many associated with the adhesion phenomena. Overall, the work supports the importance of the early contacts between bacteria and host cell as a crucial step for *B. cenocepacia* infection

and opened new insights regarding the bacterial adaptation that take place in the early stages of infection.

Key words: *Burkholderia cenocepacia*, Pathogenicity, Virulence factors, Trimeric autotransporter adhesins, Host-cell interaction

Resumo

Burkholderia cenocepacia é um patogénico oportunista capaz de estabelecer infeção e causar doença em pacientes com Fibrose Cística (FC) e outros indivíduos imunocomprometidos. A resistência intrínseca a várias classes de antibióticos, a vasto painel de fatores de virulência e a capacidade de adaptação a diferentes ambientes, facilitam a colonização e persistência de *B. cenocepacia* no hospedeiro. O arsenal de fatores de virulência de *B. cenocepacia* é amplo e diversificado e inclui proteínas de superfície altamente especializadas. Entre estas, Adesinas Triméricas Autotransportadas (ATAs) representam uma classe única de proteínas que são conhecidas por desempenhar papéis importantes na patogenicidade. O objetivo geral desta tese é aprofundar o conhecimento relativo aos passos iniciais de interação *B. cenocepacia*-hospedeiro, elucidando em particular os papéis desempenhados por ATAs nesse processo. Os resultados permitiram uma caracterização funcional de duas ATAs de *B. cenocepacia* – BcaC e BCAM2418. Ambas demonstraram ser proteínas multifuncionais e importantes intervenientes durante a adesão bacteriana a células e componentes da matriz extracelular. A expressão desses ATAs genes provou estar sobre uma regulação estrita. *bcaC* demonstrou ser regulado negativamente por uma histidina cinase vizinha enquanto que a expressão de *BCAM2418* aumentou durante os contactos inicias da bactéria com a célula hospedeira. A eliminação de O-glicanos tanto de mucinas como da superfície de células do epitélio bronquial provou diminuir a expressão do gene *BCAM2418* e inviabilizar a adesão bacteriana. O uso de um anticorpo anti-BCAM2418 causou uma demarcada redução na adesão de *B. cenocepacia* a células do brônquio e mucinas e a inibição de virulência *in vivo*. Usando *microarrays* de glicanos, epítopos glicosilados do hospedeiro foram identificados como alvos de interação com BCAM2418, e espécies do género *Burkholderia* demonstraram interagir de diferentes formas com variadas classes de carboidratos associados a FC. Por fim, a modulação transcricional e adaptação de *B. cenocepacia* em consequência dos primeiros contactos com o hospedeiro foi analisada com recurso a vesículas gigantes de membrana plasmática (VGMPs) como alternativa celular. Sequenciação de RNA indicou que os primeiros contactos físicos entre bactéria e VGMPs causam uma mudança na transcrição

de genes relacionados com o metabolismo central, sistemas de transporte e características de virulência, incluindo muitas associadas com o fenómeno de adesão. Em suma, o trabalho desenvolvido nesta tese suporta a importância das interações iniciais entre bactéria e a célula hospedeira como passo fundamental para a infeção de *B. cenocepacia*, e trouxe novos conhecimentos relativos à adaptação bacteriana quer ocorre nos estadios iniciais de infeção.

Palavras chave: *Burkholderia cenocepacia*, Patogenicidade, Fatores de virulência, Adesinas triméricas autotransportadas, Interação com célula hospedeira

Acknowledgements

The achievements of this work were only possible thanks to the help and support of many people and institutions. Firstly, I would like to acknowledge my supervisor Professor Arsénio Fialho for his guidance, support and advises; and Doctor Dalila Mil-Homens, my co-supervisor, for all the motivation, ideas, and constant support during the development of this thesis which was crucial for the success of the work.

Secondly, I have to acknowledge Professor Isabel Sá-Correia as head of the Biological Sciences Research Group (BSRG) and the director of BIOTECnico program, for the opportunity to embrace this renowned doctoral program and to work in such excellent team.

I also acknowledge the members of my *Comissão de Acompanhamento de Tese*, for their help and suggestions during the process of my work.

I would also like to take this opportunity to thank Professor Lokesh Joshi, from the Glycoscience Group at National University of Ireland in Galway, for have accepted to receive me in my PhD abroad experience. A special thank you to Doctor Michelle Kilcoyne and all her team in the Carbohydrate Signaling Group who have helped me in an extraordinary way. Her profound expertise, enthusiasm and guidance allowed me a unique opportunity to expand my scientific knowledge.

I would also like to acknowledge all the co-authors of the papers presented - Doctor Sandra Pinto from the Biospectroscopy and Interfaces Research Group (BSIRG) for the collaboration and help to obtain the best confocal microscopy images; and Doctor Marta Alves from *Centro de Química Estrutural* for the collaboration in the scanning electron microscopy imaging and all the help in elevating the obtained results.

I acknowledge *Fundação para a Ciência e a Tecnologia* (FCT) PhD grant PD/BD/116940/2016 under the framework of the *Instituto Superior Técnico* BIOTECnico PhD program in Biotechnology and Biosciences. The work carried out during this PhD was financed by the funding received by iBB and Institute for Bioengineering and

Biosciences from FCT (UID/BIO/ 04565/2020) and *Programa Operacional Regional de Lisboa* 2020 (Project N. 007317).

I would like to thank to my colleagues, and close friends – Nuno Bernardes for taken me under his wing and for sharing late hours of work, long lasting brainstorming's and never-ending crazy ideas that helped me to see clarity in the middle of troubled horizons; and Ana Rita for her strength, infinite warmth and bright smile, it was a honor to have witnessed her growth and plenitude in the more difficult of times.

To all my fellows in BSRG, specially Mónica Rato, Joana Feliciano, Tiago Pita, Sara Salazar, and Mafalda Cavalheiro for all the help, talks and laughs my deep and sincere thank you. You were the light of my days.

To my friends, especially Joana Madureira, Ana Pontes, Cláudia Palma, and Carlos Serra, thank you for all the dinners and fun gatherings, for having accompanied me during this journey and for your constant concern.

Finally, the most important acknowledgments. To Pedro for his love, encouragement, and infinite pride, thank you for giving me my ultimate goal in life. To my ginormous family, for teaching me the value of hard work and honor, for always supporting my choices and for never having doubted my capacities and goals. To my parents and sister, thank you for always be my safe harbor.

Table of Contents

List of Figures

List of Tables

List of Acronyms

ABC - ATP-binding cassette

AHL - N-acyl homoserine lactone

BAM - β-barrel assembly machinery

Bcc - *Burkholderia cepacia* complex

BcCV- *Burkholderia cenocepacia* containing vacuole

BD - Binding domain

BDSF - *Burkholderia* diffusible signal factor (*cis*-2-dodecenoic acid)

BSA – Bovine serum albumin

Cbl – Cable pili

CF – Cystic fibrosis

CFTR – Cystic fibrosis transmembrane conductance regulator

CFU – Colony forming unit

CK13 – Cytokeratin 13

COG – Clusters of orthologous groups

DMEM – Dulbecco's modified Eagle medium

DTT – Dithiothreitol

ECL – Enhanced chemiluminescence

ECM – Extracellular matrix

FBS – Fetal bovine serum

FDR – False discovery rate

FEG-SEM - Field-emission-gun scanning electron microscopy

FGFR-1 - Fibroblast growth factor receptor-1

Flp – Fimbrial low-molecular weight protein

Fuc – Fucose

Gal – Galactose

GalNac – N-acetylgalactosamine

Glc – Glucose

GPMV – Giant Plasma Membrane Vesicle

HSA – Human serum albumin

HBS – HEPES buffered saline

Hep_Hag – Invasin motif

HIM – Hemagglutinin domain

HK – Histidine kinase

IL – Interleukin

IS - Insertion sequences

KEGG – Kyoto encyclopedia of genes and genomes

LB - Luria-Bertani broth medium

LPS – Lipopolysaccharide

MEM – Minimum essential medium

MOI – Multiplicity of infection

Neu5Ac - N-Acetylneuraminic acid

NF-κB – Nuclear factor kappa B

NGC – Neoglycoconjugate

OAg – O-antigen

OD – Optical density

Omp – Outer membrane protein

PBS – Phosphate buffer saline

PBS-T - Phosphate buffer saline-Tween

PCL - Periciliary liquid

PCR – Polymerase chain reaction

PFA – Paraformaldehyde

POTRA – Polypeptide transport associated domain

QS – Quorum sensing

RFU - Relative fluorescence units

RIN - RNA integrity number

RNAseq – RNA sequencing

RR – Response regulator

RT-PCR – Real-time polymerase chain reaction

SD – Standard deviation

SDS - Sodium dodecyl sulfate

SE – Standard error

SEC - General protein export system

SEM - Scanning electron microscopy

T3SS – Type 3 secretion system

T4SS – Type 4 secretion system

T5SS – Type 5 secretion system

T6SS – Type 6 secretion system

TAA – Trimeric autotransporter adhesin

TAM – Translocation and assembly module

TBS - Tris-buffered saline

TBS-T - Tris-buffered saline-Tween

TCA - Tricarboxylic acid

TCS – Two-component system

TE - Tris-EDTA

TecA - Type VI secretion system effector

TLR - Toll-like receptor

TNF - Tumor necrosis factor

TNFR-1 - Tumor necrosis factor receptor 1

Tp – Trimethoprim cassette

wt – wild-type

Yop - Yersinia outer protein

I. INTRODUCTION

Review paper

Pimenta AI, Fialho AM. New insights into the pathogenesis of *Burkholderia cenocepacia*: special emphasis on trimeric autotransporter adhesins as primary mediators of attachment. (in preparation)

I.1 Members of the genus *Burkholderia*: multiple lifestyles

Burkholderia cenocepacia belong to *Burkholderia* genus with more than 140 species and candidate species (lpsn.dsmz.de/genus/burkholderia). *Burkholderia* genus is a group of Gram-negative β-proteobacteria described as obligate aerobic non-spore-forming bacilli that could be found in distinct ecological niches and adopt different life cycles, revealing their highly versatile metabolism and genetic diversity (Mahenthiralingam and Vandamme, 2005; Company, et al. 2008; Lewis and Torres, 2016). Some of its members are known to be problematic plant pathogens, while others have developed beneficial interactions with their plant hosts and proven to bring beneficial ecological effects like a better water management, protection against fungal infections, and improved nitrogen fixation (Coenye and Vandamme, 2003; Company, et al. 2008). Other species have demonstrated to be very efficient biocontrol (biopesticides) and bioremediation agents that degrade toxic man-made compounds including groundwater pollutants that are found in pesticides and herbicides (Mahenthiralingam, et al. 2005; Mahenthiralingam, et al. 2008). Nevertheless, *Burkholderia* isolates have been increasingly identified as important human pathogens that cause persistent, hard to treat, chronic infections. In this scenario, *Burkholderia mallei*, *Burkholderia pseudomallei*, primary pathogens for humans and animals, and bacteria belonging to *Burkholderia cepacia* complex (Bcc), opportunistic human pathogens, like *Burkholderia cenocepacia*, are especially critical (Drevinek and Mahenthiralingam, 2010; Lewis and Torres, 2016).

First identified as *Pseudomonas cepacia* in the 1950 by W. H. Burkholder, *B. cepacia* was known for being a plant pathogen widely isolated from the biosphere (Burkholder, 1950). *P. cepacia* isolates were initially classified as closely related pseudomonads, given their phenotypic diversity. However, in 1992, several species, including *P. cepacia*, were transferred from the *Pseudomonas* genus to the new genus *Burkholderia* based on new molecular taxonomic analysis like 16S rRNA sequences and DNA–DNA homology values (Yabuuchi, et al. 1992; Mahenthiralingam and Vandamme, 2005). In the late 1990s, Vandamme and colleagues divided *B. cepacia* strains into five groups of

phenotypically similar isolates called genomovars (I-V) (Vandamme, et al. 1997). In the following years four new genomovars have been described, but with the improvement in identification tests, all of them have been formally named as species. More recently, differences in clinical outcomes, transmissibility, pathogenic or beneficial behavior towards plants, and presence, or absence of genes led to new taxonomic studies and new evaluation of the *B. cepacia*-like bacteria (Coenye, et al. 2001; Mahenthiralingam and Vandamme, 2005). These studies identified novel *Burkholderia* species that were normally misidentified as *B. cepacia*, such as *B. cenocepacia* (Coenye, et al. 2001). The new closely related species were collectively referred as *B. cepacia* complex (Bcc) species, sharing a high level of 16S rDNA (98-100%), and *recA* (94–95%) sequence identity and moderate degrees of whole-genome DNA-DNA hybridization (30-50%) (Mahenthiralingam and Vandamme, 2005). All of Bcc species have been isolated from environmental and human clinical sources. They are common contaminants of cosmetic and pharmaceutical solutions, water supplies, sterile medical solutions, and disposable hospital equipment leading to serious nosocomial infections. Lately, Bcc bacteria have emerged as extremely problematic opportunistic human pathogens in patients with cystic fibrosis (CF) and chronic granulomatous disease, and immunocompromised individuals, with an increasing number of infections (Coenye and Vandamme, 2003, Mahenthiralingam, et al. 2005). Nowadays, Bcc includes at least 22 closely related species (Estrada-de Los Santos, et al. 2018).

I.1.1 Cystic Fibrosis: etiology and pathophysiology of the disease

CF is the most common autosomal recessive disorder among Caucasians. It is an incurable, chronic disease, which causes severe damages to respiratory tract. There are about 100 000 worldwide cases and approximately 1000 new cases added each year. CF affects children and young adults worldwide, with a life expectancy of mid-30s due to chronic lung infections that are associated with high mortality (Klimova, et al. 2017; Rafeeq and Murad, 2017).

CF is a disease caused by mutations on the CF transmembrane conductance regulator gene (*cftr*) that encodes for a transmembrane chloride channel of low conductance (Roussel and Lamblin, 2003; Kreda, et al. 2012). Malfunctions of CFTR cause an imbalance of electrolytes like Cl^- and Na^+ across the epithelium: CF respiratory cells have defective chloride export and elevated sodium import (Figure I.1). This imbalance causes the migration of water from the airway surface liquid to the epithelial cells resulting in a dehydrated and highly viscous mucus secretions in the lungs. The increased mucus thickness and viscosity facilitate the acquisition and persistence of bacterial infections (Figure I.1) (Lamblin, et al. 2001; Kreda, et al. 2012; Venkatakrishnan et al, 2014). The composition of normal mucus contains a mixture of 98% water and 2% solids (mostly mucins - heavily O-linked glycosylated proteins). In CF lungs this balance is altered with a reduction in the amount of water to approximately 90% and a rise in the mucin content to 3-9%. The increased mucin concentration creates a more static mucus and an impaired mucociliary clearance, that instead of acting as a protective barrier, starts to harbor bacteria enhancing infection and inflammation (Ridley and Thornton, 2018).

Chronic bacterial colonization and exacerbations of lung infections are the major cause of morbidity and mortality in CF patients. Some studies shown that besides physiological changes across the lung epithelium, CF patients present different glycosylation in airway mucins. Nevertheless, the exact differences between the glycosylation of mucins, tissues, and cell in healthy and CF-lungs and the direct contribution of CFTR malfunction are still unclear (Lamblin, et al. 2001; Schulz, et al. 2007). Furthermore, the CF-lung alterations in the mucin-linked glycans seems to promote and facilitate the interaction of respiratory pathogens with the host cells (Venkatakrishnan et al. 2014; McClean and Callaghan, 2017).

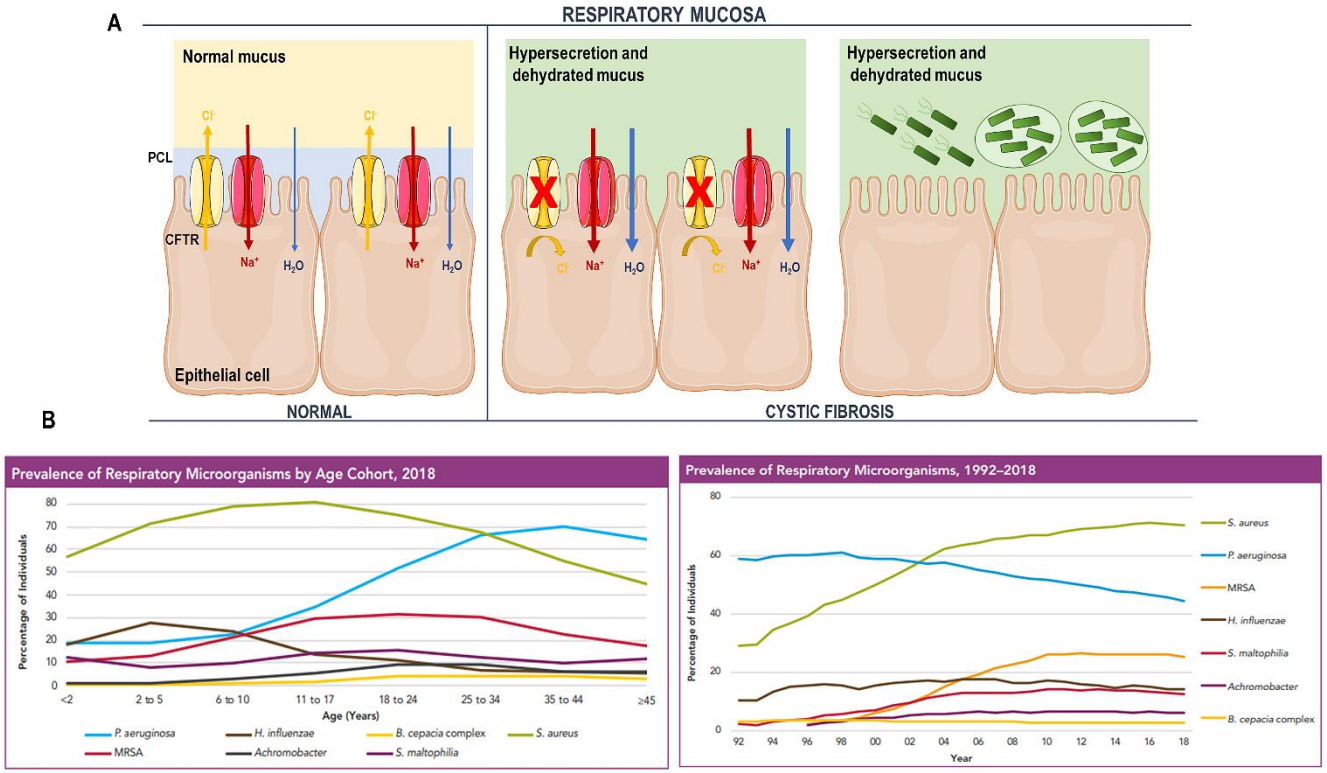

Figure I.1. Bacterial infection in CF airways. (A) On normal respiratory epithelia, a thin mucus layer is located on top of the periciliary liquid (PCL) layer. PCL layer facilitates efficient mucuciliary clearance. Malfunctions in the CF transmembrane conductance regulator (CFTR) cause an imbalance of electrolytes like Cl^- and Na^+ across the epithelium: CF respiratory cells have defective chloride export and elevated sodium import. This imbalance causes the migration of water from the airway surface liquid to the epithelial cells resulting in a dehydrated and highly viscous mucous secretions in the lungs. The increased mucus thickness and viscosity facilitate the acquisition and persistence of bacterial infections. Bacteria are able to penetrate the mucus secretions by flagellar activity and can create microcolonies and biofilm structures where they can persist, setting a stage for chronic infection. (B) Prevalence of respiratory microorganisms by age cohort in CF patients and the evolution of the overall prevalence through the years (1992-2018). Data obtained from the 2018 Annual Data Report to the Center Directors from Cystic Fibrosis Foundation Patient Registry.

Pseudomonas aeruginosa, *Staphylococcus aureus*, *Haemophilus influenzae*, *Stenotrophomonas maltophilia, Achromobacter spp.* and members of the Bcc are the most common isolated species from the lungs of CF patients (Figure I.1B) (Gibson, et al. 2003). Despite *P. aeruginosa* being the most prevalent bacteria causing chronic CF lung infection, Bcc species are the most problematic considering treatment and eradication (LiPuma, 2010). Moreover, Bcc strains are transmissible by social contact and extremely difficult to eradicate due to their intrinsically high resistance to antibiotics (Scoffone, et al. 2017). The poor prognoses and high risk of death after lung transplantation resulting from Bcc infections in CF patients cause the discard of potential recipients from the lung transplant list (Olland, et al. 2011).

I.1.2 *Burkholderia cenocepacia*: lessons from a versatile opportunistic human pathogen

Among Bcc bacteria, *B. cenocepacia* has proven to be one of the most challenging opportunistic pathogens causing persistent, hard to treat, chronic infections in CF patients. In those individuals, *B. cenocepacia* can cause severe respiratory infections that lead to a rapid deterioration of lung function associated with necrotizing pneumonia, bacteremia and sepsis that frequently results in death. In past decades, several research groups dedicated their efforts to study this bacterium and its impact in the many stages of infection. The capacity to adapt to different environments and host niches, the intrinsic resistance to several classes of drugs and its arsenal of virulence factors facilitates *B. cenocepacia* colonization and persistence inside the host.

I.1.2.1 *B. cenocepacia* genomes

Up to date approximately 200 *B. cenocepacia* genomes have been examined and sequences (Burkholderia genome database, Winsor, et al. 2008). All of them containing three large chromosomal replicons, codifying more than 7000 genes, and ranging from 6 to 9 Mb (Mahenthiralingam et al. 2005). J2315, the type strain of *B. cenocepacia* and

a member of the epidemic ET12 lineage, was the first one to have its genome sequenced and available (Holden, et al. 2009). The genome consists of three circular chromosomes of approximately 3.870, 3.217 and 0.876 Mb, and a plasmid (pBC2315) of 92.7 Kb, all of them characterized for having a high percentage of GC content ranging from 62.8% to 67.3%. Among all genomic elements, *B. cenocepacia* J2315 has 7281 annotated genes, including 74 tRNA and 18 rRNA (Holden, et al. 2009). *B. cenocepacia* J2315 plasmid comprises several types of insertion sequences (IS) and large genomic islands that facilitate the dissemination of genes between genetically divergent bacteria, promoting genomic plasticity and bacterial adaptability (Holden, et al. 2009). Genome sequence analysis revealed that *B. cenocepacia* J2315 possessed 22 different types of IS, 4 of which in more than 5 copies per genome. The transposition activity of mobile elements in bacteria is enhanced in response to several stress conditions like high temperature, starvation and oxidative stress mediated by toxic reactive oxygen species common during CF infection. This mechanism may represent a form of rapid IS-mediated evolution that *B. cenocepacia* might carry out during infection (Drevinek, et al. 2010).

I.1.2.2 Global epidemiology of infections caused by *B. cenocepacia*

B. cenocepacia is the most dominant Bcc species isolated from CF patients across the world. *B. cenocepacia* alone account for more than 30% of all Bcc infections in the CF population and comprise most of the epidemic strains described so far (Lipuma, 2010). *B. cenocepacia* CF infections have one of the poorest prognoses among Bcc species, normally associated with a high risk of developing fatal cepacia syndrome. Likewise, *B. cenocepacia* infections might occur in immunocompetent individuals, like HIV or cancer patients that present acute bronchitis and/or pneumonia (Mann, et al. 2010). Moreover, an increasing number of bacteremia cases caused by Bcc among non-CF hospitalized patients have been reported (Bressler, et al. 2007). The accumulating reports of nosocomial outbreaks caused by *B. cenocepacia* led to the recognition of these bacteria as emergent nosocomial pathogens among non-CF patients, in particular among oncology patients (Mann et al., 2010).

Using *recA* gene sequence analysis, *B. cenocepacia* (former Bcc genomovar III) was subdivided into four phylogenetic clusters, IIIA to IIID, being IIIA and IIIB the most represented groups among clinically relevant isolates (Drevinek and Mahenthiralingam, 2010). Three *B. cenocepacia* epidemic strains have been responsible for considerable morbidity and mortality in the CF community in the past years. The lineage ET-12 (Edinburgh-Toronto epidemic Electrophoretic Type 12 clone; IIIA subgroup) includes strains responsible for *B. cenocepacia* epidemic outbreaks that caused devastating infections in the CF population in Canada, and Europe (Mahenthiralingam, et al. 2005). Opposite to ET-12, PHDC (Philadelphia-District of Columbia clone) and Midwest strains that are dominant clones in the USA are part of the subgroup IIIB (Coenye and LiPuma, 2002; Speert, et al. 2002). In past years, the prevalence of *B. cenocepacia* in CF patients worldwide have been variable. Albeit the constant high incidence of *B. cenocepacia* in several European CF populations, *B. multivorans* (genomovar II) is rising to the proportion *B. cenocepacia* and is currently the most prevalent in USA and Canada (Baldwin, et al. 2008; Scoffone, et al. 2017). Nowadays, it is acknowledged the rapid evolution that *Burkholderia* species demonstrate under stress conditions during infections or *in vitro*, resulting of the occurrence of mutations that could accumulate in clonal lineages. Moreover, CF patients infected with similar Bcc species (genotypically) can manifest different outcomes as a result of distinct virulence traits that could be developed during infection (Sass, et al. 2011; Hassan, et al. 2019a; Hassan, et al. 2019b).

The progression of *B. cenocepacia* infection depends on both host and strain and exploits a variable array of virulence factors. A comprehensive description of *B. cenocepacia* virulence is explored in the next subchapter, which highlights in detail the main mechanisms that *B. cenocepacia* uses to prevail in the human host.

I.2 *Burkholderia cenocepacia* – challenges of host-pathogen crosstalk

I.2.1 Characterizing the dynamics underlying *B. cenocepacia* infections: review and update

B. cenocepacia has the capacity to adapt to a great range of environments, including the human body. The ability to cause damage to the host is what differentiate commensal from pathogenic bacteria (Duell, et al. 2016). This damage allows the pathogen to colonize and spread to new locations in the host and could be the result of a series of events. *B. cenocepacia* possess a complex network of tools from surface structures to secreted toxins or enzymes that allow it to adhere to host cells and grow in extra- or intracellular niches (Valvano, et al. 2005). The process of *B. cenocepacia* host-adaptation might continue over time, throughout chronic colonization (Saldías and Valvano, 2009). The phenotypic modifications attained during the establishment of an infection allow pathogens to manage new environmental pressures such as inflammatory responses, nutrient deficiency, antimicrobial therapies, and variations in osmolarity, pH or in the levels of oxygen (Cullen and McClean, 2015). Interactions between *B. cenocepacia* and the lung epithelium are very versatile and are mediated by a wide range of virulence factors. All three *B. cenocepacia* chromosomes and plasmid encode proteins required for bacterial survival, including proteins involved in regulatory, transport and metabolic functions. Virulence determinants are often non-essential to the pathogen, mediate the direct contact with the host and are crucial for the pathogenesis of *B. cenocepacia*. The first steps of pathogen-host interaction are penetration of the mucosal layer and the following adhesion to the host where many molecules have been reported as targets for *B. cenocepacia*. The following stage in *B. cenocepacia* pathogenesis is the invasion of the lung cells and translocation across the respiratory epithelium (McClean and Callaghan, 2009).

I.2.2 Adherence of *B. cenocepacia* to host cells

Bacteria have developed an abundance of mechanisms to engage host cells and facilitate colonization by subverting their cellular signaling networks. Bacterial surface displays a vast range of highly specialized surface bound and secreted molecules that can facilitate adherence and aid the colonization of the host (Figure I.2). Adhesion not only allows bacteria to stick to host cell surfaces creating a stable environment for growth, but it also causes physiological alterations needed for the adaptation to the host. These changes can affect bacterial metabolism, and regulation of virulence factors that lead the infection.

In the airways of healthy individuals, a mucus layer protects the epithelial cells from airborne pathogens by trapping and mechanically eliminating them by mucociliary clearance (Venkatakrishnan et al. 2014). In CF lungs, the increased mucus viscosity and impaired mucociliary clearance enable the entrapment of *B. cenocepacia* and facilitate its access to the epithelial surface and further adhesion (McClean and Callaghan, 2009; Venkatakrishnan, et al. 2014). *B. cenocepacia* can adhere to the host cells through specific interactions between bacterial surface molecules and host membrane protein and glycolipid receptors, but also secretory mucins and extracellular matrix proteins (McClean and Callaghan, 2009; Saldías and Valvano, 2009). To date, the cable pili (Cbl), their associated adhesin (AdhA) and trimeric autotransporter adhesins (TAAs) (BcaA and BcaB, formerly BCAM0224 and 0223) are the only well-documented adhesins in Bcc species (Goldberg, et al. 2011; Mil-Homens and Fialho, 2011; Mil-Homens and Fialho, 2012). Nevertheless, other structures like flagella, outer membrane proteins (Omp) or lipoproteins have been reported to mediate *B. cenocepacia* attachment towards the host cell (Figure I.2) (Tomich, et al. 2002; McClean, et al. 2016; Dennehy, et al. 2017).

The cable pili, a specific fimbria expressed in *B. cenocepacia* strains of ET-12 lineage, and its associated 22-kDa adhesin AdhA have been shown to be important players in the adherence to mucin and cytokeratin 13 in epithelial cells (Sajjan, et al. 2000a; Saijan, et al. 2000b; Urban, et al. 2005). They are also required for the invasion of respiratory epithelium causing cytotoxicity and inducing pro-inflammatory responses by stimulating

IL-8 production (Urban, et al. 2005; Goldberg, et al. 2008). Only a subset of Bcc isolates produces both cable pili and AdhA. *B. cenocepacia* isolates that expressed the cable pilus phenotype shown to be able to bind to secretory mucins and lung explants from CF patients (Saijan, et al. 2000a; Sajjan, et al. 2002), while the epithelial cell receptor for AdhA was identified as cytokeratin 13, a protein that is enriched in CF epithelial cells (Saijan, et al. 2000b). Despite the combined expression of AdhA and Cbl pili be required for optimal binding to cytokeratin 13, *B. cenocepacia* strains which did not show Cbl pili on their surface maintained their capacity of interaction (Urban, et al. 2005). Transcriptomic studies demonstrated the downregulation of the Cbl pilus gene cluster during growth in CF sputum, suggesting that the complete cable pilus structure may not be as important adhesive component as initially assumed (Drevinek, et al. 2008). However, *adhA* gene was activated in sputum suggesting that in the absence of cable pilus expression AdhA adhesin may be incorporated onto other *B. cenocepacia* surface components (Drevinek, et al. 2008). More recently, studies indicate that *B. cenocepacia* strains also bind to a second epithelial receptor – TNF receptor 1 (TNFR1). Nevertheless, this interaction did not seem to require AdhA adhesin, but is partly responsible for stimulating a robust IL-8 production from CF airway epithelial cells through the activation of TNFR1-related signaling pathway (Sajjan, et al. 2008).

More recently, BcaA (BCAM0224), a trimeric autotransporter adhesin (TAA) from *B. cenocepacia*, was found to interact with TNFR1 on the surface of epithelial cells, being able to regulate components of the TNF signaling pathway and to induce a significant production of the pro-inflammatory cytokine, IL-8 (Mil-Homens, et al. 2017). This was the first study to demonstrate that a TAA could be involved in the induction of inflammatory response during *B. cenocepacia* infections (Mil-Homens, et al. 2017). In past years, *B. cenocepacia* TAAs have been studied and identified as multifunctional proteins with major roles in *B. cenocepacia* virulence (Mil-Homens, et al. 2010; Mil-Homens, et al. 2014; Mil-Homens, et al. 2012). Besides its role as inducer of inflammation, BcaA functions have been associated with adherence to extracellular matrix components (ECM), like collagen-type I, which enable the bacteria to associate with target eukaryotic host cells. It also mediates bacterial adhesion to and invasion of cultured human bronchial epithelial cells and seems to be required for the overall *B.*

cenocepacia virulence (Mil-Homens, et al. 2010; El-Kirat-Chatel, et al. 2013; Mil-Homens, et al. 2014). Like BcaA, the role played by BcaB (BCAM0223) during the initial steps of *B. cenocepacia* infection was also characterized (Mil-Homens, et al. 2012). BcaB mutant showed a significant reduction in adherence to bronchial epithelial cells and vitronectin, an ECM component, when compared to the parental strain, revealing BcaB importance in *B. cenocepacia* pathogenesis. However, despite BcaB requirement for maximal adherence of *B. cenocepacia*, it was not necessary for invasion of respiratory cells (Mil-Homens, et al. 2012).

B. cenocepacia flagellum is known for making bacteria motile, but also serves as adhesin and facilitate host cells invasion (Tomich, et al. 2002). Furthermore, *B. cenocepacia* K56-2 mutants that lacked flagella showed a 40% reduction of mice mortality, after 3 days of infection (Urban, et al. 2004). In addition, *B. cenocepacia* flagellin was shown to instigate a host signaling cascade through interaction with the surface exposed toll-like receptor 5 (TLR5), which initiates an innate immune response through NFκB activation and IL-8 secretion (Urban, et al. 2004). The synthesis and assembly of the flagella requires the articulation of many elements. In *B. cenocepacia* J2315, genes that codify for proteins involved in the flagella structure are distributed within five clusters on chromosome 1 and as two individual genes found on chromosome 2 and 3 (Drevinek and Mahenthiralingam, 2010). Moreover, their expression seems to undergo specific regulation during the course of infection. Kalferstova, et al. (2015) showed that bacterial isolates from patients with cepacia syndrome condition present a non-motile phenotype as consequence of a reduced expression of flagellar genes. Those results seem to indicate that during chronic infection, *B. cenocepacia* loses its motility (flagellar structure) resulting in a poor prognosis for the occurrence of cepacia syndrome (Kalferstova, at al. 2015). In a different study, the downregulation of flagellar-associated genes using a rat chronic respiratory infection model suggests that the expression of those genes is not required in an established infection (O'Grady and Sokol, 2011). However, upregulation of flagellar genes has been reported in *B. cenocepacia* growing in CF sputum, which may reveal its importance during the first stages of infection (Drevinek¸et al. 2008).

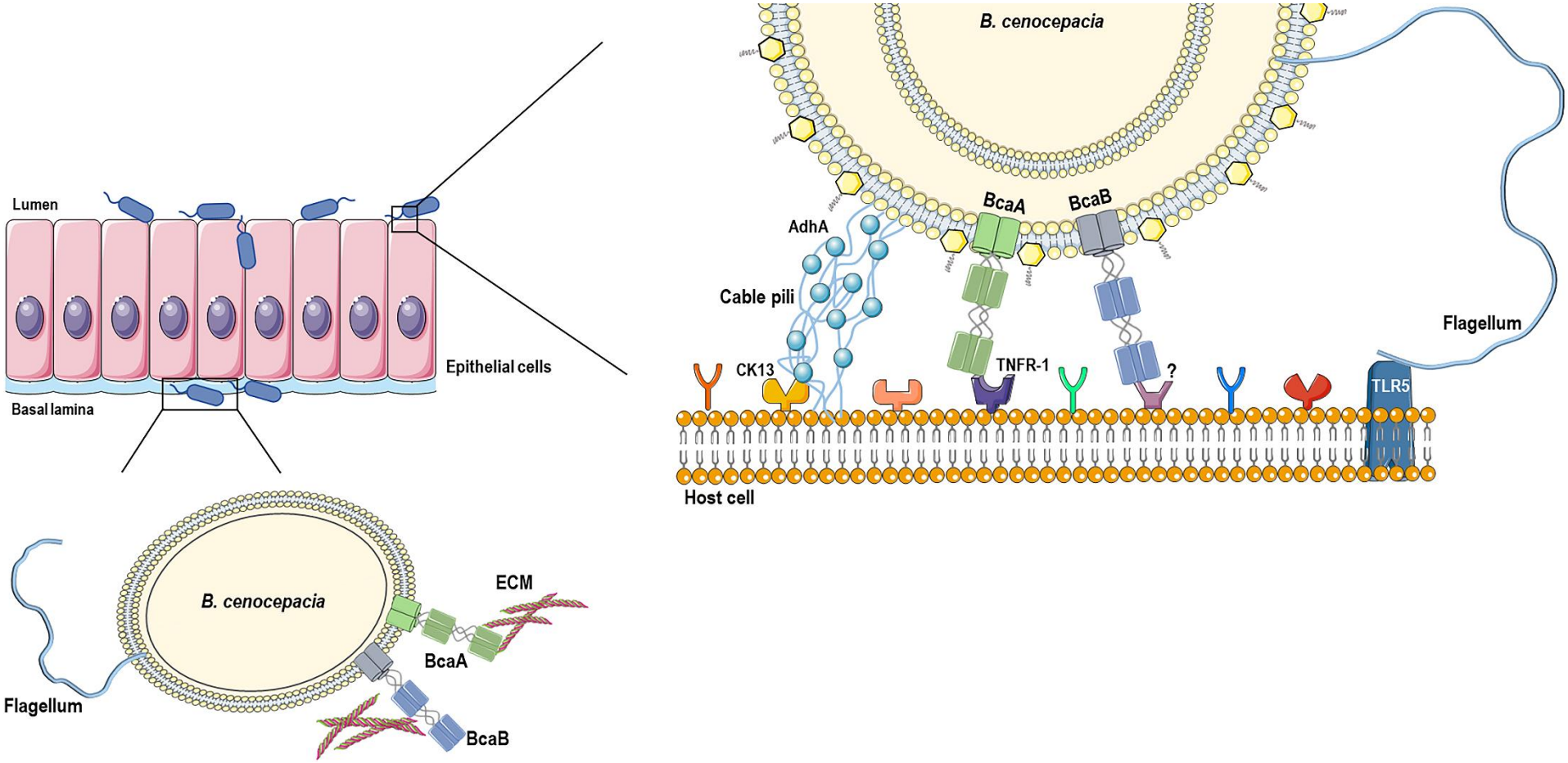

Figure I.2 – **Major adhesion factors of *B. cenocepacia*.** The scheme represents bacterial adhesive molecules and their interactions with the host cells. Cable pili and AdhA adhesin (blue spheres), that binds to cytokeratin 13 (CK13), are represented. Flagellin is known to interact with Toll-like receptor (TLR5) and mediate inflammatory response. BcaA and BcaB TAAs are also characterized. BcaA binds to TNF receptor 1 (TNFR-1) present on the surface of host cells and to extracellular matrix components (ECM), like collagen-type I. BcaB mediates *B. cenocepacia* adhesion to host cells through an unknown cellular receptor. BcaB also adhere to vitronectin, an ECM component.

I.2.3 Strategies and mechanisms used by *B. cenocepacia* to entry and survival inside host cells

Despite being predominantly extracellular, *B. cenocepacia* can survive intracellularly in free-living amoebae, phagocytes, murine and human macrophages in culture, and respiratory epithelial cells (Valvano, 2015; Ganesh, et al. 2020). *B. cenocepacia* can survive intracellularly with minimal or no replication and accumulate in an acidic vacuole (Lamothe, et al. 2007; Rosales-Reyes, et al. 2020). Survival and persistence within host cells facilitate bacterial escape from microbicidal events and play a key role in pathogenesis (Valvano, et al. 2005; Aubert, et al. 2016).

The capacity of *B. cenocepacia* to invade epithelial cells *in vitro* seems to correlate with their capacity to infect *in vivo*. *In situ* localization of *B. cenocepacia* in sections of lungs recovered from CF patients indicated their presence between bronchial epithelial cells. The obtained result suggested that bacteria can be highly invasive, migrating from the airways across the epithelium to invade the deeper tissues and capillaries initiating septicemia (Saijan, et al. 2001). Bacterial isolates were also found to transmigrate across squamous epithelial cell cultures, causing moderate to severe epithelial damage (Saijan, et al. 2002). Several mechanisms of *B. cenocepacia* host cell invasion have been proposed, but the ability to enter and survive inside epithelial cells seems to be strain dependent (Saldías and Valvano, 2009). *B. cenocepacia* can engage a set of different strategies to enter the epithelium and different routes of internalization could be achieved depending on the type and localization of the cellular receptor involved. Some strains can form biofilms on the apical cell surface, causing the disruption of the glycocalyx and rearrangements of the actin cytoskeleton which causes the destruction of the epithelial cell. While others can penetrate the epithelium between cells (paracytosis) causing limited damage (Figure I.3) (Schwab, et al. 2002).

The internalization of *B. cenocepacia* into epithelial cells occurs via a membrane-bound vacuole through a process involving actin rearrangements. After internalization, bacteria either escape into the cytoplasm, or modify bacteria-containing vacuoles to impair normal endocytic pathway and prevent fusion with lysosomes, allowing

trafficking to the endoplasmic reticulum to replicate (Saijan, et al. 2006; Saldías and Valvano, 2009). The mechanism used by *B. cenocepacia* to subvert the normal endocytic pathway in epithelial cells is still unknown. Nevertheless, the requirement of live bacteria seems to be essential, since heat-killed bacteria are found to follow the classical endocytic pathway (Saijan, et al. 2006). Also, the expression of secretion systems, namely type III (T3SS) and IV (T4SS), contribute to the survival and replication of *B. cenocepacia* in eukaryotic cells. Mutations in either systems appear to mistarget intracellular *B. cenocepacia* to a lysosomal degradative pathway causing a decrease in the intracellular bacterial survival rate (Valvano, et al. 2005; Saijan, et al. 2008; Saldías and Valvano, 2009).

Macrophages form the first line of defense against infection in the respiratory tract. Albeit they are programed to ingest and kill foreign pathogens, *B. cenocepacia* can survive with minimal or no replication within murine and human macrophages *in vivo* and *in vitro* (Lamothe, et al. 2007; Saijan, et al. 2008; Walpole, et al. 2020). *B. cenocepacia* macrophage internalization was found to occur through the induction of micropinocytosis. Upon contact with macrophages, *B. cenocepacia* seems to induce membrane rearrangements via T3SS, contributing to macrophage entry and macropinosome-like compartment formation (Rosales-Reyes, et al. 2018). Engulfed bacteria have the capacity to redirect host cell intracellular traffic. *B. cenocepacia*-containing vacuoles (BcCVs) exhibit a significant delay in fusion with lysosomes and fail to acidify their lumen, maintaining a luminal pH around 6.4 (Figure I.3) (Lamothe, et al. 2007; Valvano, 2015). The unsuccessful acidification of BcCVs is thought to be a consequence of the delay on the recruitment of a phagosomal vacuolar ATPase (Valvano, 2015; Rosales-Reyes, et al. 2020). Also, a delay on the normal assembly of a functional NADPH oxidase complex (~6 h) on the BcCVs membrane was observed and seems to be responsible for the reduction of superoxide production (Keith, et al. 2009). The overcome of oxidative damage is an ability that contributes to the intracellular survival of *B. cenocepacia*. Inside vacuolar structures, this ability requires bacterial adaptation to different environments, with the modulation of expression of specific genes, such as membrane transporters or enzymes (Saldías and Valvano, 2009). Alternative sigma factors RpoN or RpoE, stress response regulators, were found to be

involved in *B. cenocepacia* survival inside macrophages and though to be involved in the bacterial adaptation to oxidative stress conditions (Flannagan and Valvano, 2008; Saldías, et al. 2008). Recent work has demonstrated that the inability of bacteria-containing vacuoles to fuse with lysosomes could be linked to the capacity of *B. cenocepacia* to impair the recruitment of GTPases, major regulators of phagosome maturation (Figure I.3) (Huynh, et al. 2010; Aubert, et al. 2015; Walpole, et al. 2020). In addition to the delayed BcCV maturation, the inactivation of GTPases recruitment by *B. cenocepacia* leads to the overtake of the host cell actin cytoskeleton. The absence of functional GTPases, result in the accumulation of projections of filamentous actin nearby BcCVs membranes which appear to be responsible for the delayed maturation of the vacuolar structures (Aubert, et al. 2016; Walpole, et al. 2020). The inactivation of GTPases by *B. cenocepacia* was found to be mediated by type VI secretion system (T6SS) effector protein TecA (Valvano, 2015; Aubert, et al. 2015; Aubert, et al. 2016; Walpole, et al. 2020). The T6SS also prevents the recruitment of soluble subunits of the NADH oxidase complex to the membrane of BcCVs, is required to induce cell death in infected cells and contributes to the overall survival capacity of *B. cenocepacia* inside macrophages (Valvano, 2015; Aubert, et al. 2016). Intracellular *B. cenocepacia* can also induce macrophage pyroptosis, a highly inflammatory form of programmed cell death, through the secretion of a bacterial deamidase, which ultimately leads to *B. cenocepacia* release (Figure I.3) (Aubert, et al. 2016; Gomes, et al. 2018; Rosales-Reyes, et al. 2020). Macrophages despite being a critical site for *B. cenocepacia* replication inside the host, could act as a platform for the transition from intracellular *B. cenocepacia* to acute pro-inflammatory infection (Mesureur, et al. 2017; Gomes, et al. 2018).

Several studies have pointed to the fact that altered trafficking and acidification of BcCVs was greatly amplified in CFTR-defective macrophages, when compared to normal ones (Lamothe and Valvano, 2008; Assani, et al. 2017). Some evidence indicates that malfunctioning CFTR leads to defective autophagy which might alter the capacity of macrophages to clear intracellular bacteria (Lamothe and Valvano, 2008; Luciani, et al. 2011). In this scenario, a defective CFTR enhances the *B. cenocepacia*-mediated maturation defect of BcCVs, revealing a possible synergic effect in downregulating autophagy. Furthermore, Assani et al. (2017) demonstrated CF macrophages have

defective oxidative responses due to a decreased phosphorylation of NADPH oxidase components (Assani, et al. 2017). The decreased oxidative burst was found to be enhanced by the presence of intracellular *B. cenocepacia*. These results could be involved in the basis of *B. cenocepacia* increased persistence within CF patients compared to healthy individuals (Lamothe and Valvano, 2008; Saldías and Valvano, 2009; Assani, et al. 2017).

The interaction between *B. cenocepacia* and other cells involved in the host immune system have been suggested. Neutrophils are an important member of the innate immune response against pathogenic bacteria in the lungs. Upon infection, neutrophils are recruited and engaged in bacterial phagocytosis. Bacteria were then destroyed by a combination of oxidative and non-oxidative processes. In CF lungs, neutrophils are responsible for the inflammatory process with a constant neutrophilic infiltration (Sandías and Valvano, 2009). *B. cenocepacia* exopolysaccharide seems to interfere with the human neutrophils by constraining chemotaxis and scavenging reactive oxygen species (ROS) production (Bylund, et al. 2006). Moreover, neutrophils exposed to *B. cenocepacia* isolates revealed an increased apoptosis and necrosis levels, which compromises the clearance of bacteria from the lungs (Bylund, et al. 2005). Neutrophils necrosis also cause the release of their toxic contents which are ingested by macrophages and lead to the release of elevated levels of proinflammatory cytokines triggering persistent inflammation and tissue destruction in infected CF lungs (Saldías and Valvano, 2009). Dendritic cells are essential in regulating immune response, they capture and process foreign antigens and then present them on their surface to the cells of the innate immune system. Dendritic cells were found to bind and engulf *B. cenocepacia* which induces the release of proinflammatory cytokines. In addition, *B. cenocepacia* seems to interfere with the normal function of dendritic cells by inducing necrosis (Figure I.3) (Saldías and Valvano, 2009).

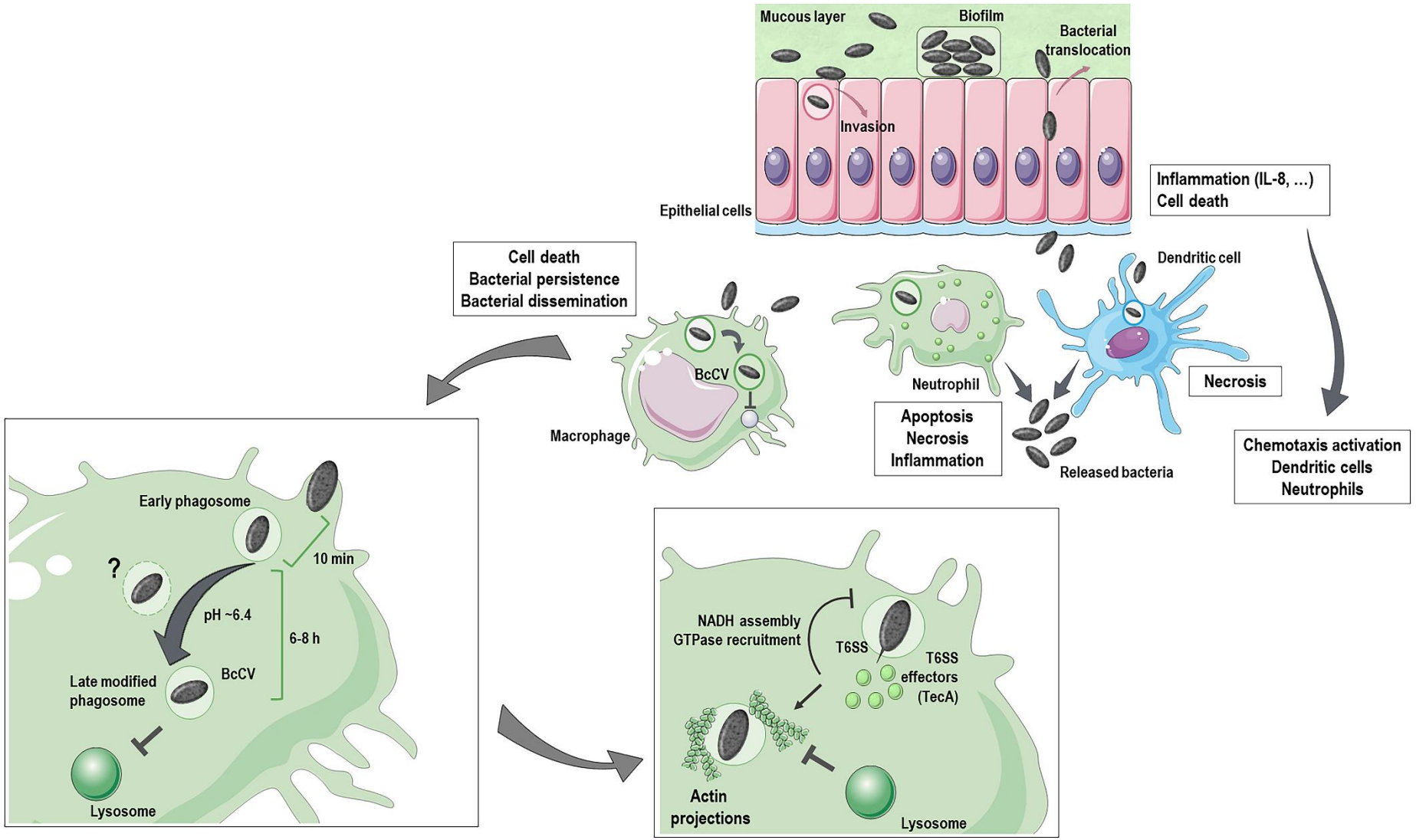
Mucous layer
Biofilm
Bacterial translocation
Invasion
Epithelial cells
Inflammation (IL-8, ...)
Cell death
Cell death
Bacterial persistence
Bacterial dissemination
Dendritic cell
BcCV
Neutrophil
Necrosis
Macrophage
Apoptosis
Necrosis
Inflammation
Released bacteria
Chemotaxis activation
Dendritic cells
Neutrophils
Early phagosome
10 min
?
pH ~6.4
6-8 h
Late modified phagosome
BcCV
Lysosome
NADH assembly
GTPase recruitment
T6SS
T6SS effectors (TecA)
Actin projections
Lysosome

Figure I.3 – **Proposed model of *B. cenocepacia* interactions with epithelial and immune cells from CF airways.** Bacteria adhere to receptors on the apical surface of lung epithelial cells and proceed to transepithelial migration either by intracellular invasion or by paracellular translocation (paracytosis). *B. cenocepacia* can also form biofilms on the surface of the epithelium. The effects of intracellular bacteria in macrophages, neutrophils and dendritic cells are represented. In most cases, the engulfment of *B. cenocepacia* leads to host cell death and consequent release of the bacteria to the extracellular space, that may cause bacterial persistence and an extended inflammatory response that damages the host tissue. In macrophages, engulfed bacteria have the capacity to redirect host cell traffic. *B. cenocepacia*-containing phagosome exhibits a significant delayed maturation (6-8h). BcCVs (*B. cenocepacia*-containing vacuoles) fail to acidify their lumen, maintaining a pH around 6.4. BcCVs fusion with lysosomes is inhibit. The possibility that during this process the bacteria escape the vacuole (dashed lines) and live in the cytosol is not clearly established. T6SS of *B. cenocepacia* plays an important role in intracellular survival inside macrophages. T6SS effectors, like TecA, are injected into the cytosol where they affect the recruitment of GTPases and components of the NADPH oxidase to the membrane of the phagosome. TecA induces filamentous actin polymerization around the phagosome membranes. The formed actin clusters delay phagosomes maturation and prevent their fusion with lysosomes.

I.2.4 *B. cenocepacia* adaptation to host lungs during chronic infections

The process of chronic colonization is based on the ability of bacteria to adapt over time, being able to adjust themselves to environmental pressures, co-infecting species, and antimicrobial therapies. These adaptations can occur due to inflammatory responses, hypoxia, nutrient deficiency or antibiotics and cause phenotypic and genotypic alterations in bacterial pathogens, that include metabolic shifts, morphological alterations, biofilm formation and motility, antimicrobial resistance and host immune system evasion and modulation (Mira, et al. 2011; Ganesan and Sajjan, 2012; Kalferstova, et al. 2015; Cullen, et al. 2018; Hassan, et al. 2019b).

During chronic infection *B. cenocepacia* suffers a clonal expansion, as the result of mutations and selective pressures occurring in the CF lung environment. Multiple phenotypic variants emerge from the clonal population and become established in the patient's airways (Coutinho, et al. 2011). Diverging populations can exist simultaneously in the same host for several years. Diversification can be driven by multiple adaptive mutations, sometimes in the same target, that occur in parallel and facilitates persistence of the bacterial community during changes in environmental conditions (Lieberman, et al. 2014). Hypermutation has also been associated with *B. cenocepacia* persistence in CF patients. Hypermutable bacteria normally present defects in the DNA repair system leading to an increased rate of spontaneous mutations that play a key role in the evolution of the pathogen. Martina et al. (2014) demonstrated the prevalence of *B. cenocepacia* hypermutators among chronically infected CF patients. Data revealed that 76.5% of the *B. cenocepacia* hypermutators were defective in *mutS* and/or *mutL*, genes that encode proteins involved in mismatch repair, and that they are positively selected in CF chronic lung infections (Martina, et al. 2014).

Moreover, alterations in genomic and proteomic expression in the course of infection were found to occur in *B. cenocepacia* isolates (Madeira, et al. 2011; Mira et al. 2011; O'Grady and Sokol, 2011; Kalferstova, et al. 2015; Cullen, et al. 2018). Aside from that, processes of DNA methylation also seem to contribute to the epigenetic regulation of gene expression, causing alteration in biofilm formation, cell aggregation, and motility

(Vandenbussche, et al. 2020). Madeira, et al. (2011) found that proteins of the functional categories of energy metabolism, translation, iron uptake, nucleotide synthesis and protein folding and stabilization were more abundant in a *B. cenocepacia* clonal variant (isolated during persistent infection), compared to the first isolate recovered, suggesting an increased protein synthesis, DNA repair activity, iron uptake capacity and stress resistance. The level of proteins related with peptidoglycan, membrane lipids and lipopolysaccharide biosynthesis were also found to be different in the two clonal variants (Madeira, et al. 2011). Concerning the comparison of genetic expression of the same sequential *B. cenocepacia* isolates, Mira, et al. (2011) showed that almost 1000 genes were found to be differently expressed in the two clonal variants. Induced genes included those involved in translation, iron uptake, efflux of drugs and adhesion to epithelial cells and mucins. Moreover, changes in expression of genes involved in adaptation to nutrient- and oxygen-limited environments of the CF lung were suggested to be central features in the *B. cenocepacia* transcriptional shift during long-term colonization (Mira, et al. 2011). A different study assessed the adaptation of *B. cenocepacia* to the host environment, using a rat chronic respiratory infection model (O'Grady and Sokol, 2011). When compared to cultures grown *in vitro*, genes associated with flagellar motility and Flp type pilus formation were found to be down-regulated *in vivo*. On the other hand, genes encoding for T4SS, and proteins involved in osmotic stress, adaptation and intracellular survival, nutrient transport, as well as those encoding outer membrane proteins were significantly induced *in vivo* (O'Grady and Sokol, 2011). Using microarrays, Kalferstova, et al. (2015) compared the transcriptomes of different *B. cenocepacia* isolates – from the bloodstream of infected CF patients at the time of cepacia syndrome and from the sputum, recovered months prior. The blood isolates revealed induced expression of virulence genes involved in T3SS and bacterial exopolysaccharide cepacian, while genes encoding for flagellar proteins were found to be downregulated when compared to the sputum isolates. The loss of motility was observed in most of the isolates recovered form patients with cepacia syndrome, indicating that a nonmotile phenotype could represent a warning sign for the development of fatal cepacia syndrome in CF patients infected with *B. cenocepacia* (Kalferstova, et al. 2015). Despite the repression of the expression of genes involved in flagella production and in chemotaxis during chronic infections, some reports have

pointed out to their upregulation during rapid growth in sputum-based medium (Sass, et al. 2011; Kumar and Cardona, 2016). This repression may reflect a short-term response of *B. cenocepacia* to early growth during infection, where flagella and motility might act as important virulence determinants (Tomich, et al. 2002). Moreover, Kumar and Cardona (2016) suggested that it is likely that flagellin and flagellar structure may play a role in the initial stages of colonization in response to the nutritional environment of the CF lung (Kumar and Cardona, 2016). The nutritional conditions of the CF lung were proven to induce expression of multiple flagella on the cell surface of *B. cenocepacia*, increasing bacteria motility and facilitating the spread and development of *B. cenocepacia* chronic infection (Kumar and Cardona, 2016). More recently, the growth in low-iron conditions and the anoxic persistence of *B. cenocepacia* has gaining importance as a mechanism of adaptation (Sass, et al. 2013; Cullen, et al. 2018; Sass and Coenye, 2020). Studies indicate that bacterial growth under low oxygen conditions lead to the regulation of a specific group of genes – the *lxa* (low oxygen-activated) locus, that are predicted to be involved in metabolism, transport, electron transfer and regulation (Sass, et al. 2013; Cullen, et al. 2018). Proteins encoded by *lxa* locus genes were also found to be upregulated during chronic infection, highlighting the involvement of the *lxa* locus in the adaptation of *B. cenocepacia* during *in vivo* colonization of the hypoxic CF lung (Cullen, et al. 2018). Likewise, conditions of iron starvation, commonly encountered inside the CF host, proven to act as a *stimulus* for central metabolism and oxidative stress regulation in *B. cenocepacia* (Sass and Coenye, 2020). Such restrictions might lead to the involvement of small RNAs as mediators of response, in order to maintain iron homeostasis under conditions of iron starvation (Sass and Coenye, 2020).

Proteomic and transcriptomic alteration in *B. cenocepacia* during long term colonization could also be a result of intricated regulatory systems that can sense and respond to the surrounding environment. An important molecular method to perceive and transduce specific signals is quorum sensing (QS) (Abisado, et al. 2018). QS is a cell-cell communication system known to coordinate population density-dependent changes in behavior, involving the production of and response to diffusible or secreted signals, such as N-acyl homoserine lactones (AHL) and *cis*-2-dodecenoic acid also known as *Burkholderia* diffusible signal factor (BDSF). QS can coordinate interactions both within

a species and between species in the context of bacterial sociality (Abisado, et al. 2018). In *B. cenocepacia*, several QS systems have been identified and shown to modulate virulence functions like toxin, protease, lipase and siderophore production, as well as swarming phenotype and biofilm formation (Subramoni and Sokol, 2012; Schmid, et al. 2017; Yang, et al. 2017). Several studies have supported the hypothesis of a role for QS during *B. cenocepacia* chronic infection. Evidences of AHLs detected in sputum and respiratory secretions from CF patients chronically colonized by *B. cenocepacia* and the overexpression of functional QS genes in long term isolates support such assumption (Mira, et al. 2011; McKeon, et al. 2011). The use of QS by bacterial populations to communicate and coordinate behaviors during host colonization contribute for the success of pathogenic bacteria during infection (Abisado, et al. 2018). In the case of *B. cenocepacia*, such interactions coordinate the expression of specific virulence-associated genes that ultimately result in phenotypic adaptations, such as enhanced invasion capacity and antibiotic resistance, that impacts disease progression (Subramoni and Sokol, 2012; Ganesh, et al. 2020). Besides QS, other processes of interaction between *B. cenocepacia* and other species of bacteria during long-term CF infections has also been reported (Welp and Bomberger, 2020). In order to outcompete other species of co-colonizing pathogens, *B. cenocepacia* had to adapt and establish specific antibacterial mechanisms (Perault, et al. 2020). Among those, *B. cenocepacia* T6SS seems to play an important role in interbacterial predation. T6SS mediate the injection of toxic effector proteins inside bacterial competitors, making the CF-lung more susceptible to *B. cenocepacia* infection and the nutrients more available for growth and colonization (Spiewak, et al. 2019; Perault, et al. 2020).

B. cenocepacia adaptation during long-term colonization contribute to the occurrence of physiologic and phenotypic alterations. The cell wall morphology of *B. cenocepacia* appears to suffer consistent and progressive alterations during the course of chronic infection. From the common rod shape, *B. cenocepacia* seems to change over time its height and shape reaching a morphology closer to *cocci* (Hassan, et al. 2019b). Concerning adhesion, *B. cenocepacia* isolates obtained in the initial stages of infection seems to adhere better when compared to a clonal variant isolated during persistent infection. This reduction in the ability to adhere could be correlated to variations of the

lipopolysaccharide (LPS) structure at level of the O-antigen (OAg) (Hassan, et al. 2019a). *B. cenocepacia*, unlike other members of Bcc complex, shown to have the tendency to lose the OAg along chronic infection, which seems to increase with the duration of infection. Moreover, it is suggested that the loss or modifications of the OAg could be critical during the *B. cenocepacia* infection process, particularly during adhesion and to overcome host defense mechanisms (Hassan, et al 2019a; 2019b).

Biofilm formation during infection has been associated with the capacity of *B. cenocepacia* persist in patients with CF. *B. cenocepacia* biofilms are a matrix of extracellular polymeric molecules composed of DNA, polysaccharides, and proteins. The decreased antibiotic diffusion, nutrient availability and metabolic changes inside biofilm matrix could lead to the development of antibiotic resistance (Caraher, et al. 2007; Scoffone, et al. 2017). Van Acker et al. (2013) demonstrated that *B. cenocepacia* biofilms contain tolerant persister cells that are able to survive to ROS and are often more tolerant to antimicrobials than planktonic cells (Van Acker, et al. 2013). Furthermore, *B. cenocepacia* biofilms appear to be enhanced in the presence of neutrophils, probably due to the incorporation of cellular debris into the biofilm structure. Mature biofilms also induce neutrophil necrosis and mask bacteria from being recognized by the host cells affecting the production and secretion of IL-8 (Murphy and Caraher, 2015). Moreover, the formation of *B. cenocepacia* microcolonies seems to allow the bacterial persistence in the apical mucus layer of airway epithelial cell cultures, improving cell invasion and extensive cell damage (Ganesan and Sajjan, 2012).

B. cenocepacia is intrinsically resistant to several classes of antibiotics such as polymyxins, cephalosporins, aminoglycosides and most β-lactams, and can develop *in vivo* resistance to essentially all classes of antimicrobial drugs (Drevinek and Mahenthiralingam, 2010; Scoffone, et al. 2020). Antibiotic resistance is a well-known feature of chronically colonizing pathogens specially those associated with CF infections. Bacteria acquire and utilize mechanisms of enzymatic inactivation and modification (β-lactamases, aminoglycoside-inactivating enzymes), alteration of drug targets, cell wall impermeability, porins and active efflux pumps (Cullen and McClean, 2015; Scoffone, et al. 2017; Chiarelli, et al. 2020). During long-term infection, resistance mechanisms could be altered and modulated as result of exposure to different antimicrobial compounds.

Bcc bacteria could develop different patterns of antimicrobial resistance depending on the environmental conditions. Bacterial strains isolated from CF-lungs were found to present a higher degree of antibiotic resistance than the ones isolated from non-CF patients. This may be directly related to *B. cenocepacia in vivo* adaptation to the elevated concentrations of administered antibiotic overtime, since early *B. cenocepacia* clonal isolates were found to be more susceptible to the most classes of antimicrobial agents (Zhou, et al. 2007; Coutinho, et al. 2011; McAvoy, et al. 2020).

B. cenocepacia has the capacity to subvert the innate immune system stimulating disproportionate pro-inflammatory cytokine release. The interaction of *B. cenocepacia* with innate immune receptors such as TLRs or TNFR1 was addressed above. The bacterial interaction with such kind of receptors is expected to be beneficial to the host as it prompts pro-inflammatory responses and the recruitment of neutrophils to the site of infection. However, interaction of bacteria with cytokine receptors may increase in a disproportional way the host immune response which can lead to damage in the lungs often observed in infected CF-lungs (Vandivier, et al. 2009; Ganesan and Sajjan, 2012). Several *B. cenocepacia* products like LPS, flagella, pili and adhesins were found to be recognized by both epithelial and inflammatory cells and stimulate a pro-inflammatory response (Urban, et al. 2004; Sajjan, et al. 2008; Mil-Homens, et al. 2017). Flagella from *B. cenocepacia* K56-2 was shown to stimulate chemokine and cytokine responses both *in vitro* and *in vivo* by interacting with TLR5 (Urban et al., 2004). More recently, it was found that *B. cenocepacia* flagella not only modulated the host pro-inflammatory response but could also be associated with immune system evasion. Hanuszkiewicz, et al. (2014) identified a flagellin glycosylation system in *B. cenocepacia* and showed the contribution of glycosylated flagellin to evasion of human innate immune responses (Hanuszkiewicz, et al. 2014). Non-glycosylated flagellin was more pro-inflammatory than its glycosylated form, also glycosylation was associated with reduced efficacy of TLR5 stimulation and consequent signal transduction. The obtained results led the authors to suggest that the presence of glycans may alter the flagellin recognition by TLR5, reducing *B. cenocepacia* recognition by the innate immune system facilitating its persistence in the human lungs (Hanuszkiewicz, et al. 2014). Mil-Homens et al. (2014) demonstrated the role of TAA BcaA in the *B. cenocepacia* evasion of the human innate immune system,

by providing resistance against the serum bactericidal activity via the complement classical pathway (Mil-Homens, et al. 2014). The mechanism by which BcaA affect the classical complement pathway is still unknown, but it was suggested that recruitment or mimicking of complement regulators/inhibitors and the modulation or inhibition of complement proteins by direct interactions could take place. BcaA promotes adhesion of *B. cenocepacia* towards vitronectin, an inhibitor of the complement cascade. This ability to bind vitronectin could be used by *B. cenocepacia* to inhibit complement-mediated attack or as a bacterial camouflage with nonimmunogenic proteins to delay *B. cenocepacia* recognition by the human immune system (Mil-Homens, et al. 2014).

The progression of *B. cenocepacia* infection requires a series of stages that involves a close interconnection between bacteria and host. Since the early stages of adherence to adaptation to long term colonization, *B. cenocepacia* uses an armory of mechanisms and virulence factors. Among them, trimeric autotransporter adhesins (TAAs) are crucial players in several processes of pathogenesis acting as multifunctional proteins. In the following subchapter the main features of this class of proteins are reviewed and a detailed description of some well-studied TAAs was achieved.

I.3 Trimeric autotransporter adhesins: more than bacterial surface appendages

Trimeric autotransporter adhesins (TAAs) are members of the autotransporter proteins family - one of the largest groups of extracellular proteins widely spread in Gram-negative bacteria. They are designated autotransporter due to the type V secretion system (T5SS) used as translocation mechanism that appears to be independent of any source of energy (Henderson, et al. 2004). Autotransporter proteins have a common organization with a C-terminal β-barrel translocator domain, an extracellular passenger domain and an N-terminal signal. The β-barrel functions as a pore by which the N-terminal domain passes through during the biogenesis process, remaining covalently attached to the C-terminal part of the protein (Benz and Schmidt, 2011). TAAs have a typical trimeric surface modular architecture with a C-terminal anchor and a variable extracellular set of fiber-like stalk and globular-like head regions. While the membrane anchor domain is the defining feature of this group of proteins, highly conserved between all the TAA members, head and stalk organization is adaptable and vary among TAAs (Cotter, et al. 2005a; Łyskowski, et al. 2011). YadA (*Yersinia* adhesin A) from *Yersinia enterolitica* and *Yersinia pseudotuberculosis* is the prototype of this family of proteins (Koretke, et al. 2006). The sizes of TAAs can vary between 340 residues (putative TAA from *Fusobacterium nucleatum*) (Desvaux, et al. 2005) and 5035 residues (*Bartonella tribocorum*, BadA) (Kaiser, et al. 2011). Their lengths could differ between species or even between different strains (Szczesny and Lupas, 2008).

Normally, the head and stalk domains appear in a repetitive and modular way and could be distinguished from several related types. Within this modular arrangement, the head mediated the binding to the host and the stalk hurls the head from the membrane, enhancing the distance between the binding domains and the bacterial surface. Also, this repetitive fashion could help the occurrence of recombination events that may lead to environmental adaptation phenomena or selective evolution (Linke, et al. 2006; Bassler, et al. 2015). TAAs play a wide range of roles in virulence and bind to a large set of molecules, such as host cell receptors, ECM components or ever other TAAs. They can

also interfere with the host cell immune response through the inhibition of some pathways of complement or antibody-related ones (Kline, et al. 2009; Stones and Krachler, 2015).

I.3.1 Structural organization

In the past years, as several TAA crystal structures have been solved, it became possible to relate assembly with function and create a more accurate knowledge of these trimeric proteins. Until now only conformations of protein fragments have been solved, such as YadA (PDB 1P9H, Nummelin, et al, 2004), BadA (PDB 3D9X, Szczesny, et al. 2008), AtaA (*Acinetobacter* sp.) (PDB 3WP8, Koiwai, et al. 2016) and BpaA (*Burkholderia pseudomallei*) (PDB 3LAA, Edwards, et al. 2010) head structures; EibD (*E. coli*) (PDB 2XQH, Leo, et al. 2011), AtaA (PDB 3WPO, PDB 3WPA, PDB 3WPR, Koiwai, et al. 2016) and YadA (PDB 3H7X, Alvarez, et al. 2010) partial stalk domains; Hia (*Haemophilus influenzae*) (PDB 1S7M, Yeo, et al. 2004; PDB 3EMI, Meng, et al. 2008) and SadA (*Salmonella enterica*) (PDB 2YO2, 2YNZ, 2YO3, Hartmann, et al. 2012) neck domains; and YadA (PDB 2LME, Shahid, et al. 2015) and Hia (PDB 2GR7, Meng, et al. 2006) membrane anchor domains.

TAAs are usually large proteins with an extracellular region of considerable dimension. Their length can vary up to 10-fold from the smaller TAA to the larger one (Figure I.4) (Bassler, et al. 2015). This variation could be a result of the intricate modular organization of the passenger region with a repetitive array of consistent domains surrounded by extended sequences with arrangements of lower complexity, typically organized in coiled-coil structures (Szczesny and Lupas, 2008; Bassler, et al. 2015) (Figure I.4). These segments of the passenger domain could include a significant amount of short amino acid motifs repetitions with unknown function or structure (Szczesny and Lupas, 2008; Mil-Homens, et al. 2010; Campos, et al. 2013).

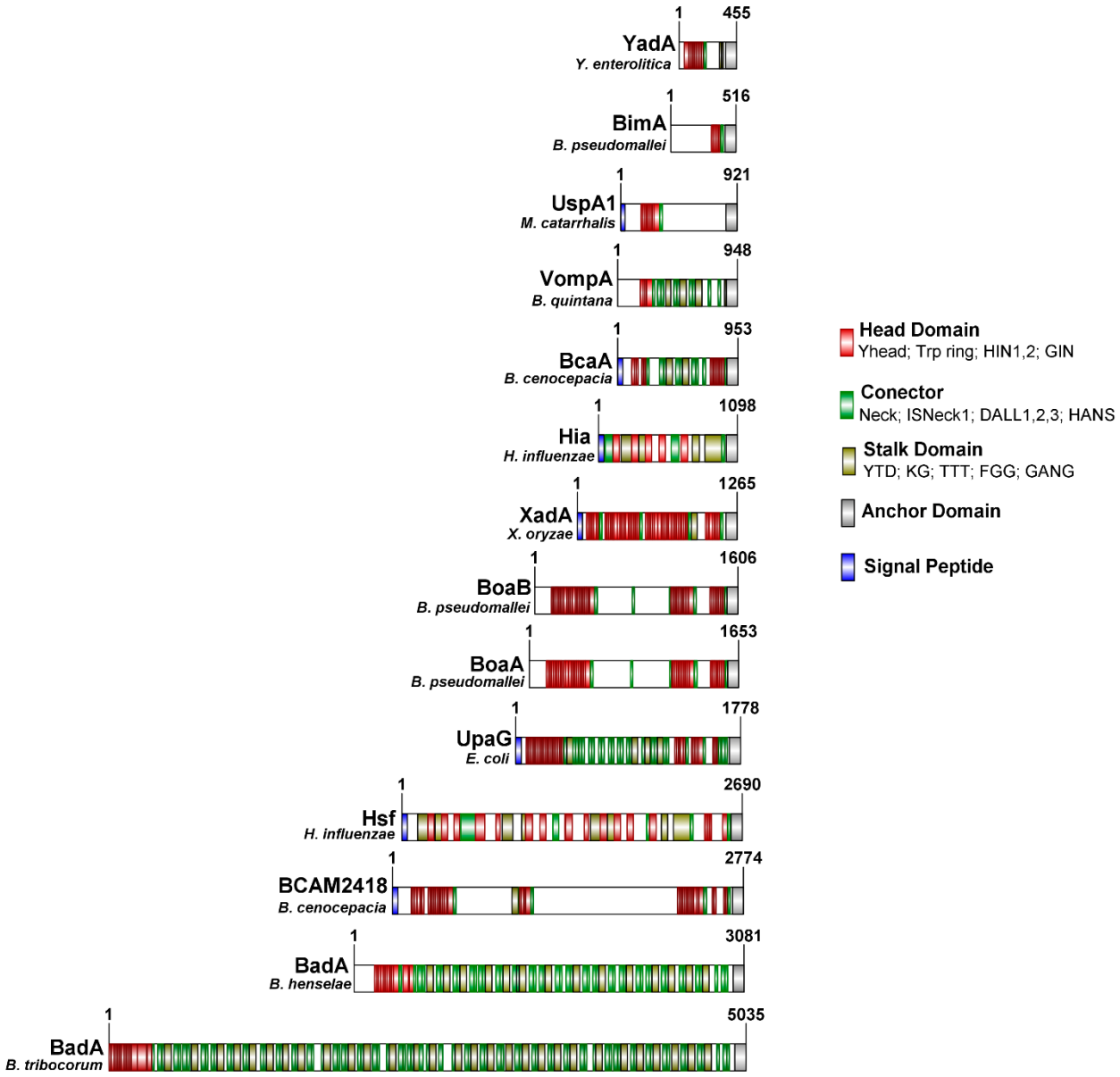

Figure I.4. Schematic representation of the modular organization of several TAAs from different Gram-negative species. The protein and the species of origin are represented. The domain composition was determined using the daTAA tool (discontinued in 2017) (Szczesny and Lupas, 2008). The illustrations are to scale (based on sequence length). All TAAs contain a signal peptide (SP), passenger domain and anchor domain. The sub-domain organization in passenger domain varies among TAAs. The TAAs length are largely variable among species. Also, homologous proteins also shown a significant size variation between them (BadA from *B. hensealae* or *B. tribocorum*). The TAA repetitive and modular features are notorious.

The trimeric C-terminal region forms a β-barrel structure in the outer membrane. This barrel is constituted by 12 β-sheets and it is highly stable and heat-, trypsin- and SDS-resistant (Roggenkamp, et al. 2003; Koretke, et al. 2006; Lehr, et al. 2010). Each

monomer forms an amphipathic α-helix followed by 4 β-strands that interact with the other two monomers side-by-side to build the hydrophilic membrane pore with approximately 20 Å in diameter (Meng, et al. 2006). After the trimerization the helices form a coiled-coil structure capable to stabilize the homotrimer and to block the entrance of the pore (Koretke, et al. 2006). Molecular dynamics simulations studies on the translocator domain of Hia shown that the presence of α-helixes is a key-element for the stability and integrity of the trimer, and their elimination from the protein causes representative conformal alterations on the trimeric pore such as distortion of the β-barrel or loss of symmetry (Holdbrook, et al. 2013). The translocator domain of individual monomers has ~70-80 residues in length and it seems to be sufficient for the translocation of the passenger domain into the bacterial external surface (Surana, et al. 2004; Mikula, et al. 2012). Also, the oligomerization of the three chains could be driven by the translocation domain, and so the folding and transport are inherent to the anchor domain. The C-terminal trimerization seems to be a necessary step for the passenger domain translocation through the β-barrel pore (Meng, et al. 2006; Mikula, et al. 2012).

The stalk structures have the simplest arrangement, and their length could vary greatly between different TAAs (Szczesny and Lupas, 2008). The fibrous stalk domain function as spacer projecting the head domains from the bacterial surface and is usually constituted by coiled-coil sequences that may fluctuate periodically from both left-handed and right-handed structures (Lupas and Gruber, 2005; Moutevelis and Woolfson, 2009; Łyskowski, et al. 2011). The stalk is highly repetitive containing several copies of conserved sequence motifs. In order to increase stalk flexibility or rigidity, it is thought that the coiled-coil sequences may be surrounded by specific motifs or minidomains formed by an elongated hairpin (Leo, et al. 2011; Bassler, et al. 2015). These motifs are largely spread in TAAs, they may (i) increase the rigidity of the stalk, since they are denser than nearby stalk segments; or (ii) increase the flexibility releasing the tension triggered by superhelical stalk turns (Bassler, et al. 2015).

The YadA passenger domain with 23 nm represent the simplest model of the extracellular extension of trimeric adhesins with only one stalk domain and one head domain (YadA-like domain (Ylhead)) in the N-terminal region (El Tahir and Skurnik, 2001). In more complex TAAs, head and stalk domains could alter several times until

reaching the anchor (Bassler, et al. 2015) (Figure I.4). The globular-like head domains are known to mediate the interactions between TAA and other molecules potentiating functions like agglutination, binding to host proteins (ECM proteins or host cell receptors) or even resistance to the immune system (Nummelin, et al. 2004; Conners, et al. 2008; Biedzka-Sarek, et al. 2008; Leo, et al. 2010; Kaiser, et al. 2012; Singh, et al. 2014). Ylhead domain is the most widely distributed in TAAs, but there are several other domains with analogous topology such as GIN domains, tryptophan ring domains (TrpRing), FxG domains, and GANG domains, that can be present in a repetitive fashion in the passenger domain of trimeric adhesins (Meng, et al. 2006; Bassler, et al. 2015; Singh, et al. 2015). The head domains could be not only repetitive in structure but also in sequence (Łyskowski, et al. 2011). Due to structural differences between head and stalk domains the connection among these two segments must occur through the presence of a conserved connector or "neck" that provides a sleek transition to and from the stalk. Neck domains are the most conserved segment among TAAs sharing the same architecture varying from 19 to 22 residues (Hoiczyk, et al. 2000; Bassler, et al. 2015).

I.3.2 Biogenesis – type Vc secretion system

Secretion systems in Gram-negative bacteria have been numbered from I to VI (Green and Mecsas, 2016). The more well-known difference between type V (autotransporter system) and the other secretion systems is its apparent simplicity. Type V secretion system (T5SS) is subdivided in Va (autotransporter system - classical monomeric autotransporter proteins), Vb (two-partner secretion system - TPS) and Vc (trimeric autotransporter system) (Leo, et al. 2012; Green and Mecsas, 2016). More recently, type Vd (patatin-like passenger domains), Ve (intimin/invasin pathway) and "type V-like" secretion systems have been reported (Figure I.5) (Leo, et al. 2015; Casasanta, et al. 2017; Coppens, et al. 2018; Bernstein, 2019). Proteins that are exported by these systems share common biogenesis mechanisms (SEC-pathway) and structural features like the presence of a signal peptide that promotes translocation across the inner membrane, an extracellular passenger domain, and a domain that anchors the protein

to the outer membrane , normally forming a β barrel structure (Kostakioti, et al. 2005; Bernstein, 2019). Type V secretion is a process that occur in two major steps: (i) the signal peptide-containing protein chains are guided to the SEC machinery in the inner membrane; (ii) the trimeric anchor is formed at the outer membrane and the passenger domains are translocated, folded and processed in order to acquire the final conformation at the external face of the bacteria (Figure I.5) (Dautin and Bernstein, 2007; Leo, et al. 2012). For TAAs three copies of the protein chain are required for the translocation, the trimerization of the C-terminal anchor domain is mandatory for the ongoing secretion process (Cotter, et al. 2006; Mikula, et al. 2012). TAA passenger domains remained covalently attached to the β-anchor after secretion. Given the trimeric nature of TAAs, they must develop a specific strategy to deal with the physical and mechanical restrictions of multimerization and simultaneous transport and folding of the trimeric passenger domains (Hodak and Jacob-Dubuisson, 2007). Several models have been predicted in order to explain this process (Ieva and Bernstein, 2009; Leyton, et al. 2012; Sikdar, et al. 2019; Ryoo, et al. 2020).

Considered the hairpin model, the unfolded protein passes the inner membrane in a SEC-dependent manner, the C-terminal β-barrel is folded into the outer membrane while the passenger domain remains unfolded in the periplasm with the help of chaperones to prevent misfolding and proteolytic degradation. Once the β-barrel is formed the passenger domain forms a hairpin that is inserted into the membrane pore. The rest of the polypeptide chain is then able to pass through the pore of the β-barrel using as driving force the free energy gained by folding the passenger domain on the cell surface (Henderson, et al. 2004; Barnard, et al. 2007; Leo, et al. 2012; Fan, et al. 2016). One of the restraints associated with this model is related with the timeline of trimerization of the passenger domain. It is thought that the assembly of the passenger domains must happen only after the passage through the β-barrel pore, since totally folded trimeric passenger domains will be enabled to fit in the already formed membrane β-channel. And so, it is critical that the extracellular domain remains unfolded in the periplasm and during the passage through the outer membrane (Hodak and Jacob-Dubuisson, 2007; Hagan, et al. 2010). In this step several scenarios could take place: the passenger domain could begin to be extruded with a hairpin loop formation,

with the C-terminal end of the passenger domain being secreted first; or, in the other hand, the N-terminal end of the passenger domain may be the first part to be externalized without the necessity of formation of intermediate structures. In both cases and considered the simultaneously of the three domains translocation, the pore must have a diameter large enough to accommodate up to six unfolded protein chains (considered the hairpin loops) or three unfolded passenger domains, respectively (Łyskowski, et al. 2011; Fan, et al. 2016; Bernstein, 2019).

A different model suggests the need for accessory proteins – the Bam complex (β-barrel assembly machinery), to assist the translocation (Sikdar, et al. 2019). In Gram-negative bacteria, the 200 kDa Bam complex is well known for its role in folding and insertion of Omps β-barrel in the outer membrane (Sauri, et al. 2009; Lehr, et al. 2010). Bam complex is a heterooligomer formed by BamA (an Omp), BamB, BamC, BamD and BamE (lipoproteins) (Figure I.5) (Han, et al. 2016). Although the well-studied interference of Bam in Omps and classical autotransporter biogenesis, the role in TAA assembly and translocation is still poorly understood (Sauri, et al. 2009; Ieva and Bernstein, 2009; Leo, et al. 2012; Ryoo, et al. 2020). Bam assistance during TAA biogenesis could occur by providing a channel for the migration of the passenger domain, or by helping the stabilization of the trimeric pore (Han, et al. 2016). It could also interfere with the C- to N-terminal translocation of the passenger domain (Leo, et al. 2012). The translocation across the outer membrane through the trimeric autotransporter pathway could be divided in a series of sequential steps (Sidkar, et al. 2019). First, the three polypeptides structures that form the β-barrel domain fold into an asymmetrical trimer in the periplasm; then the partially assembled anchor domain is directed to the Bam complex which facilitates its insertion into the outer membrane. Subsequently, translocation occurs through a hybrid channel formed by open forms of the β-barrel domain and BamA barrel (Figure I.5). This proposal could clarify how TAA passenger domains, that contain tertiary structure, could fit, and be secreted by the constricted pore created by the anchor domain (Saurí, et al. 2012). Translocation is then rapidly guided by the folding of the passenger domains since the formation of a coiled-coil structure in the extracellular space drives the rapid secretion of the remaining trimer. After the complete translocation, the β-barrel pore closes and dissociates from BamA (Sidkat, et

al. 2019; Kiessling, et al. 2020). The β-barrel domain remains bound to the Bam complex until all three passenger domains are fully secreted and the resolution of the hairpin structures is completed (Sidkat, et al. 2019; Ryoo, et al. 2020). This model proposition defies the self-transporter aspect of the type Vc secretion system, in which the β-barrel domain catalyzes the secretion of the covalently linked passenger domain, suggesting that the Bam complex plays at least an indirect role in the secretion process (Fan, et al. 2016; Bernstein, 2019; Sidkar, et al. 2019; Kiesslin, et al. 2020).

Apart from SEC machinery and the Bam complex, the involvement of the translocation and assembly module (TAM) in the correct folding of the TAAs have also been suggested (Kiessling, et al. 2020). TAM complex comprises a 60 kDa Omp, called TamA, that possess three domains projected into the periplasm, which interact with a C-terminal domain of TamB, an inner-membrane anchored protein (Heinz, et al. 2015). Due to the lack of ATP in the periplasm and an electrochemical gradient at the outer membrane it is generally assumed that the translocation of the TAA's passenger domains is driven by their ongoing folding. Nevertheless, TAM assistance during the passenger domains secretion could be a possible solution for this energy problem since TAM complex crosses the periplasmic space and might act as a bridge between the inner and the outer membranes of the cell (Kiessling, et al. 2020). Selkrig, et al. (2012) shown that TamA and TamB could form a hetero-oligomer translocation machinery with BamA that can use autotransporters polypeptides as reaction substrates (Selkrig, et al. 2012). This creates a new point on the Bam-complex translocation model, introducing an alternative pathway in which TAM and BAM could act together. Moreover, in the absence of TamA, interactions between TamB and BamA were established in some bacterial species, indicating that the role of TamA in the translocation process could be replaced by BamA (Figure I.5) (Stubenrauch, et al. 2016; Kiessling, et al. 2020).

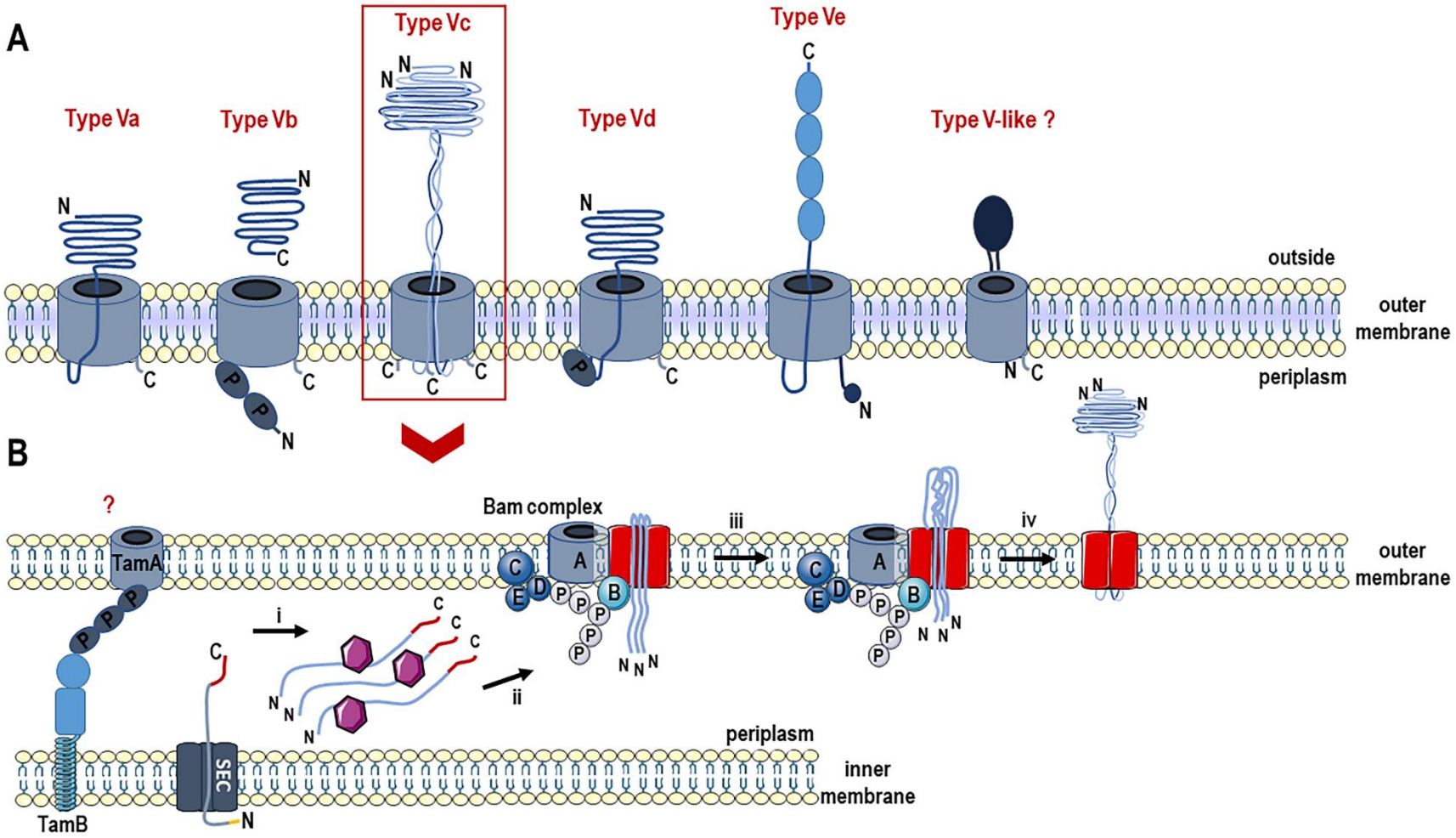
A
Type Va
Type Vb
Type Vc
Type Vd
Type Ve
Type V-like ?
outside
outer membrane
periplasm
B
?
TamA
TamB
Bam complex
i
ii
iii
iv
SEC
periplasm
inner membrane
outer membrane

Figure I.5 - **Topology models of the different type V secretion systems.** (**A**) Proteins in type V (and type V-like) secretion pathways consist of a β barrel anchor domain and an extracellular passenger domain. The β barrel and passenger domains are usually covalently linked, but in the type Vb pathway the β barrel and the extracellular component are separate polypeptides. In the type Vc pathway both domains are formed through the assembly of three identical subunits. The passenger domain is located at the N terminal of the protein in the type Va, Vb, Vc, and Vd pathways, but it is found at the C terminal in the type Ve. In the type V-like pathway the extracellular domain is in a loop that connects the first two β strands of the β barrel domain. POTRA domains are labelled as P. (**B**) Schematic outline of TAAs translocation through inner membrane and outer membrane of Gram-negative bacteria. TamB domains interact with one of the POTRA domains of TamA, forming a bridge between both outer and inner membranes. The role of Tam complex during TAA translocation is still poorly understood. TAAs are transported through the inner membrane into the periplasm as monomers by SEC machinery. In the periplasm, chaperons (purple structures) act to maintain the unfolded state of TAA monomers. The partially folded β barrel domain is then targeted to the outer membrane, where it binds to BamA and BamB. Both autotransporter and BamA β barrels are in an open conformation. Translocation involves the progressive movement of passenger domain segments through the channel. In the end of the translocation process, the passenger hairpin is completed resolved. The β barrel domain is then released from the Bam complex.

I.3.3 Trimeric autotransporter adhesins: distribution in Gram-negative bacteria

TAAs are largely distributed in α-, β-, and γ-proteobacteria that could infect several hosts such as humans or plants (Figure I.6). The sequences of these proteins are also found in bacteriophages and virulence plasmids (Linke, et al. 2006; Szczesny and Lupas, 2008). Nevertheless, in recent years, more distantly related TAAs have begun to be discovered in new bacterial clades such as Verrucomicrobia, Bacteroidetes, Synergistetes, Fusobacteria and Firmicutes (Negativicutes) (Koretke, et al. 2006; Bassler, et al. 2015). Furthermore, TAAs are also found in unicellular Cyanobacteria and in marine metagenome sequences (not assigned phylogenetically yet) (Bassler, et al. 2015). Kim et al. (2006) have shown that the phylogenetic relations of TAAs mimic at some level the phylogeny of the species in which these proteins are represented. In that sense and given their existence in phages genomes, TAA encoding genes may have suffered lateral transference within closely related species (Kim, et al. 2006). In some species, like in *Burkholderia* sp., there can be detected the presence of several TAA paralogues. This occurrence could be consequence of gene duplication events. In the other hand, sequence similarity does not directly imply similar protein sizes. Increases and decreases in consistent residues repeats in passenger domains are mainly responsible for size variations observed in closely homologues or even between paralogues (Mil-Homens and Fialho, 2011; Campos, et al. 2013). This phenomena may be the result of repeat duplication of a genetic element that could be potentiated by environmental adaptation or by an attempt to raise the virulence features (immune escape, e.g.) of this class of adhesins (Riess, et al. 2004; Meng, et al. 2006; Balder, et al. 2010; Atack, et al. 2015).

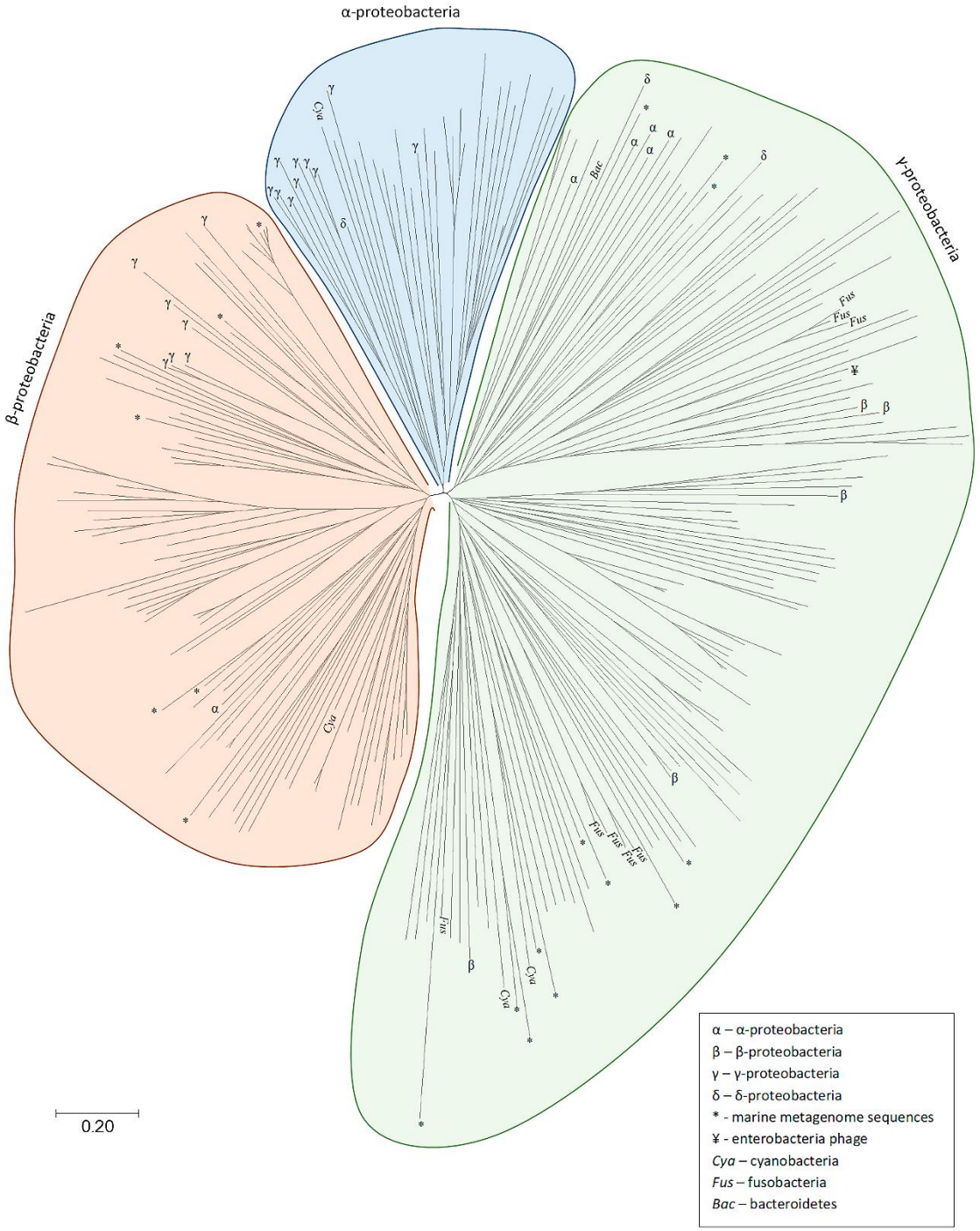

Figure I.6 Phylogenetic tree of TAAs' sequences. A total of 532 TAA protein sequences were obtained from daTAA database (discontinued in 2017) (Szczesny and Lupas, 2008). The tree was based on Muscle multiple alignment and drawn with the MEGA7: Molecular Evolutionary Genetics Analysis software using a neighbor-joining test with bootstraps (500 replicates) (Kumar, et al. 2016).

There are a quite large number of TAAs across a widely representative number of genera. The phylogenetic relation among these exemplars is presented in the phylogenic tree on Figure I.6. It is possible to notice the presence of three major clusters that represent mostly α-, β-, and γ-proteobacteria, respectively. In the majority of the cases, TAAs from the same clades are closely located. Yet, it is noteworthy that some proteins seem to be independent from each other, revealing a possible different origin. TAAs from Fusobacteria appear to be clustered nearby γ-proteobacteria TAA sequences, while representatives of Cyanobacteria TAAs seem to be dispersed among all three major clusters (Figure I.6).

I.3.4 Roles in bacterial virulence

As told above TAAs signature function is their adhesion capacity. As could be expected as an attempt of bacteria to adapt to different environmental conditions, TAAs could not only adhere to biotic structures but also to non-living materials such as glass or plastic (Ishikawa, et al. 2014). In living systems, TAAs could mediate attachment to host cell receptors or interactions between bacteria that lead to autoaggregation or biofilm formation – important features in bacterial virulence (Henderson and Nataro, 2001; Khalil, et al. 2020) (Figure I.7). There are evidences that support the recognition of these proteins as key players in bacterial infection, colonization, invasion, attachment to ECM molecules, host tissues and cellular surface binding and dissemination (Mil-Homens and Fialho, 2012; Keller, et al. 2015; Mühlenkamp, et al. 2017). Also, TAAs potentiate the infectious phenotype of pathogenic Gram-negative bacteria by promoting the escape of host defenses, either by serum-resistance or resisting to phagocytosis (Kirjavainen, et al. 2008; Schindler, et al. 2012). The autoaggregation and biofilm formation promoted by TAAs interaction with themselves create another mechanism of immune system escape (Spahich and St Geme, 2011; Khalil, et al. 2020) (Figure I.7).

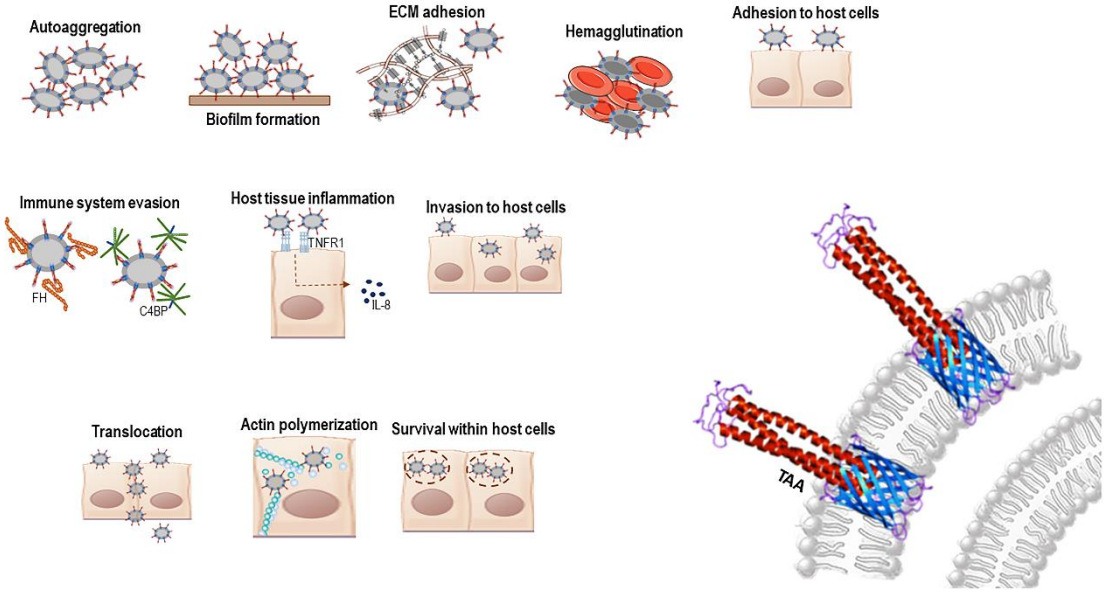

Figure I.7 - **Schematic representation of the virulence functions associated with TAAs.** TAAs can play a wide range of roles in bacterial virulence and bind to a representative set of molecules, such as host cell receptors, components of the ECM or ever other TAAs. They can also interfere with the host cell immune response through the inhibition of some pathways of complement or antibody-related ones.

The passenger domain seems to be the most active structure, mediating the majority of TAA associated functions, specifically with the presence of a network of repetitive head domains and stalks. Nevertheless, in some cases, like DsrA protein of *Haemophilus ducreyi*, translocator domain and the C-terminal passenger domain could be able to act as an effector structure with adhesive properties (Leduc, et al. 2009). The binding activity of TAAs seems to be associated with specific tri-dimensional characteristics as well as with amino acid sequences in this binding structures. In some cases, a simple amino acid alteration could alter the affinity of a binding domain (El Tahir, et al. 2000; Yeo, et al. 2004; Cotter, et al. 2005b; Cotter, et al. 2006). The number of binding domains is not a constant feature of TAAs, different TAAs could have different sets of binding sites that could vary greatly. Hia and Hsf have 2 and 3 binding domains that have distinct affinities (Radin, et al. 2009; Singh, et al. 2014). Whereas other TAAs can have more than 20 binding sites with affinity for the same molecule, like the ECM component, collagen (Daigneault and Lo, 2009). In a more extensive way, the trimeric formula of TAAs seems to be essential for their adherence properties. The disruption or the unbalance between

the three passenger domains causes the unfolding of the extracellular part of the protein and abolish the adhesion functions of TAAs (Cotter, et al. 2006).

It is known that TAAs can adhere to different cellular receptors, depending on the type of host-pathogen interaction. Hia, from the respiratory tract pathogen *H. influenzae*, adheres to respiratory epithelial cells, while YadA of enteropathogenic *Yersinia* species binds to the intestinal mucosa (Singh, et al. 2014; Drechsler-Hake, et al. 2016). Studies about the binding mechanisms of *B. cenocepacia* TAA BcaA to respiratory epithelium reveal that TAA can bind to collagen, recognize specific cellular receptors, and form hydrophobic interaction that could act as a string capable of resisting to high forces. Both connections are made by low binding affinity that might endorse epithelial colonization (El-Kirat-Chatel, et al. 2013). Studies about BcaA show the interaction of this adhesin with TNFR1 that at last causes the overproduction of the proinflammatory cytokine IL-8 which leads to a severe inflammation state. This unnatural state of inflammation adversely affects host cell survival and tissue integrity providing the means for bacterial epithelium translocation and invasion of mucosa profounder regions (Mil-Homens, et al. 2017). Likewise, YadA induces a host proinflammatory state in response to *Y. enterolitica* infection. YadA interaction with β1 integrin triggers IL-8 secretion in epithelial cells that seems to cause the activation of NF-Bκ transcription factor. This process might implicate the involvement of small GTPases and MAP kinases (Schmid, et al. 2004). In *B. pseudomallei*, it was identified a TAA (BimA) capable of binding actin and promote the polymerization of the actin filamentous and consequently the movement of the bacteria within and between host cells (Stevens, et al. 2005; Lazar Adler, et al. 2011). BimA has a passenger domain with a repetitive set of head domains with still unknown function, and two characterized motifs that shown to be elemental for binding and polymerization of actin (Sitthidet, et al. 2011).

Despite adhesion properties, host serum resistance is one of the major transversal functions of TAAs. This ability can be performed by different means, from inhibition of complement pathways to interfere with the membrane attack complex (MAC) (Lambris, et al. 2008). The trimeric stability is essential for these interactions. Some TAAs had developed the ability of binding complement inhibitors such as C4b binding protein (C4BP) or factor H that prevent the activation of inflammatory effector components and

the final complement complex. YadA is capable of directly recruit individual partners of complement cascade, like C3b or iC3b, without the need of additional serum factors. The binding of YadA to these molecules strategically attract large amounts of factor H causing the limitation of terminal complement complex formation and allow the survival of *Y. enterolitica* (Schindler, et al. 2012). The bacterial camouflage with non-immunogenic proteins such as vitronectin is another strategy to evade the host immune system. The vitronectin act as a shield for the TAA immunogenic epitopes contributing to serum resistance (Leduc, et al. 2009; Mil-Homens, et al. 2014). The vitronectin-dependent serum resistance is a proficiency executed by different TAAs, such as Hsf (Hallström, et al. 2006), BcaA (Mil-Homens, et al. 2014) or UspA2 (Attia, et al. 2006). Also, vitronectin has been associated to the negative regulation of MAC formation by inhibit C5b–C7 complex formation and C9 polymerization (Attia, et al. 2006; Hallström, et al. 2006). The presence of trimeric adhesins on the surface of a bacteria improve not only their pathogenic potential with the enhancement of a virulent phenotype but also the defenses of the bacterial cell to the host immune system attack during infection.

The next section will discuss the acquire knowledge of some well-studied TAAs from different bacterial pathogens.

I.3.5 *Yersinia* spp. YadA

YadA has a lollipop-like structure with a TAA typical C-terminal translocator domain, a single N-terminal head domain and a coiled-coil stalk linked by a connector (Linke, et al. 2006). The head domain is connected to the anchor domain by a right-handed supercoil stalk (Koretke, et al. 2006). The structure of YadA anchor domain was solved by solid-state nuclear magnetic resonance (Shahid, et al. 2015).

YadA is an important virulence factor expressed by the enteropathogenic *Yersinia* species *Y. enterolitica* and *Y. pseudotuberculosis* (Koretke, et al. 2006). *Y. enterolitica* can cause a variety of diseases in humans from diarrhea to septicemia, it colonizes the intestinal mucosa, and the expression of YadA is crucial for the development of the infection (El Tahir and Skurnik, 2001). It seems that the dissemination and intestinal

invasion of *Y. enterolitica* occurs via mononuclear phagocytes subsets, which promote pathogen translocation to the mesenteric lymph nodes and spleen (Drechsler-Hake, et al. 2016). YadA is known for its capacity of adhesion to collagen, vitronectin, fibronectin, laminin, host cells receptors mediated by β1-integrin and to other YadA copies, promoting bacterial agglutination. By inhibiting the complement cascade, YadA also confers serum resistance to *Y. enterolitica* (Heise and Dersch, 2006; Kirjavainen, et al. 2008; Biedzka-Sarek, et al. 2008; Schütz, et al. 2010).

YadA coding gene is located on the virulence plasmid pYV which expression is activated by a temperature sensitive regulator (37 °C). The plasmid exists in the pathogenic species of *Yersinia* and encodes, besides YadA, a type three secretion system (T3SS) and effector proteins (Yersinia outer proteins – Yops) (Cornelis, et al. 1989; Köberle, et al. 2009; Mühlenkamp, et al. 2017; Bancerz-Kisiel, et al. 2018). The production of YadA seems to be stimulated by the RNA chaperone Hfq. Hfq-dependent action at a transcriptional, post-transcriptional and post-translational levels seems to be involved in the control of the number of YadA copies present on the surface of the bacteria in different environments (Kakoschke, et al. 2016; Bancerz-Kisiel, et al. 2018; Leibiger, et al. 2019). Recently, OmpR was identified as a new *yadA* regulator, being responsible for repricing its expression in specific environments (Nieckarz, et al. 2016).

The YadA-fibronectin-β1 integrin bound on the surface of epithelial cells is a crucial step for *Yersinia* Yops entrance into the cells through T3SS (Heise and Dersch, 2006; Keller, at al. 2015). YadA can indirectly bind to a wide set of host cell receptors. Besides β1-integrins, YadA can interact with αV-integrins to induce Yops injection. The presence of β1-integrin on fibroblasts membrane is essential to trigger the injection of Yops but the presence of αV-integrins could also be required as a synergic partner (Leo and Skurnik, 2011; Keller, et al. 2015). New results have been achieved in order to fully understand the requirements for Yops injection and the interference of YadA, cellular receptors and ECM molecules. It was found that besides fibroblasts and epithelial cells, *Y. enterolitica* target cells from the immune system for Yops injection (Köberle, et al. 2009; Deuschle, et al. 2015; Drechsler-Hake, et al. 2016). The data demonstrated that YadA is essential for Yop injection into leukocytes. The injection of Yops into leukocytes is crucial for *Yersinia* immune resistance since their action inside the host cell cause alterations of

signal transduction processes affecting the host immune responses (Trülzsch, et al. 2007; Köberle, et al. 2009).

Moreover, YadA expression on *Yersinia* surface modulates the immune system complement cascade contributing for bacterial serum resistance. The lytic terminal complement complex is blocked by the binding of serum complement factor H and C4BP to YadA. The factor H and C4BP form a shield around the outer membrane and prevent the deposition of C3b opsonin and C9 complement factor, inhibiting the formation of membrane attack complexes and the killing of the bacteria (Kirjavainen, et al. 2008; Biedzka-Sarek, et al. 2008; Leibiger, et al. 2019). C4BP is the major negative regulator of the classical and the lectin pathways of the complement. C4BP-YadA binding prevents C4b-medited opsonization and also leads to a reduction of C3b accumulation on the bacterial surface (Blom, 2002; Kirjavainen, et al. 2008). Furthermore, YadA seems to mediate immune invasion by binding vitronectin that acts as a negative regulator of terminal complement complex by inhibiting the lytic pore formation (Mühlenkamp, et al. 2017). The N-terminal region of YadA is also responsible for enhancing red blood cells hemagglutination, autoagglutination and biofilm formation. Bacterial autoagglutination and formation of dense microcolonies mediated by YadA expression could contribute to a phagocytosis resistance phenotype (El Tahir and Skurnik, 2001; Heise and Dersch, 2006; Freund, et al. 2008).

I.3.6 Hia and Hsf from *Haemiphilus influenzae*

Haemophilus influenzae has two homologous TAAs –Hia (*Haemophilus influenzae* adhesin) and Hsf (*Haemophilus* surface fibril). Hsf is found among all typeable strains, while Hia is present only in non-encapsulated strains of *H. influenzae* (St Geme and Cutter, 2000; Cotter, et al. 2005b; Watson, et al. 2013; Osman, et al. 2018). Hia and Hsf proteins share 81% of similarity and 72% of identity (Meng, et al. 2008). Both TAAs have analogous architecture with the highest homology in N- and C-terminal ends. The main difference between Hsf and Hia is the dimension of the passenger domain. With a set of extra head domains and neck structures, Hsf is typical extended in comparison to Hia

(Cotter, et al. 2005b; Meng, et al. 2008). Hsf has a unique structure among TAAs, its oddly long passenger domain is not a straight fiber-like structure but rather a folded and twisted protein (Singh, et al. 2015). As Hsf is expressed in capsulated strains of *H. influenzae*, the extra length of Hsf passenger domain is a necessity that allows the protein to extend itself past the polysaccharide capsule (Cotter, et al. 2005b).

Hia and Hsf passenger domains possess two binding domains (BD) with an acidic pocket required for adherence to epithelial cells. Given trimerization, each BD contains three potential sites for interaction with host receptors, allowing the interaction with different parts of the receptor or even with independent receptor molecules (Yeo, et al. 2004; Cotter, et al. 2005b; Cotter, et al. 2006; Radin, et al. 2009). BD1 and 2 are in opposite parts of the passenger domains and both contribute to *H. influenzae* adhesion to the surface of epithelial cells. It is likely that both BDs might participate in a bivalent interaction, increasing avidity and stabilizing bacterial adherence to host cells. A stable binding between pathogen and host cell may be especially important in the upper respiratory tract, where bacteria are vulnerable to clearance by mucociliary action (Laarmann, et al. 2002; Osman, et al. 2018; Atack, et al. 2020). BD1 is located closer to the C-terminal domain of Hia and Hsf and has proven to have a stronger affinity towards host cell receptors than BD2 (Laarmann, et al. 2002). Different affinities are a reflection of alterations in amino acid configurations in the acidic pockets, the variation of an aspartic acid in BD1 to a glutamine in BD2 diminish the affinity of the last one (Yeo, et al. 2004). In Hsf the sequence between HsfBD1 and HsfBD2 is three times longer than the sequence between HiaBD1 and HiaBD2 which may permit the interaction of HsfBD2 with cellular host receptors (Cotter, et al. 2005b). The passenger domain of Hsf still includes a third BD region – HsfBD3. This binding domain seems to not influence the bacterial adhesion to epithelial cells once it does not contain the common BD acidic pocket. The presence of HsfBD3 between HsfBD1 and HsfBD2 could be required to allow Hsf stabilization or to mediate adhesion (Cotter, et al. 2005b). The proposed mode of action of Hia and Hsf BD1 and BD2 towards host cell molecules comprises two sequential steps. The initial interaction is played by BD2, which is located at the N-terminal extremity of the passenger domain and is responsible for the approximation of the bacterial to the host cell. BD2 is then replaced by BD1, given its higher affinity towards

host cell ligands. The switch between BDs causes conformal alterations that bring the bacteria closer to the host cell, enhancing the attachment to the epithelial cell layer (Radin, et al. 2009; Spahich and St. Geme, 2011). Recently, Atack et al. (2020) demonstrated that Hia is a lectin with high specificity for host glycans. Through BD1, Hia mediates high affinity interaction between *H. influenzae* and sialic acid structures (Neu5Ac-α2,6-lactosamine) present on the membranes of human cells (Atack, et al. 2020). Moreover, detailed results revealed that HiaBD1 and BD2 can interact with distinct ligands on the surface of host cells (Atack, et al. 2020).

Several studies have disclosed the interaction between Hsf and the ECM component vitronectin mediated by both BD1 and BD2 (Hallström, et al. 2006; Singh, et al. 2014). It was proposed that vitronectin interaction act as an input to *H. influenzae* adhesion and internalization into host cells. Evidence seem to support an adapted adhesion mechanism by which BD2 binds to vitronectin as a connection between the epithelial integrins and the pathogen. The BD1 may act as a second vitronectin binding site or bind directly with a cellular receptor instead (Hallström, et al. 2006; Singh, et al. 2014). Moreover, vitronectin is also a key player in different processes of host immune responses. It is the major regulator of the complement membrane attack complex (MAC) which is formed on the surface of the pathogen and causes the disruption of the cell membrane, it is also an inhibitor of the terminal lytic pathway of the complement system (Singh, et al. 2011; Riesbeck, 2020). Singh et al (2014) demonstrated that Hsf bound to vitronectin protects *H. influenzae* from serum-mediated host immune responses, preventing the formation of MAC (Singh, et al. 2014; Riesbeck, 2020)

I.3.7 *Burkholderia* spp. trimeric autotransporter adhesins

I.3.7.1 *Burkholderia pseudomallei*: the diverse roles of trimeric autotransporter adhesins

B. pseudomallei is found in water and soils worldwide and is the causative agent of melioidosis, a febrile illness with acute and chronic disease states that could affect several organs with a mortality rate of up to 40% (Inglis and Sagripanti, 2006; Wiersinga

et al. 2012). Some *B. pseudomallei* strains can express a considerable number of TAA coding genes – *B. pseudomallei* K96243 and 1026b contain genes for nine putative trimeric adhesins (Lazar Adler et al. 2011; Campos, et al. 2013). The number of TAAs expressed on a particular strain seems to be directly related with its virulent potential. (Lazar Adler, et al. 2015). *B. pseudomallei* adhere and invade epithelial cells, macrophage-like cells and can survive and proliferate for prolonged periods within phagocytic cells (Kespichayawattana, et al. 2004; Wiersinga et al. 2006; Muangsombut, et al. 2008). Once inside the host, *B. pseudomallei* can induce actin polymerization by the action of the TAA BimA located at one pole of the bacteria. The control of host actin allows the propulsion of the bacteria inside the cell and can induce bacterial spread across the infected tissue through the fusion of adjacent host cell membranes. The survival inside the host can also be used by *B. pseudomallei* as a mechanism of innate and humoral immune system escape (Stevens, et al. 2005; Galyov, et al. 2010; Yip, et al. 2020). BimA has a similar YadA C-terminal and a set of head domains with a similar sequence and structure to those found in actin modulating proteins (Stevens, et al. 2005; Galyov, et al. 2010). The existence of a 13 residues repeat on the passenger domain of BimA seems to be essential for the recruitment of bacterial or cellular factors and for the intracellular dissemination but not for actin polymerization (Sitthidet, et al. 2011). The action of BimA inside the host cell cause the formation of elongations of the cellular membrane that allow the spread of *B. pseudomallei* from cell-to-cell while evading immune defenses (Stevens, et al. 2005). The cellular ubiquitous scaffold protein Ras GTPase-activating-like protein acts as a functional player regulating the organization and length of the actin filamentous formed by BimA (Jitprasutwit, et al. 2016). The high immunogenicity of BimA raise attention for its use as a diagnostic tool (Suwannasaen, et al. 2011; Lazar Adler, et al. 2011).

Alongside BimA there are several characterized TAAs that play a role in *B. pseudomallei* virulence. Some of the most studied include: BoaA, BoaB that act as adhesins and can mediate replication inside macrophage-like cells; BpaC that contributes to serum resistance and BbfA required for biofilm formation and overall bacteria virulence (Balder, et al. 2010; Lazar Adler, et al. 2013; Lazar Adler, et al. 2015; Schnetterle, et al. 2017; Yip, et al. 2020).

The mode of action of BpaC is still unknown but could be due to interactions with different complement pathways such as the classical or lectin pathways. Besides serum survival, BpaC was also associated with intracellular bacteria survival in phagocytic cells (Lazar Adler, et al. 2015). BoaA and BoaB are very much similar (63.1% identical in 1026b strain), they share the same C-terminal domain and numerous serine-rich SLST regions across the passenger domain. The SLST short motifs are frequently a portion of larger repeats formed by ~10 to 20 residues that occupy a large part of the BoaA and BoaB passenger domains. These repetitions do not have any specific secondary structure or defined function and are not usual in other species outside *Burkholderia* genus (Balder, et al. 2010; Campos, et al. 2013). The number of these repetitions across the passenger domain is directly related to the size variation of the protein. The addition or loss of these sequences can be used as a mechanism to regulate the length of the passenger domain. Also, the high serine content could be related with glycosylation potential of BoaA and BoaB (Campos, et al. 2013; Chaze, et al. 2014). Considering the functional and sequence similarities between both proteins, Balder et al. (2010) speculate that the expression of BoaA and BoaB could be a result of gene duplication, since their coding genes are present in chromosome 1 and 2, respectively, and *boaB* is preceded by an invertase and a transposase. The elimination of *boaA* and *boaB* significantly decrease the ability of *B. pseudomallei* mutants to grow inside murine macrophages, although the mechanism involved is not known yet (Balder, et al. 2010). The biofilm formation capacity revealed by *B. pseudomallei* seems to be related with the expression BbfA. Lazar Adler et al. (2013) shown results that this TAA influences the initial adhesion of *B. pseudomallei* to abiotic surfaces, microcolony formation, and biofilm maturation (Lazar Adler, et al. 2013). The ability of *B. pseudomallei* to form biofilms is important for bacterial persistence in the environment and inside the host, which might enhance its infectious potential (Nandi, et al. 2010).

I.3.7.2 *Burkholderia cenocepacia*: multifunctional trimeric autotransporter adhesins

The epidemic strain *B. cenocepacia* J2315 contains seven TAA encoding genes distributed across the chromosomes 2 and 3. BcaA (BCAM0224) was considered as a multifunctional virulence factor (Mil-Homens and Fialho, 2011). It is composed of 953

amino acids and contains a YadA-like C-terminal domain, an extended N-terminal signal sequence and a passenger domain that includes several domains: Hep_Hag, HIM, collagen-binding domains and tandem repeats (Mil-Homens, et al. 2010). Its encoding gene is founded exclusively in ET-12 *B. cenocepacia* strains (Mil-Homens, et al. 2010). Alongside with other two TAA encoding genes (*bcaB* and *bcaC*), *bcaA* is located in a cluster with a two-component system, which may regulate their expression in particular conditions and modulate the virulence-associated features of *B. cenocepacia* (Mil-Homens, et al. 2010). Mil-Homens et al. (2010) observed that the expression of *bcaA* is enhanced under conditions that tend to mimic the environment in CF lungs such as high osmolarity, oxygen limited conditions, and oxidative stress (Bhatt and Weingart, 2008; Mil-Homens, et al. 2010). Using *Galleria mellonella* larvae as infection model, Mil-Homens et al. (2010) shown evidences that the elimination of *bcaA* causes a significant reduction in virulence, in comparison to *B. cenocepacia* wild-type strain (Mil-Homens, et al. 2010). BcaA has been associated with a set of virulence-related functions like biofilm formation, motility, evasion of host immune system, bacterial adhesion and invasion of epithelial cells, binding to ECM components such as vitronectin and collagen type I, and binding to cellular receptor TNFR1 (Mil-Homens, et al. 2010; El-Kirat-Chatel, et al. 2013; Mil-Homens, et al. 2014; Mil-Homens, et al. 2017).

Single-molecule atomic force microscopy studies unraveled the binding mechanisms of BcaA and demonstrated its binding properties - large binding strength, low affinity, multi-specificity, and spring elasticity. This multifunctional adhesin undertake both homophilic and heterophilic low affinity interactions with a range of different targets (El-Kirat-Chatel, et al. 2013). BcaA can also recognize specific receptors on pneumocytes membrane that might promote *B. cenocepacia* adhesion to host cells. BcaA-collagen heterophilic and BcaA-BcaA homophilic bounds seem to be a result of low affinity interactions that might allow epithelium colonization and *B. cenocepacia* autoaggregation, respectively (El-Kirat-Chatel, et al. 2013). Mutation of *bcaA* leads to the impairment of swarming motility that seems to contribute for the abolishment of biofilm formation (Mil-Homens, et al. 2014). Since flagella motility is essential for the first step of biofilm formation both characteristics can be conjugated and so, BcaA may

be an important asset for different stages of biofilm formation and maintenance (Verstraeten, et al. 2008; Mil-Homens, et al. 2014).

The capacity of *B. cenocepacia* to escape host immune system seems to involve BcaA as well. The mechanisms by which BcaA mediates immune resistance is still poorly understood, but Mil-Homens et al. (2014) shown evidences that BcaA mutant was serum sensitive and that classical complement pathway is the main killing mechanism involved. BcaA could use its vitronectin binding capacity in order to inhibit complement-related attack or to form a shield on *B. cenocepacia* surface with non-immunogenic molecules (Mil-Homens, et al. 2014). This protection may camouflage the highly immunogenic trimeric adhesins and keep them away from the immune system recognition and targeting (Mil-Homens, et al. 2014). Mil-Homens et al. (2017) revealed the first evidence that a TAA could induce a proinflamatory response in pulmonary epithelial cells through TNFR1 binding. TNFR1, a receptor for tumor necrosis factor-α (TNF-α), widely distributed on the respiratory epithelium is also the receptor for BcaA high-affinity interaction with bronchial epithelial cells (Baud and Karin, 2001; Mil-Homens, et al. 2017). In a normal process of infection, TNF-α is produced when the presence of a bacterial pathogen is sensed by the binding to TNFR1 on cellular membrane. This interaction leads to a signaling response that ultimately leads to an inflammatory response and IL-8 cytokine production and release (Baud and Karin, 2001). Exacerbated IL-8 production caused by *B. cenocepacia* infection could compromises tissue integrity and be a new pathway for pathogen penetration and survival inside host tissues (Kaza, et al. 2011; Ganesan and Sajjan, 2012; Mil-Homens, et al. 2017).

BcaB (BCAM0223) encoding gene is found immediately downstream of *bcaA*, located in the *B. cenocepacia* TAA cluster. *bcaB* encodes for a TAA with 1500 residues that contains an anchor domain with homology to the C-terminal translocator domain of YadA and eight noncontiguous coiled-coil clusters of HIM motif repeats and five clusters of Hep-Hag motif repeats. HIM and Hep-Hag are short repeat motifs commonly found in bacterial hemagglutinins and invasins (Mil-Homens and Fialho, 2012). The disruption of *bcaB* in *B. cenocepacia* caused a significant decrease in hemagglutination, adhesion to cells, and bacterial virulence. Moreover, like BcaA, BcaB is also involved in the process

of *B. cenocepacia* adherence to vitronectin and serum resistance (Mil-Homens, et al. 2013).

I.3.8 Trimeric autotransporter adhesins for biomedical applications

The highly immunogenic repetitive organization of TAAs make these proteins a useful tool in immune protection and a potential vaccine candidate (Thibau, et al. 2020). Several studies have pointed out that neutralization of TAA-host cell interaction can attenuate the course of infection. Therefore, the use of TAAs as vaccine ingredients could be an important strategy to impair infection evolution, since they show to be immunogenic antigens both in model animals and natural hosts (Cutter, et al. 2002; Comanducci, et al. 2002; Weynants, et al. 2007; Durant, et al. 2007; Fusco, et al. 2014). The use of TAAs as a component of a vaccine was achieved with the application of NadA from *Neisseria meningitides*, in a multifactorial vaccine approved by European Medicines Agency (Malito, et al. 2014). Components of the vaccine target the interaction of the TAA NadA with its ligand, the human receptor LOX-1 (Liguori, et al. 2018). Also, a vaccine produced with UspA2 TAA from *Moraxella catarrhalis*, proved to successfully protect patients with chronic obstructive pulmonary against non-typeable *M. catarrhalis* (Van Damme, et al. 2019). Considering the biogenesis mechanism of autotransporter proteins, the TAA secretion system can also be used as an autodisplay in vaccine design (Jose, 2006; Jong, et al. 2014). Type Vc secretion system can be an important tool for construction of recombinant multimeric vaccines. This mechanism can promote the formation and exposure of trimeric forms of antigens becoming a form of increase vaccine immunogenicity since multimeric forms of proteins have stronger immunogenicity than monomeric ones (Jose 2006; Baker, et al. 2010). Moreover, the differential expression of TAA genes during infection could turn their detection into a disease-associated molecular biomarker method for diagnosis (Mil-Homens and Fialho, 2011; Fagnocchi, et al. 2013). Likewise, the structural conservation of trimeric autotransporter domains make TAAs of particular interest to be used as target for an anti-adhesion therapy. By preventing bacteria adhesion to the cells of an infected host,

anti-adhesion treatments make pathogens more susceptible to physical clearance (Kiessling, et al. 2020).

I.3.9 Conclusion and future perspectives

TAAs can be considered the “Swiss-army knife” of pathogenic Gram-negative bacteria as they can promote an expanded set of virulence-related functions, from adhesion to actin polymerization or escape to host immune system. The highly immunogenic profile of TAAs makes them useful in immune protection and as potential vaccine candidates apart of the potential value as disease biomarker on diagnostic (Qin, et al. 2015).

In past years there were achieved several milestones in TAAs investigation. New studies about their biogenesis and secretion mechanisms, functional and structural features revealed new functions and mechanisms in the infection process which helped to position TAAs as important tools of pathogenicity and potential targets to subvert bacterial infections. Nevertheless, knowledge about the regulation mechanisms involved in the expression of these proteins is still poorly established. In the future it will be important to understand the means by which TAA encoding genes are regulated in response to specific environments and how it may control the virulence of the pathogenic bacteria inside the host. Furthermore, a more profound understanding of the details of TAA secretion as well as the host molecules that can promote bacterial adhesion is necessary.

I.4. Thesis aims and outline

The ability of *B. cenocepacia* to cause disease and persist inside the host remains one of the most problematic threats for CF patients. This pathogen is well-known for its large set of virulence factors capable to promote an aggressive infection that, in many cases, leads to a patient's death. The close interconnection between *B. cenocepacia* and the host has also been well documented and seems to be essential for bacterial adaptation during host colonization.

This thesis will be focused on the first steps of *B. cenocepacia*-host cell interaction, with a special emphasis on a specific class of *B. cenocepacia* virulence factors – TAAs. The mechanism of bacterial adhesion is the culmination of a set of cause-effect interactions that require both host cell and bacterium. Some of these processes involve the recognition and binding of bacterial receptors to host ligands and the consequent adaptation to such contacts.

TAAs have been classified as multifunctional proteins that could take action in the early stages of Bcc infection. *B. cenocepacia* J2315 genome encodes seven different TAAs and some of them have been previously described and characterized (Mil-Homens and Fialho, 2011; Mil-Homens and Fialho, 2012; Mil-Homens, et al. 2014). This work aimed to achieve an in-depth knowledge of two new *B. cenocepacia* J2315 TAAs, regarding their main functions, mechanisms of regulation and host-cell interaction during the early stages of infection. Moreover, the identification of host-cell ligands for *B. cenocepacia* attachment and the bacterial transcriptional shift in response to such physical interactions were also major goals of this work. Therefore, specific aims were pursued in the past four years in order to accomplish the overall purpose of this thesis. The work developed so far will be presented and organized in six main chapters:

Chapter I is a detailed literature overview concerning Bcc diversity and clinical importance; and *B. cenocepacia* interaction with the host, detailing the mechanisms involved in adherence, survival inside the host and adaptation. The state of art of TAAs and their biological traits is also perused.

Chapter II covers the phenotypic characterization of TAA-defective *bcaC* mutant of *B. cenocepacia*. Also, the relation between the histidine kinase BCAM0218 and a putative regulatory network targeting the expression of bcaC is approached.

Chapter III comprises the study of the transcription of TAA encoding genes during *B. cenocepacia*-host cell contact. In particular, the patterns of *BCAM2418* TAA gene expression are detailed reported and extracellular components of host membrane are assessed as possible signals for the differential expression of the TAA gene *BCAM2418*.

Chapter IV addresses the inhibitory effects of an antibody produced against the *B. cenocepacia* TAA BCAM2418. The anti-BCAM2418 antibody inhibits bacterial adhesion, confers protection to infection and enables identification of host glycans as adhesin targets.

Chapter V describes the profile of *B. cenocepacia* gene expression during the early contacts with the surface of the host-cell. Giant plasma membrane vesicles were produced from bronchial epithelial cells and used as a *stimulus* to assess the transcriptomic shift of *B. cenocepacia* after host membrane sensing, the obtained results are presented in detail in this chapter.

Chapter VI provides a unified discussion of all the results presented in this work, with a special highlight on the improvement that these outcomes may bring to the actual scientific state of art.

Finally, a complete list of publications and communications is provided.

II. PHENOTYPIC CHARACTERIZATION OF TRIMERIC AUTOTRANSPORTER ADHESIN-DEFECTIVE *bcaC* MUTANT OF *BURKHOLDERIA CENOCEPACIA*: CROSS-TALK TOWARDS THE HISTIDINE KINASE BCAM0218

Journal paper

Pimenta AI, Mil-Homens D, Pinto SN, Fialho AM. Phenotypic characterization of trimeric autotransporter adhesin-defective *bcaC* mutant of *Burkholderia cenocepacia*: cross-talk towards the histidine kinase BCAM0218. *Microbes Infect*. 2020; S1286-4579(20)30096-4. doi:10.1016/j.micinf.2020.05.018

II.1 Abstract

Burkholderia cenocepacia is a virulent species belonging to the *Burkholderia cepacia* complex (Bcc) and one of the most problematic agents of chronic lung infection in cystic fibrosis patients. *B. cenocepacia* possesses a large panel of virulence traits that include trimeric autotransporter adhesins (TAAs). Such proteins are obligate homotrimers anchored in the outer membrane. They are players in the adhesion events that occur between bacteria and biotic/abiotic surfaces. In this study, we constructed two insertional-mutants for TAA *bcaC* and histidine kinase (HK) *BCAM0218* genes, which are clustered together within the *B. cenocepacia* K56-2 TAA cluster. The *bcaC*-mutant affected *B. cenocepacia* adhesion to extracellular matrix proteins and red blood cells hemagglutination. BcaC contributed to enhancing *B. cenocepacia* K56-2 adhesion to bronchial epithelial cells. The expression of *bcaC* affected biofilm formation negatively. Due to a *BCAM0218* disruption, the *bcaC* expression increased significantly, indicating that they are functionally linked. The overexpression of *bcaC* in the *BCAM0218*-mutant background rescued at least part of the BcaC functions. Altogether, these findings revealed the multifunctionality of BcaC as a novel *B. cenocepacia* K56-2 virulence factor and postulated the involvement of a sensor HK (BCAM0218) in the control of this TAA gene.

II.2 Introduction

Burkholderia cepacia complex (Bcc) bacteria are respiratory pathogens in cystic fibrosis (CF) and immunocompromised patients. They utilize a panel of virulence factors that cause chronic inflammation and disease. Complications of such acute respiratory infections are severe and can result in permanent and fatal damage to the lungs' airways. Among the twenty-two species of Bcc known to cause disease in CF patients, *Burkholderia cenocepacia* is one of the most virulent (Mahenthiralingam, et al. 2005; Depoorter, et al. 2016). *B. cenocepacia* is naturally resistant to several classes of antibiotics and possesses a broad set of virulence features that contribute to its

enhanced pathogenicity (Drevinek and Mahenthiralingam, 2010; Rhodes and Schweizer, 2017). *B. cenocepacia* can also adapt to different environments by using a broad set of regulatory mechanisms (Cullen and Mcclean, 2015).

One of the virulence factors found in Bcc bacteria belongs to the class of trimeric autotransporter adhesins (TAAs) (Mil-Homens and Fialho, 2011). These proteins are members of the Type V secretion system (T5SS; subtype Vc) and have been emerging as important virulence factors in Gram-negative bacteria (Cotter, et al. 2005; Koretke, et al. 2006; Rahbar, et al. 2019). TAAs are obligate homotrimeric proteins anchored in the outer membrane of bacterial cells. The C-terminal anchor domain, conserved among TAAs, is composed of a trimeric β-barrel that allows the extrusion of the passenger domain via a type V protein secretion pathway. The N-terminal extracellular passenger domain is composed of the neck, stalk, and head regions that could vary in number, organization, and complexity among TAAs (Cotter, et al. 2005; Bassler, et al. 2015). Besides mediating host cell adhesion, they proved to be involved in many other virulence traits, such as biofilm formation, serum resistance, hemagglutination and invasion of host cells (Zhang, et al. 2004; Lazar Adler, et al. 2013; El-Kirat-Chatel , et al. 2013; Mil-Homens, et al. 2017).

The genome of *B. cenocepacia* J2315 contains seven TAA encoding genes distributed across the chromosome 2 (*bcaA*, *bcaB*, *bcaC*, *BCAM1115* and *BCAM2418*) and 3 (*BCAS0236* and *BCAS0335*) (Mil-Homens and Fialho, 2011; Mil-Homens and Fialho, 2012; Mil-Homens, et al. 2014). Among those, three form part of a gene cluster (TAA cluster) consisting of eleven genes encoding two hypothetical proteins (*BCAM0216* and *BCAM0217*), two hybrid histidine kinases (HK) (*BCAM0218* and *BCAM0227*), three response regulators (RR) (*BCAM0221*, *BCAM0222*, and *BCAM0228*), one outer membrane protein (*BCAM0220*) and three TAAs (*bcaA*, *bcaB* and *bcaC*) (Figure II.1A) (Mil-Homens and Fialho, 2012). TAA encoding genes *bcaA* and *bcaB* have been characterized in detail, and their relevance in the virulence of *B. cenocepacia* disclosed (Mil-Homens and Fialho, 2012; Lazar Adler, et al. 2013; El-Kirat-Chatel, et al. 2013; Mil-Homens, et al. 2014). However, a deeper understanding of the structure/function of the adjacent subset of HKs and RRs is needed. McCarthy et al. (2010) demonstrated that the HK BCAM0227 and its cognate RR BCAM0228 are part of a two-component system (TCS)

that enables *B. cenocepacia* to sense *cis*-2-dodecenoic acid (BDSF), a quorum-sensing signal molecule involved in the expression of virulence factors, other than the ones existing in the TAA cluster (Mccarthy, et al. 2010).

Besides the two TCSs found at the TAA cluster, the genome of *B. cenocepacia* J2315 encodes at least 26 other TCSs (Winsor, et al. 2008; Schaefers, 2020). A typical TCS is composed by a HK and a RR. The external stimuli are sensed by the HK, which in turn phosphorylate the regulatory domain of the RR, changing its DNA binding affinity (Stock, et al. 2000; West and Stock, 2001). In past years efforts have been made to characterize new TCSs and their importance in Bcc bacteria physiology and pathogenesis (Aubert, et al. 2008; Merry, et al. 2015). Oxygen- and quorum-sensing systems are some of the most studied TCSs in Bcc species. Though their precise functional network is still not entirely understood, Bcc TCSs are proven to be linked to regulation of bacterial pathogenic fitness like biofilm formation, motility, adherence, and virulence in different models (Merry, et al. 2015; Aubert, et al. 2008; Schaefers, et al. 2017; Cui, et al. 2018; Schaefers, 2020).

In the present study, we aimed to disclosure the role of *bcaC* TAA (previously named *BCAM0219*) in *B. cenocepacia* K56-2 virulence. For that, we constructed a *bcaC*-insertional mutant in *B. cenocepacia* K56-2 and evaluated various virulence-related traits. Our findings indicated that *bcaC* encodes for a large multifunctional TAA that had hemagglutination activity and simultaneously was required for bacteria-extracellular matrix (ECM) adhesion and maximal host cell adherence. Also, we characterized the role of the neighbor *BCAM0218* HK encoding gene, suggesting that it was a critical player that negatively controls the expression of the *bcaC* TAA gene. Taken together, the findings of this work represented a step forward for a better characterization of the subset of *B. cenocepacia* TAA encoding genes.

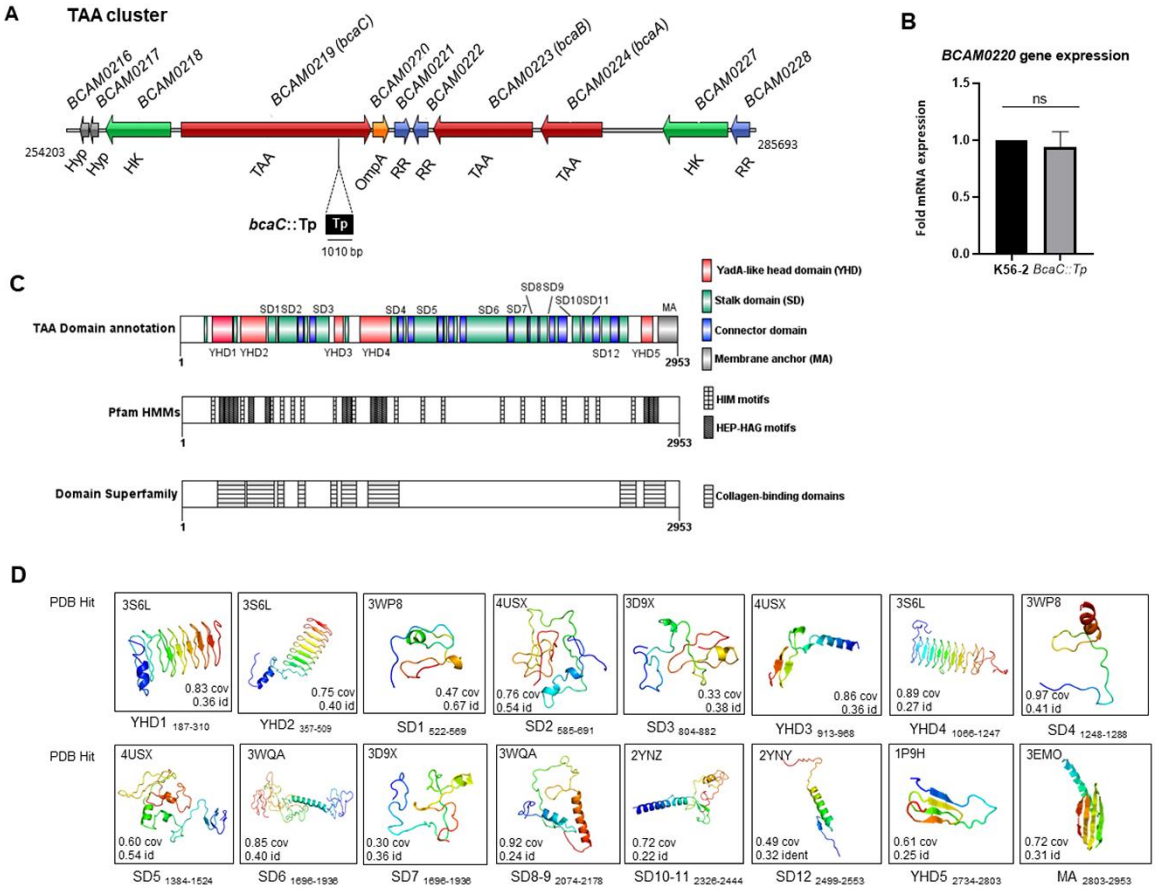

Figure II.1. **Bioinformatic analysis of BcaC and impact of *bcaC* inactivation on the expression of the neighboring gene *BCAM0220*. (A)** Organization of the *B. cenocepacia* K56-2 region surrounding the *bcaC* gene, previously denominated TAA cluster. The region includes eleven genes encoding two hypothetical proteins (Hyp) (*BCAM0216*, *BCAM0217*), two hybrid histidine kinases (HK) (*BCAM0218* and *BCAM0227*), three response regulators (RR) (*BCAM0221*, *BCAM0222*, and *BCAM0228*), one outer membrane protein (OmpA) (*BCAM0220*) and the three TAAs (*bcaA*, *bcaB*, and *bcaC*). The *B. cenocepacia* K56-2 *bcaC* mutant was obtained by insertional mutagenesis of a trimethoprim resistance cassette, as indicated in the figure. **(B)** Expression of *BCAM0220* gene determined in wild-type and *bcaC*-negative mutant backgrounds. Transcription levels of *B. cenocepacia* K56-2 *BCAM0220* were obtained by qRT-PCR. Results were normalized to the expression of the housekeeping *sigA* gene. Expression levels are represented as relative values in comparison to the expression levels in standard LB growth. All the results are from three independent experiments; bars indicate SD. **(C)** Schematic illustration of the domain organization of BcaC protein from *B. cenocepacia* K56-2 using daTAA program (http://toolkit.tuebingen.mpg.de/dataa) (Szczesny and Lupas, 2008). The protein comprises the typical membrane-anchor domain of TAAs at the C-terminal, several YadA-like head domains and stalk and connector domains. **(D)** Predicted structure of the BcaC TAA - The 3D structure of each BcaC predicted domain was modeled using Phyre2 web portal (http://www.sbg.bio.ic.ac.uk/phyre2) (Kelley, et al. 2015). Using the Pfam database (http://pfam.sanger.ac.uk/), numerous Hep-Hag repeats, and hemagglutinin domains (HIM) were found. The structural features of the YadA collagen-binding domain superfamily were identified as well using InterPro online tool (https://www.ebi.ac.uk/interpro/).

II.3 Material and Methods

II.3.1 Bacterial strains and growth conditions

B. cenocepacia clinical isolate K56-2 (clonally related to *B. cenocepacia* J2315 strain) was used. Bacteria were cultured in Luria-Bertani (LB) broth at 37 °C with orbital agitation at 250 rpm. When appropriate, the medium was supplemented with 150 mg/L of ampicillin, 100 mg/mL of chloramphenicol (for *E. coli*), 150 mg/L of trimethoprim, 600 mg/mL of kanamycin (for *B. cenocepacia* K56- 2 mutants), or 100 mg/L chloramphenicol (for the *B. cenocepacia* mutant complementation). For functional studies, the parental and mutant *B. cenocepacia* strains were grown in 24-well plates, at 37 °C with orbital agitation at 70 rpm, for 17 h under conditions of limited oxygen supply in LB broth supplemented with 300 mM NaCl and 10 mM H_2O_2. The limited oxygen supply was achieved by growing cultures in incubation jars containing an atmosphere generator for microaerophilic conditions.

II.3.2 Cell lines and cell culture

Two human bronchial epithelial cell lines were used: 16HBE14o- cells (healthy bronchial cells) and CFBE41o- cells (CF airway) (Cozens, et al. 1994; Bruscia, et al. 2002). Cells were maintained in fibronectin-collagen coated flasks in minimum essential medium with Earle's salt (MEM) supplemented with 10% fetal bovine serum, 0.292 g/L L-glutamine, and penicillin-streptomycin (100 U/mL) in a humidified atmosphere at 37 °C with 5% CO_2.

II.3.3 Bioinformatic analysis of BcaC and BCAM0218

BcaC and BCAM0218 protein and DNA sequences were taken from *Burkholderia* genome online database - www.burkholderia.com (Winsor, et al. 2008). The study of the modular organization of the specific domains of BcaC was performed through the online database Domain annotation of trimeric autotransporter adhesins (daTAA) (http://toolkit.tuebingen.mpg.de/dataa/browse) (Szczesny and Lupas, 2008). The 3D

structure of each BcaC predicted domain was modeled using Phyre2 web portal (http://www.sbg.bio.ic.ac.uk/phyre2) (Kelley, et al. 2015), specific motifs were searched using Pfam database (http://pfam.sanger.ac.uk/) and InterPro online tool (https://www.ebi.ac.uk/interpro/). BCAM0218 domains were analyzed using SMART algorithm (Letunic and Bork, 2018), and the transmembrane helices were predicted using TMHMM server v.2.0 (http://www.cbs.dtu.dk/services/TMHMM/). Specific active residues were scanned using Motif Scan (https://myhits.isbsib.ch/cgi-bin/motif_scan) and ScanProsite tool (https://prosite.expasy.org/scanprosite/) (de Castro, et al. 2006).

II.3.4 Construction of *bcaC*- and *BCAM0218*-negative *B. cenocepacia* K56-2 mutants

A 1620-bp fragment of the *bcaC* gene (94-1714 bp) and a 1694-bp fragment of the *BCAM0218* gene (772-2466 bp) from *B. cenocepacia* K56-2 were amplified by PCR, using the primers: fr219F1 (5'- CGGGGTACCAATGGTTCGCTGACGCTTTGC-3') and fr219R1 (5'-CCCAAGCTTGTCCTTCAACTGACCGAGGTTCAA-3'); fr218F1 (5'-GGGGTACCGACGGGCAGAAGCATTTCATGACT-3') and fr218R1 (5'-CCCAAGCTTATGTTCAGGTCGGTCAACACCA-3') which contain a *Hind*III and a *Kpn*I restriction sites. The PCR-produced fragments were digested and cloned into pDrive (Qiagen) to generate pD0219 and pD0218, respectively. The trimethoprim resistance cassette (Tp) was excised from pUC-Tp and cloned into the pD0219 and pD0218 via the unique *Sph*I restriction site, resulting in pD0218_Tp and pD0218_Tp, respectively. These plasmids were transformed into *B. cenocepacia* K56-2 by electroporation. Transformants were selected on LB agar supplemented with kanamycin and trimethoprim for 48 h at 37 °C. To distinguish between single-and double-crossover mutants, trimethoprim-resistant colonies were screened by replica plating for kanamycin sensitivity. The candidate insertion mutants were further characterized by using gene-specific primers, 218F2 (5'-CCATCCGCCATCTCTTCGC-3') and 218R2 (5'-TCATCGCTTCATCACCGATGTGTTG-3'), and fr219F1 and fr219R1. The non-polarity of *bcaC*::Tp and *BCAM0218*::Tp mutants were confirmed by RT-PCR. To do that, we measured the expression levels of *BCAM0220* (RT_0220Fw 5'-CCGCAACGTGATGAACTACCT-3' and RT_0220Rv 5'-GCCTTCGGAGACGAACGA-3') and *BCAM0216* (RT_0216Fw 5'-CGACGCCTCGTATCAACACA-3' and RT_0216Rv 5'-

GAGAACTGTCGGCCAAATCC-3') and *BCAM0217* (RT_0217Fw 5'-GTCCATTCACACGAGTCTTTCC-3' and RT_0217Rv 5'-CCGTTTTCCATCTGTGGA-3'), respectively in the *bcaC*::Tp and *BCAM0218*::Tp mutants.

II.3.5 Complementation of the *B. cenocepacia* K56-2 *BCAM0218*::Tp mutant

The coding sequence of the *BCAM0218* gene from *B. cenocepacia* K56-2 was amplified by PCR, using the primers 218F3 (5'-TCATCGCTTCATCACCGATGTGTTGG-3') and 218R3 (5'-TACGGGTAGGCGGTAGAGAA-3') which contain a *Nde*I and *Xba*I restriction sites. This DNA fragment was digested and cloned into plasmid pIN177 (Gomes, et al. 2018) before transformation into *E. coli* DH5α and selection with chloramphenicol. The resulting plasmid, pN0218, was introduced into the *BCAM0218*::Tp mutant by electroporation, being replicative in *Burkholderia*.

II.3.6. Bacterial adherence to ECM proteins

Bacterial adherence to ECM proteins was tested, as described before, with some modifications (Mil-Homens, et al. 2010). Briefly, 96-well polystyrene microplates were coated with 10 mg/mL laminin, fibronectin, and collagen types I and IV (in phosphate-buffered saline (PBS)) and placed at 4 °C, overnight. The wells were washed twice with PBS and saturated with a 2% (w/v) bovine serum albumin (BSA) solution for 1 h at room temperature. Cultures of *B. cenocepacia* K56-2, *bcaC*::Tp and *BCAM0218*::Tp mutants, *BCAM0218*::Tp pN0218 (complementation) and *BCAM0218*::Tp pIN117 (control) (initial OD_{640} 0.2) were grown for 17 h at 37 °C, 70 rpm, under the above established conditions. Equal amounts (200 mL) of a bacterial suspension of 5 x 10^6 CFU/mL were added to the ECM-coated wells. After incubation for 2 h at 37 °C, unbound bacteria were removed, and adherent bacteria were washed twice with PBS. The wells were then treated with 200 mL of a 0.5% (v/v) Triton X-100 solution to desorb the bound bacteria. Plates were incubated for 2 h at room temperature under orbital agitation. Serial dilutions of the bacterial suspensions were prepared in PBS and plated on LB agar plates. Results are expressed as a ratio of the wild-type (wt) and corrected with the initial bacterial dose applied. Results are mean values of at least 5 repeats from 3 independent experiments.

II.3.7. Biofilm formation assay

Parental and mutant *B. cenocepacia* K56-2 strains (initial OD_{640} 0.2) were grown for 17 h at 37 °C, 70 rpm, under the above established conditions (section II.3.1). The cultures were diluted in LB to an OD_{640} of 0.05 and 200 µL of the cell suspensions were inoculated into wells of a 96-well polystyrene microplate (U-bottom). Plates were statically incubated at 37 °C for 4 h, the supernatant removed (unbound bacteria), and each well was washed once with PBS. Fresh LB media was added, and the plates were statically incubated at 37 °C for 24 and 48 h. For biofilm quantification, the culture medium and non-adherent bacteria were removed, and wells were rinsed twice with PBS. The biofilms were fixed with 200 µL of cold methanol and incubated for 15 min at room temperature. The methanol was removed, and the plates were dried at 37 °C. Adherent bacteria were stained with 200 µL of a 1% (w/v) crystal violet solution for 20 min at room temperature. After three gentle rinses with deionized water, the dye was solubilized with 95% ethanol for 15 min at room temperature under orbital agitation. Measurement of the solution absorbance was performed at 595 nm using a microplate reader. Results are median values of at least 5 repeats from 3 independent experiments.

II.3.8. Hemagglutination assay

Fresh blood (ABO blood types) from healthy human donors was collected and gently mixed with 3.8% of sodium citrate in a final ratio of 9:1. An equal amount of Alsever solution (2.05% dextrose; 0.8% sodium citrate, 0.055% citric acid, and 0.42% sodium chloride) was added, and the resulting suspension was immediately mixed. Red blood cells were separated by centrifugation at 3000 rpm for 10 min. The supernatant was removed, and the red blood cells were washed three times with five volumes of PBS, pH 7.4, and centrifuged at 3000 rpm for 10 min. A suspension of red blood cells with 50% hematocrit was prepared in PBS and kept in 4 °C before use. Parental and mutant *B. cenocepacia* K56-2 strains (initial OD_{640} 0.2) were grown for 17 h at 37 °C, 70 rpm, under the above established conditions. Cells were harvested by centrifugation, washed twice with PBS pH 7.4, and resuspended in PBS to an OD_{640} of 10. The cells were serially diluted (dilution factor of each transfer, ½) and placed (30 µL) in 96-well plates (U bottom). To

each well, an equal volume of red blood cells (2% (v/v) in PBS) was added. The plates were mixed gently and incubated for 1 h at room temperature. PBS solution was used as a negative control. Each assay consisted of three to five replicates. Hemagglutination was detected by visual inspection of the suspension with a direct comparison to the negative control.

II.3.9. Adhesion to human bronchial epithelial cells

Adhesion assays were carried out on non-CF 16HBE14o- and CF CFBE41o- bronchial epithelial cells as described previously (Mil-Homens and Fialho, 2012). Cells were seeded in polystyrene 24-well plates one day before infection at 5 x 10^5 cells/well in supplemented medium. Then, the cell monolayers were washed with PBS and maintained in MEM medium without supplements. Parental and mutant *B. cenocepacia* K56-2 strains were used to infect host cells at a multiplicity of infection (MOI) of 50:1. The infected monolayers were incubated at 37 °C in 5% CO_2 for 30 min to allow bacterial adherence. Cells were washed three times with PBS and lysed with lysis buffer (10 mM EDTA, 0.25% Triton X-100) for 30 min at room temperature. The adhered bacteria were quantified by plating serial dilutions of the cell lysates. Results are expressed as percentage of adhesion relatively to the initial bacterial load added to the cells.

II.3.10. Confocal laser scanning microscopy assays

Confocal laser scanning microscopy assays were performed as previously described (Mil-Homens and Fialho, 2012). Briefly, bacteria were stained by pIN29 plasmid, which encodes DsRed, a red fluorescent protein (Vergunst, et al. 2010). Plasmid was introduced into *B. cenocepacia* K56-2, *bcaC*::Tp and *BCAM0218*::Tp mutants by electroporation. Bacteria strains were grown in supplemented LB broth as described above. After 17 h of growth, bacteria were collected, harvested by centrifugation, and washed with PBS. Adhesion assays were performed as explained above, but glass coverslips were placed into 24-well plates and coated with a 0.1% (w/v) poly-L-lysine solution (Sigma) before cell seeding. After 30 min of adhesion, cells were washed three times with PBS and fixed with 4% paraformaldehyde during 30 min at room

temperature. Samples were washed to eliminate any traces of paraformaldehyde and incubated with a membrane dye AlexaFluor 633 conjugate WGA (ThermoFisher) (1:200 dilution in PBS), during 1 h in the absence of light. Cells were washed twice with PBS and incubated with Hoechst 33342 Solution (Thermo-Fisher) for nuclei staining (1:2000 dilution, in PBS) during 15 min, at room temperature and in the dark. Then the coverslips were mounted in Vectashield (Vector Laboratories). All samples were examined on a Leica TCS SP5 (Leica Microsystems CMS GmbH, Mannheim, Germany) inverted microscope (model DMI6000) with a 63X water (1.2-numerical-aperture) apochromatic objective.

II.3.11. Total RNA isolation

Total RNA was isolated from *B. cenocepacia* K56-2 grown in 24-well plates, at 37 °C with orbital agitation at 70 rpm, and under the conditions described above (section II.3.1). Harvested cells were treated with RNAprotect Bacteria Reagent (Qiagen) following the manufacturer's instructions. Bacterial lysis was achieved by enzymatic lysis with lysozyme and proteinase K. Total RNA was purified from the bacterial lysate using RNeasy mini kit (Qiagen), according the manufacturer's protocol. To avoid contamination with genomic DNA, RNA was treated with RNase-free DNA digestion kit (Qiagen) in column during the purification process, for 1 h at room temperature. After the RNA isolation, a second DNase treatment was performed overnight at 37 °C, using 1 µL DNase (2.7 Kunitz units) for 1.5 µg of RNA, followed by inactivation for 5 min at 65 °C, according to the manufacturer's instructions. The total RNA concentration was estimated using a UV spectrophotometer.

II.3.12. Reverse transcription PCR

For RT-PCR total RNA was converted to cDNA and then analyzed with Power SYBR Green Master Mix (Applied Biosystems), using primers to amplify *BCAM0216* (0216_Fw 5'-CGACGCCTCGTATCAACACA-3'; 0216_Rv 5'-GAGAACTGTCGGCCAAATCC-3'), *BCAM0217* (0217_Fw 5'-GTCCATTCACACGAGTCTTTCC-3'; 0217_Rv 5'-CCGTTTTCCATCTGTGGA-3'), *BCAM0218* (0218_Fw 5'-CGGCGATCTGAAGGTTGCA-3'; 0218_Rv 5'-

AGCGCTAGTGCTTCGATCGA-3'), *bcaC* (bcaC_Fw 5'-TCTCGGGTACGCGATTGAC-3'; bcaC_Rv 5'-TGTTATACAGCTGAAACGACCTTACG-3'), *BCAM0220* (0220_Fw 5'-CCGCAACGTGATGAACTACCT-3'; 0220_Rv 5'-GCCTTCGGAGACGAACGA-3') and *sigA* gene (used as an internal control) (sigA_Fw 5'-GCCGATGCGTTTCGGTAT-3'; sigA_Rv 5'-GCGTGACGTCGAACTGCTT-3'). All samples were analyzed in triplicate, and the amount of mRNA detected normalized to control *sigA* mRNA values. Relative gene expression was calculated by using the ΔΔCT method (Livak and Schmittgen, 2001).

II.3.13. Statistical analysis

Data are expressed as mean or median values of a minimum of three independent experiments ± standard deviation (SD). Statistical analysis was carried out by using GraphPad Prism6 software. Relative comparisons were made between corrected values with ANOVA test for significance. A P value of <0.05 was considered statistically significant.

II.4 Results

II.4.1. Bioinformatic analysis of BcaC and impact of *bcaC* inactivation on the expression of the neighboring gene BCAM0220

bcaC gene is situated in the TAA cluster and arranged in a bicistronic unit with *BCAM0220* OmpA. Immediately upstream is located the *BCAM0218* gene, which encodes for a sensor HK that, along with the RRs (BCAM0221 and BCAM0222) may form a two-component regulatory system (Figure II.1A) (Mil-Homens and Fialho, 2011; Mil-Homens and Fialho, 2012). *B. cenocepacia* K56-2 *bcaC* mutant was obtained by insertional mutagenesis with a trimethoprim resistance cassette, as indicated in the Figure II.1A. To confirm that *bcaC* inactivation did not caused a polar effect, the expression of the neighbor *BCAM0220* gene was studied. RT-PCR assays using mRNA isolated either from the *B. cenocepacia* K56-2 wild type and from the *bcaC*-negative

mutant showed an identical amount of BCAM0220 expression, thereby confirming the lack of polarity (Figure II.1B).

The 8862-bp *bcaC* gene from *B. cenocepacia* K56-2 encodes a protein with 2953 residues previously described as a TAA (Mil-Homens and Fialho, 2011). Its head-stalk-anchor domain organization and the presence of the TAA signature C-terminal anchor was confirmed by using the daTAA web program (http://toolkit. tuebingen.mpg.de/dataa) (Szczesny and Lupas, 2008) (Figure II.1C). The 3D structure of each BcaC predicted domain was modeled using Phyre2 web portal (http://www.sbg.bio.ic.ac.uk/phyre2) (Kelley, et al. 2015), confirming the typical four beta strands structure of the monomeric membrane anchor and the presence of five and twelve YadA-like head and stalk domains, respectively. In Figure II.1D, we showed the top 3D models for each of these BcaC domains. The stalk domains were primarily composed of alpha helices and connecting loops. In contrast, the YadA-like heads appeared as layers of parallel beta-sheets. Using Pfam database (http://pfam.sanger.ac.uk/), the presence of fifteen Hep_Hag (Pfam PF05658), and eighteen HIM (Pfam PF05662) motifs, associated with bacterial hemagglutinins and invasins, was also scanned and identified along with the extracellular domains of BcaC. The structural features of the TAA YadA collagen-binding domain super family were identified as well using InterPro online tool (https://www.ebi.ac.uk/interpro/). Both Hep_Hag motifs and collagen-binding domains appeared to be associated with the head domains identified by daTAA, while HIM motifs seemed to mostly co-localize with the predicted stalk domains (Figure II.1C).

II.4.2. Effect of the *bcaC* mutation on *B. cenocepacia* K56-2 adherence to ECM proteins and biofilm formation

We assessed the capacity of *B. cenocepacia* K56-2 *bcaC*::Tp mutant to adhere to immobilized human ECM molecules such as fibronectin, laminin, collagen type I and IV (Figure II.2A). After 2 h of contact, adherent bacteria were quantified by CFU-plating assay. The obtained data indicated that the mutation of BcaC caused a decrease in *B. cenocepacia* adhesion to fibronectin, laminin, and collagen I and IV.

The fitness for biofilm formation was also determined for the mutant strain and compared to *B. cenocepacia* K56-2 wt strain (Figure II.2B). Biofilm quantification was performed by measuring crystal violet absorbance after 24 h and 48 h of static incubation. Results showed a significant increase in biofilm formation in the absence of a functional BcaC TAA ($P < 0.0001$).

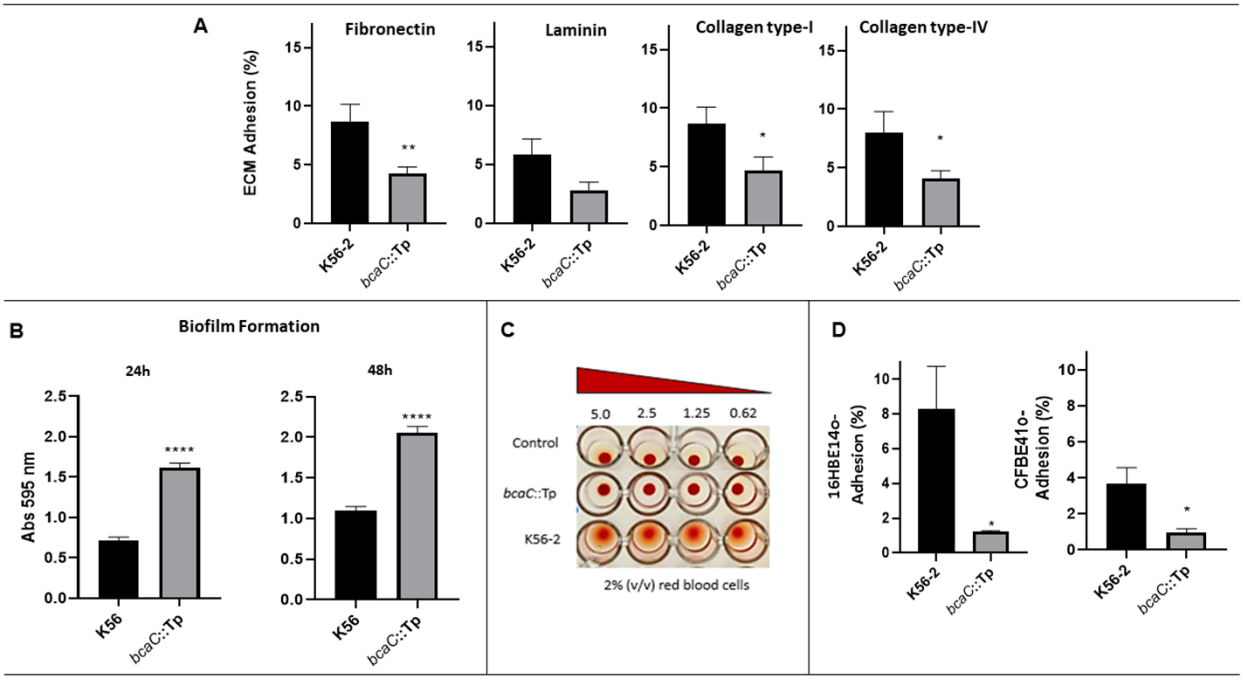

Figure II.2. Effect of the *bcaC* mutation on adherence to ECM proteins, biofilm formation, hemagglutination, and on adherence of cultured bronchial epithelial cells. (A) Adherence of wt *B. cenocepacia* K56-2 (black bars) and *bcaC*::Tp mutant (gray bars) to ECM proteins (fibronectin, laminin, and collagen type I and IV). All the results are from three independent experiments; bars indicate SD (*$P < 0.05$; **$P < 0.01$). **(B)** Static biofilm formation in polystyrene microtiter plates by wt *B. cenocepacia* K56-2 (black bars) and *bcaC*::Tp mutant (gray bars) at 24 and 48 h. Biofilm growth was quantified by the solubilization of crystal violet-stained cells with ethanol. The wt and the mutant strain after the 24 and 48 h grew identically. All the results are from three independent experiments; bars indicate SD (***$P < 0.0001$). **(C)** Hemagglutination ability of the wt *B. cenocepacia* K56-2 and *bcaC*::Tp mutant, using 2% human red blood cells. Values above the hemagglutination images indicate OD of the bacterial suspension added to the red blood cells. PBS was used as a negative control. **(D)** Adherence to 16HBE14o- (non-CF) and CFBE41o- (CF) epithelial cell lines by *bcaC*::Tp mutant (gray bars) expressed as percentage of adhesion relatively to the initial bacterial load added to the cells. *bcaC*-negative mutant adhered less efficiently than the wt strain (*$P < 0.05$).

II.4.3. The impact of *bcaC* mutation on human red blood cells hemagglutination and on adhesion to host cells

Hemagglutination activity was described as one of *B. cenocepacia* virulence traits, and its association with other *B. cenocepacia* TAA was already verified (Mil-Homens and Fialho, 2012). *In silico* analysis of BcaC revealed the presence of several hemagglutination associated motifs (Hep-Hag and HIM) organized across the passenger domain (Figure II.1C). To assess the influence of BcaC in *B. cenocepacia* K56-2 hemagglutination, the activity of the *bcaC*::Tp mutant was tested. The hemagglutination assay was performed with 2% (v/v) of red blood cells and with four crescent inoculum concentrations (OD_{640} 5, 2.5, 1.25 and 0.62). PBS was used as a negative control. Wild type K56-2 caused hemagglutination at all bacterial densities tested while none was seen with BcaC mutant (Figure II.2C). This indicated that BcaC played a role in the hemagglutination activity of this strain and that such capacity was independent of the blood type.

Aiming to determine the role of BcaC on host cell adhesion, two human bronchial epithelial cell lines (16HBE14o- and CFBE41o-) were used, and a CFU-based assay detected cell-adherent bacteria. *B. cenocepacia* K56-2 *bcaC*::Tp mutant adhered with less efficiency to both cell lines when compared to the wt strain (Figure II.2D).

II.4.4 Insertional inactivation of BCAM0218 enhances the expression of the trimeric autotransporter gene *bcaC*

The *BCAM0218* gene from *B. cenocepacia* K56-2 encodes for a hybrid HK whose function is still poorly understood. Its location in the *B. cenocepacia* genome has been determined as part of the TAA cluster (approximately 30-kb in chromosome 2) alongside with a set of virulence-associated genes (Mil-Homens and Fialho, 2011; Mil-Homens and Fialho, 2012). The *BCAM0218*-insertional mutant was constructed and used as a background to assess the expression of the upstream *bcaC* gene (Figure II.3A). A comparison of *bcaC* expression in the wt strain *versus* the *BCAM0218*-negative mutant showed that the level of the trimeric adhesin gene expression was much higher in the mutant strain (Figure II.3B). This feature and the lack of polar effects of *BCAM0218*-

negative mutant on its neighbors' genes (*BCAM0216* and *BCAM0217*) (Figure II.3B) suggested that the HK BCAM0218 may act as a negative regulator of the TAA *bcaC* expression.

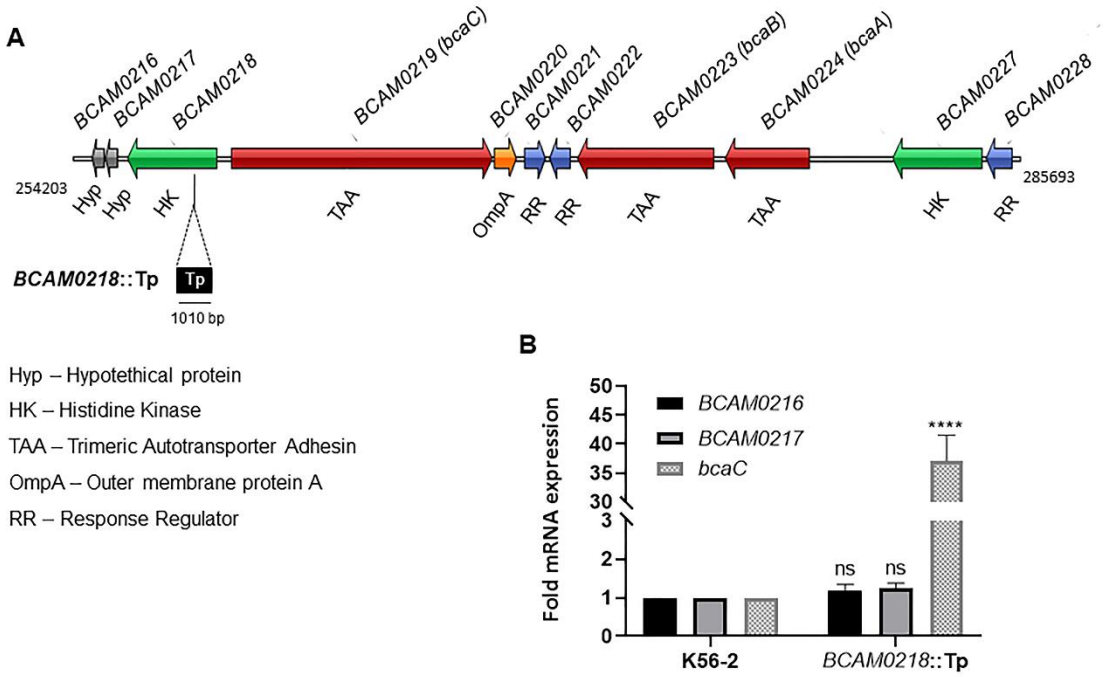

Figure II.3. Insertional inactivation of BCAM0218. (A) Organization of the *B. cenocepacia* K56-2 TAA cluster. The *B. cenocepacia* K56-2 *BCAM0218* mutant was obtained by insertional mutagenesis of a trimethoprim resistance cassette, as indicated in the figure. **(B)** Expression of *BCAM0216*, *BCAM0217* and *bcaC* TAA coding gene determined in wt and *BCAM0218*-negative mutant backgrounds. Transcription levels were obtained by qRT-PCR from parental and *BCAM0218*::Tp mutant strains were grown under limited oxygen supply in LB broth supplemented with NaCl and H_2O_2. Results were normalized to the expression of the housekeeping *sigA* gene. Expression levels are represented as relative values in comparison to the expression levels in standard LB growth. All the results are from three independent experiments; bars indicate SD (****P < 0.0001).

II.4.5. Bioinformatic analysis of the hybrid histidine kinase BCAM0218

The 3033-bp *BCAM0218* gene from *B. cenocepacia* K56-2 encodes a protein with 1010 amino acids that is a member of the hybrid histidine kinase family. Sequence analysis using SMART (Letunic and Bork, 2018) revealed the presence of a histidine kinase phosphoacceptor domain (residues 525-590), a histidine kinase-like ATPase (residues 637-751), a CheY-like receiver domain (residues 769-880) and a C-terminal histidine

phosphotransfer domain (residues 906-1000) (Figure II.4A). The BCAM0218 N-terminal includes the sensory input domain, which was predicted to have two transmembrane segments embedded within the inner membrane and a large loop located in the periplasm (Figure II.4B). Using the N-terminal sequence of BCAM0218$_{60\text{-}372}$ (periplasmic sensory domain) as a query, we searched by PSI-BLAST (Altschul, et al. 1997) for related proteins. BCAM0218 homologs in the NCBI database were only found in other members of the *Burkholderiales* order, with 90.7-20.9% amino acids sequence identities. The function of this hybrid sensor kinase was not reported for any of the BCAM0218 homologs.

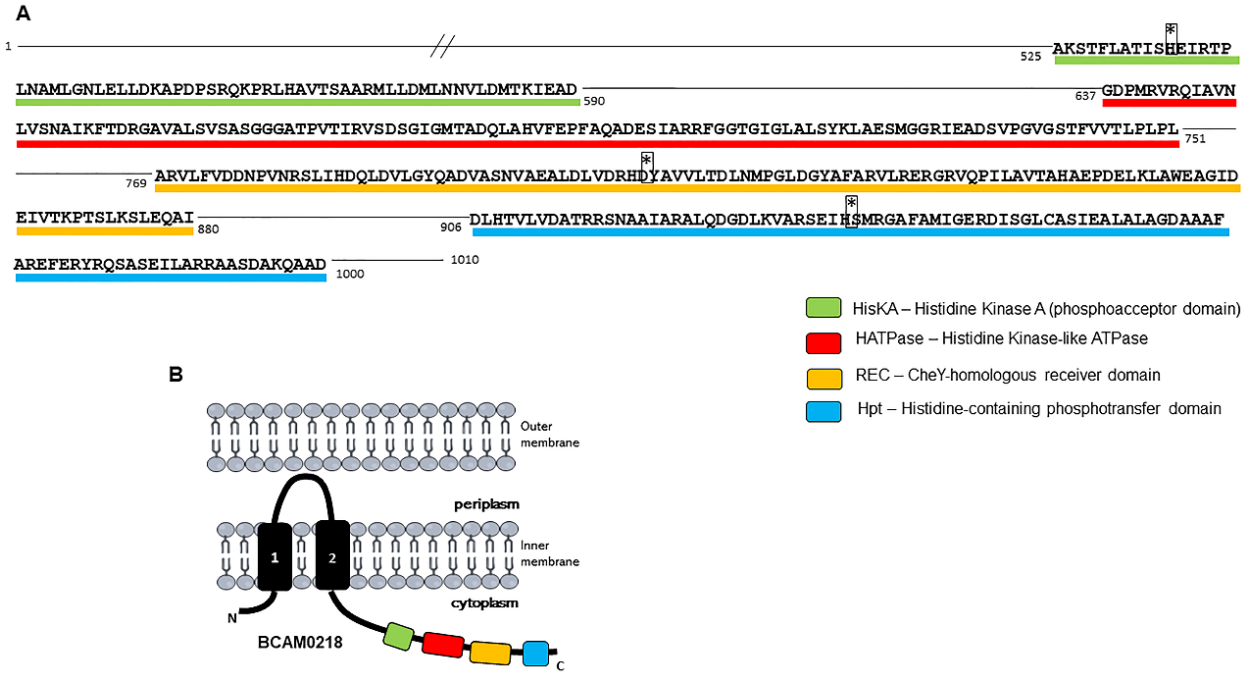

Figure II.4. Bioinformatic analysis of the HK BCAM0218. (**A)** Domain architecture of BCAM0218 revealing the existence of a histidine kinase phosphoacceptor domain (residues 525-590), a histidine kinase-like ATPase (residues 637-751), a CheY-like receiver domain (residues 769-880) and a C-terminal histidine phosphotransfer domain (residues 906-1000). Important residues H535, D819, and H940 are marked with asterisks within rectangles. (**B)** Predicted topology of BCAM0218, which has two predicted transmembrane segments in the inner membrane and a large loop in the periplasm.

II.4.6. Disruption of *BCAM0218* gene complements, at least in part, the phenotypes of the *bcaC* mutant

The above RT-PCR results showed that with a not functional HK BCAM0218, an overexpression of *bcaC* was observed. Thus, we proceeded to ask whether such *bcaC*

overexpression suppressed the TAA mutant phenotypes. As showed in Figures II.5 and II.6, we demonstrated that in three of the four phenotypic traits studied the overexpression of *bcaC* in the *B. cenocepacia* K56- 2 *BCAM0218*::Tp mutant background altered the fitness of the bacteria. Such overexpression caused an increased in ECM and cell adhesion when compared to the *bcaC*::Tp mutant strain and the restoration of the hemagglutination activity that was abolished in *bcaC* mutant strain. Moreover, the inactivity of BCAM0218 HK seemed to not only be able to restore the wt phenotype but even to surpass this threshold. This trait was particularly evident for host cell adhesion (Figure II.6). As shown in Figure II.6A and B, the *BCAM0218*-negative mutant adhered to host bronchial epithelial cells much more efficiently than the wt and *bcaC*-negative strains. Analysis of the stained cells by confocal immunofluorescence microscopy confirmed this result. Moreover, the *BCAM0218* complementation in *trans* restored the wt phenotype and displayed an expression pattern for *bcaC* to a level comparable to that of the wt strain (Figure II.6C). Overall, these analyses reveal that when functional, BCAM0218 HK negatively regulates the expression of the TAA encoding gene *bcaC*.

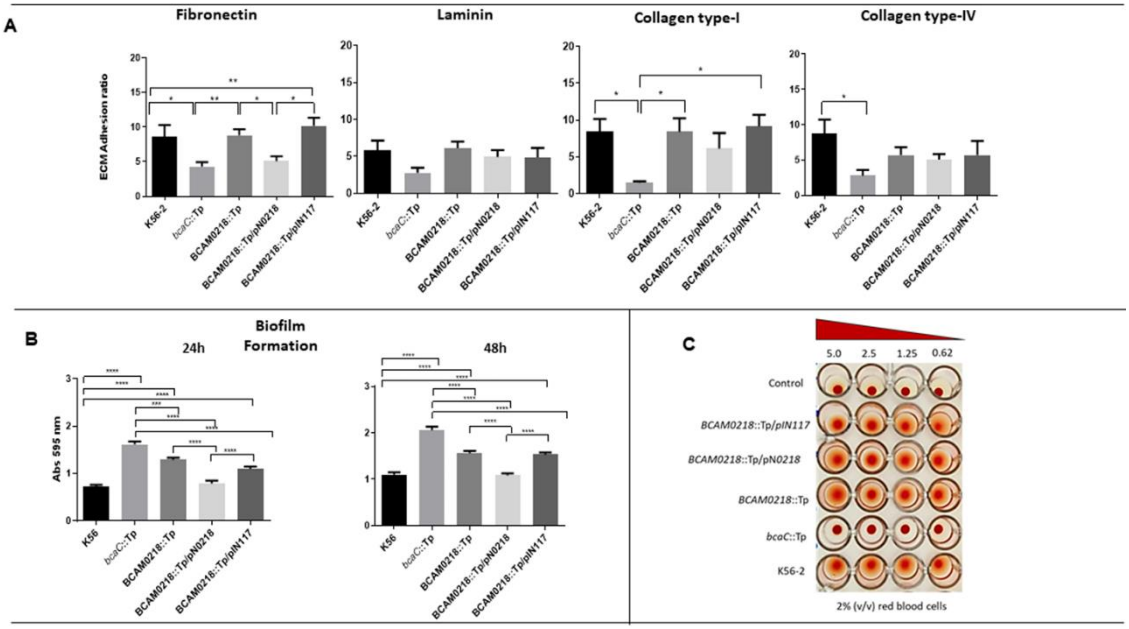

Figure II.5. Effects of the *BCAM0218* mutation on adherence to ECM proteins (A), biofilm formation (B) and hemagglutination (C). Complementation of the mutant was achieved using pIN177-*BCAM0218* (pN0218) plasmid and the empty plasmid (pIN117) as a control. The overexpression of *bcaC* in the *B. cenocepacia* K56-2 *BCAM0218*::Tp mutant background (Figure II.3) causes pronounced effects on phenotype, thereby permitting the functional analysis of BcaC. All the results are from three independent experiments, bars indicate SD (*P < 0.05; **P < 0.01; ***P < 0.001; ****P < 0.0001).

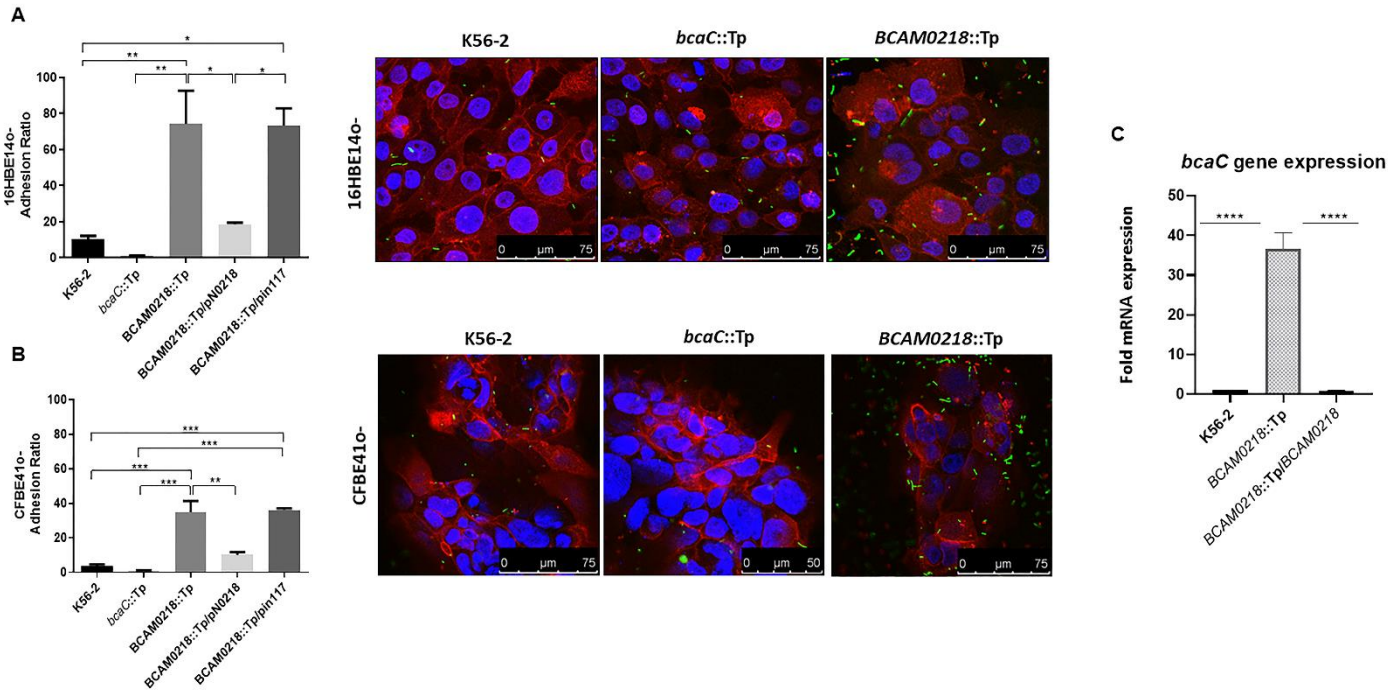

Figure II.6. *BCAM0218* mutation affects *B. cenocepacia* K56-2 adherence to host cells. Fluorescence confocal microscopy images of *B. cenocepacia* K56-2, *bcaC*::Tp and *BCAM0218*::Tp mutant strains adhering to 16HBE14o- (**A**) and CFBE41o-bronchial epithelial cells (**B**). Eukaryotic cell plasma membranes and nuclei were labeled with AlexaFluor 633-WGA (red) and Hoechst 33342 (blue) fluorophores, respectively. Bacteria were labeled with DsRed (represented in green). Adherence to 16HBE14o- and CFBE41o-epithelial cells by *B. cenocepacia* K56-2, *bcaC*::Tp and *BCAM0218*::Tp mutant strains is expressed as percentage of adhesion relatively to the initial bacterial load added to the cells. Complementation of the mutant was achieved using pIN177-*BCAM0218* (pN0218) plasmid and the empty plasmid (pIN117) as a control. All the results are from three independent experiments, bars indicate SD (*P < 0.05; **P < 0.01; ***P < 0.001). **(C)** Expression of *bcaC* TAA coding genes determined in wt, *BCAM0218*-mutant and *BCAM0218* complemented strains background. Transcription levels were obtained by qRT-PCR from bacteria growth under limited oxygen supply in LB broth supplemented with NaCl and H_2O_2. Results were normalized to the expression of the housekeeping *sigA* gene. Expression levels are represented as relative values in comparison to the expression levels in standard LB growth. All the results are from three independent experiments; bars indicate SD (****P < 0.0001).

II.5 Discussion

B. cenocepacia is known for its vastly set of virulent traits that, in most cases, seems to be regulated in response to specific environmental alterations (Sousa, et al. 2017). Among those, a variable set of adhesin genes have been annotated, and some confirmed through experimental validation (Saldías, et al. 2009; McClean, et al. 2009; Mil-Homens and Fialho, 2011; Dennehy, et al. 2016). Overall, they play crucial roles in the early steps of bacterial infection and are subject to regulation in response to environmental changes (Sheets and St Geme, 2011; Sieira, et al. 2017; Pimenta, et al. 2020a). In this work, we continued the characterization of the *B. cenocepacia* K56-2 TAA cluster previous described (Mil-Homens and Fialho, 2012). We focused on the characterization of a *B. cenocepacia* K56-2 strain with an insertional mutation in the *bcaC* gene encoding the third trimeric autotransporter adhesin of the cluster. Unfortunately, despite many efforts, we failed to clone the entire *bcaC* gene, and hence we were unable to perform the mutant complementation analysis. However, we analyzed the gene immediately upstream (*BCAM0218*), which encodes a hybrid HK that is likely, at least partly, responsible for rescue the phenotypic defects caused by the *bcaC* deficiency. In order to further discard a possible effect of the trimethoprim resistance cassette in the phenotypes observed, RT-PCR assays were performed (Figures II.1B and II.3B).

A *bcaC*-mutant strain was created, and the related phenotypes analyzed (Figure II.2). To uncover the relevance of the *BCAM0218* HK coding gene as a putative modulator of the BcaC activity, a *BCAM0218*-mutant strain was constructed, and its phenotypic variations evaluated. The results showed an interference of BCAM0218 in the expression of the *bcaC* gene. The absence of a functional HK caused a significant increase in the *bcaC* gene expression, indicating an inhibitory role for BCAM0218 towards BcaC (Figure II.3). Moreover, the overexpression of *bcaC* in the *BCAM0218*-mutant background rescued some of the phenotypes that were associated with the BcaC functions (Figure II.5).

Concerning adherence to immobilized ECM, the *bcaC*-negative mutant adhered less efficiently to all tested matrixes when compared to the wt. *In silico* analysis of the passenger domain of BcaC, highlighted the presence of nine putative collagen-binding

domains, indicating this TAA as a putative collagen-binding protein (Figure II.1C). Collagen is the most abundant protein in mammalian ECM, being widely distributed in lung tissues (Shoulders and Raines, 2009). It has been reported as an important ligand for host-pathogen interaction, colonization, and persistence (Liu, et al. 2018). Various bacterial TAAs were previously described as collagen-binding proteins, being able to enhance bacterial adherence to host tissues and improving the survival capacity and overall virulence of the bacteria (Singh, et al. 2016; Daigneault and Lo, 2009).

Despite the reduced capacity to adhere to ECM proteins, the *bcaC*-mutant had an enhanced ability to form a biofilm. It seemed that the presence of BcaC (*BCAM0218*-mutant) adversely affected the establishment of biofilm on a hydrophobic polystyrene surface (Figure II.2B). Under the experimental conditions used, we could not detect a direct association of the *bcaC* expression and biofilm formation.

Biofilm formation was substantially increased in the *bcaC* mutant compared to the wt (Figure II.2B). However, in the *BCAM0218*::Tp mutant background, which activated the overexpression of *bcaC*, the biofilm formation capacity was still greater than that of the wt (Figure II.5B). Thus, it appeared that, at least under the experimental conditions used, BcaC was required in the early stages of adherence, but in late stages of biofilm settlement, its presence was not needed or even inhibitory. We hypothesized that the large size of the BcaC (2953 residues) could be inconvenient for the mature and more compact biofilm structure, being only necessary for the establishment of the early adhesion steps.

Hemagglutination is one of the many features associated with TAAs role in virulence of Gram-negative bacteria (Pearson, et al. 2006; Mil-Homens and Fialho, 2012). *In silico* analysis and experimental validation revealed the importance of BcaC for the hemagglutination-positive phenotype of *B. cenocepacia* K56-2 (Figures II.2 and II.5). The presence of Hep_Hag motifs (eighteen predicted) in the head domains of BcaC (Figure II.1C) may indicate that there are multiple sites for immune recognition, and thereby may represent an interesting target for vaccine development. Finally, we assessed the effect of the *bcaC* and *BCAM0218* mutations on host cell adhesion. Results indicate that *bcaC*::Tp mutant impaired cell adhesion. On the other hand, *bcaC* overexpression (in the *BCAM0218*::Tp mutant background) caused a significant increase in bacterial adherence

to host cells, which is much higher than that of the wt *B. cenocepacia* K56-2 (Figure II.6). *B. cenocepacia* possess a large set of different molecules that can mediate adhesion to host cell (McClean and Callaghan, 2017). It is reasonable to postulate that the absence of a TAA in the extracellular surface of *B. cenocepacia* was not enough to cause a profound functional impact in the overall bacterial adhesion capacity. Nevertheless, the rise in a specific TAA transcript seemed to be enough to improve the adherence capacities of *B. cenocepacia* K56-2 in more than 10 times.

Overall, our results indicated that the TAA *bcaC* and the predicted HK BCAM0218 were functionally linked. Moreover, a disruption of the HK *BCAM0218* gene had a direct impact on *bcaC* expression, thereby revealing its phenotypic associated features. The *in silico* analysis of BCAM0218 predicted that this protein is a hybrid HK as it contained a histidine phosphotransfer domain, an ATP binding domain, and an internal aspartate-containing receiver domain (Figure II.4). Furthermore, the presence of two closely linked response regulators (RR) (*BCAM0221* and *BCAM0222*) within the TAA cluster (Figure II.1A) raised the question as to whether these two RRs are cognate partners. Various studies have shown that two-component systems (TCS) (sensor HKs and their cognate RRs) are linked with the regulation of the adherence events during the bacterial infection process. This is the case of the ArlS-ArlR and AgrC-AgrA *loci* of *Staphylococcus aureus* (Fournier and Hooper, 2000; Choudhary, et al. 2018), the PhoQ/PhoP *locus* of *Salmonella enterica* serovar Typhimurium (Lambert and Smith, 2008), the BvgA-BvgS *locus* of *Bordetella pertussis* (Herrou, et al. 2009) and the FixL-FixJ *locus* of *Burkholderia dolosa* (Schaefers, et al. 2017). For these TCSs, the input *stimuli* are diverse and involve quorum sensing (AgrC-AgrA), osmosensing (PhoQ/PhoP), and oxygen sensing (FixL-FixJ). For the HK BCAM0218 used in this work to disclosure the role of *bcaC* TAA, it remains to be elucidated the chemical or environmental nature of the *stimuli* perceived. Moreover, it is not known whether the TCS involving HK BCAM0218 acts directly or indirectly on *bcaC* gene transcription. Research is underway in our laboratory focusing on understanding the mechanisms of action of the HK BCAM0218.

In sum, we performed the functional analysis of a TAA mutant of *B. cenocepacia* K56-2, which was defective in one (*bcaC*) of the three TAA genes found in the TAA cluster. The phenotypic analysis of this mutant revealed that BcaC had multiple virulence associated

functions. Interestingly, we also reported for the first time, that the HK BCAM0218 negatively modulates BcaC functions. We believe that the TAA cluster composed of three multifunctional trimeric autotransporter adhesins is linked to a TCS system (HK BCAM0218; RR BCAM0221 and BCAM0222) that integrates and coordinates the multiples roles of TAAs during the infection process of *B. cenocepacia*.

Data availability statement

All data are provided in full in the results section of this chapter.

Acknowledgments

This work was supported by the Portuguese Science and Technology Foundation (FCT) BIOTECnico Ph.D. program grant PD/BD/116940/2016. FCT also provides post-doctoral research grants for D. Mil-Homens (SFRH/BPD/91831/2012). Funding received by iBB e Institute for Bioengineering and Biosciences from FCT (UID/BIO/04565/2020) and Programa Operacional Regional de Lisboa 2020 (Project N. 007317) is acknowledged. We thank Dieter Gruenert, Pacific Medical Center Research Institute, San Francisco, CA, for providing us with the 16HBE14o- and CFBE41o-cell lines. We also acknowledge John LiPuma from the University of Michigan, who kindly provided a Burkholderia strain. We also thank Annette Vergunst from INSERM, Université de Montpellier, France, for kindly provided plasmids pIN29 and pIN177.

Declaration of Competing Interest

The authors have no conflict of interest to declare.

III. *BURKHOLDERIA CENOCEPACIA* CELL CONTACT CONTROLS THE TRANSCRIPTION ACTIVITY OF THE TRIMERIC AUTOTRANSPORTER ADHESIN *BCAM2418* GENE

Journal paper

Pimenta AI, Mil-Homens D, Fialho AM. *Burkholderia cenocepacia*-host cell contact controls the transcription activity of the trimeric autotransporter adhesin *BCAM2418* gene. *MicrobiologyOpen*. 2020;9(4):e998. doi:10.1002/mbo3.998

III.1 Abstract

Cell-to-cell early contact between pathogens and their host cells is required for the establishment of many infections. Among various surface factors produced by bacteria that allow an organism to become established in a host, the class of adhesins is a primary determinant. *Burkholderia cenocepacia* adheres to the respiratory epithelium of cystic fibrosis patients and causes chronic inflammation and disease. Cell-to-cell contacts are promoted by various kinds of adhesins, including trimeric autotransporter adhesins (TAAs). We observed that among the 7 TAA genes found in the *B. cenocepacia* K56-2 genome, two of them (*BCAM2418* and *BCAS0236*) expressed higher levels of mRNA following physical contact with host cells. Further analysis revealed that the *B. cenocepacia* K56-2 *BCAM2418* gene showed an on–off switch after an initial colonization period, exhibited a strong expression dependent on the host cell type, and enhanced its function on cell adhesion. Furthermore, our analysis revealed that adhesion to mucin-coated surfaces dramatically increased the expression levels of *BCAM2418*. Abrogation of mucin O-glycans turned *BCAM2418* gene expression off and impaired bacterial adherence. Overall, our findings suggested that glycosylated extracellular components of host membrane might be a binding site for *B. cenocepacia* and a signal for the differential expression of the TAA gene *BCAM2418*.

III.2 Introduction

Bacterial initial contact to host cells has been defined as a crucial step in the overall host–pathogen interaction process (Pizarro-Cerdá and Cossart, 2006). During the early stages of infection, the ability of bacteria to sense environmental changes and physical barriers of the host makes them more prone to alter and adapt their metabolism, regulation, and virulence (Stones and Krachler, 2016). Bacteria could perceive this surface sensing through chemical signals or mechanical forces (Cox, et al. 2018). Although poorly understood, it has been described that the sense and adherence of the bacteria to the host could lead to a prompt transcription modulation of a panel of

virulence-associated genes, adhesive molecules, surface antigens, and toxins (Kansal, et al. 2013; Alsharif, et al. 2015; Katsowich, et al. 2017). These physiological alterations can result in a more robust bacterial adhesion that thereby favors colonization and persistence in the host cell (Li, et al. 2012; Kansal, et al. 2013; Stones and Krachler, 2016).

Burkholderia cenocepacia is a human contact-dependent pathogenic bacterium known for its capacity of adherence and intrinsic interaction with the host, causing severe and persistent opportunistic lung infection in cystic fibrosis (CF) patients (Chiarini, et al. 2006, Baldwin, et al. 2007). In CF airways, the hypersecretion of mucus (containing water, ions, mucins, and other macromolecules) contributes to the formation of a viscoelastic material that facilitates bacterial adhesion and impairs host immune responses (Xia, et al. 2005; Mullen, et al. 2010; Colomb, et al. 2014). Besides this cell surrounding material, airway epithelial cells contain membrane-anchored mucins that represent a group of highly O-glycosylated transmembrane glycoproteins (MUC1, MUC4, and MUC16 as the most representative). These membrane-tethered glycoproteins have signaling functions and serve as a protective barrier against invading pathogens (Kim, 2012; Cullen, et al. 2017; Dhar and Mcauley, 2019). In contrast to that, in some bacteria, it has been described the use of the mucin carbohydrate moieties as receptors for host cell infection, followed by the modulation of virulence genes expression (Navabi, et al. 2012; Ohneck, et al. 2018). *B. cenocepacia* uses very complex machinery for primary adherence with host cells in which few adhesion factors or appendages have been described (Sajjan, et al. 2000; Saldías, et al. 2009; Mil-Homens and Fialho, 2011; Dennehy, et al. 2016; McClean, et al. 2016). Among those, the subclass of trimeric autotransporter adhesins (TAAs) (Linke, et al. 2006) deserves particular attention.

TAAs form a large and diverse group of outer membrane proteins widely distributed in Gram-negative bacteria. They belong to a subfamily of autotransporter proteins and are secreted to the outer surface of the bacteria via the type Vc secretion system. These proteins have a typical trimeric surface modular architecture, composed of three identical monomers, with a C-terminal anchor and a variable extracellular set of fiber composed of stalk and globular-like head regions. While the membrane anchor domain is the defining feature of this class of proteins, highly conserved among all the TAA

members, head and stalk organization is adaptable and vary among TAAs (Cotter, et al. 2005; Łyskowski, et al. 2011; Bassler, et al. 2015).

B. cenocepacia J2315 possess 7 TAA-encoding genes distributed between chromosome 2 (*bcaA*, *bcaB, bcaC*, *1115*, and *2418*) and 3 (*BCAS0236* and *0335*) (Mil-Homens and Fialho, 2011, 2012; Mil-Homens, et al. 2014). They have been implicated in the binding to a considerable set of molecules, such as host cell receptors, components of the extracellular matrix or even other TAAs (El-Kirat-Chatel, et al. 2013; Mil-Homens, et al. 2017). Results showed that TAAs are involved in several virulence-associated features, such as biofilm formation, evasion to host immune system, motility, invasion of host cells, hemagglutination, and induction of inflammation (Mil-Homens and Fialho, 2011, 2012; Mil-Homens, et al. 2014, 2017).

In this work, we aimed to uncover the relevance of *B. cenocepacia* TAAs in the early stages of infection. In particular, our findings revealed the transcriptional alteration of *BCAM2418* gene induced by the physical contact of the bacterium with bronchial epithelial cells. Moreover, we found that overexpression of *BCAM2418* gene contributed to the bacterial cell adhesion to host cells and was dependent on recognition of O-linked glycans from the host cell membranes. Overall, this study not only defined the behavior of the TAAs during the step of bacterial adhesion but also provided insights aiming to determine potential targets for therapeutic proposals.

III.3 Material and Methods

III.3.1 Bacterial growth conditions

The *B. cenocepacia* clinical isolate K56-2 is clonally related to the reference strain J2315 (Holden, et al. 2009) and was kindly provided by Prof. J. J. LiPuma (University of Michigan, USA). Bacteria were routinely cultured in Luria–Bertani (LB) broth (NZYTech), at 37 °C with orbital agitation (250 rpm).

III.3.2 Human cell lines and cell culture conditions

Two human bronchial epithelial cell lines were used: 16HBE14o- cell line, which is healthy lung cells expressing a functional CF transmembrane conductance regulator, and CFBE41o- cell line, which is homozygous for the delta F508 mutation corresponding to a CF airway. Both immortalized cell lines were kindly provided by Dr. Gruenert and coworkers (Cozens, et al. 1994; Bruscia, et al. 2002). Cells were routinely maintained in fibronectin/collagen type-I-coated flasks in Minimum Essential Medium with Earle's salt (MEM) (Gibco, ThermoFisher) supplemented with 10% fetal bovine serum (FBS) (Lonza), 0.292 g/L L-glutamine (Sigma-Aldrich) and Penicillin/Streptomycin 100 U/mL (Gibco, ThermoFisher). Human lung carcinoma cell line A549 (ATCC® CCL-185™) and human cervix adenocarcinoma cell line HeLa (ATCC® CCL-2™) were grown in Dulbecco's Modified Eagle Medium (DMEM) (Gibco, ThermoFisher) supplemented with the same components as described above. The four cell lines were incubated at 37 °C in a humidified atmosphere with 5% CO_2.

III.3.3 Quantitative assessment of TAAs genes expression upon host cell contact

The transcript levels of TAAs encoding genes *bcaA*, *bcaB, bcaC*, *1115*, *2418*, *BCAS0236*, and *0335* were determined by quantitative real-time PCR (qRT-PCR). qRT-PCR was performed with the 7500 RTPCR system (Applied Biosystems) according to the manufacturers' protocols. Total RNA was isolated from adherent *B. cenocepacia* K56-2 cells (30 min incubation) to the four human cell lines described above. Bacterial lysis was achieved by enzymatic lysis with lysozyme and proteinase K (Qiagen). Total RNA was purified from a bacterial lysate using RNeasy mini kit (Qiagen), according to the manufacturer's protocol. To avoid contamination with genomic DNA, RNA was treated with RNase-free DNAse digestion kit (Qiagen) in a column during the purification process, for 1 h at room temperature. To remove the DNA contamination from isolated RNA, overnight DNase (1 µL for 1.5 µg of RNA) treatment was performed at 37 °C followed by inactivation for 5 min at 65 °C. The total RNA concentration was estimated using a UV spectrophotometer (ND-1000 UV-Vis, NanoDrop Technologies).

For qRT-PCR experiments, total RNA was converted to cDNA using TaqMan kit (Applied Biosystems) and then analyzed with Power SYBR Green master mix (Applied Biosystems), using primers to amplify TAA-encoding genes and *sigA* gene (used as an internal control; Table III.1). All samples were analyzed in triplicate, and the amount of mRNA detected normalized to control *sigA* mRNA values. Relative quantification of genes expression was calculated by using the ΔΔCT method (Livak and Schmittgen, 2001).

Table III.1 – List of RT-PCR primers used in this study

Gene	Primer	Sequence
sigA	Forward	5'-GCCGATGCGTTTCGGTAT-3'
	Reverse	5'-GCGTGACGTCGAACTGCTT-3'
bcaC (BCAM0219)	Forward	5'-TCTCGGGTACGCGATYGAC-3'
	Reverse	5'-TGTTATACAGCTGAAACGACCTTACG-3'
bcaB (BCAM0223)	Forward	5'-GCAATCGGCCGGAACTC-3'
	Reverse	5'-TCGTCTATGCCTCGGTCCAT-3'
bcaA (BCAM0224)	Forward	5'-TCACGAGGCGAATTGTCAAC-3'
	Reverse	5'-GAGACGTTCACGACATCCGTATC-3'
BCAM1115	Forward	5'-TTGCCGCAGGCGTATCT-3'
	Reverse	5'-CCTTCAGCACCCAGTTG-3'
BCAM2418	Forward	5'-CGCCAATACCTTCGTTCCA-3'
	Reverse	5'-CGGGATAGGCATTGGTGTTG-3'
BCAS0236	Forward	5'-AACGTGAATCAGCTGAATGCG-3'
	Reverse	5'-GGTCTGCTGGATCTGCT-3'
BCAS0335	Forward	5'-CGACGTAGCTGCCGTTCTT-3'
	Reverse	5'-ATTTCGTCGACCGCGGTAAC-3'

III.3.4 Bacterial adhesion to epithelial cells

Adhesion experiments were carried out on 16HBE14o-, CFBE41o-, A549, and HeLa cell lines as described previously (Mil-Homens and Fialho, 2012), with some modifications. Cells were seeded in polystyrene microplates one day before infection at 1×10^6 cells/mL in a supplemented medium. The cells were infected with a multiplicity of infection (MOI) of 50:1. After infection, plates were centrifuged at 700 g for 5 min. The infected

monolayers were incubated for different time periods (15 min, 30 min, 2 h, 3 h, and 5 h min) at 37 °C in an atmosphere containing 5% CO_2. After incubation, each well was washed three times with PBS. For adhesion determination, the host cells were lysed by incubation with lysis buffer (10 mM EDTA, 0.25% Triton X-100) for 30 min at room temperature. The adhered bacteria were quantified by plating serial dilutions of the cell lysates. Results are expressed as a percentage of adhesion relatively to the initial bacterial dose applied. For further expression assays, the supernatant containing the non-adherent bacteria was recovered, and each well was washed three times with PBS. Cells and adherent bacteria were harvested by scratching and further resuspension in PBS. All the samples were centrifuged, suspended in RNAprotect Bacteria Reagent (Qiagen), and centrifuged again. The recovered pellets were stored at −80 °C.

III.3.5 Extracellular digestion of surface-exposed host cell membrane components

16HBE14o- cells were seeded 1 day before infection at 1×10^6 cells/mL. Before infection experiment, cellular monolayers were washed two times with HBS (HEPES buffer saline) and incubated with different digestive enzymes: pronase E (Sigma-Aldrich; 3.12 µg/mL in HBS), trypsin (Gibco, ThermoFisher; 6.25 µg/mL in HBS,) for 1 h, O-glycosidase (New England BioLabs; 2,500 U/well), and PNGase F (New England BioLabs; 2,500 U/well) for 6 h, in PBS (pH 7.4) at 37 °C CO_2 incubator. The supernatants with the resulting enzymatic-produced cellular fragments were recovered and inoculated with 5×10^7 CFU/mL of *B. cenocepacia* K56-2. The samples were incubated for 30 min at 37 °C. The concentrations of all the enzymes were optimized to guarantee the cellular and bacterial viability throughout the assay. HBS and serum-free MEM were used as controls. The treated cellular monolayers were washed three times with HBS, and 1 mL of serum-free MEM was added to each well. The cells were infected with a MOI of 50:1. After infection, plates were centrifuged at 700 g for 5 min. The infected monolayers were incubated for 30 min at 37 °C in an atmosphere containing 5% CO_2. After incubation, the supernatant containing the non-adherent bacteria was recovered, and each well was washed three times with PBS. Cells and adherent bacteria were harvested by scratching and further resuspension in PBS. All the samples were centrifuged, suspended in RNAprotect

Bacteria Reagent (Qiagen), and centrifuged again. The recovered pellets were stored at −80 °C.

III.3.6 Adherence to mucins

Bacterial adherence to mucins (mucin from the porcine stomach, type III, bound sialic acid 0.5%–1.5%, Sigma-Aldrich) was tested as described before with some modifications (Tomich and Mohr, 2003). Briefly, polystyrene microplates were coated with 1 mg/mL mucins (in PBS) and placed at 4 °C, overnight. Extracellular matrix proteins fibronectin and collagen type I were used as controls (10 µg/mL) (Mil-Homens, et al. 2010). The wells were washed twice with PBS and saturated with a 2% (w/v) bovine serum albumin (BSA) (NZYTech) solution for 1 h at room temperature. The wells were washed twice with PBS. Approximately 5×10^7 CFU/mL was added to each coated well. The plates were incubated 15, 30 min, 2, 3, or 5 h at 37 °C and washed 3 times with sterile PBS to remove unbound bacteria. The mucin-coated plates were also subjected to O-glycosidase treatment, as described previously. Adhesion to treated and untreated mucin-coated wells was performed during 2 h at 37 °C.

For adhesion determination, the wells were treated with 0.5% (v/v) Triton X-100 solution to desorb the bound bacteria. Plates were incubated for 2 h at room temperature under orbital agitation. One hundred microliters of the content of each well were removed, diluted in PBS, and plated on LB agar plates. Results are expressed as a percentage of adhesion relatively to the initial bacterial dose applied. For further expression assays, the wells were scratched, and the released bacteria suspended in PBS. The samples were centrifuged, suspended in RNAprotect Bacteria Reagent (Qiagen), and centrifuged again. The recovered pellets were stored at −80 °C.

III.3.7 Statistical analysis

All experiments were performed in a minimum of three independent replicates. Relative comparisons were made between corrected values with ANOVA test for significance. A P value < 0.05 was considered statistically significant.

III.4 Results

III.4.1 *B. cenocepacia* K56-2 TAAs transcripts are produced at different levels after bacterial adhesion to bronchial epithelial cells

We started this work by analyzing the expression profile of the 7 TAA genes in response to host cell contact (30 min). Thus, we performed quantitative real-time PCR from RNA samples obtained after *B. cenocepacia* adhesion to 16HBE14o- cells. The results of Figure III.1 showed a differential expression pattern for all the TAA mRNAs. The expression data were represented in comparison with the basal TAA mRNAs expression obtained from cells that were not subjected to contact with the host cells. The contact with bronchial epithelial cells caused different responses in the TAA-encoding genes suggesting a differentiated role for TAAs. Based on the levels of their transcript's expression, TAA genes were divided into two groups. The first one with considerably higher levels of expression (from 100- to more than 400-fold) included *bcaC*, *2418* and *BCAS0236*. A second group with lower expression values included *bcaA*, *bcaB*, *1115*, and *BCAS0335*. *BCAM2418* and *1115* mRNAs were the ones with higher and lower values of expression, respectively, spanning a difference of approximately 400× between them. *BCAM2418* and *BCAS0236* were the only genes that presented significantly different levels of expression when compared to basal control ($P < 0.001$ and $P < 0.0001$; Figure III.1). Based on the increased expression of these two genes, we postulated a prominent role of their implicating proteins in the process of bacterial adhesion to host cells. Therefore, we decided to pursue this study by characterizing the *BCAM2418* gene, the one that has the higher shift in expression levels.

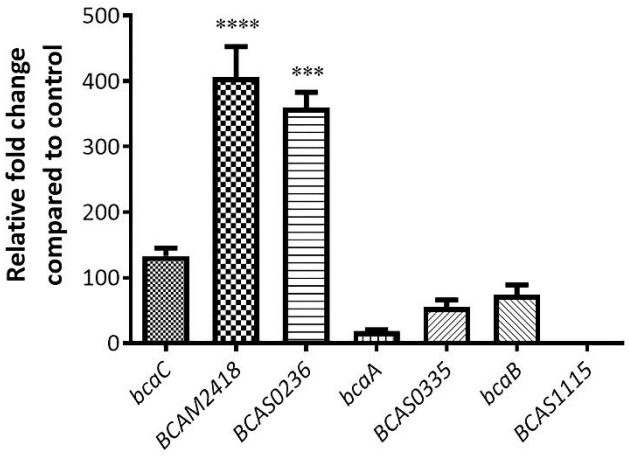

Figure III.1. Expression profile of TAA coding genes after adhesion to bronchial epithelial cells. Transcription levels of the 7 *B. cenocepacia* K56-2 TAA coding genes were obtained by qRT-PCR after 30 min of adhesion to 16HBE14o- cells. Results were normalized to the expression of the housekeeping *sigA* gene. Expression levels are represented as relative values in comparison to the expression levels in standard LB growth. All the results are from three independent experiments, and bars indicate SD. Expression of *BCAM2418* and *BCAS0236* is significantly higher when compared to standard LB growth. (*** P< 0.001; ****P< 0.0001).

III.4.2 *BCAM2418* transcriptional levels after adhesion are reliant on the nature of host cells

To determine whether *BCAM2418* expression after cellular contact was a direct response to a specific type of cell, we analyzed *BCAM2418* expression patterns after adhesion to a set of human cell lines. Figure III.2A represented the results obtained for *BCAM2418* expression after adhesion to HeLa, A549, 16HBE14o-, and CFBE41o- cell lines. It was notorious the difference in the levels of *BCAM2418* mRNA after adhesion to different cells. The contact with human bronchial epithelial cells, either from a CF or a functional airway, induced an increase in this gene expression. Adhesion to lung or cervix cell lines did not lead to any alteration in the expression levels.

The expression of *BCAM2418* was also evaluated in non-adherent bacteria, meaning the bacteria recovered in the supernatant after the adhesion assays. The obtained data (Figure III.2A) indicated that non-adherent bacteria had lower levels of *BCAM2418* mRNA when compared to adherent bacteria. These differences were especially evident

after adhesion to bronchial epithelial cells. *BCAM2418* expression was induced after bacterial contact with the cellular surface once the non-adherent bacteria did not show the same transcriptional response.

In parallel with the determination of *BCAM2418* gene expression, the adhesion capacity to different host cell lines was also assessed (Figure III.2B). The results were expressed in percentage of adhesion relatively to the initial bacterial load added to the cells. The results indicated that adhesion to A549 and HeLa cell lines was inferior when compared to adhesion to the bronchial epithelial cell lines. Bacterial cell adhesion assays to plastic were performed as a negative control. These results followed the same trend of the expression ones, with variations on adhesion percentages coupled to the type of cells used in the assay. Overall data indicated that *B. cenocepacia* K56-2 had a higher adhesion capacity toward bronchial epithelial cells (non-CF and CF) than to other types of cells.

III.4.3 *BCAM2418* gene expression profile during the early stages of infection

To follow the levels of *BCAM2418* expression after adhesion to 16HBE14o- cell line (approximately 400-fold mRNA expression), we evaluated the transcription of this gene at early and later time points of cellular contact (from 15 min to 5 h). The results represented in Figure III.3 showed a timeline pattern of *BCAM2418* expression that reached a peak after 30 min of adhesion. The same did not occur in the recovered non-adherent bacteria (not shown). The expression of this TAA gene began to increase soon after the first contact with the host cell (t = 15 min), starting to decrease after the adhesion process taken place (t = 2 h). Moreover, after 5 h of cellular contact, the levels of *BCAM2418* expression were lower than the ones obtained after the initial 15 min.

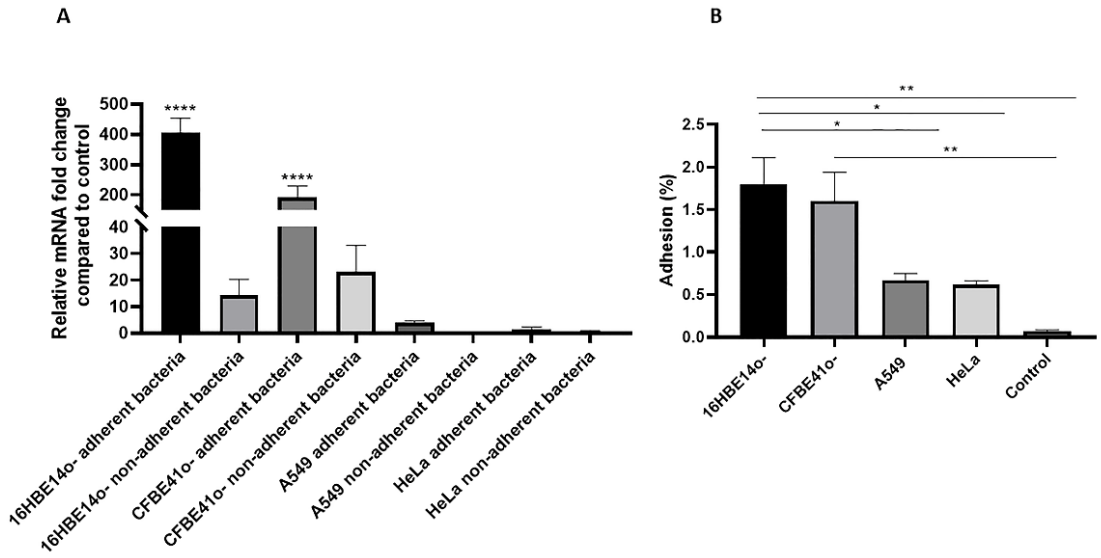

Figure III.2. ***BCAM2418*** **transcriptional levels after adhesion to human epithelial cells.** (**A**) Transcriptional levels of the *B. cenocepacia* K56-2 *BCAM2418* coding gene were obtained by qRT-PCR after adhesion to four lines of human epithelial cells: 16HBE14o- (bronchial, non-CF), CFBE41o- (bronchial, CF), A549 (lung), and HeLa (cervix). Expression results were also analyzed in non-adherent bacteria samples. Results were normalized to the expression of the housekeeping *sigA* gene. Expression levels are represented as relative values in comparison to the expression levels in standard LB growth. All the results are from three independent experiments, and bars indicate SD. Expression of *BCAM2418* after adhesion to 16HBE14o- and CFBE41o- cell lines are significantly higher when compared to standard LB growth. (****P < 0.0001). (**B**) Adherence to 16HBE14o-, CFBE41o-, A549, and HeLa cell lines expressed as a percentage of adhesion relatively to the initial bacterial load added to the cells. Adherence to A549 and HeLa cell lines was significantly lower when compared to adherence to both 16HBE14o- and CFBE41o- cell lines (*P < 0.05). Adherence to plastic was used as negative control.

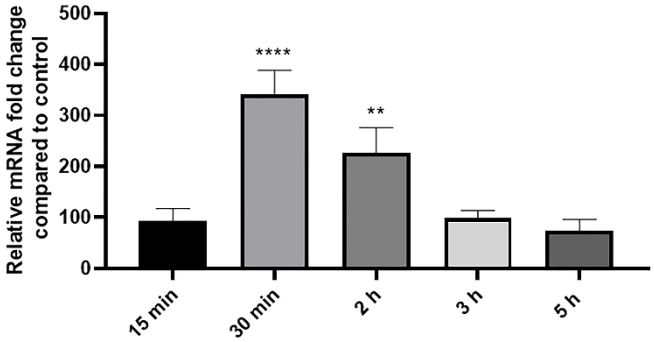

Figure III.3. ***BCAM2418*** **transcriptional levels over different times of host cellular contact.** Transcription levels of *BCAM2418* coding gene were obtained by qRT-PCR after different times of adhesion to 16HBE14o- cell line—15, 30 min, 2, 3, and 5 h. Results were normalized to the expression of the housekeeping *sigA* gene. Expression levels are represented as relative values in comparison to the expression levels in standard LB growth. All the results are from three independent experiments, and bars indicate SD. Expression of *BCAM2418* after 30 min and 2 h of adhesion to 16HBE14o- cells is significantly higher when compared to standard LB growth. (****P < 0.0001; **P < 0.01)

III.4.4 Enzymatic treatment of the host cell surface before adhesion cause a decrease in *BCAM2418* transcripts

To evaluate the requirement of a native cellular surface as a *stimulus* to induce *BCAM2418* expression, we proceeded with the enzymatic treatment of the host cell surface before the cellular adhesion. As shown in Figure III.4A, the treatment with proteases (pronase E or trypsin) or O- and N-glycosidases before the adhesion event caused a significant reduction in *BCAM2418* expression in comparison with untreated 16HBE14o- cells. This "shaving" strategy based on limited proteolytic digestion of host surface components (proteins and carbohydrates) correlated with a significant decrease (at least two times lower) of *BCAM2418* transcripts (Figure III.4A). In line with these data, we observed that incubation of *B. cenocepacia* cells with the supernatants containing the surface released components impacted on the *BCAM2418* gene transcription (Figure III.4A). Interestingly apart from N-glycosidase-treated cells, the values of *BCAM2418* expression after bacterial incubation with those supernatants were higher than the ones obtained after the adhesion to the respective treated cellular monolayers (Figure III.4A). These results raised the possibility that the carbohydrate-binding proteins or other glycoconjugates found on the host cell surface may serve as the recognition signals that directly or indirectly control the rate of *BCAM2418* expression. Moreover, the *BCAM2418* expression profile observed seemed to be finely tuned according to the glycosidase enzymatic pretreatment of the cells. Thus, we hypothesize that O- but not N-glycans may serve as a host cell signal to enhance the *BCAM2418* gene expression. As a complementary approach, we had also assessed the rate of *B. cenocepacia* K56-2 adhesion to enzyme-treated cells. As showed in Figure III.4B, although slightly reduced when compared to untreated ones, the proteolytic digestion of host cell membrane constituents did not seem to affect cell adhesion significantly.

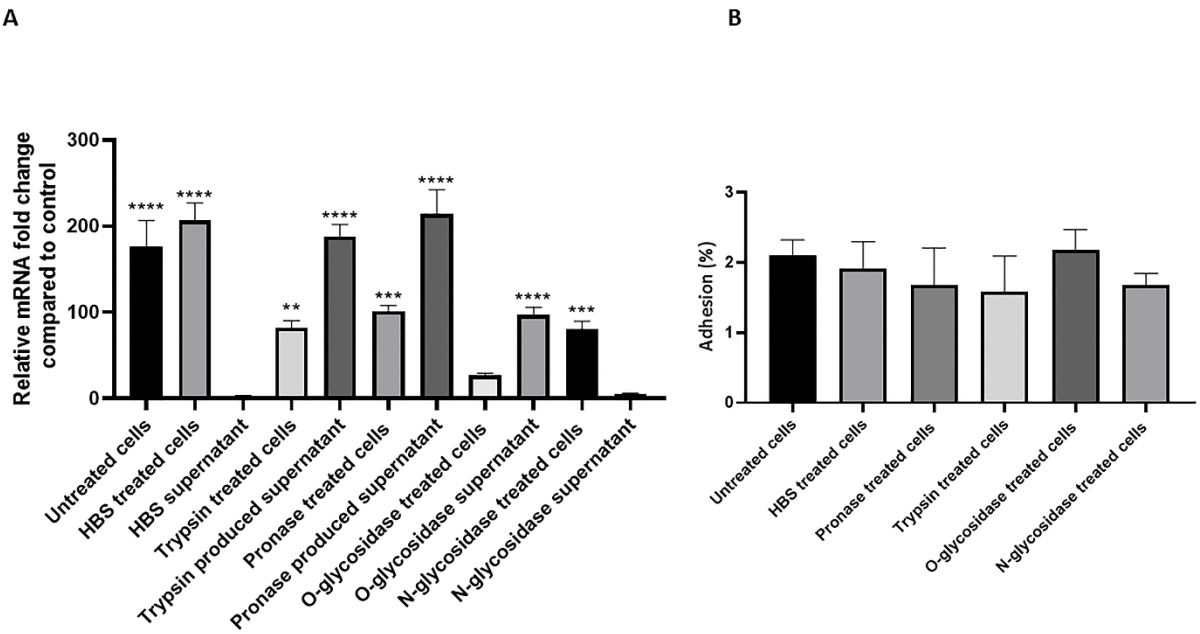

Figure III.4. *BCAM2418* transcript levels and *B. cenocepacia* adhesion after enzymatic treatment of the host cell surface before adhesion. (**A**) Transcription levels of *B. cenocepacia* K56-2 *BCAM2418* coding gene were obtained by qRT-PCR after adhesion to untreated 16HBE14o- cell line, HBS-, pronase-, trypsin-, O-glycosidase-, and N-glycosidase-treated cells. Expression results were also analyzed in bacteria incubated with the supernatant containing the enzymatically produced fragments of the treated cellular surface. Results were normalized to the expression of the housekeeping *sigA* gene. Expression levels are represented as relative values in comparison to the expression levels in standard LB growth. All the results are from three independent experiments; bars indicate SD. Expression of *BCAM2418* after adhesion to untreated 16HBE14o- cells and to HBS control is significantly higher when compared to standard LB growth. (****P < 0.0001). *BCAM2418* transcription levels after bacterial incubation with pronase, trypsin, and O-glycosidase produced supernatant are significantly higher when compared to standard LB growth (****P < 0.0001). (**B**) Adherence to 16HBE14o- cell line, HBS-, pronase-, trypsin-, O-glycosidase-, and N-glycosidase-treated cells expressed as a percentage of adhesion relatively to the initial bacterial load added to the cells. All the results are from three independent experiments, and bars indicate SD. Adherence to treated cells was not significantly different in comparison to untreated ones (**P < 0.01; *** P < 0.001; **** P < 0.0001).

III.4.5 Adhesion properties and *BCAM2418* expression-based comparison of *B. cenocepacia* K56-2 to mucins and extracellular matrix proteins

Since one of the primary O-glycosylated-type proteins of mucus is mucin, we tested the adherence capacity of *B. cenocepacia* K56-2 to mucins and the impact on *BCAM2418* gene expression profile. Two extracellular matrix (ECM) proteins, namely fibronectin and collagen type I, were used as controls. As shown in Figure III.5A, the *B. cenocepacia*

K56-2 exhibited significantly higher binding to mucins when compared to ECM proteins. After 3 and 5 h of mucin contact, the rate of adhesion reached approximately 20 and 50%, respectively. In contrast, the percentages of adhesion to the ECM proteins were like the ones obtained with the BSA control and relatively constant in all the adhesion times assessed. Interestingly, we also observed that the effect of high cell adhesion on a mucin layer was directly linked with the levels of *BCAM2418* transcripts. The data indicated that the expression levels of this TAA gene significantly increased over time. The longer the bacteria contact with mucins, the higher the amount of *BCAM2418* transcripts produced (Figure III.5B). Taken together, the results described above revealed that *B. cenocepacia* K56-2 could sense the environment through promoting a specific interaction with mucins which thereby triggered the expression of the *BCAM2418* gene.

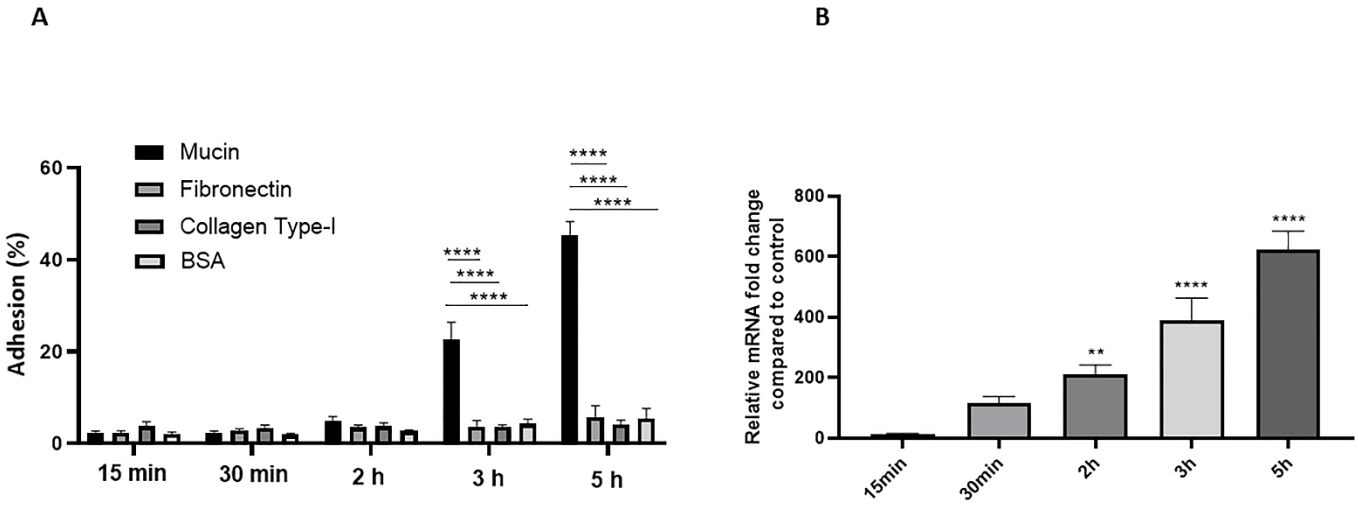

Figure III.5. *B. cenocepacia* adherence to mucins and *BCAM2418* transcript levels over different times of contact. (**A**) Adherence of *B. cenocepacia* K56-2 to BSA (control), collagen type I, fibronectin, and mucins during defining timelines—15, 30 min, 2, 3, and 5 h. Results are expressed as the percentage of adhesion relatively to the initial bacterial load added to the cells. BSA was used as a negative control of the assay. All the results are from three independent experiments, and bars indicate SD. The binding capacity to mucins increases over time. The adhesion percentage to mucins is significantly higher after 3 h and 5 h of contact (****P < 0.0001). (**B**) *BCAM2418* transcript levels after adherence to mucins in a defined timeline. Transcription levels of *B. cenocepacia* K56-2 *BCAM2418* coding gene were obtained by qRT-PCR after adhesion to mucin coatings during 15, 30 min, 2, 3, and 5 h. Results were normalized to the of the housekeeping *sigA* gene. Expression levels are represented as relative values in comparison to the expression levels in standard LB growth. All the results are from three independent experiments, and bars indicate SD. Expression of *BCAM2418* after 2, 3, and 5 h of mucin adhesion is significantly higher when compared to standard LB growth. (**P < 0.01; ****P < 0.0001)

III.4.6. Enzymatic deglycosylation of mucins is linked to the ablation of *BCAM2418* expression and a significant reduction of bacterial adhesion

By placing *B. cenocepacia* K56-2 cells in contact with a mucin layer, we observed a significant overexpression of the *BCAM2418* gene and enhancement of the bacterial adhesion. To further investigate this finding, we proceed with the enzymatic deglycosylation of mucins with an O-glycosidase. As such, we intended to discriminate if the bacterial cell surface recognition was exerted through the binding to the protein itself, their O-linked glycan cores, or both. As shown in Figure III.6A, after the enzymatic deglycosylation of mucins, the *BCAM2418* gene expression was abolished. However, the incubation of *B. cenocepacia* K56-2 cells with the supernatant containing the O-linked glycans released from mucins significantly enhanced the mRNA expression of *BCAM2418*. Moreover, we also found that the pretreatment of mucins with the O-glycosidase enzyme could effectively reduce bacterial adhesion (Figure III.6B). Taken together, these results indicated that *B. cenocepacia* K56-2 bound to mucins by mediating recognition to the O-glycans attached to the external mucin surface. Furthermore, such recognition was mediated, at least in part, via activation of the trimeric autotransporter adhesin gene *BCAM2418*.

III.5 Discussion

B. cenocepacia epidemic strains of the ET-12 lineage are reported to have 7 TAA-encoding genes (Mil-Homens, et al. 2010; Mil-Homens and Fialho, 2011). Mil-Homens and colleagues unveil the multifunctional functions of two *B. cenocepacia* K56-2 TAAs (BcaA and BcaB) clustered together in chromosome 2 (Mil-Homens and Fialho, 2011, 2012; Mil-Homens, et al. 2014, 2017). The existence of these surface proteins contributes to the overall pathogenicity of this bacterium (Mil-Homens and Fialho, 2012; Mil-Homens, et al. 2014). It is known that TAAs can mediate host cell adherence through different types of interactions. These contacts vary from non-specific events to highly specific bindings between adhesins and host receptors (Ofek, et al. 2013). Therefore, TAAs are critical players in defining bacterial tropism to particular host tissue and are

determinants of the early stages of infection (Thanassi, 2011). We started this work by assessing the expression levels of the 7 TAA-encoding genes after 30 min of adherence to host bronchial cells (Figure III.1). TAA genes revealed a different pattern of expression, which may indicate different aptitudes of bacterial adhesion. Among those, *BCAM2418* was the TAA gene with the highest expression after contact with 16HBE14o- cells. Little is known about BCAM2418 function for *B. cenocepacia* pathogenicity; *in silico* analyses revealed BCAM2418 as a protein with unique features, like its length, its structural polymorphism and its extensive serine-rich repetitive motifs (Mil-Homens and Fialho, 2011).

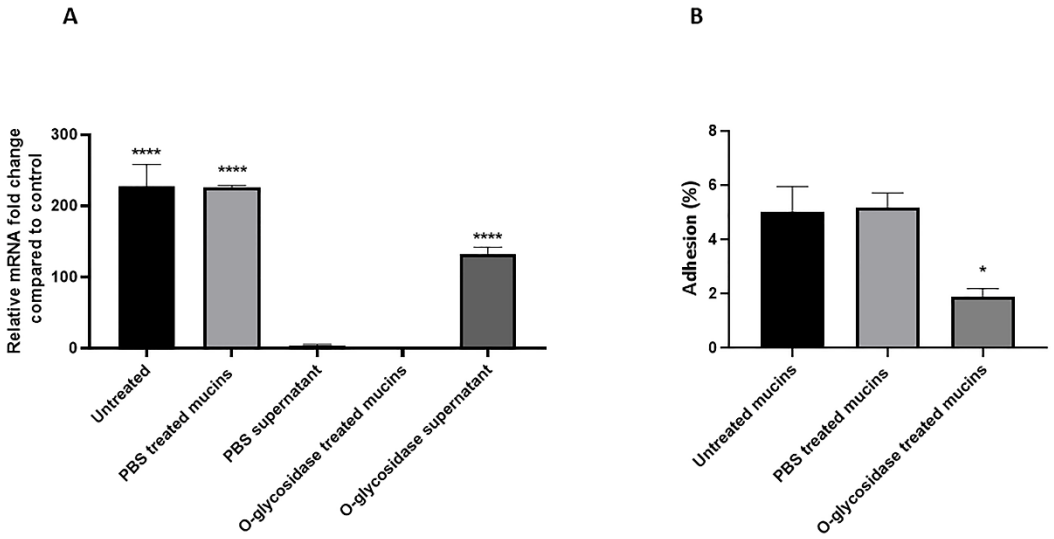

Figure III.6. *BCAM2418* transcript levels and *B. cenocepacia* adhesion after enzymatic treatment of the mucin-coated surfaces before adhesion. (**A**) Transcription levels of *B. cenocepacia* K56-2 *BCAM2418* coding gene were obtained by qRT-PCR after adhesion to untreated mucin-coated wells, HBS- and O-glycosidase-treated mucin-coated wells. Expression results were also analyzed in bacteria incubated with the supernatant containing the enzymatically produced fragments of the treated surface. Results were normalized to the expression of the housekeeping *sigA* gene. Expression levels are represented as relative values in comparison to the expression levels in standard LB growth. All the results are from three independent experiments; bars indicate SD. Expression of *BCAM2418* after adhesion to untreated mucin-coated wells and HBS control is significantly higher when compared to standard LB growth. (****P < 0.0001). *BCAM2418* transcription levels after bacterial incubation with O-glycosidase produced supernatant are significantly higher when compared to standard LB growth (****P < 0.0001). (**B**) Adherence to mucin-coated wells, HBS- and O-glycosidase-treated wells expressed as a percentage of adhesion relatively to the initial bacterial load added to the cells. All the results are from three independent experiments, and bars indicate SD. Adherence to treated mucins was significantly different in comparison to untreated ones (*P < 0.05).

To begin to address the cell specificity of *BCAM2418* gene response, we compared the bacterial adhesion in a panel of four cell lines. Interestingly, from both bronchial cells tested, 16HBE14o- (non-CF) and CFBE41o- (CF), the contact with the non-CF ones triggered a notable increase in *BCAM2418* expression. These results followed the same trend that the performed adhesion assays, in which the higher adhesion rates were achieved after contact with the non-CF cells (Figure III.2). It was possible that, at least *in vitro* and under the experimental conditions used, non-CF cells were preferentially recognized by *B. cenocepacia* K56-2 when compared to the other studied human cell lines, including the CF cells. Also, direct contact with the host cell was likely a need for *BCAM2418* overexpression once the non-adherent bacteria did not show increased levels of *BCAM2418* transcription. *BCAM2418* expression appeared not to be prompted by any component of the retained supernatant that may content cellular products and secreted molecules. This fact enhanced the assumption that was the physical recognition of a cellular target component by *B. cenocepacia* that led to the increased expression of this TAA mRNA. This hypothesis was reinforced by previous studies that point out the interaction of *B. cenocepacia* and other Bcc species with extracellular molecules of airway cell lines as an essential set point of infection (Pacello, et al. 2016; Mil-Homens, et al. 2017).

The host cell proximity was a requirement to stimulate the *BCAM2418* transcription. *BCAM2418* expression followed a differential expression pattern that varied with the time of cellular contact (Figure III.3). The highest level of expression was obtained after 30 min of *B. cenocepacia*-16HBE14o- adhesion. The presence of BCAM2418 TAA on the surface of the bacteria could play an essential role in the initial steps of infection. The variation in adhesin genes expression after a particular *stimulus* was mostly linked to their function and requirement to play a particular role in pathogenesis (Sheets and St Geme, 2011; Berne, et al. 2015). Unfortunately, despite many efforts, we failed to obtain a *BCAM2418* mutant, and hence, we were unable to perform the mutant phenotypic analysis and determine the impact of this gene product.

Previous studies shown the specificity of Bcc species to interact with lung epithelial cells (Sajjan, et al. 2004; McClean and Callaghan, 2009). In this scenario, we aimed to disclosure the cellular component that is recognized by *B. cenocepacia* K56-2 and

prompted an overexpression of *BCAM2418* gene. It is known that protein or glycoconjugate host receptors mediate binding of Bcc species to the airway epithelium through bacterial surface components such as flagella, pili, and non-pilus adhesins (Urban, et al. 2005; McClean and Callaghan, 2009; Drevinek and Mahenthiralingam, 2010). In this work, a 16HBE14o- cellular monolayer was enzymatically altered using either proteases (trypsin or pronase E) or glycosidases (O- or N-linked). The cell surface "shaving" significantly reduced the *BCAM2418* transcription in adherent *B. cenocepacia* K56-2 but did not affect the bacterial adhesion (Figure III.4). Moreover, the bacterial incubation with the resulting supernatant fraction restored the signaling and subsequent *BCAM2418* overexpression. It became clear the requirement of a physical contact with a protein/O-linked glycoprotein component of the host cell surface to turn on the *BCAM2418* expression. These findings led us to hypothesize that membrane-anchored O-glycosylated mucins may act as a host cell receptor for *B. cenocepacia* K56-2 that directly or indirectly lead to the overexpression of the *BCAM2418* gene. To further validate this finding, we evaluated bacterial adhesion and *BCAM2418* gene expression on a mucin-coating surface; ECM-coated plates were used as control. The effect of mucins, but not the ECM proteins, on bacterial adhesion and further *BCAM2418* overexpression was noteworthy and increased over time (Figure III.5). In this scenario, we were interested in investigating if the adhesion properties and the *BCAM2418* gene expression response to mucin exposure are dictated by the O-glycans present in mucins or instead by the core protein itself. For these experiments, deglycosylated mucins were used to corroborate that mucin-associated glycans play a crucial role in the activation of the *BCAM2418* gene with possible implications in bacterial adhesion (Figure III.6).

In the context of CF disease, it is established that *Pseudomonas aeruginosa* and various Bcc species use secretory mucins to adhere to lung epithelial cells (McClean and Callaghan, 2009). Moreover, mucin glycan domains can serve as releasable decoys to prevent infection (Lindén, et al. 2009; Lillehoj, et al. 2019). Paradoxically, other pathogens have been described to use transmembrane mucins to enter the host cells. This is the case of various *Salmonella enterica* serovars, *Staphylococcus aureus*, and *Helicobacter pylori* where the mucin glycan-rich domains serve as receptors for infection (Vesterlund, et al. 2006; Navabi, et al. 2012; Gipson, et al. 2014; Huang, et al. 2016; Li,

et al. 2019). However, until recently, the structure elucidation of the mucin glycan moieties and their bacterial counterparts involved in the binding events remains difficult to determine. Taken together, our present findings suggested that membrane-tethered glycosylated mucins exposed on the surface of lung epithelial cells may represent a group of receptors mediating the primary association of *B. cenocepacia* K56-2 with host cells. We also hypothesizede that the TAA BCAM2418, among other putative adhesive factors, operates to promote the initial contact of the bacteria in the infection process.

Comparative DNA sequence analysis of *BCAM2418* genes (structural and promoter regions) of various *B. cenocepacia* isolates revealed that their lengths greatly vary according to the number of repetitive elements. These data supported the hypothesis that the *BCAM2418* gene may be subject to phase and antigenic variation during disease. Phase variation permits the on/off switch in expression, while antigenic variation leads to the alteration in the amino acid sequence of extracellular regions of the protein to prevent recognition by the host immune system (Poole, et al. 2013). Previous studies have revealed the alteration in TAAs expression in define infection-linked conditions and environments (Sheets and St Geme, 2011; Lu, et al. 2013). *Haemophilus* cryptic genospecies Cha TAA was found to vary its peptide repeat number gradually during the infection time course. Sheets and St. Geme found that the expansion of Cha amino acid tandem repeats caused a decrease in Cha binding capability; and also, that this expansion and contraction of the Cha neck motifs could, in theory, balance the bacteria necessity to colonize with the need to disperse in the host or evade the immune system (Sheets, et al. 2008; Sheets and St Geme, 2011). *In silico* analyses of BCAM2418 revealed the presence of an extensive number of amino acid repeats that vary in size but seems to maintain an SLST signature (Mil-Homens and Fialho, 2011). The overexpression of *BCAM2418* might be a mechanism to induce variation in the number of these repeat motifs. This antigenic variation could, in turn, play a similar role to the one reported for Cha TAA. Nevertheless, we could not rule out the alteration in *BCAM2418* expression as a result of an on/off switch. Furthermore, the serine and threonine enrichment of these repetitions may be related to putative O-linked glycosylation of BCAM2418 extracellular domains (Zhou and Wu, 2009; Iwashkiw, et al. 2013). O-linked glycosylation systems have been described in bacterial systems in

the past years, particularly among pathogenic bacteria (Vik, et al. 2009; Hanuszkiewicz, et al. 2014). The glycosylation of bacterial proteins is usually related to surface and outer membrane proteins. Their sugar enrichment was shown to be linked to adhesive and invasive capacities and protective immunity (Szymanski and Wren, 2005; Lu, et al. 2015). Thus, integrated *in silico* and experimental results could bring new insights regarding BCAM2418 importance as an essential virulence factor and as a new key player in the earlier steps of *B. cenocepacia* infection.

In summary, we first profiled the expression of the 7 virulence-associated trimeric autotransporter adhesin (TAA) genes from *B. cenocepacia* K56-2 during the early stage of bacteria–host cell interaction. Among those, we found that *BCAM2418* gene expression shows an on–off switch and a fine-tuned control in response to a time frame and a particular host cell environment. We also found that physical contact between the bacterium and the host cell is required to trigger the expression of the *BCAM2418* TAA with the consequent increase of bacterial adhesion. Finally, we hypothesized that the glycosylated extracellular domain of transmembrane mucins might be cell surface receptors used by *B. cenocepacia*. Further research using mucin-based technologies will contribute to advance our understanding of the mechanisms underlying the early stages of the bacteria–host crosstalk.

Data availability statement

All data are provided in full in the results section of this chapter.

Acknowledgments

The Portuguese Science and Technology Foundation (FCT) BIOTECnico PhD program (grant PD/BD/116940/2016) supported this work. FCT also provides postdoctoral research grants for D. Mil-Homens (SFRH/BPD/91831/2012). Funding received by iBB—Instituto for Bioengineering and Biosciences from FCT (UIDB/04565/2020) and Programa Operacional Regional de Lisboa 2020 (Project N. 007317) is acknowledged. We thank Dieter Gruenert, Pacific Medical Center Research Institute, San Francisco, CA,

for providing us with the 16HBE14o- and CFBE41o- cell lines. We also acknowledge John LiPuma from the University of Michigan, who kindly provided a Burkholderia strain.

Declaration of Competing Interest

The authors have no conflict of interest to declare.

IV. *BURKHOLDERIA CENOCEPACIA* BCAM2418-INDUCED ANTIBODY INHIBITS BACTERIAL ADHESION, CONFERS PROTECTION TO INFECTION AND ENABLES IDENTIFICATION OF HOST GLYCANS AS ADHESIN TARGETS

Journal paper

Pimenta AI, Kilcoyne M, Bernardes N, Mil-Homens D, Joshi L, Fialho AM. *Burkholderia cenocepacia* BCAM2418-induced antibody inhibits bacterial adhesion, confers protection to infection and enables identification of host glycans as adhesin targets. 2020 (Submitted to Cellular Microbiology, under revision).

IV.1 Abstract

Trimeric Autotransporter Adhesins (TAA) found in Gram-negative bacteria play a key role in virulence. This is the case of *Burkholderia cepacia* complex (Bcc), a group of related bacteria able to cause infections in patients with cystic fibrosis. These bacteria use TAAs, among other virulence factors, to bind to host protein receptors and their carbohydrate ligands. Blocking such contacts is an attractive approach to inhibit Bcc infections. In this study, using an antibody produced against the TAA BCAM2418 from the epidemic strain *Burkholderia cenocepacia* K56-2, we were able to uncover its roles as an adhesin and the type of host glycan structures that serve as recognition targets. The neutralization of BCAM2418 was found to cause a reduction in the adhesion of the bacteria to bronchial cells and mucins. Moreover, *in vivo* studies showed that the anti-BCAM2418 antibody exerted an inhibitory effect during infection in *Galleria mellonella*. Finally, inferred by glycan arrays, we were able to predict for the first time, host glycan epitopes for a TAA. We showed that BCAM2418 favored binding to 3'sialyl-3-fucosyllactose, histo-blood group A, α-(1,2)-linked Fuc-containing structures, Lewis structures and GM1 gangliosides. Additionally, the glycan microarrays demonstrated similar specificities of *Burkholderia* species for their most intensely binding carbohydrates.

IV.2 Introduction

Members of the denominated *Burkholderia cepacia* complex (Bcc; group of 22 species), can cause severe infections in humans and animals (Scoffone, et al. 2017). Among those, *Burkholderia cenocepacia* and *Burkholderia multivorans* are particularly dangerous for cystic fibrosis (CF) patients (Scoffone, et al. 2017). They are highly adapted to the respiratory tract, show intrinsic resistance to commonly used antibiotics, and elicit an unusual chronic inflammation (Mahenthiralingam, et al. 2008). In some cases, these infections progress to a necrotizing pneumonia and a generalized sepsis (cepacia

syndrome) (Mahenthiralingam, et al. 2008; Scoffone, et al. 2020). Based on such factors, therapeutic options against *Burkholderia* species are limited to few agents and new drugs and alternative therapies are urgently needed. One potential solution forward is through the use of anti-adhesion therapies.

B. cenocepacia is known to have a complex network of surface proteins with adhesion properties for host molecules. Such group of proteins (adhesins) is needed for the initial recognition and binding to host cell molecules including extracellular matrix (ECM) components and mucins (Sajjan, et al. 2000; Saldías, et al. 2009; Mil-Homens and Fialho, 2011; Dennehy, et al. 2016; Pimenta, et al. 2020a; Pimenta, et al. 2020b). Among the adhesins, the trimeric autotransporter adhesins (TAAs) represent a target protein model for anti-adhesion therapies. TAAs are represented across Bcc species and are known as key virulence factors (Mil-Homens and Fialho, 2011; 2012; Mil-Homens, et al. 2014; Mil-Homens, et al. 2017). TAAs are cell surface proteins secreted to the outer membrane by the type Vc secretion system. They have a modular architecture with a C-terminal anchor and a variable extracellular set of fiber-like stalk and globular-like head regions. The C-terminal anchor is highly conserved whereas the head and stalk regions of the passenger domain vary among TAAs (Cotter, et al. 2005; Łyskowski, et al. 2011).

The *B. cenocepacia* J2315 genome encodes for seven TAAs distributed between chromosome 2 and 3 (Mil-Homens and Fialho, 2011; 2012; Mil-Homens, et al. 2014; Pimenta, et al. 2020b). BCAM2418 is one of the largest TAAs, comprising 2775 amino acids and exhibiting a high proportion of serine residues consensus motifs distributed across its extracellular passenger domain (Mil-Homens and Fialho, 2011). We recently described that the expression of *BCAM2418* requires physical contact between bacteria and epithelial host cells and displays a fine-tuned control during time and is particularly relevant in the early stages of infection (Pimenta, et al. 2020a). Moreover, we found that the surface exposed head-stalk domains of BCAM2418 mediates bacterial binding to O-linked glycans conjugated to host cell-surface mucins (Pimenta, et al. 2020a). Thus, the actions of the *B. cenocepacia* BCAM2418 TAA represent a paradigm for how adhesins are key players at the bacteria-host cell interface.

Host glycans represent a large set of ligands for bacterial binding in several tissues, being important in host-bacteria cross-talk during infection (Taylor, et al. 2018). Glycan-based

microarrays have become a powerful technique for glycan-binding analysis, supporting the screening of bacterial interactions with specific carbohydrate structures (Flannery, et al. 2015; Martinez, et al. 2020). Glycan microarrays can be tailored to carry relevant structures or patterns providing high-throughput information on protein-carbohydrate interactions using a small amount of sample (Geissner, et al. 2014; 2019; Martinez, et al. 2020). The identification of carbohydrate ligands for a range of proteins, toxins and whole bacteria have been performed in past years for several species and specific proteins like *Burkholderia* lectins (Audfray, et al. 2012; Deng, et al. 2014; Day, et al. 2015; De Oliveira, et al. 2017; Sýkorová, et al. 2020).

The purpose of this study was to assess the inhibitory effects of an antibody produced against the TAA BCAM2418 from the epidemic strain *B. cenocepacia* K56-2*. In vitro* and *in vivo* results revealed that the antibody exhibited specific responses. Moreover, following interrogation of a glycan microarray with fluorescently labelled *Burkholderia* species, it was possible to infer the interactions of bacteria with their glycan ligands. Overall, this work revealed the importance of BCAM2418 as a mediator of host-bacteria cross-talk during infection, and may direct future vaccine development.

IV.3 Material and Methods

IV.3.1 Bacterial growth conditions

B. cenocepacia clinical isolates K56-2 and J2315 were provided by Prof. J. J. LiPuma, University of Michigan. *B. contaminans* IST408 and *B. multivorans* VC13401 clinical isolates were previously described (Coutinho, et al. 2015; Silva, et al. 2016). *Escherichia coli* BL21-DE3 was a purchased strain (Invitrogen). Bacteria were routinely cultured in Luria–Bertani (LB) broth, at 37 °C with orbital agitation (250 rpm).

IV.3.2 Human bronchial cell line and cell culture

16HBE14o- bronchial epithelial cells were immortalized and characterized by Dr. Gruenert and co-workers (Cozens, et al. 1994) and kindly provided. Cells were routinely maintained in fibronectin/vitrogen coated flasks in Minimum Essential Medium with Earle's salt (MEM) (Gibco, ThermoFisher) supplemented with 10% fetal bovine serum (FBS) (Lonza), 0.292 g/L L-glutamine (Sigma-Aldrich) and penicillin/streptomycin 100 U/mL (Gibco, ThermoFisher) in a humidified atmosphere at 37 °C with 5% CO_2.

IV.3.3 Production and purification of a BCAM2418 fragment

A fragment of *BCAM2418* gene, encoding 135 amino acids (aa) of the passenger domain (aa 100 to 234), was amplified using *B. cenocepacia* K56-2 genomic DNA as template and primers FrBCAM2418Fw (5'-CGGGATCCGTTGCGGGCTGTAACTCCA-3') and FrBCAM2418Rv (5'-CCCAAGCTT**TCA**TATTGCAGTTGGCCGT-3'), containing, respectively, *Nde*I and *Hind*III restriction sites (underlined) and a stop codon (bold). The fragment was cloned into pWH844 plasmid with a 6xHis tag at its N-terminus and the resulting construction was introduced by electroporation into *E. coli* BL21-DE3. To overexpress the $BCAM2418_{100\text{-}234}$ fragment, cells were incubated overnight in LB medium at 37 °C with 150 mg/L of ampicillin and cultured, at an initial optical density at 640 nm (OD_{640}) of 0.1, in LB medium with ampicillin. The cells were grown until an OD_{640} 0.6 and induced with IPTG (Sigma-Aldrich) at a final concentration of 0.5 mM for 6 h at 30 °C, 250 rpm. Cells were harvested by centrifugation at 8,000 rpm for 10 min at 4 °C and resuspended in buffer A (20 mM sodium phosphate, 500 mM NaCl, 20 mM imidazole, pH 7.8).

Cells were disrupted by sonication and the purification steps were performed by histidine affinity chromatography, using HisTrap FF columns (GE Healthcare). Briefly, disrupted cells were centrifuged for 30 min, at 12,000 rpm and 4 °C; the pellet was resuspended in a solution of 0.1% Triton X-100 and the suspension was centrifuged in the same conditions. The resulting pellet was resuspended in a solution of 8 M urea, 2.5 mM DTT, in buffer A, and incubated for 1 h at room temperature with mild agitation. The sample was centrifuged at 12,000 rpm for 30 min, the supernatant was collected, and the concentration of urea was adjusted to 6 M. The sample was then loaded into a

1 ml HisTrap FF column (GE Healthcare) equilibrated with buffer A with 6 M of urea, in an AKTA purifier system, following the manufacturer's instructions. The amount of urea was reduced by a continuous gradient (from 6 M to 1 M) over 60 column volumes and a flow rate of 0.5 mL/min. BCAM2418$_{100\text{-}234His}$ fragment elution was achieved with a continuous imidazole gradient (from 20 to 500 mM) in the same buffer (buffer A, 1 M urea).

IV.3.4 Generation of an anti-BCAM2418 antibody

After purification, endotoxins and pyrogens from *E. coli* host strain were removed from the elution fractions using 1 mL Detoxi-Gel™ Endotoxin Removing Gel (Thermo Scientific) following the manufacturer's instructions. Finally, BCAM2418$_{100\text{-}234His}$ fragment was concentrated by centrifugation at 4 °C with Amicon Ultra centrifugal filters (Millipore) with a molecular mass cutoff of 3 kDa. BCAM2418$_{100\text{-}234His}$ fragment concentration was estimated using a UV spectrophotometer (ND-1000 UV-Vis, NanoDrop Technologies, USA). The purity of the fragment was analyzed by 15% acrylamide sodium dodecyl-polyacrylamide gel electrophoresis (SDS-PAGE). Polyclonal antibodies against BCAM2418 were produced by goat immunization (Sicgen) with recombinant BCAM2418$_{100\text{-}234His}$ fragment. The resulting immunized serum was then purified by affinity chromatography (Sicgen), and the resulting purified anti-BCAM2418 antibody was used in all experiments.

IV.3.5 Bacterial membrane extracts

Bacterial cultures of *B. cenocepacia* K56-2, *B. cenocepacia* J2315, *B. multivorans* VC13401, *B. contaminans* IST408 and *E. coli* BL21-DE3 were grown overnight in 200 mL of LB broth, as mentioned above. After growth, bacteria were harvested by centrifugation at 9,000 rpm at 4 °C for 10 min. Bacterial pellets were resuspended in 50 mM Tris-HCL (pH 7.4) buffer, containing a protease inhibitor mixture (Roche), 1 mM phenylmethylsulfonyl fluoride (PMSF) (Sigma), 50 µg/mL DNase (Qiagen), and 50 µg/mL RNase (Sigma). The bacterial suspension was sonicated in ice. Cell debris was removed by centrifugation at 10,000 rpm for 15 min at 4 °C, and the supernatant was

ultracentrifuged at 24,000 rpm for 1 h at 4 °C. The final pellet containing total membranes was resuspended in 50 mM Tris-HCl (pH 7.4) buffer, containing a protease inhibitor mixture (Roche) and 1 mM PMSF (Sigma). The total protein quantification was performed by using a Bradford protein assay kit (Bio-Rad Laboratories).

IV.3.6 Immunoprecipitation and confirmation of BCAM2418 TAA

Bacterial membrane extracts were used for immunoprecipitation of BCAM2418 TAA. Briefly, 150 µg of membrane proteins were mixed with 50 µg anti-BCAM2418 antibody and incubated overnight at 4 °C. Then, 100 µL Pierce™ Protein G Agarose (Thermo Scientific) were added and the mix was incubated for 2 h at room temperature with mild agitation. Four rinses with 500 µL of immunoprecipitation buffer (25 mM Tris-HCl, 150 mM NaCl, pH 7.4) were performed, the sample was then centrifuged and the resulting pellet containing the protein G beads and the precipitated BCAM2418 was resuspended in 50 µL of sample buffer (Laemmli buffer with 5% (v/v) 2-β-mercaptoethanol and 5% (v/v) bromophenol blue), boiled for 10 min and separated by 6% SDS-PAGE.

For western blot analysis, proteins were transferred onto nitrocellulose membranes using a TransBlot Turbo transfer system (Bio-Rad). Membranes were blocked with 5% (w/v) non-fat dry milk in phosphate-buffered saline (PBS) containing 0.5% (v/v) Tween 20 (PBS-T) (blocking solution) for 1 h at room temperature. Blocked membranes were then incubated with purified anti-BCAM2418 antibody (1:2,000 dilution in blocking solution) overnight at 4 °C, washed three times for 5 min each wash with PBS-T and incubated with secondary antibody rabbit anti-goat conjugated to horseradish peroxidase (1:2,000 dilution in PBS-T) (Santa Cruz), for 1 h at room-temperature. Membranes were washed 5 times with PBS-T and proteins were detected by the addition of ECL 1 (2.5 mM luminol, 400 µM ρ-coumaric acid, 100 mM Tris-HCl pH 8.6) and ECL 2 (0.15% H_2O_2, 100 mM Tris-HCl pH 8.6) reagents as a substrate and the chemiluminescence captured by Fusion Solo (Viber Lourmat) equipment.

IV.3.7 Adhesion of epithelial cells

Adhesion experiments were carried out on 16HBE14o- bronchial cells as described previously (Mil-Homens and Fialho, 2012), with some modifications. Cells were seeded in polystyrene 24 well microplates 1 day prior to infection at 1 x 10^6 cells/mL in supplemented medium. Bacterial strains were grown as described above. The cells were infected with a multiplicity of infection (MOI) of 50:1. After infection, plates were centrifuged at 700 x g for 5 min. The infected monolayers were incubated for 30 min at 37°C in an atmosphere containing 5% CO_2. After incubation each well was washed three times with PBS. For adhesion determination the host cells were lysed by incubation with lysis buffer (10 mM EDTA, 0.25% Triton X-100) for 30 min at room temperature. The adhered bacteria were quantified by plating serial dilutions of the cell lysates.

The ability of the antibody (anti-BCAM2418) to inhibit adhesion to epithelial cells was also assessed. Bacterial suspensions were incubated with anti-BCAM2418 goat polyclonal antibody (0.01 to 0.5 mg/mL) for 90 min at room temperature. Samples were washed once with PBS and used to infect cell monolayers as described above. Results were expressed as a percentage of adhesion relatively to the initial bacterial dose applied. All the experiments were repeated at least three times and the mean of three experiments reported.

IV.3.8 Adherence to mucin

Bacterial adherence to mucin (mucin from porcine stomach, type III, Sigma-Aldrich) was tested as described before with some modifications (Pimenta, et al. 2020a). Briefly, polystyrene 24 well microplates were coated with 1 mg/mL mucins (in PBS) and placed at 4 °C overnight. The ECM proteins fibronectin and collagen type I were also used (10 µg/mL) to coat microplates (Mil-Homens, et al. 2010). The wells were washed with PBS and saturated with a 2% (w/v) bovine serum albumin (BSA) solution for 1 h at room temperature and washed twice with PBS. Approximately 5 x 10^7 CFU of bacteria were added to each coated well. The number of CFUs was calculated based on the load of bacteria used in the adhesion assays described above. The plates were incubated for 3 h at 37 °C and washed three times with PBS to remove unbound bacteria. For adhesion

determination the wells were treated with 0.5% (v/v) Triton X-100 in PBS to desorb the bound bacteria. Plates were incubated for 2 h at room temperature under orbital agitation. One hundred microliters of the content of each well were removed, diluted in PBS and plated on LB agar plates. The adherence inhibition by anti-BCAM2418 antibody was also assessed as described above. Control plates were performed to evaluate the effect of Triton X-100 on the viability of the different *Burkholderia* strains. Results are expressed as a percentage of adhesion relatively to the initial bacterial dose applied. All the experiments were repeated at least three times and results reported as the mean of three experiments.

IV.3.9 *Galleria mellonella* killing assay

Galleria mellonella killing assays were performed as described before (Seed and Dennis, 2008; Mil-Homens and Fialho, 2012) with some modifications. Bacterial cultures were grown as previously described. The OD_{640} of the bacterial cultures was measured and the appropriate volume of cells was collected, centrifuged, and washed with PBS. The activity of anti-BCAM2418 antibody to prevent bacterial virulence was also analyzed. Bacterial suspensions (1 x 10^7 CFU) were incubated with 0.05 mg/mL of anti-BCAM2418 90 min at room-temperature. Tenfold dilutions were performed to obtain 1 x 10^2 *B. cenocepacia* K56-2 CFU, 1 x 10^4 *B. cenocepacia* J2315 CFU, 0.5 x 10^7 *B. multivorans* VC13401 CFU, 10 *B. contaminans* IST408 CFU and 1 x 10^7 *E. coli* BL21-DE3 CFU per injection. Those concentrations were optimized to guarantee a survival rate suitable for killing assays and were confirmed by inoculating serial dilutions on LB agar plates. A micrometer was used to control the volume of a disposable hypodermic micro-syringe, and a 5 µL aliquot of each bacterial dilution was injected into the larvae *via* the hindmost left proleg, which had been previously surface sanitized with 70% (v/v) ethanol. For each condition, 10 larvae were used and as a control a set of larvae was injected with an anti-BCAM2418 antibody suspension in PBS (0.05 mg/mL). Following injection, larvae were placed in petri dishes and stored in the dark at 37°C. Larval survival was followed over a period of 3 days at 24 h intervals, and caterpillars were considered dead when they displayed no movement in response to touch. Kaplan-Meier survival curves were plotted using results from three independent experiments, and differences in survival rates

were calculated by using a log rank (Mantel-Cox) statistical test. All analyses were performed with GraphPad Prism, version 8.0.1, software.

IV.3.10 Fluorescent labeling of bacteria

Bacteria cultured overnight in LB broth at 37 °C and 180 rpm were collected, washed three times in low-salt Tris-buffered saline (TBS) (20 mM Tris-HCl, 100 mM NaCl, 1mM $CaCl_2$, 1 mM $MgCl_2$, pH 7.4), and resuspended to an OD_{600} of 1.0 in TBS. All staining procedures were carried out in the dark and labeled bacteria were subsequently kept in the dark. Bacteria were labelled with 7.5 µM (*Burkholderia* strains) or 10 µM (*E. coli* BL21-DE3) fluorescent dye SYTO 82® (Invitrogen) for 1 h at 37 °C with gentle continuous rotation (180 rpm) (Kilcoyne, et al. 2014; Flannery, et al. 2020). The cells were then washed five times in TBS to remove excess staining and were resuspended to an OD_{600} of 2.0 in TBS with 0.05% Tween 20 (TBS-T).

IV.3.11 Construction of neoglycoconjugate microarrays and interrogation for bacterial binding

Neoglycoconjugate (NGC) microarrays were printed essentially as previously described (Singh, et al. 2018; Flannery, et al. 2020). The microarrays were printed in 8 replicate subarrays per microarray slide consisting of 52 different NGCs and glycoproteins (probes) in replicates of 6 probes per subarray (Supplementary Table IV.S1). All subsequent procedures were carried out in the dark. Microarrays were incubated with fluorescently labelled bacteria diluted 1:2 in TBS-T using an 8 well gasket slide and incubation cassette system (Agilent Technologies) at 37 °C with gentle rotation in the dark. Labelled bacterial suspensions were also pre-incubated separately with anti-BCAM2418 antibody and a rabbit anti-mouse IgG antibody (M-8692, Sigma) at a final concentration of 0.25 mg/mL for each antibody for 90 min at room temperature and included in separate subarrays on the same microarray slide (i.e. the same experiment). The slides were washed three times with TBS-T and once in TBS. The microarrays were dried by centrifugation and were scanned immediately using the 532 nm laser in a G2505B microarray scanner (Agilent) (90% laser power, 5 µm resolution).

Separate subarrays were also incubated with anti-BCAM2418 antibody (0.25 mg/mL) and anti-mouse IgG antibody (0.25 mg/mL) as control, and detected with fluorescence-labelled secondary antibodies anti-goat (SC-2020, Santa Cruz) and anti-rabbit (SAB4600164, Sigma) (1:1,000 dilution in TBS-T), respectively. Two-step incubations were carried out in triplicate. After incubation, washing and drying, microarray slides were scanned immediately (Singh, et al. 2018). As additional controls, microarray incubations with fluorescence-labelled secondary antibodies anti-goat and anti-rabbit (1:1,000 dilution in TBS-T) were also performed. Binding intensities (RFU) from incubations with anti-BCAM2418 and anti-mouse IgG antibodies alone were considered as controls and were subtracted from the intensities from bacteria-anti-BCAM2418 and bacteria-anti-mouse IgG antibodies binding to presented glycans, respectively. The experiments were performed on three separate occasions or alternatively in just one slide, three separate times.

IV.3.12 Microarray data extraction, and analysis

Fluorescence intensity data was extracted from .tif files using GenePix Pro v.5.1 software (Molecular Devices) and a proprietary *.gal file using adaptive diameter (70–130%) circular alignment based on 230 µm features and exported to Excel (v.2010, Microsoft, Redmond, WA, USA) as a text file, where subsequent data processing and analysis was performed (Kilcoyne, et al. 2014; Flannery, et al. 2020). Local background was subtracted, and background corrected median feature intensity (F532median-B532 or F633median-B633) was used for each feature intensity value. The median of six replicate features per subarray was handled as a single data point for graphical and statistical analysis. Data were normalized to the mean for three replicate microarray slides subarray by subarray using subarray total intensity mean. Binding data was presented as a bar graph of mean intensity with an error bar of one standard deviation (SD) of three experimental replicates or in cases of one experiment as a bar graph of median intensity of the six technical replicates. Obtained data scaled to a fluorescence intensity maximum of 7,000 relative fluorescence units (RFU) was subjected to unsupervised clustering with complete linkage and Euclidean distance using Hierarchical Clustering Explorer v3.0 (HCE 3.0, University of Maryland).

IV.3.13 Statistical analysis

All experiments were performed in a minimum of three independent replicates. Relative comparisons were done between corrected values with ANOVA test for significance. A P-value < 0.05 was considered statistically significant. For microarray data, Tukey's multiple comparisons test was used to estimate statistical significance between two different conditions, with a P-value of <0.05 considered significant.

IV.4 Results

IV.4.1 Generation, purification, and Western blot analysis of the anti-BCAM2418 antibody

The anti-TAA antibody was generated in serum of goats using a *B. cenocepacia* K56-2 BCAM2418 N-terminal 135 residues-long fragment, located in the extracellular TAA passenger domain. Despite being annotated for *B. cenocepacia* J2315, BCAM2418 TAA ortholog in *B. cenocepacia* K56-2 share a very similar amino acid sequence (Figure IV.1A). Thus, in order to facilitate interpretation, K56-2 TAA protein will be referred to by the same annotation (BCAM2418) in the course of this work.

Nevertheless, it was interesting to notice that two *B. cenocepacia* K56-2 genome sequences were found to be available on Genbank: *B. cenocepacia* K56-2Valvano (NZ_ALJA00000000.2) and *B. cenocepacia* strain K56-2 (NZ_LAUA00000000.1). A comparative sequence analysis between both genomes and *B. cenocepacia* J2315 indicated the presence of large differences between *BCAM2418* homolog sequences. In the first sequence two ORFs are predicted in this region instead of one, and a large deletion is present in the middle of the sequence of *BCAM2418* ortholog gene. While the second genome sequence indicates an identical protein sequence to J2315 BCAM2418. Preliminary tests were performed to assess the features of the *BCAM2418* sequence in our K56-2 laboratory strain and the presence of a unique ORF was confirmed, indicating a similar organization to J2315 BCAM2418 TAA.

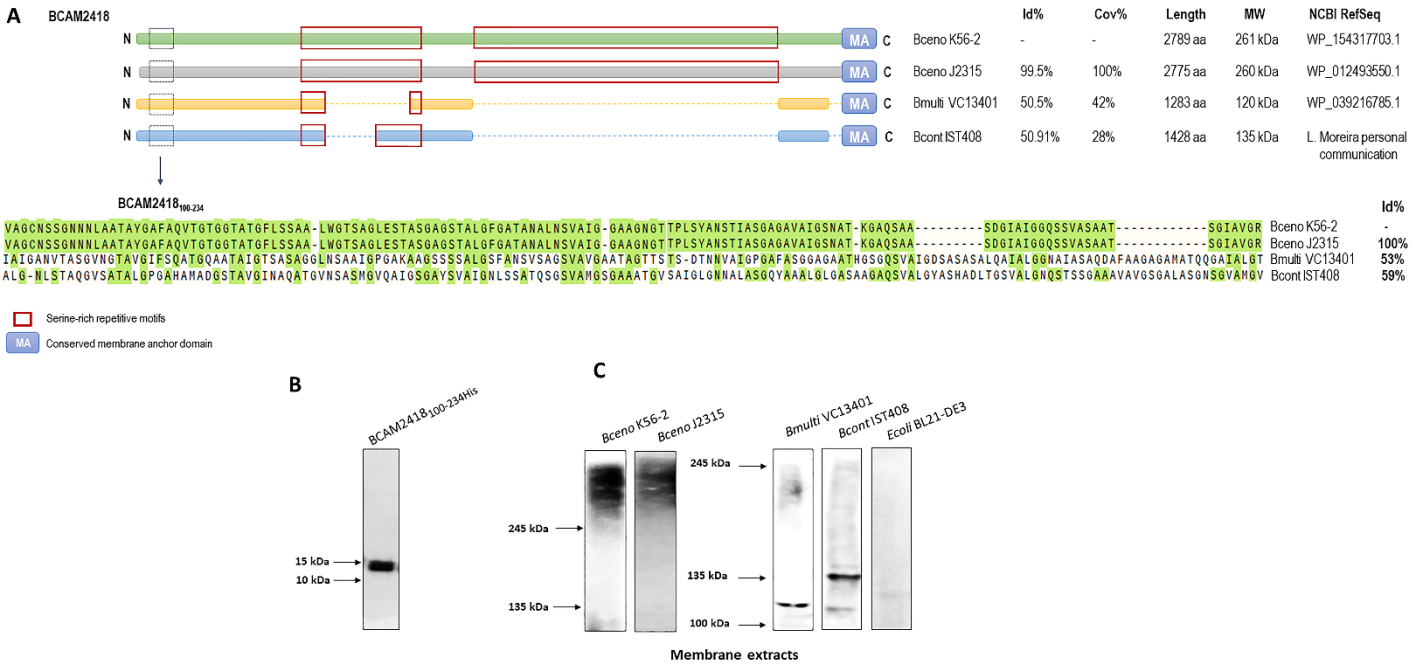

Figure IV.1. BCAM2418 homologs and Western blot analysis of the anti-BCAM2418 antibody
Blastp analysis of BCAM2418 homologous proteins (**A**). Sequence identity (Id) and alignment coverage (Cov) are represented in percentage. Length, molecular weight (MW) and NCBI reference sequence (RefSeq) are also referred for all proteins. Multiple alignment between BCAM2418$_{100\text{-}234}$ fragment and BCAM2418 homologs is represented; residues painted in green are conserved among the protein sequences. Denatured Western blot of BCAM2418$_{100\text{-}234His}$ fragment (**B**) and immunoprecipitated membrane extracts of *B. cenocepacia* (Bceno) K56-2, *B. cenocepacia* (Bceno) J2315, *B. multivorans* (Bmulti) VC13401, *B. comtaminans* (Bcont) IST408 and *E. coli* (Ecoli) BL21DE3 (**C**), probed with a polyclonal antibody specific for BCAM2418.

Aside from *B. cenocepacia* K56-2 and J2315 BCAM2418 proteins, two homologous sequences were also identified in *B. multivorans* VC13401 and *B. contaminans* IST408 and their representation is found on Figure IV.1A. Despite their differences in size and homology along the sequence, all proteins share a conserved C-terminal anchor domain, that is the TAAs defining feature. The shortening of VC13401 and IST408 proteins seems to coincide with the serine-rich repetitive motifs-enriched sequence distinctive of *B. cenocepacia* BCAM2418 passenger domain (Figure IV.1A).

The purified BCAM2418$_{100\text{-}234His}$ fragment (13 kDa) verified the working efficiency of the anti-BCAM2418 antibody (Figure IV.1B). The membrane proteins of *B. cenocepacia* K56-2, J2315, *B. multivorans* VC13401, *B. contaminans* IST408 and *E. coli* BL21-DE3 were

isolated and Western blotting confirmed the recognition of the native homologous proteins by the antibody, which were absent in *E. coli* BL21-DE3 extracts as expected (Figure IV.1C). Regarding *B. cenocepacia* strains, the lower-mass product, with an estimate molecular mass of >245 kDa, could represent BCAM2418 monomers which are supposed to have a molecular mass of approximately 260 kDa. The product detected at very high molecular mass might be due to trimeric forms characteristic of TAAs (Mil-Homens, et al. 2014) that were not fully reduced or might reflect the aggregation of BCAM2418 molecules in the sample (Figure IV.1C). Concerning *B. multivorans* and *B. contaminans* strains, the detected products are in concordance with the estimated molecular mass of BCAM2418 homolog proteins – 121 and 135 kDa, respectively (Figure IV.1A and IV.1C).

IV.4.2 Anti-BCAM2418 antibody inhibits *B. cenocepacia* K56-2 adhesion to mucins and host cells

In previous work (Pimenta, et al. 2020a), the expression of *BCAM2418* TAA gene showed to be time-modulated in response to specific host infection-related conditions. The increase in *BCAM2418* transcript levels upon physical contact of the bacteria with the host cell surface and mucin-coated surfaces raised questions regarding its role during cell adhesion (Pimenta, et al. 2020a). We therefore evaluated the ability of the anti-BCAM2418 antibody to inhibit adhesion of *B. cenocepacia* K56-2 to bronchial epithelial cells. *B. cenocepacia* host-cell adhesion decreased with the applied doses of antibody (Figure IV.2A) and indicated that an anti-BCAM2418 concentration of 0.05 mg/mL was enough to reduce *B. cenocepacia* K56-2 adhesion to bronchial epithelial cells by approximately 46% ($P < 0.01$). A pre-incubation with a maximum concentration of 0.5 mg/mL of antibody caused an 88% bacterial adhesion reduction ($P < 0.0001$) (Figure IV.2A).

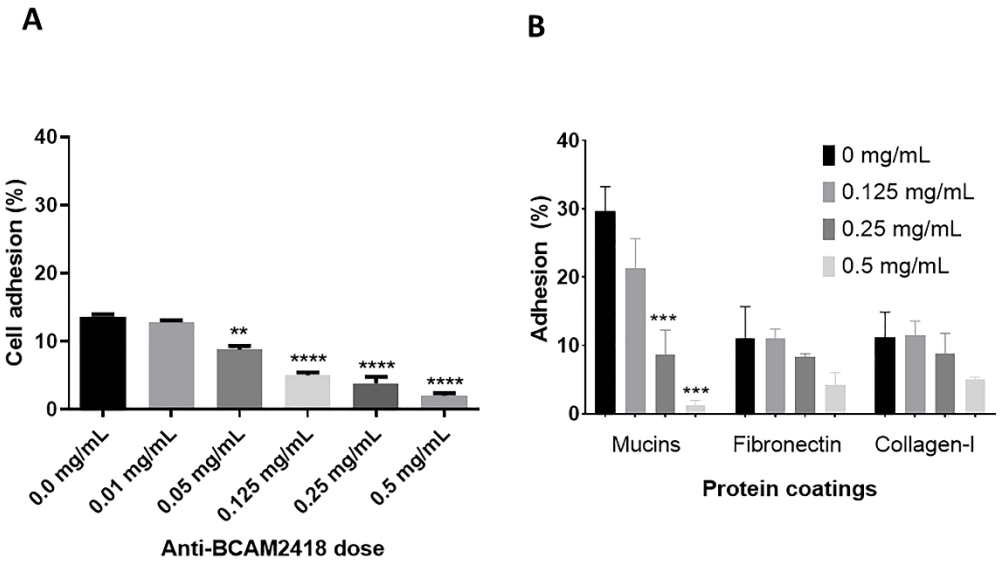

Figure IV.2. Anti-BCAM2418 antibody reduces *B. cenocepacia* K56-2 adhesion to host-cells and protein coatings. Adherence of *B. cenocepacia* K56-2 to bronchial epithelial cell line 16HBE14o- (**A**) and mucins, fibronectin, and collagen type-I (**B**). Anti-BCAM2418 treated and untreated bacteria were tested. Anti-BCAM2418 antibody doses ranged from 0.01 mg/mL to 0.5 mg/mL. Results were expressed as percentage of adhesion relatively to the initial bacterial load added to the cells. Bars represent the mean of three independent experiments and error bars indicate SD. (**P <0.01; ***P <0.001; ****P <0.0001).

We also examined the impact of the anti-BCAM2418 antibody on the proficiency of *B. cenocepacia* K56-2 to adhere to mucins and ECM protein coatings (Figure IV.2B). Different concentrations of anti-BCAM2418 (0.125 mg/mL to 0.5 mg/mL) tested indicated a dose-dependent reduction in bacterial adherence. The most relevant decrease was observed for bacterial adherence to mucin, in which bacteria pre-incubation with a 0.25 mg/mL anti-BCAM2418 solution caused a 75% decline in the adhesion potential of the *B. cenocepacia* (P <0.001). Moreover, when an antibody concentration of 0.5 mg/mL was used, a 96% reduction of bacteria-mucin adherence was observed (P <0.0001). Bacteria-antibody pre-incubation also led to a consistent decrease in bacterial adhesion to fibronectin and collagen type-I coated-surfaces (Figure IV.2B).

IV.4.3 Anti-BCAM2418 antibody decreases host-cell adhesion of different Bcc strains

To assess the specificity of anti-BCAM2418 antibody in the inhibition of host-cell adhesion, four Bcc clinical isolates (*B. cenocepacia* K56-2 and J2315, *B. multivorans* VC13401 and *B. contaminans* IST408) and *E. coli* BL21-DE3 were tested (Figure IV.3).

Bacteria-antibody pre-incubation was performed with 0.05 mg/mL anti-BCAM2418 and adhesion to host-cells was done with a MOI of 50:1. The action of anti-BCAM2418 was more efficient for *B. cenocepacia* strains (K56-2 and J2315) causing a decrease in bacterial adhesion of 45.8% (P <0.0001) and 43.8% (P <0.01), respectively (Figure IV.3). The presence of anti-BCAM2418 reduced bacterial adhesion by 17.9% (P <0.0001) for *B. multivorans* VC13401. For *B. contaminans* IST408 and *E. coli* BL21-DE3, the reductions were of 12.1 and 6.5%, respectively.

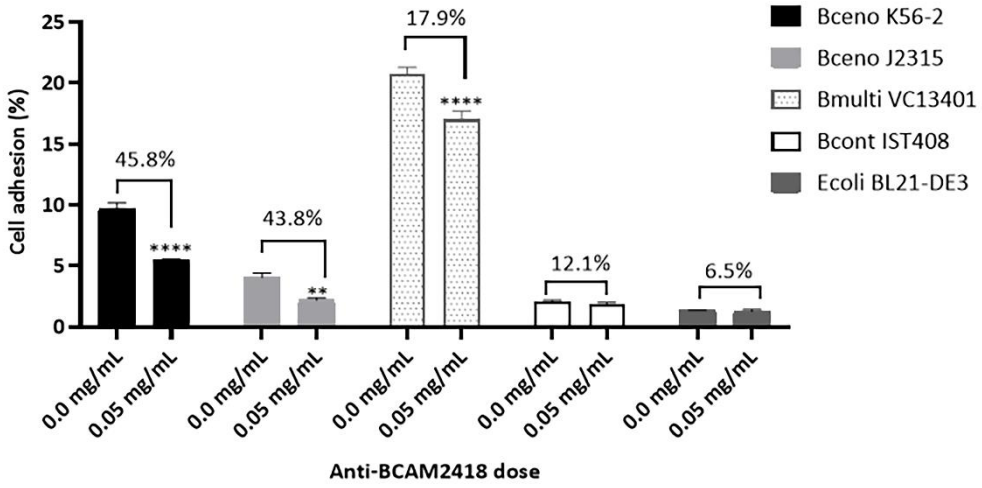

Figure IV.3. Anti-BCAM2418 antibody decreases host-cell adhesion of *Burkholderia* species. Adherence inhibition of *B. cenocepacia* K56-2, *B. cenocepacia* J2315, *B. multivorans* VC13401, *B. contaminans* IST408 and *E. coli* BL21-DE3 towards bronchial epithelial cell line 16HBE14o- after treatment with anti-BCAM2418 antibody (0.05 mg/mL). Results were expressed as percentage of adhesion relatively to the initial bacterial load added to the cells. Presented results are the mean of three independent experiments, error bars indicate SD. (**P <0.01; **** P <0.0001).

IV.4.4 Anti-BCAM2418 antibody affords full protection to the larvae *Galleria mellonella* against *B. cenocepacia* K56-2 infection

To further analyze the specificity of anti-BCAM2418 antibody against different *Burkholderia* strains, virulence assays using the insect model *Galleria mellonella* were performed. Bacterial strains were pre-incubated with a 0.05 mg/mL anti-BCAM2418 suspension prior to injection. The neutralization of *B. cenocepacia* K56-2 BCAM2418 TAA led to an inhibition of the bacterial killing ability (Figure IV.4A). The bacteria-antibody pre-incubation was enough to obtain 100% of larvae survival over 3 days. Thus, in the presence of the anti-BCAM2418 antibody, *B. cenocepacia* K56-2 developed an avirulent behavior. Regarding *B. cenocepacia* J2315, the presence of anti-BCAM2418 reduced larva killing by the bacteria. Nevertheless, in comparison to *B. cenocepacia* K56-2 the survival increase caused by J2315 strain pre-incubated with antibody was not significant (Figure IV.4B). When compared to untreated bacteria, the percentage of larvae survival after injection with neutralized K56-2 and J2315 strains increased by 92.2% and 4.3%, respectively ($P < 0.001$ and $P < 0.05$) (Figure IV.4A and IV.4B). Regarding the other tested *Burkholderia* strains and *E. coli,* pre-incubation with anti-BCAM2418 prior to injection caused no alterations in the killing capacity of the bacteria when compared with untreated ones (Figure IV.4C, IV.4D and IV.4E).

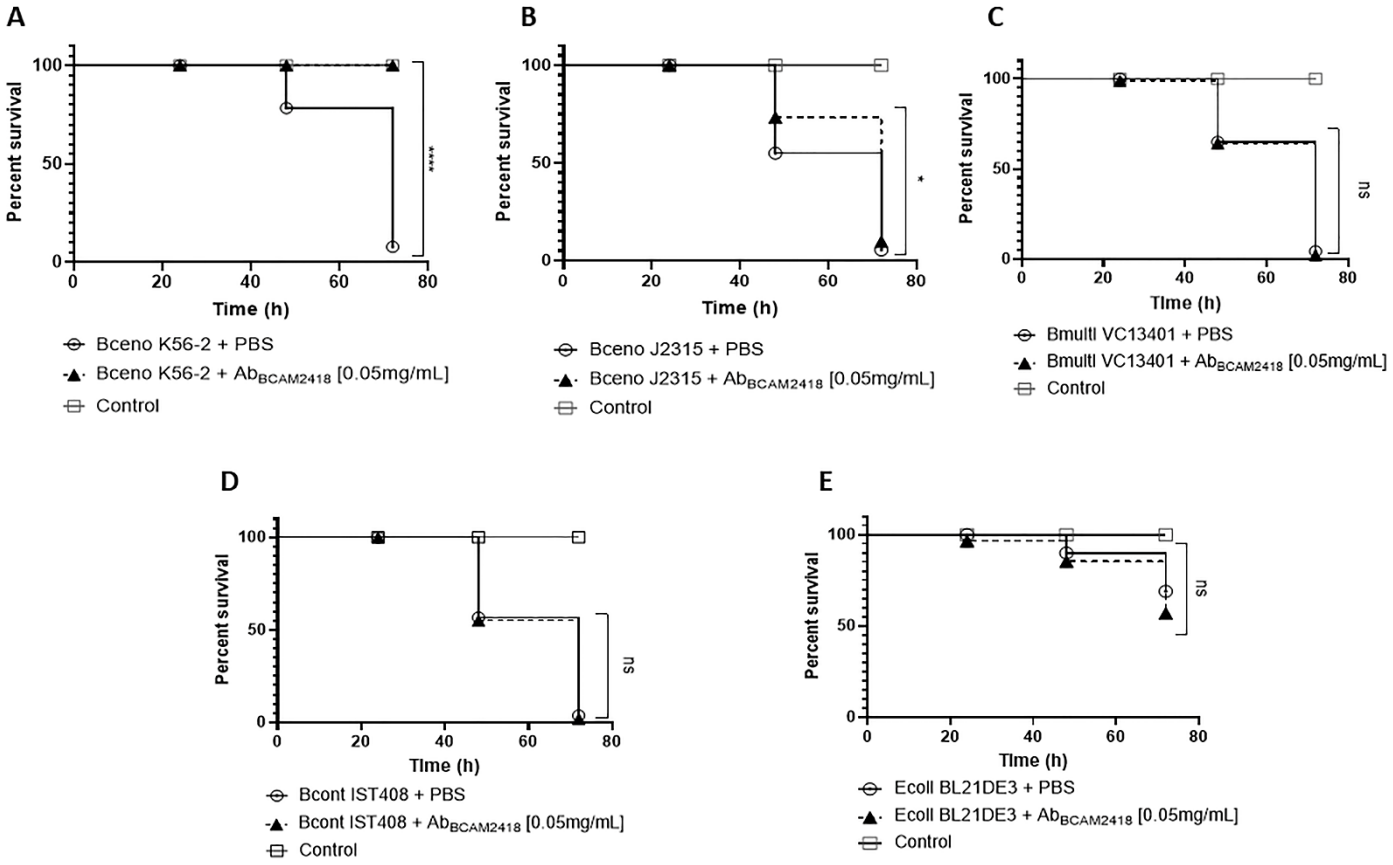

Figure IV.4. Anti-BCAM2418 antibody protects the larvae *Galleria mellonella* against bacterial infection. Kaplan-Meier graphs of *G. mellonella* survival after injection with *B. cenocepacia* K56-2 (**A**), *B. cenocepacia* J2315 (**B**), *B. multivorans* VC13401 (**C**), *B. contaminans* IST408 (**D**) and *E. coli* BL21-DE3 (**E**). Anti-BCAM2418 treated (0.05 mg/mL) and untreated bacteria were tested. Uninfected larvae injected with a solution of PBS with anti-BCAM2418 (0.05 mg/mL) were used as control. Results represent the mean of three independent determinations for 10 animals per treatment. (ns non-significant; *P<0.05; ****P<0.0001).

IV.4.5 Anti-BCAM2418 antibody on glycan microarrays: glycan ligands for *Burkholderia* adhesion to host cells

We investigated whether the anti-BCAM2418 antibody could affect the accessibility of the *Burkholderia* species to host glycans using carbohydrate microarrays. Bacteria, either pre-incubated or not with anti-BCAM2418 antibody, were exposed to 52 glycosylated molecules for 1 h on the microarray surface (Figure IV.5). Differences between treated and untreated bacteria were considered relevant (represented as red bars, Figure IV.6) when [untreated/anti-BCAM2418 treated bacteria] ratio was <0.6; and [anti-mouse IgG treated bacteria/anti-BCAM2418 treated bacteria] ratio was >1.1.

While statistical analysis indicates the robustness of the obtained result, ratio calculation indicates the biological relevance of the anti-BCAM2418 binding inhibition. In case of normalized negative RFU values, the result was considered non-determined (nd). Overall, the results presented in clearly indicated that the anti-BCAM2418 antibody pre-incubation led to a diminished interaction between *Burkholderia* species (through BCAM2418 or its orthologs) and the tested glycans (Figure IV.6 and Supplementary Tables IV.S2, IV.S3 and IV.S4). These results were much more relevant among the two *B. cenocepacia* strains (K56-2 and J3215), and indeed gained significance for K56-2. In contrast, very minor changes were observed in the *E. coli* BL21-DE3.

B. cenocepacia K56-2 pre-treated with the anti-BCAM2418 antibody demonstrated reduced binding to 32 out of the 52 glycosylated molecules tested (Supplementary Tables IV.S2, IV.S3 and IV.S4). Among those, the anti-BCAM2418 decreased binding to 3'sialyl-3-fucosyllactose (Neu5Ac-α(2,3)-Gal-β(1,4)-[Fuc-α(1,3)]-Glc) but not to 3´- and 6'-sialyllactose (Neu5Ac-α(2,3)-Gal-β(1,4)-Glc). Therefore, the internal α-(1,3)-linked Fuc on 3'sialyl-3-fucosyllactose may be key to BCAM2418-mediated binding. We also observed a significant decreased binding to histo-blood group A (BGABSA) but not to histo-blood group B (BGBHSA) in the presence of the anti-BCAM2418 antibody, indicating a preference for BCAM2418 for terminal α-linked GalNAc (group A) over α-linked Gal (group B) and potentially a tolerance for internal α-(1,2)-linked Fuc (H antigen). Additionally, the anti-BCAM2418 antibody also affected the binding to other galactosyl epitopes, supporting the indicated specificity of BCAM2418 for only terminal α-linked Gal residues (Gal-α(1,3)-Gal-β(1,4)-GlcNAc; Gal-α(1,3)-Gal; and Gal-α(1,2)-Gal). An identical pattern was observed for terminal α-(1,2)-linked Fuc-containing structures (lacto-N-fucopentaose I and lacto-N-difucohexaose I, respectively, on NGCs lacto-N-fucopentaose I-BSA and lacto-N-difucohexaose I-BSA) and indicating that BCAM2418-mediated binding to the blood group B structure probably depended on the terminal α-linked Gal as well as the α-(1,2)-linked Fuc. Another highly relevant group encompassed oligosaccharides containing Lewis structures, modified with or without sialyl- and sulfo-groups. However, we observed two exceptions; the bacterial binding to 6(SO_4)Gal-β(1,3)-[Fuc-α(1,4)]-GlcNAc and 3(SO_4)Gal-β(1,4)-[Fuc-α(1,3)]-GlcNAc was quite low or

no binding was seen for all tested conditions. Finally, binding to the GM1 gangliosides, GM1 and asialo-GM1, was also reduced by anti-BCAM2418 antibody (Figure IV.6).

The binding intensity data for the 52 glycans were subjected to hierarchical clustering and generated two major clusters (I and II) (plus a small cluster (III) with outliers) (Figure IV.7). Cluster I included the glycans in which the pre-incubation of *B. cenocepacia* K56-2 with anti-BCAM2418 antibody significantly decreased binding. This may be indicative of the type of glycans recognized by the BCAM2418 adhesin. The glycans included were the histo-blood groups (A, B and H; on the NGCs BGABSA, BGBHSA and H2BSA), the Lewis structures (a, b, x and y; on the NGCs LeaBSA, LebBSA, LexBSA and LeyHSA) and other relevant glycoconjugates such as asialo-GM1 ganglioside (on the NGC aGM1HSA).

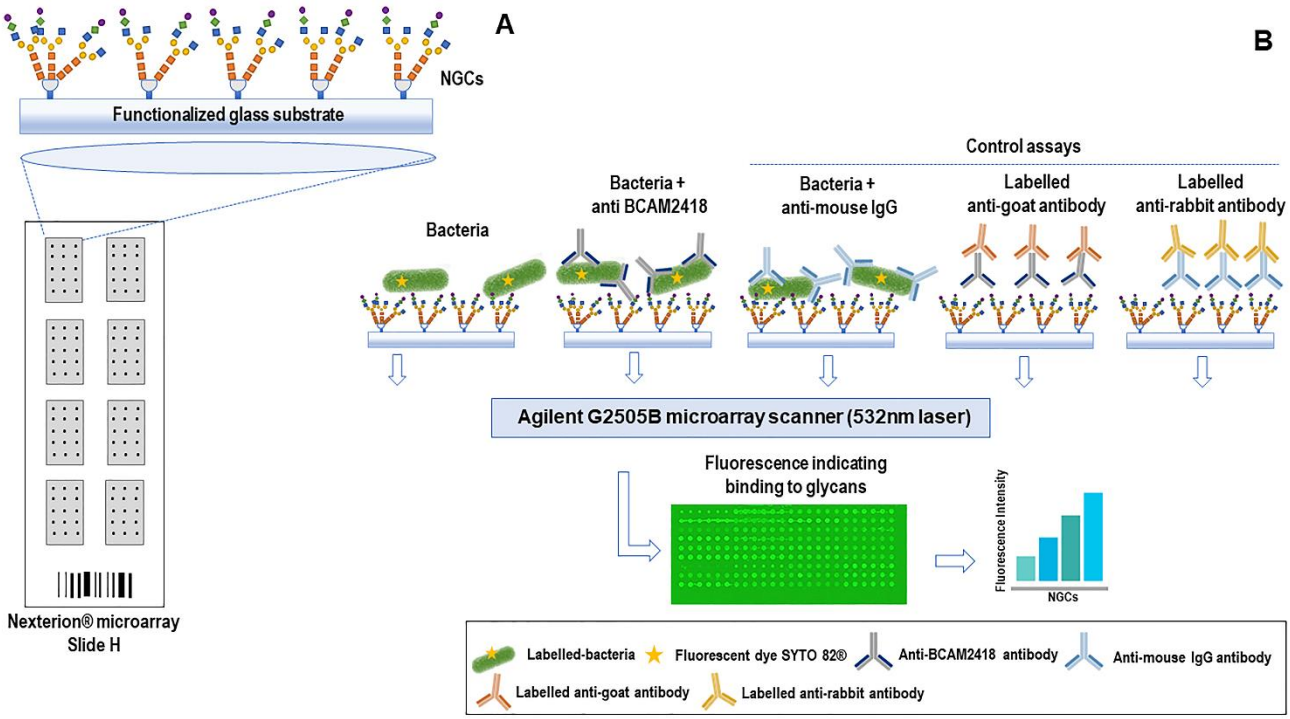

Figure IV.5. Schematic representation of the protocol used for interrogation of NGC microarrays for bacterial binding. Representative presentation of NGC structures on microarrays to profile bacterial interaction. Fifty-two different structures were printed onto Nexterion® slide H microarray slides in 6 replicates, with 8 identical subarrays per slide. Bacteria cultured overnight were internally labelled with fluorescent dye SYTO 82®. Labelled bacterial suspensions were also pre-incubated with anti-BCAM2418 antibody and a rabbit anti-mouse IgG antibody at a final concentration of 0.25 mg/mL, for 90 min at room-temperature. Microarrays were incubated with fluorescently labelled bacteria for 1 h at 37 °C with gentle rotation in the dark. The slides were scanned using the 532 nm laser in a microarray scanner. Microarrays were also incubated only with anti-BCAM2418 antibody and anti-mouse IgG antibody as a control. As complementary controls, microarray incubations with anti-BCAM2418 antibody, with a rabbit anti-mouse IgG antibody and with fluorescence-labelled secondary antibodies anti-goat and anti-rabbit were performed. Fluorescence intensity data was extracted using GenePix Pro v.5.1 software and local background was subtracted.

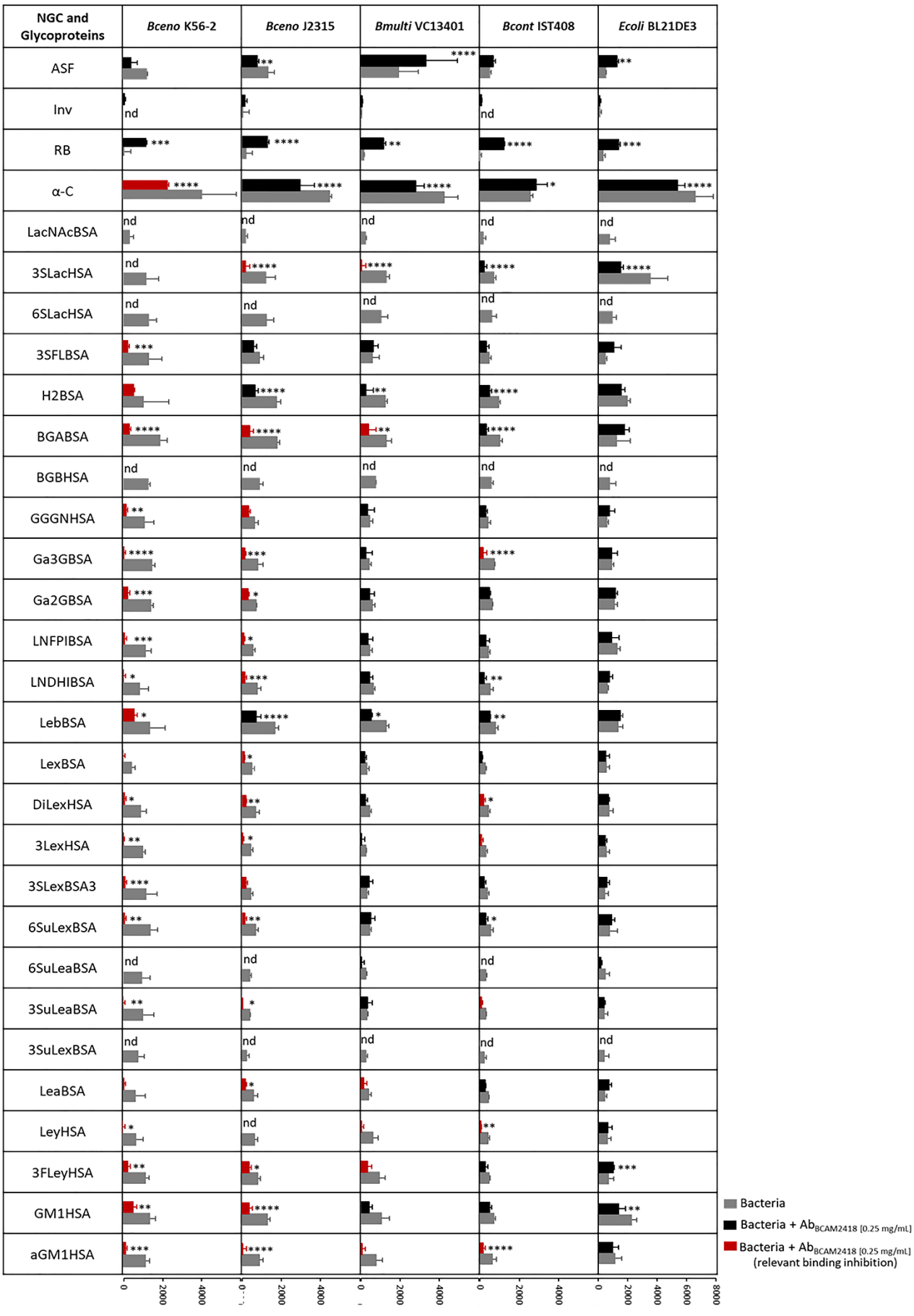
NGC and Glycoproteins
Bceno K56-2
Bceno J2315
Bmulti VC13401
Bcont IST408
Ecoli BL21DE3
ASF
Inv
RB
α-C
LacNAcBSA
3SLacHSA
6SLacHSA
3SFLBSA
H2BSA
BGABSA
BGBHSA
GGGNHSA
Ga3GBSA
Ga2GBSA
LNFPIBSA
LNDHIBSA
LebBSA
LexBSA
DiLexHSA
3LexHSA
3SLexBSA3
6SuLexBSA
6SuLeaBSA
3SuLeaBSA
3SuLexBSA
LeaBSA
LeyHSA
3FLeyHSA
GM1HSA
aGM1HSA
nd
0
2000
4000
6000
8000
Fluorescence Intensity (RFU)
Bacteria
Bacteria + Ab BCAM2418 [0.25 mg/mL]
Bacteria + Ab BCAM2418 [0.25 mg/mL] (relevant binding inhibition)

Figure IV.6. Anti-BCAM2418 antibody treatment altered *Burkholderia* binding to specific host glycans. Bacteria, pre-incubated or not with anti-BCAM2418 antibody (0.25 mg/mL), were incubated with different glycans on a carbohydrate microarray. *B. cenocepacia* (Bceno) K56-2, *B. cenocepacia* (Bceno) J2315, *B. multivorans* (Bmulti) VC13401, *B. comtaminans* (Bcont) IST408 and *E. coli* (Ecoli) BL21DE3 were tested. Binding intensities (RFU) from incubations with anti-BCAM2418 and anti-mouse IgG antibodies alone were considered as controls and were subtracted from the intensities from bacteria-anti-BCAM2418 and bacteria-anti-mouse IgG antibodies binding to presented glycans, respectively. In cases of resulting negative RFU (fluorescence intensity) after subtraction of negative controls, the result was considered non-determined (nd). RFU values resulting from the binding of untreated and treated labeled bacteria are represented by grey and black bars, respectively. Differences between treated and untreated bacteria were considered relevant (represented as red bars) when [untreated/anti-BCAM2418 treated bacteria] ratio was <0.6; and [anti-mouse IgG treated bacteria/anti-BCAM2418 treated bacteria] ratio was >1.1. The median of six replicate features per subarray was handled as a single data point for graphical and statistical analysis. Data were normalized to the mean for three replicate microarray slides subarray by subarray using subarray total intensity mean. Binding data was presented as a bar graph of mean intensity with an error bar of one standard deviation of three experimental replicates. (*P <0.05; **P <0.01; ***P <0.001; ****P <0.0001). While statistical analysis indicates the robustness of the obtained result, ratio calculation indicates the biological relevance of the anti-BCAM2418 binding inhibition.

IV.4.6 Probing live bacteria-glycan interactions using glycan microarrays: carbohydrate specificity of *Burkholderia* species

We next investigated the carbohydrate-binding specificities of *B. cenocepacia*, *B. multivorans* VC13401 and *B. contaminans* IST408 using carbohydrate microarrays. Fluorescence intensities varied between the four strains/species of *Burkholderia* but were generally higher for *B. cenocepacia* K56-2, indicating a stronger interaction with the printed glycans (Figure IV.8). Overall, the most intensely binding ligands for *Burkholderia* species included the glycoproteins α-crystallin (α-C) and asialofetuin, blood group A (on NGC BGABSA), Lewis b (on NGC Lewis b-BSA), lacto-N-tetraose (on NGC lacto-N-tetraose-APD-HSA) and the gangliosides (GM1 and asialo-GM1 pentasaccharides (on NGCs GM1 or aGM1-pentasaccharide-APD-HSA). In contrast, the low-affinity ligands included the glycoproteins RNase B and invertase and LacNAc and Lewis x (on NGCs LacNAc-BSA and Lewis x-BSA, respectively). *E. coli* BL21-DE3 showed a more outlier behavior concerning its interaction ability towards the tested glycoconjugates.

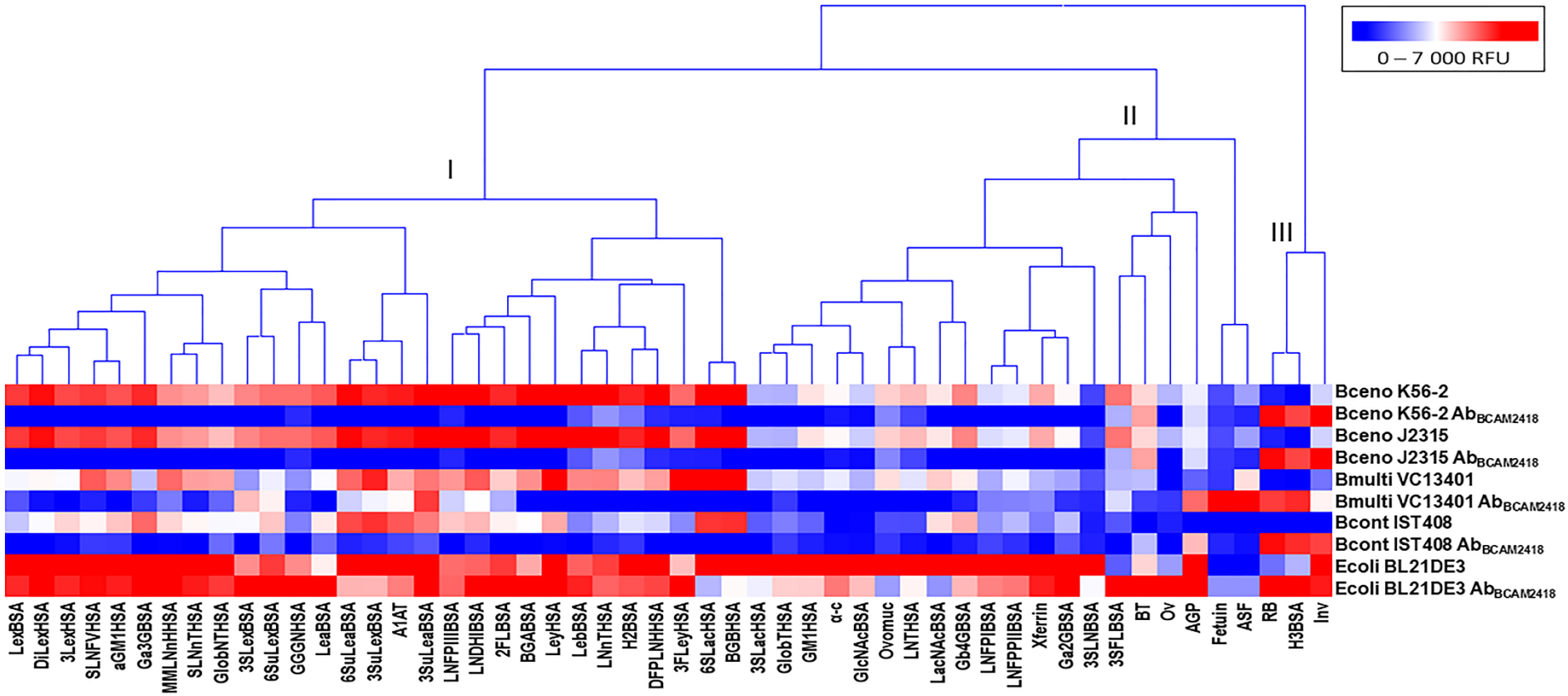

Figure IV.7. Hierarchically clustered heatmap of *Burkholderia* NGC binding profiles. Heat maps with dendrograms of hierarchical clustering generated using HCE 3.0. Fifty-two glycans were subjected to hierarchical clustering and generated two major clusters (I and II) (plus a small cluster (III) with outliers). Mean values of three technical replicates plotted and scaled to a maximum intensity of 7,000 RFU. Color indicates fluorescence intensities as in the legend, with low intensity depicted as blue, medium intensity in white and high intensity in red. Anti-BCAM2418 treated (0.25 mg/mL) and untreated bacteria were represented.

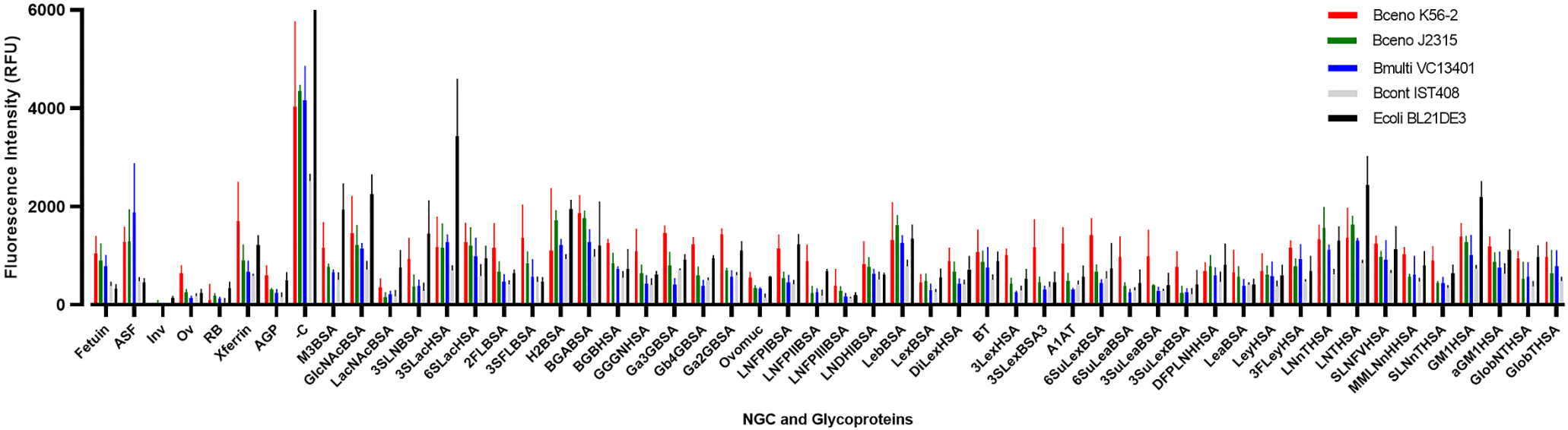

Figure IV.8. Interaction of live *Burkholderia* strains with carbohydrates. NGC microarrays were probed with fluorescently labeled *B. cenocepacia* (Bceno) K56-2, *B. cenocepacia* (Bceno) J2315, *B. multivorans* (Bmulti) VC13401, *B. contaminans* (Bcont) IST408 and *E. coli* BL21-DE3. The bar chart shows the mean fluorescence intensities (RFU) from one subarray of three replicate microarray slides; values for each subarray are medians for six feature replicates. Error bars indicate one standard deviation of the mean for the individual probes for three microarray slides.

IV.5 Discussion

BCAM2418 is one out of seven TAA genes of *B. cenocepacia* K56-2 (Mil-Homens and Fialho, 2011). Several TAAs from *B. cenocepacia* and other Gram-negative pathogens have been characterized. The main functions of this class of proteins are adhesion-related ones, biofilm formation and autoaggregation (Cotter, et al. 2005; El-Kirat-Chatel, et al. 2013; Mil-Homens, et al. 2017). Like other TAAs from *B. cenocepacia*, it seems that BCAM2418 could be an intervening protein during the early contacts with the host (Mil-Homens and Fialho, 2012; Mil-Homens, et al. 2014). Previous work showed that *BCAM2418* gene is upregulated upon bacterial contact with host cells, reaching a maximum level of expression after 30 min of adhesion (Pimenta, et al. 2020a). This indicates a fine-tuned regulation event that seemed to function in the early steps of infection and may derive from cross-talk between the bacterium and O-glycosylated host cell surface components (Pimenta, et al. 2020a). Given the failed efforts to construct a *BCAM2418* mutant (Pimenta, et al. 2020a), we aimed to produce an antibody that could neutralize the action of BCAM2418 allowing the investigation of its function(s) during infection.

Anti-BCAM2418 was produced by goat immunization using a 135-residue N-terminal fragment of *B. cenocepacia* K56-2 BCAM2418 as antigen. The resulting antibody recognized BCAM2418 isolated from bacterial membranes (Figure IV.1). Bacteria pre-incubated with the antibody exhibited diminished adhesion, in a dose-dependent manner, of *B. cenocepacia* K56-2 towards bronchial epithelial cells, mucins and ECM proteins (fibronectin and collagen type-I) (Figure IV.2). The present results together with the proven overexpression of *BCAM2418* gene in the same bacterial adhesion context (Pimenta, et al. 2020a) revealed the relevance of this protein in *B. cenocepacia* pathogenicity.

Bcc bacteria are closely related species that have an interspecies identity of 94-95% (*recA* gene variability) (Chiarini, et al. 2006). TAA genes are largely represented in Bcc genomes compared to other Gram-negative bacteria. The density of TAAs is variable among Bcc genomes, but their functions seem to be closely related (Mil-Homens and

Fialho, 2011). Here we evaluated the effect of anti-BCAM2418 towards various Bcc bacteria (*B. cenocepacia* K56-2, *B. cenocepacia* J2315, *B. multivorans* VC13401 and *B. contaminans* IST408), testing them in adhesion and *in vivo* virulence assays (Figure IV.3 and IV.4). The effect of the antibody on cell adhesion was more effective targeting *B. cenocepacia* K56-2 and *B. cenocepacia* J2315 (46 and 44% inhibition) compared to the other two Bcc species (*B. multivorans* VC13401 and *B. contaminans* IST408), while only a modest effect (6%) was observed in *E. coli* BL21-DE3 (Figure IV.3). When the role of anti-BCAM2418 was tested in virulence using *G. mellonella* larvae as a heterologous invertebrate host, data indicate that during a 72 h infection period, the anti-BCAM2418 antibody provided full protection against *B. cenocepacia* K56-2 (Figure IV.4). In contrast, we observed a weak protective effect in *B. cenocepacia* J2315, and no protection at all in *B. multivorans* VC13401, *B. contaminans* IST408 and *E. coli* BL21-DE3. Concerning *B. multivorans*, *B. contaminans* strains, the obtained results were in concordance with the low identity registered between BCAM2418 and respective homologous proteins (Figure IV.1A), indicating a poor neutralizing capacity of anti-BCAM2418 towards those isolates. Regarding J2315 strain, the effect of the anti-TAA antibody was reduced considering the high similarity between the *B. cenocepacia* K56-2 BCAM2418 135 amino acids fragment used as antigen and *B. cenocepacia* J2315 sequence (Figure IV.1A). Despite the high similarities between J2315 and K56-2 clonal isolates, the behavior of both strains were quite variable under laboratory conditions, which may explain the differences in cellular adhesion, virulence using *G. mellonella* model and the consequent deficient effect of the anti-BCAM2418 antibody. Additionally, differences identified in *B. cenocepacia* sequenced genomes raise questions concerning potential differences between K56-2 strains propagated in the different laboratories.

Overall, our findings suggested that the anti-BCAM2418 antibody prevented *B. cenocepacia* K56-2 infection by blocking BCAM2418-mediated attachment to the host cell surface. The data indicated an important role played by this TAA in the early stages of bacteria-host interaction as proposed before (Pimenta, et al. 2020a). Other adhesin-specific antibodies were described to confer host-cell protection against pathogens during adhesion. For example, Girard et al. (2006), reported the use of anti-intimin chicken egg yolk antibodies to prevent the adherence of enterohemorrhagic *E.*

coli (EHEC) (Girard, et al. 2006), while Cook et al. (2007) demonstrated the anti-adhesion properties of polyclonal antibodies raised against EHEC strain O157:H7 adherence-associated proteins (Cook, et al. 2007).

We next examined whether the anti-BCAM2418 affected the binding of the *Burkholderia* species to host glycans (Figure IV.5). The 52 selected probes on the glycan microarray presented glycan structures commonly encountered on the host cell surface, as part of mucins, and other glycoproteins or glycolipids (Colomb, et al. 2014; Jeffries, et al. 2016; Dingjan, et al. 2017). Pre-incubation of the interrogated bacteria with anti-BCAM2418 antibody caused a widespread reduction in the binding of *Burkholderia* strains to the printed glycans (Figure IV.7). However, the most significant inhibitory effect was observed for the two strains of *B. cenocepacia,* K56-2 and J2315, supporting the relevance of BCAM2418 TAA-mediated binding during the early contacts between *B. cenocepacia* K56-2 and the host. Previous studies reported that virulent strains of *Helicobacter pylori* expressing the surface adhesin BabA were able to bind to host ABH/Lewis glycans (Lindén, et al. 2002). In addition, similar results were reported for FedF, the adhesin on F18 fimbriae from enterotoxigenic *E. coli*. FedF mediates binding by recognizing ABH type 1 and sulfated H type 2 blood group antigens (Moonens, et al. 2012).

Apart from evaluating the *B. cenocepacia* K56-2 adhesin BCAM2418 ligand specificities, glycan microarrays were used to determine and compare the binding specificity profiles of the *Burkholderia* species. *B. cenocepacia* strains were shown to interact in a similar way with a comparable panel of glycoconjugates. In the case of *B. multivorans* VC13401, despite recognizing almost the same glycans as the other *Burkholderia* strains, the intensity of interaction was lower. The same occurred for *B. contaminans* IST408; on the other hand, the results obtained for *E. coli* BL21-DE3 showed a generalized binding among all the tested glycoconjugates (Figures IV.7 and IV.8). Those differences could naturally occur because of variations on the fluorescent dye uptake by the bacteria, generating higher or lower intensity values during NGC interaction. Also, differences in the bacterial-surface composition, like the presence of exopolysaccharide in *Burkholderia* species, could alter the presentation and accessibility of adhesive

molecules and might lead to a distinct interaction between a specific strain and the panel of tested glycans (Conway, et al. 2004; Flannery, et al. 2020).

Burkholderia species bound to all three ABH blood group antigens, although displayed a higher binding intensity to group A. Blood group antigens and Lewis structures are fucosylated oligosaccharides expressed on human cell surfaces and secretions, including mucin-rich lung mucus. In the CF-lungs, glycans on mucins, including blood group antigens and Lewis structures, act as ligands for opportunistic pathogens (Ruiz-Palacios, et al. 2003; Imberty, et al. 2004; Chessa, et al. 2008; Ishijima, et al. 2011; Audfray, et al. 2013). *Burkholderia* species also interact with Lewis structures and here displayed higher binding intensities with Lewis b. To date, in CF patients, the relationship between blood groups and severity of bacterial infections has been investigated only for *P. aeruginosa,* the most common pathogen encountered in CF disease (Taylor-Cousar, et al. 2009). *P. aeruginosa* recognizes sialyl and sulfo-sialyl-Lewis x epitopes abundantly found on respiratory mucins (Scharfman, et al. 2000). Moreover, in agreement with our findings, Sulák et al. (2010) reported that *B. cenocepacia* expresses soluble lectins (BC2L-A, B, C and D) with specificity for fucosylated human histo-blood group epitopes Lewis b and Lewis y (Sulák, et al. 2010).

In this work, *Burkhloderia* species also interacted with gangliosides GM1 and asialoGM1 and with lacto-N-tetraose. GM1 and asialoGM1 are used as ligands by a number of respiratory pathogens, including *Burkholderia* species (Krivan, et al. 1988; McClean and Callaghan, 2009). Lacto-N-tetraose is found in human milk as a free oligosaccharide and binds to bacterial lectins and toxins as a decoy ligand, thereby preventing bacteria-host cell interactions (El-Hawiet, et al. 2015). Thomas and Brooks (2004) demonstrated its efficacy as an anti-adhesion molecule directly on living bacteria, including *B. cenocepacia* and *B. pseudomallei* (Thomas and Brooks, 2004). Finally, the *Burkholderia* species bound to asialofetuin and α-crystallin (Yet, et al. 1988; Augusteyn, 2004). The carbohydrate moieties of these glycoproteins are recognized by lectins from diverse origins (Dam, et al. 2005). It is interesting to speculate whether such molecules could act on *Burkholderia* species as potential anti-adhesive molecules.

In conclusion, we accessed the inhibitory effects of an antibody produced against the *B. cenocepacia* K56-2 TAA BCAM2418. The inhibition of BCAM2418 caused a reduction in

the adhesion of the bacteria to bronchial cells and mucins and a suppression of *B. cenocepacia* K56-2 infection in the non-mammalian model *Galleria mellonella*. The presented results indicated that the neutralization of TAA-host cell interaction can attenuate the course of infection. Therefore, the use of TAAs as vaccine ingredients or as a target for an anti-adhesion therapy cold be an important strategy to impair infection evolution (Bentancor, et al. 2012; Van Damme, et al. 2019). Finally, we were able to infer, for the first time, the glycan structures recognized by a TAA. Moreover, our glycan microarray dataset was also employed to determine glycan binding specificities of live *Burkholderia* and expand the understanding on the molecular underpinning of Bcc pathogenesis in the context of CF disease.

Data availability statement

All data are provided in full in the results section of this chapter and in supplementary data (Tables IV.S1, IV.S2, IV.S3 and IV.S4).

Acknowledgments

This work was supported by the Portuguese Science and Technology Foundation (FCT) BIOTECnico Ph.D. program grant PD/BD/116940/2016. Funding received by iBB – Instituto for Bioengineering and Biosciences from FCT (UID/BIO/04565/2020) and Programa Operacional Regional de Lisboa 2020 (Project N. 007317) is acknowledged.

Declaration of Competing Interest

The authors have no conflict of interest to declare.

V. *BURKHOLDERIA CENOCEPACIA* TRANSCRIPTOME ANALYSIS DURING THE EARLY CONTACTS WITH BRONCHIAL EPITHELIAL CELL-DERIVED GIANT PLASMA-MEMBRANE VESICLES

Journal paper

Pimenta AI, Bernardes N, Alves MM, Mil-Homens D, Fialho AM. *Burkholderia cenocepacia* transcriptome analysis during the early contacts with bronchial epithelial cell-derived giant plasma-membrane vesicles. 2020 (Submitted to Scientific Reports, under revision).

V.1 Abstract

Burkholderia cenocepacia is known for its capacity of adherence and intrinsic interaction with the host, causing severe opportunistic lung infections in cystic fibrosis patients. In this work we produced Giant Plasma Membrane Vesicles (GPMVs) from a bronchial epithelial cell line and used them as a cell-like alternative to investigate how *B. cenocepacia* response upon host cell contact. RNA-sequencing was performed and the analysis of the *B. cenocepacia* K56-2 transcriptome after the first contact with the surface of host cells opened new insights regarding the bacterial adaptation and virulence-associated alterations that take place in the early stages of infection. The sensing of host membranes led to a transcriptional shift that caused a cascade of metabolic and physiological adaptations to the host specific environment. Many of the differentially expressed genes encode proteins related with central metabolic pathways, transport systems, cellular processes, and virulence traits. The understanding of the changes in gene expression that occur in the early steps of infection can uncover the first mechanisms used to invade and subvert the host cell, providing new strategies to restrain *B. cenocepacia* lung infections.

V.2 Introduction

Burkholderia cenocepacia is well known for its capacity of adherence and intrinsic interaction with the host, causing severe opportunistic lung infections in cystic fibrosis (CF) patients (Chiarini, et al. 2006; Baldwin, et al. 2007). *B. cenocepacia* has many virulence factors that contribute for its capacity to colonize the lung epithelium of CF patients and to cause disease. The set of virulence factors include a broad variety of adhesins, invasins, secretion systems, extracellular enzymes and toxins, and quorum sensing systems (McClean and Callaghan, 2009; Drevinek and Mahenthiralingam, 2010). Regarding bacterial adhesion, the machinery used is wide and largely complex and

several surface molecules have been described (Sajjan, et al. 2000; Tomich, et al. 2002; Mil-Homens and Fialho, 2011).

Bacterial contact to host cells has been known as a pivotal step in the host-pathogen interaction (Pizarro-Cerdá and Cossart, 2006). The capacity to sense environmental changes and physical barriers of the host makes the pathogen able to alter and adapt its metabolism, regulation, and virulence (Stones and Krachler, 2016). This surface sensing could be perceived by the bacteria through chemical signals or mechanical forces (Cox, et al. 2018). Although poorly understood, some reports indicate that the sense and adherence of bacteria to host cells could lead to a prompt transcription modulation of several virulence-associated genes, like adhesive molecules and other surface antigens (Li, et al. 2012; Kansal, et al. 2013; Katsowich, et al. 2017).

The study of the complete bacterial transcriptome upon adhesion to host cells could be a must-have tool in the study of pathogens behavior. In recent years, several transcriptional profiling studies have been performed during bacterial infection. Simultaneous transcriptomic analysis of bacterial and their host cells are currently performed to understand the overall alterations that occur in the context of host-pathogen interactions (Baddal, et al. 2015). Nonetheless, the isolation and further analysis of RNA from adherent bacteria could be demanding and hard to achieve concerning the limiting number of available organisms per cell. For that reason, the adhesion to an *in vitro* membrane system free from contaminant host material could be an easy alternative to extract bacterial RNA with appropriate quantity and quality and to perform further transcriptomic studies.

Giant plasma membrane vesicles (GPMVs) are a model to study the cellular membrane behavior. Contrary to other systems in use, GPMVs are more stable, and mimic the constitution of the plasma membrane as they are formed by a chemically induced plasma membrane vesiculation (Zemlji, et al. 2018). Despite their biological origin GPMVs lack cytoskeletal structures and the presence of complex components from the cytosol (Sezgin, et al. 2012; Levental and Levental, 2015). GPMVs research has advanced through the years and lead to break-through studies of the biophysical properties of the cellular membranes. The similarities to the host cell membranes make a new potential model to study host-pathogen interactions and fulfil a gap of knowledge.

With this work we aimed to develop a new technique that allowed an easy and efficient recovery of *B. cenocepacia* RNA after contact with host cell membranes. For that, GPMVs were produced from a bronchial epithelial cell line and adhesion assays with *B. cenocepacia* K56-2 were performed. The optimizations applied for both the GPMVs production and bacterial adhesion procedures led to a final recovery of *B. cenocepacia* RNA samples with high levels of quality and purity to perform RNA-sequencing analysis. The analysis of the *B. cenocepacia* transcriptome after the first contact with the surface of host cells opened new insights regarding the bacterial adaptation and virulence-associated alterations that take place in the early stages of infection. Furthermore, to the best of our knowledge this is the first methodological approach using GPMVs as a tool to study the mechanisms of pathogens interaction with host cells.

V.3 Materials and Methods

V.3.1 Bacterial strain and growth conditions

Burkholderia cenocepacia clinical isolate K56-2 was kindly provided by J. J. LiPuma (University of Michigan). Bacteria were cultured in Luria-Bertani (LB) broth at 37°C with orbital agitation at 250 rpm. For functional studies, bacteria from a fresh overnight culture were grown (initial OD_{640} 0.1) at 37 °C with orbital agitation at 250 rpm, for 6 h until reaching a mid-exponential phase of growth.

V.3.2 Cell line and cell culture

16HBE14o- a human bronchial epithelial cell line was used (Cozens, et al. 1994). Cells were maintained in fibronectin/vitrogen-coated flasks in minimum essential medium with Earle's salt (MEM) supplemented with 10% fetal bovine serum (FBS), 0.292 g/L L-glutamine, and penicillin-streptomycin (100 U/mL) in a humidified atmosphere at 37°C with 5% CO_2.

V.3.3 Giant Plasma Membrane Vesicles (GPMVs) production

Giant Plasma Membrane Vesicles (GPMVs) production and isolation protocol was performed as previously described (Sezgin, et al. 2012) with some alterations. 16HBE14o- cells were seeded and grown until reaching a confluence of more than 70%. Cells were washed twice with 100 µL/cm^2 of GPMV buffer (10 mM HEPES, 150 mM NaCl, 2 mM $CaCl_2$, pH7.4). GPMV reagent containing the vesiculation agents (25 mM paraformaldehyde (PFA), 2 mM DTT in GPMV buffer) was applied to the cells in the same 100 µL/cm^2 ratio. The cells were incubated at 37 °C with low agitation (100 rpm), during 1 h. The GPMV-enriched supernatant was transferred to a centrifuge tube by decantation. To pelleting the cellular debris, the GPMV suspension was centrifuged 10 min at 100xg. The resulting supernatant was carefully collected by pipetting. To perform adhesion assays GPMVs were concentrated and the vesiculation agents in the suspension were removed by ultrafiltration using an Amicon® Ultra-15 Centrifugal Filter Unit with a 100 kDa molecular cut-off. The GPMV suspension were applied to the filter unit (15 mL at a time), and centrifuged 15 min, at 3,500xg leaving at least 3 mL of final volume in the tube. Ten volumes of GPMV buffer were applied to wash the vesicles and remove PFA and DTT from the suspension. The dialyzed vesicles were recovered from the filter unit and added to a culture plate coated with a solution of 0.1% (w/v) of poly-L-lysine (Sigma-Aldrich). The plates were then centrifuged 5 min at 750xg and incubated overnight at 37 °C, with 5% CO_2, to promote GPMVs adhesion to the coated surface. The starting cell culture should be prepared in a culture area 8x higher than the surface where the purified GPMVs will be applied, in order to achieve a confluent layer of vesicles.

V.3.4 Western blot analysis

For Western blot analysis, GMPV and 16HBE14o- cellular extracts were prepared. Samples were washed twice with PBS (phosphate buffer saline) and a mixture of CLB buffer (1% (v/v) Triton X-100, 1% (v/v) NP-40, in PBS pH 7.4) and protease inhibitors was added to the samples and let to incubate for 10 min at 4 °C. GPMV and cellular monolayers were scrapped, vortexed 10 sec for three times and centrifuged at 14,000

rpm, 10 min at 4 °C. The supernatant was recovered and quantified. A volume of extract corresponding to 30 µg of the total protein was mixed with Laemmli buffer with 5% (v/v) 2-β-mercaptoethanol and 5% (v/v) bromophenol blue and stored at -20 °C. Both samples were boiled for 10 min for protein denaturation and separated by 10% SDS-PAGE. Proteins were transferred onto nitrocellulose membranes by using a Trans-Blot Turbo transfer system (Bio-Rad). Membranes were blocked with 5% (w/v) nonfat dry milk in PBS containing 0.5% (v/v) Tween 20 (PBS-T) for 1 h, incubated with anti-caveolin-1 (diluted 1:1,000), anti-flotolin-1 (diluted 1:500), anti-FGFR-1 (diluted 1:250) and anti-TNFR (diluted 1:1,000) antibodies, overnight at 4 °C. Membranes were washed three times for 5 min with PBS-T and were then incubated with a secondary antibody (diluted 1:2,000), conjugated to horseradish peroxidase (Santa Cruz), for 1 h. Proteins were detected by the addition of ECL reagent as a substrate and chemiluminescense was captured by Fusion Solo (Viber Lourmat) equipment.

V.3.5 *B. cenocepacia* adhesion to 16HBE14o- cells and derived GPMVs

Adhesion assays were carried out either on GPMVs derived from 16HBE14o cells and living 16HBE14o- cells as described previously (Mil-Homens and Fialho, 2012). Cells ($5x10^5$ cells/well) were seeded in polystyrene 24-well plates one day prior to infection in supplemented medium. Before adhesion, cells were washed with PBS and maintained in MEM medium without supplements. *B. cenocepacia* inoculum was used to infect host cells at a multiplicity of infection (MOI) of 50:1. For GPMVs adhesion, a confluent monolayer was prepared in poly-L-lysine coated 24-well plates in GPMV buffer, on day prior to adhesion. GPMVs monolayers were washed twice with GPMV buffer and maintained in the same buffer. Adhesion was performed with $5x10^7$ CFU per well of confluent GPMVs. The plates were then centrifuged 5 min at 750xg and incubated at 37 °C in 5% CO_2 for 30 min to allow bacterial adherence. Cells were then washed three times with PBS and GPMVs with GPMV buffer and lysed with lysis buffer (10 mM EDTA, 0.25% Triton X-100) for 30 min at room temperature. The adhered bacteria were quantified by plating serial dilutions of the cell lysates. Results are expressed as a percentage of adhesion relatively to the initial bacterial dose applied.

V.3.6 Scanning Electron Microscopy (SEM) imaging

Samples of *B. cenocepacia* K56-2, 16HBE14o- cells and GPMVs were visualized by SEM. Confluent monolayers of epithelial cells and GPMVs were prepared on a glass coverslip coated with poly-L-lysine on a 24-well plate a day before the assay, as previously described. *B. cenocepacia* overnight inoculum was used. A bacterial suspension of $5x10^7$ CFUs was added to a coated coverslip and to cellular and GPMVs monolayers. The plates were then centrifuged 5 min at 750xg and incubated at 37 °C in 5% CO_2 for 30 min to allow bacterial adherence. Samples were washed three times with GPMV buffer or PBS and fixed with a 2% (v/v) PFA, 2.5% (v/v) glutaraldehyde solution for 30 min at 25 °C. Samples were dehydrated with 70% (v/v) ethanol for 10 min, 95% (v/v) ethanol for 10 min, and finally absolute ethanol for 20 min. After complete air-drying, samples were mounted on a carbon conductive adhesive tape followed by gold-palladium coating (Polaron E-5100). Scanning electron microscopy (SEM) images were taken using a field-emission-gun scanning electron microscopy (FEG-SEM) Hitachi S4100 microscope operating at 20 kV with a sample-to-objective working distance of 15 mm.

V.3.7 Total RNA extraction

Total RNA was extracted from GPMV-adherent bacteria after 30 min of contact. GPMVs were produced, purified, and prepared in a coated culture plate (Ø 100 mm) one day prior to adhesion. *B. cenocepacia* adhesion was performed with $1.5x10^9$ CFU per plate of confluent GPMVs. The plates were then centrifuged 5 min at 750xg and incubated at 37 °C in 5% CO_2 for 30 min to allow bacterial adherence. After incubation, the supernatant was removed and the GPMVs monolayer carefully washed three times with GPMV buffer. The GPMVs monolayer and the adherent bacteria were scrapped and centrifuged at 9,000 rpm for 3 min and the resulting pellet was resuspended in TE buffer. Bacterial lysis was achieved by enzymatic treatment with lysozyme and proteinase K (Qiagen). Total RNA was purified from bacterial lysate using RNeasy mini kit (Qiagen), according the manufacturer's protocol. To avoid contamination with genomic DNA, RNA was treated with RNase-free DNA digestion kit (Qiagen) in column during the purification process, for 1 h at room temperature. If necessary, a second step of DNase

(Qiagen) treatment was performed (RNase-free DNA digestion kit), after RNA isolation, using 1 µL DNase for 1.5 µg of RNA to be treated, overnight at 37 °C, followed by inactivation for 5 min at 65 °C, according the manufacturer's instructions. Total RNA concentration was estimated using a UV spectrophotometer (ND-1000 UV-Vis, NanoDrop Technologies, USA).

V.3.8 Reverse Transcription PCR and Real-time PCR

For RT-PCR total RNA was converted to cDNA using Taqman Kit (Applied Biosystems) and then analyzed with Power SYBR Green Master Mix (Applied Biosystems), using primers to amplify *BCAM02418*, *bcaA, BCAM0729*, *BCAL1829*, *BCAL293*, *BCAL3068*, *BCAM1570*, *BCAM2531* and *sigA* gene (used as an internal control) (Table V.1). All samples were analyzed in triplicate and the amount of mRNA detected normalized to control *sigA* mRNA values. Relative quantification of genes expression was calculated by using the ΔΔCT method (Livak and Schmittgen, 2001).

V.3.9 RNA sequencing

RNA sequencing was conducted as a service provided by Admera Health Biopharma Services (South Plainfield, NJ, USA), using a validated Transcriptomic Analysis Pipeline. The RNA quality was assessed and samples that had an RNA integrity number (RIN) value >6.5 were used for further analysis. Three replicates of non-adherent (control) and GPMV-adherent bacteria (sample) RNA samples were used to perform mRNA paired-end library construction with a TruSeq Stranded RNA with rRNA Depletion (Illumina, San Diego, CA, USA). Before alignment of sequence reads, quality check (FastQC), removal of adapter content (used during sequencing) and quality thresholding (remove any bad quality reads (Phred Score < 30)), were performed. The RNA-Seq reads were mapped against the genome and annotations of *B. cenocepacia* J2315 (obtained from Ensembl) to identify transcripts. Quantification of differential expressed transcripts was evaluated to estimate the relative abundances between groups (sample vs control). Normalization of the expression values (Log_2_FPKM (Fragments per Kilobase per Million)) was performed and the significantly up-regulated and down-regulated genes were

identified. The significance threshold was P-value <0.01 (FDR-adjusted P-value) and fold-change ≥1.5.

Table V.1 – **List of RT-PCR primers used in this study.**

Gene	Primer	Sequence
sigA	Forward	5'-GCCGATGCGTTTCGGTAT-3'
	Reverse	5'-GCGTGACGTCGAACTGCTT-3'
bcaA	Forward	5'-TCACGAGGCGAATTGTCAAC-3'
	Reverse	5'-GAGACGTTCACGACATCCGTATC-3'
BCAM2418	Forward	5'-CGCCAATACCTTCGTTCCA-3'
	Reverse	5'-CGGGATAGGCATTGGTGTTG-3'
BCAM0729	Forward	5'-GATCTCGGCTACGTCGAGTTTT-3'
	Reverse	5'-GTATTCACGACGAATTGCGTG-3'
BCAL1829	Forward	5'-CGTGTCGATCAACAAGAGCA-3'
	Reverse	5'-GACGTGCAGTTGACGAAGAA-3'
BCAL2933	Forward	5'-TCAAGTGGATGTTCGAAAAGCA-3'
	Reverse	5'-AATGGATGTATCAGATGCTGCG-3'
BCAL3068	Forward	5'-GCGGTGAAGGAGCAGTTG-3'
	Reverse	5'-CGGATTTCGACGAAGGACTG-3'
BCAM1570	Forward	5'-TATTCGGTGAACGGCAGCTA-3'
	Reverse	5'-TCACGGTCTACAAGGGCATT-3'
BCAM2531	Forward	5'-CGACGTGAAGATCGTCGAAT-3'
	Reverse	5'-CGAACGATCCGGTCAATGG-3'

V.3.10 Bioinformatic Analysis

Heat maps of *B. cenocepacia* genes expression during adhesion to 16HBE14o- GPMVs were created using Heatmapper online platform (http://www.heatmapper.ca) (Babicki, et al. 2016). To evaluate putative functions of the differentially expressed transcripts the identified genes were analyzed using Clusters of Orthologous Groups (COG) database. Gene annotation or predicted protein function were retrieved from the *B. cenocepacia* J2315 genome at *Burkholderia* Genome Database (http://www.burkholderia.com) (Winsor, et al. 2008). Voronoi tessellations were created using Voronto mapper web service (Santamaría and Pierre, 2012). Genes were associated in Gene Ontology of KEGG pathway database obtained in ShinyGO v0.61 software. Enrichment analysis were based on hypergeometric distribution followed by FDR correction (Ge, et al. 2020).

V.3.11 Statistical Analysis

Data are expressed as mean values of a minimum of three independent experiments ± standard error (SE). Statistical analysis was carried out by using GraphPad Prism 8.0.1 software. Relative comparisons were done among corrected values with ANOVA test for significance. Fisher exact test was used to identify significantly expressed COG. A P-value of <0.05 was considered statistically significant in all analysis.

V.4 Results

V.4.1 Production and characterization of GPMVs derived from bronchial epithelial cells

The first step of this work involved the production and characterization of GPMVs from a bronchial epithelial cell line (16HBE14o-). The optimized protocol is represented in Figure V.1. Cellular vesiculation was induced by a mixture of dithiothreitol (DTT) and paraformaldehyde (PFA). GPMVs were collected from the culture supernatant, concentrated and traces of the vesiculation agents were removed by dialysis. A confluent monolayer of GPMVs was achieved by vesicle seeding and adherence in a polystyrene poly-L-lysine coated surface for one day.

The morphology of the produced GPMVs was assessed by SEM (Scanning Electron Microscopy) and the images are presented in Figure V.2A. The visualized GPMVs have a spherical-like shape with a median size of 3 to 5 μm in diameter; they present a rough surface with several structures that seem to stretch over their exterior. (Figure V.2A).

Next, we performed Western blot analysis to compare the protein compositions of GPMVs and cell membranes. TNFR-1 (tumor necrosis factor receptor-1), flotillin-1, caveolin-1, and FGFR-1 (fibroblast growth factor receptor-1) were selected as target proteins. The obtained results showed the presence of all tested proteins in both samples (plasma vesicles and cells) (Figure V.2B). Despite the result obtained for FGFR-1, the other proteins were less intense in GPMVs when compared to cells.

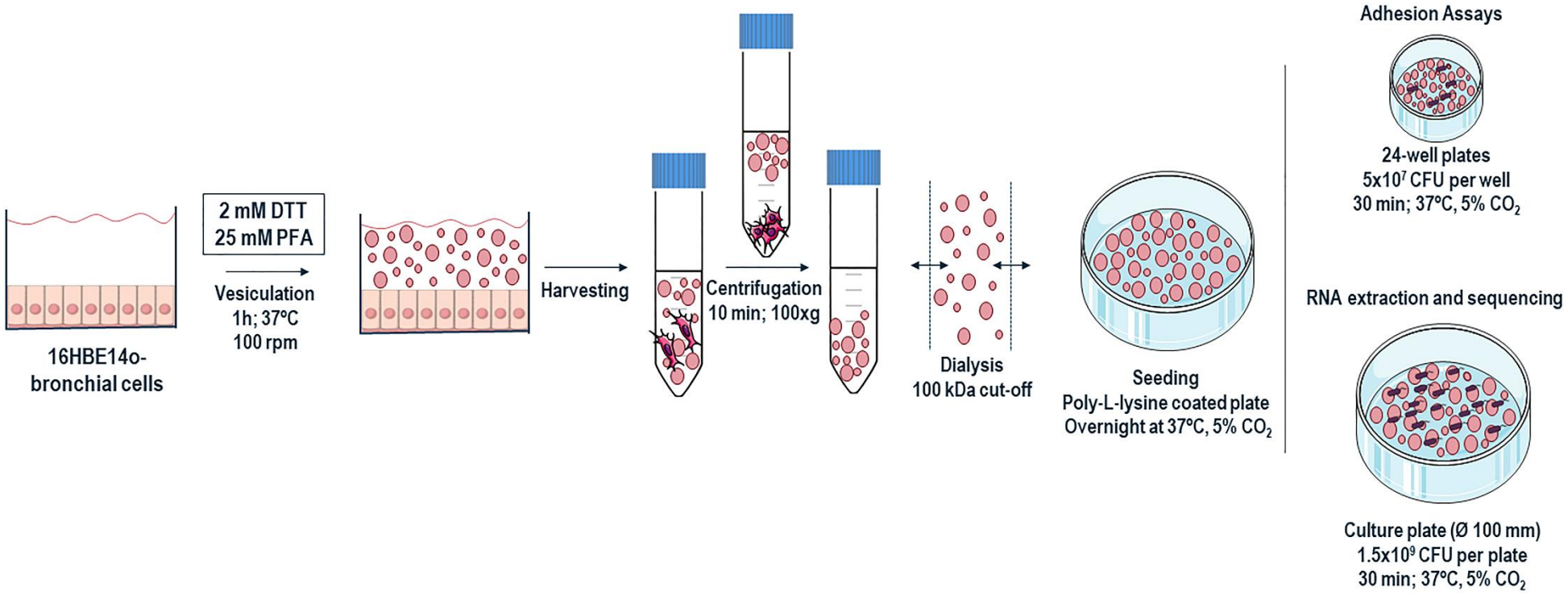

Figure V.1. Schematic representation of Giant Plasma Membrane Vesicles production and purification. Briefly, the cells were treated with GPMV-reagent containing PFA and DTT during 1h to allow vesiculation. The starting cell culture should be prepared in a culture area 8x higher than the surface where the purified GPMVs will be applied, in order to achieve a confluent layer of vesicles. After incubation, GPMV-enriched supernatant was collected and centrifuged to sediment cellular debris. The clear GPMVs suspension was dialyzed to remove the PFA and DTT. The GPMV suspension was also concentrated and seeded in a poly-L-lysine coated plate, overnight at 37 ˚C, 5% CO_2 for further assays. For adhesion assays, 24-well plates were used, and adhesion was performed with $5x10^7$ *B. cenocepacia* K56-2 CFU per well. For total RNA extraction and further RNA sequencing analysis, adhesion was performed in a culture plate of Ø 100 mm using $1.5x10^9$ *B. cenocepacia* K56-2 CFU per plate. In both cases, bacteria were allowed to adhere for 30 min, at 37 ˚C, 5% CO_2.

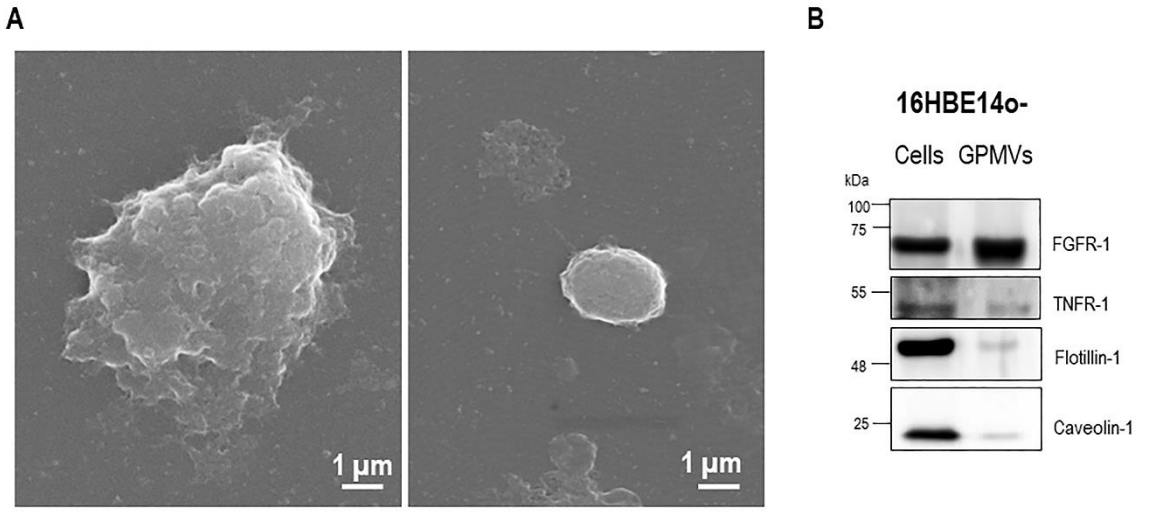

Figure V.2. Scanning electron microscopy (SEM) images of 16HBE14o- produced GPMVs (A). A scale bar is presented in every SEM image. Western Blot analysis of 16HBE14o- cellular and vesicular protein extracts. The presence of TNFR-1, Flotillin-1, FGFR-1 and Caveolin-1 was analyzed using specific antibodies. The exposure time was optimized for each target, ranging from 5 min to 10 min. NZYColour protein marker II was used (**B**).

V.4.2 *B. cenocepacia* K56-2 efficiently adheres to 16HBE14o- derived GPMVs

We next optimized a *B. cenocepacia* adhesion assay using a monolayer of 16HBE14o- derived GPMVs. As a comparative assay, adhesion to 16HBE14o- cells was also performed with the same bacterial inoculum. The obtained results are represented in Figure 3A. When compared to the adhesion values obtained after contact with 16HBE14o- cells, the percentage of *B. cenocepacia* adhesion to GPMVs was considerably superior. This increase could be related to biophysical alterations on the plasma membrane during the vesiculation, which could make GPMVs more prone to interact with pathogenic bacteria. The results indicated that GPMVs, as cell derived-membrane systems, mimicked cell membranes of 16HBE14o- cells and thereby can serve as an alternative to living systems.

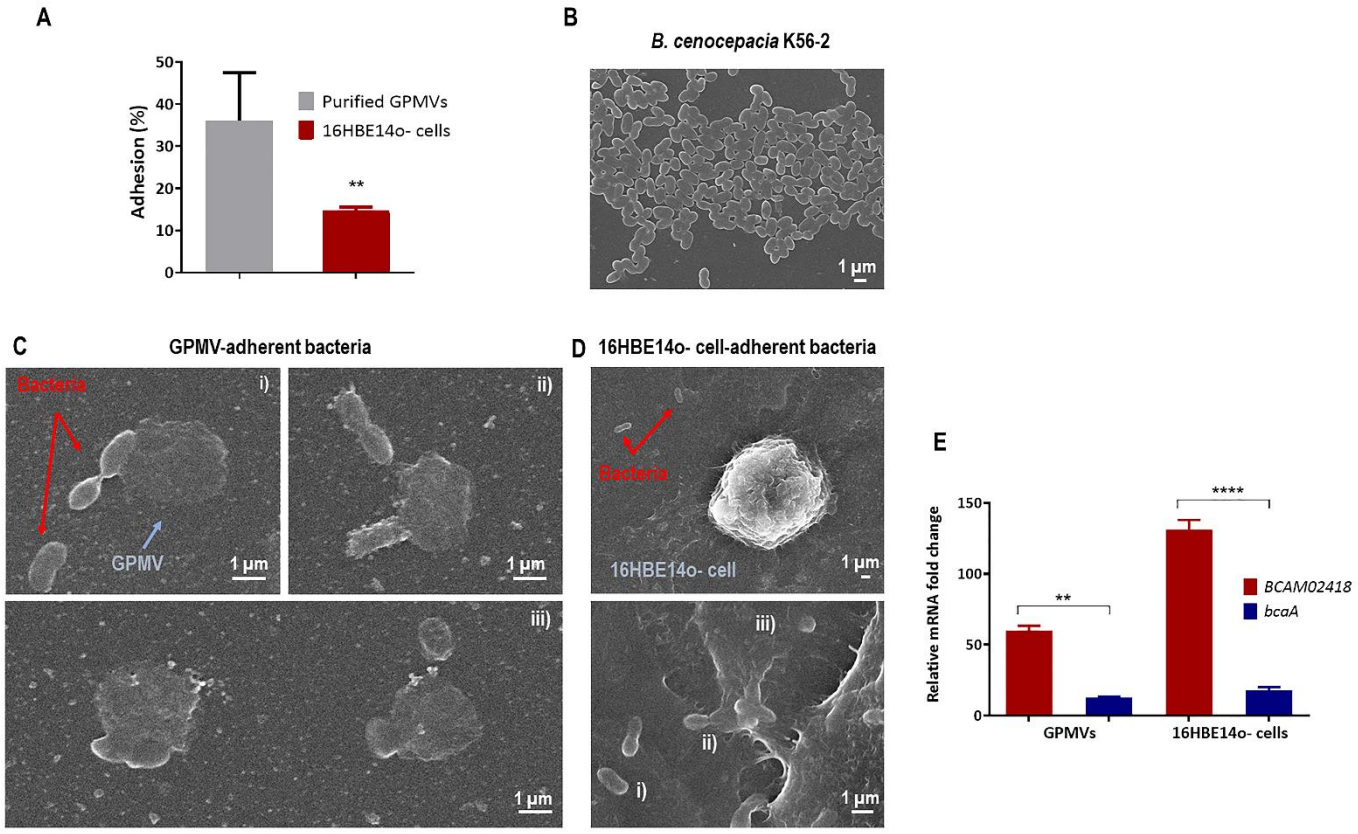

Figure V.3. *B. cenocepacia* K56-2 interaction with 16HBE14o- derived GPMVs. *B. cenocepacia* K56-2 adhesion to 16HBE14o- cells and GPMVs (**A**). Adhesion assays were performed for 30 min against 16HBE14o- GPMVs and against cells as a comparison method. *B. cenocepacia* adhere more efficiently to purified GPMVs than to cells. Also, adhesion percentage to GPMVs is higher than the adhesion to the original cells. (****P <0.0001; **P <0.01). Error bars indicate the standard error (SE). Scanning electron microscopy (SEM) images of *B. cenocepacia* K56-2 cells (**B**), bacteria-GPMV adhesion (**C**), and bacteria-16HBE14o- cell adhesion (**D**). Bacteria are highlighted by red arrows and GPMVs by blue ones. A scale bar is presented in every SEM image. Expression of *BCAM2418* and *bcaA* TAA coding genes (**F**). Transcription levels of *B. cenocepacia* K56-2 *BCAM2418* and *bcaA* were obtained by qRT-PCR from bacteria adherent to 16HBE14o- cells and GPMVs (30 min of contact). Results were normalized to expression of the housekeeping *sigA* gene. Expression levels are represented as relative values in comparison to the expression levels in standard LB growth. All the results are from three independent experiments, bars indicate SE (**P <0.01; ****P <0.0001).

To confirm *B. cenocepacia* K56-2 interaction with 16HBE14o- GPMVs, SEM images were obtained. The results are presented in Figure V.3 and show images of *B. cenocepacia* K56-2 (B), and the bacterial adherence to vesicles (C) and cells (D). Concerning the interaction between GPMVs and *B. cenocepacia* cells (Figure V.3C), bacterial cells with rod-like shape were clearly in contact with the GPMVs. This contact can be observed to occur in different stages. In an initial stage, bacteria were in contact with GPMV surface (i), in a following step, bacteria looked to be embedded inside GPMV (ii) and later a fusion-like process seemed to occur (iii). When comparing with Figure V.3D, similar events can be seen between the bacteria and the cell, where an initial contact phase can be observed (i), followed by an imbibition of the bacterial cells into the cell (ii) and fusion (iii). These observations corroborated the adequacy of our system for studying the initial interactions of *B. cenocepacia* cells.

To verify if the adhesion to GPMVs conferred the same *stimuli* to *B. cenocepacia* as the adhesion to host cells, qRT-PCR was performed using both samples – RNA extracted from bacteria adherent to GPMVs and epithelial cells (Figure V.3E). The chosen genes were used before and shown to have differential levels of expression after *B. cenocepacia* adhesion to 16HBE14o- cells (Pimenta, et al. 2020a). *BCAM2418* and *bcaA* genes codify two *B. cenocepacia* TAAs. The results in Figure V.3F indicated that after adhesion to GPMVs, *B. cenocepacia* TAAs gene transcription were activated in the same pattern that after adhesion to epithelial cells. In both cases, *BCAM2418* gene was significantly more expressed than *bcaA*. These results may indicate that GPMVs are a proper model to substitute the entire cell in the study of the early stages of host-bacteria interactions.

V.4.3 Adherence to 16HBE14o-GPMVs alter the transcriptomic profile of *B. cenocepacia* K56-2

To monitor alterations in the transcriptional profile of *B. cenocepacia* K56-2 after adhesion to bronchial cells-derived GPMVs (30 min), RNAseq was performed and the expression of the adherent (GPMV-attached) and non-adherent (planktonic control) bacteria were compared. Using a fold change cut off of ≥ 1.5 (adjusted P-value < 0.01),

the obtained RNAseq dataset indicated a total of 926 genes which expression was altered upon bacteria-GPMV contact, that represented 12.7% of *B. cenocepacia* K56-2 coding genes. From those, 496 genes (53.6%) were up-regulated and 430 (46.4%) were down-regulated (Figure V.4A), indicating that the contact with GPMV had an impact in *B. cenocepacia* K56-2 gene expression. The obtained fold change values ranged from 560.205 (*BCAL0729*) to -215.050 (*BCAL2933*).

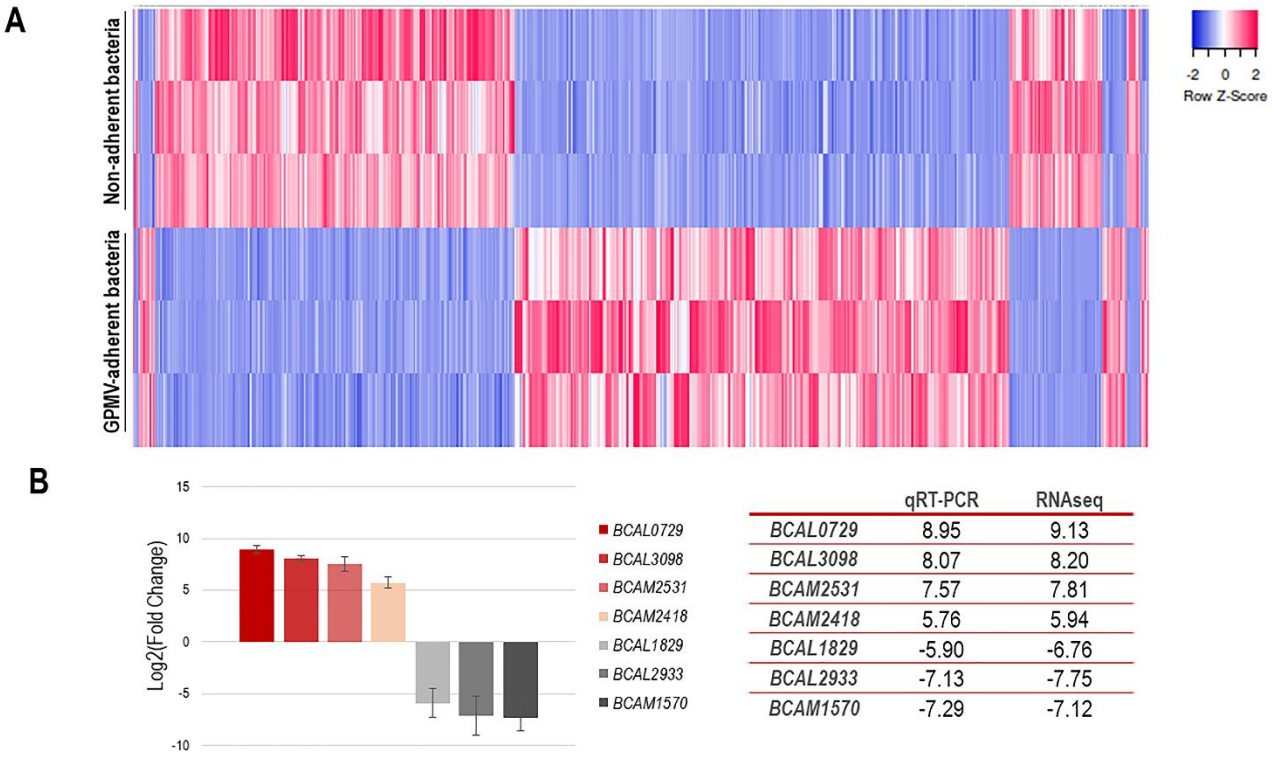

	qRT-PCR	RNAseq
BCAL0729	8.95	9.13
BCAL3098	8.07	8.20
BCAM2531	7.57	7.81
BCAM2418	5.76	5.94
BCAL1829	-5.90	-6.76
BCAL2933	-7.13	-7.75
BCAM1570	-7.29	-7.12

Figure V.4. Transcriptomic alterations after *B. cenocepacia* K56-2 adherence to 16HBE14o- GPMVs. Heat map of *B. cenocepacia* K56-2 genes expression during adhesion to 16HBE14o- GPMVs (**A**). Colors from white to pink indicate upregulated genes; colors from white to blue indicate downregulated genes. Data from three replicas are represented. Heat maps were created using Heatmapper online platform (http://www.heatmapper.ca) (Babicki, et al. 2016). Dataset validation by qRT-PCR (**B**). Transcription levels of *B. cenocepacia* K56-2 *BCAL0729*, *BCAL3098*, *BCAM2531*, *BCAM2418*, *BCAL1829*, *BCAL2933* and *BCAM1570* genes were obtained by qRT-PCR from bacteria adherent to 16HBE14o- GPMVs (30 min of contact). Expression levels are represented as Log2(Fold change) relative values in comparison to the expression levels of non-adherent bacteria. All the results are from three independent experiments, bars indicate SE (**P <0.01; ****P <0.0001).

To validate the dataset, qRT-PCR was performed using primers for seven genes, both up- and down-regulated (Figure V.4B). The high expression of *BCAL0729* (nitrogen

regulatory protein P-II 1), *BCAL3098* (putative ABC transporter substrate-binding protein), *BCAM2531* (putative ABC transporter solute-binding protein) and *BCAM2418* (trimeric autotransporter adhesin); and the low expression levels of *BCAL1829* (putative outer membrane protein), *BCAL2933* (D-amino acid dehydrogenase small subunit) and *BCAM1570* (alcohol dehydrogenase) genes were confirmed using qRT-PCR and the fold change values were comparable to the ones obtained for RNAseq.

V.4.4 Genes involved in metabolic pathways and cellular information processing are highly altered upon *B. cenocepacia* K56-2 adhesion to 16HBE14o- GPMVs

To evaluate functions of the differentially expressed transcripts the identified genes were analyzed using COG database (Figure V.5). The majority of the up-regulated genes (55.0%) were predicted to be involved in metabolism (transport and metabolism of amino acids (n=101), inorganic ions (n=59), carbohydrates (n=24), lipids (n=24), secondary metabolites biosynthesis, transport and catabolism (n=12), transport and metabolism of coenzymes (n=6) and nucleotides (n=5) and energy production (n= 42)). Around 14.3% of the highly expressed genes were involved in cellular processing and signal (cell wall/membrane/envelope biogenesis (n=19), signal transduction mechanisms (n=18), intracellular trafficking, secretion, and vesicular transport (n=13), post-translational modification, protein turnover and chaperones (n=10), cell motility (n=9), defense mechanisms (n=2) and extracellular structures (n=2)). 7.3% of the genes were corresponding to information storage and processing (transcription (n=29), replication, recombination, and repair (n=5) and translation and ribosomal biogenesis (n=2)).

Regarding down-regulated genes, 47.4% were predicted to be implicated in metabolism (energy production (n= 72), transport and metabolism of amino acids (n=41), lipids (n=28), inorganic ions (n=19), nucleotides (n=13), secondary metabolites biosynthesis, transport and catabolism (n=12), transport and metabolism of coenzymes (n=10) and carbohydrates (n=9)). About 25.1% of the transcripts were predicted to participate in cellular processing and signal (signal transduction mechanisms (n=29), post-translational modification, protein turnover and chaperones (n=28), cell

wall/membrane/envelope biogenesis (n=23), cell motility (n=13), intracellular trafficking, secretion, and vesicular transport (n=11) and cell cycle control and division (n=4)). Approximately 19.8% of the genes were corresponding to information storage and processing (translation and ribosomal biogenesis (n=47), transcription (n=27) and replication, recombination, and repair (n=11)). Considering both up- and down-regulated group of genes, 23.4% and 23.7%, respectively, were grouped as poorly characterized.

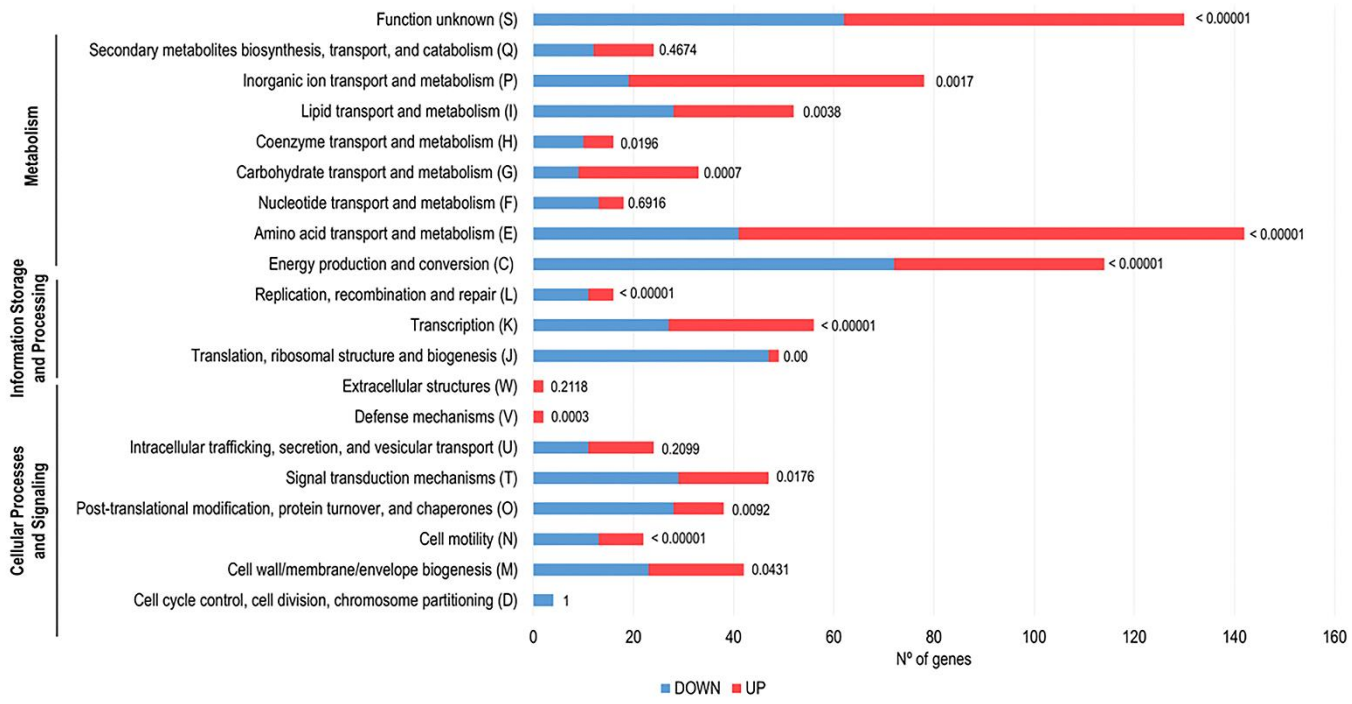

Figure V.5. Clustering, based on biological function, of the genes found to be differently expressed upon *B. cenocepacia* K56-2 adhesion to 16HBE14o- GPMVs (30 min of contact). Down-regulated genes are represented by blue bars and up-regulated genes by pink bars. Biological function information was based on the information available in the *Burkholderia* Genome database and in the COG Database.

When compared both datasets, it was notable that up-regulated genes were more involved in metabolic pathways, namely amino acid and inorganic ions transport and metabolism and energy production and conversion. Revealing a possible metabolic adaptation in consequence of the proximity and contact with the host surface. Besides metabolism (energy production and conversion and amino acid transport), the down-regulated genes played an important role in, translation and ribosome biogenesis, transcription, post-translational modifications, and signal transduction mechanisms. This may indicate a bacterial growth and cell division reduction upon host sensing.

V.4.5 Pathway analysis of the differentially expressed genes revealed distinct putative functions.

To go further in the evaluation of the functional roles of the differentially expressed genes, a KEGG pathway analysis was performed. The statistically significant changes are illustrated as Voronoi tree maps in Figure V.6. To illustrate the statistically significant alterations ($P < 0.01$; fold change ≥ 1.5), Voronoi tessellations were created using Voronto mapper web service (Santamaría and Pierre, 2012). From the totality of the genes with altered expression, only 47.8% were KEGG annotated genes. A general overview concerning the main differences between non-adherent and GPMV-adherent bacteria gene expression is shown in Figure V.6. It is noteworthy that most transcriptomic changes were concentrated on metabolism, environmental information processing, organismal systems, and genetic information processing pathways. Relating to GPMV-adherent bacteria, genes involved in processes like oxidative phosphorylation (energy metabolism), amino acid metabolism, TCA cycle and propanoate metabolism (carbohydrate metabolism) were down-regulated alongside with genes participating in translation, transcription, RNA-degradation, and replication mechanisms. On contrary, genes that encode for membrane transport structures, like ABC transporters, were up regulated. The same was the case for genes involved in sulfur metabolism (energy metabolism), quorum sensing and cell growth and death (Figure V.6).

The entries for enrichment analysis of KEGG pathways were resumed in Tables V.S1 and V.S2 (Supplementary data). Datasets for up- and down-regulated genes were analyzed

using ShinyGO v0.61: Gene Ontology Enrichment Analysis web service (Ge, et al. 2020), and the most significant enriched pathways were selected and confirmed the results obtained in Voronoi tessellations. The majority of the up-regulated pathways were found to be involved in ABC transporters and metabolic functions, in particular sulfur, taurine and hypotaurine metabolism, nitrogen metabolism, glyoxylate and dicarboxylate metabolism and fatty acid degradation and metabolism as possible alternative sources of energy. Concerning ABC transporters, 81 genes (30.7%) were found to be upregulated, including genes involved in transport of potassium, glutamate/aspartate, amino acids, sugars, like ribose and maltose, sulfate, and nitrogen. In some cases, the transcription of an entire gene cluster was observed, such as the Kdp system (*BCAL2379-2383* – *kdpA-E*), responsible for potassium transport, Glt genes (*BCAL3356-3358* – *gltI-K*) (glutamate/aspartate transport), genes involved in branched-chain amino acids import (*BCAL0015-0019*) and genes involved in sulfate uptake (*BCAL1652-1657* – *sbp, cysT, cysW, cysA, ssuR*). Also, genes involved in two-component systems (signal transduction) and in the biosynthesis of amino acids were also up-regulated. Additionally, several genes implicated in flagellar assembly (17.5%) were induced during *B. cenocepacia* adhesion alongside with 6 genes involved in bacterial chemotaxis, namely flagellar motor switch protein coding genes – *fliG* and *fliM*; and *BCAL1657* (putative ribose transport system) and *BCAM0766* (D-ribose-binding periplasmic protein precursor) which was associated with ribose-related pathways (Table V.S1).

In contrast, several metabolic pathways were down-regulated, namely oxidative phosphorylation, carbon metabolism, citrate cycle (TCA cycle), purine metabolism, biosynthesis of secondary metabolites, pyruvate metabolism, and glycolysis and gluconeogenesis. Regarding oxidative phosphorylation, 60.8% of the genes were repressed, including genes that encode F0F1 ATP synthase subunits (*BCAL0032-0037* – *atpACDFGH*), cytochrome C oxidase proteins (*BCAL0750, 0752, 0754*), cytochrome D (*BCAL0784-0785, cydAB*) and O (*BCAL2141-2144, cyoA-D*) ubiquinol oxidase subunits and succinate dehydrogenase subunits (*BCAM0969-0970*, *sdhAB*). Moreover, type I NADH dehydrogenase 14 subunit genes, that were organized in the *nuo* locus were down regulated as well (*BCAL2331-2344*, *nuoA-N*). Interestingly, *ndh* gene (*BCAM0166*)

that encodes for type II NADH dehydrogenase was found to be up regulated. Cellular processes like transcription and translation were affected upon bacterial-GPMV adhesion too. The expression of three (*rpoA*, *rpoB* and *rpoC*) out of the four RNA-polymerase subunit genes were down-regulated as well as genes involved in aminoacyl-tRNA biosynthesis, namely aspartyl-, glutaminyl-, valyl-, phenylalanyl-, histidyl- and tryptophanyl-tRNA synthetases (*aspS*, *glnS*, *valS*, *pheT*, *hisS* and *trpS*). Moreover, 49.1% of ribosomal proteins were found to be downregulated, being that 11 genes encode for 30S ribosomal subunit proteins and 17 genes for 50S subunit, which indicated an impressive reduction in ribosomal production and activity (Table V.S2). Bacterial chemotaxis also was altered upon *B. cenocepacia* K56-2 early contacts with host-cell membranes. Despite some genes that were up regulated, 32.5% of the genes involved in chemotaxis pathways were found to be down regulated, including 8 genes belonging to the chemotaxis gene cluster – *BCAL0126* (*motA*), *BCAL0129-0135* (*cheA*, *cheW*, *tar*, *cheR*, *cheD*, *cheB1* and *cheY*). Aside from that, 4 methyl-accepting chemotaxis proteins were also repressed - *BCAL0762*, *BCAM1503*, *BCAM1572* and *BCAM1804*, and *aer* (*BCAM2564*) a putative aerotaxis receptor that is known to sense environmental oxygen levels. Apart from that, expression of genes related to protein export systems, namely the SEC dependent pathway, was also repressed. Both post- and co-translational translocation were affected. In the first category were included genes that encode for translocation channel and related proteins, like *BCAL0254* (*secY*), *BCAL0742* (*secB*), *BCAL3307* (*secF*) and *BCAL3433* (*secA*). In the second one, *BCAL3453* (*ffh*) that encodes for a signal recognition particle protein involved in targeting and insertion of nascent membrane proteins into the cytoplasmic membrane (Table V.S2).

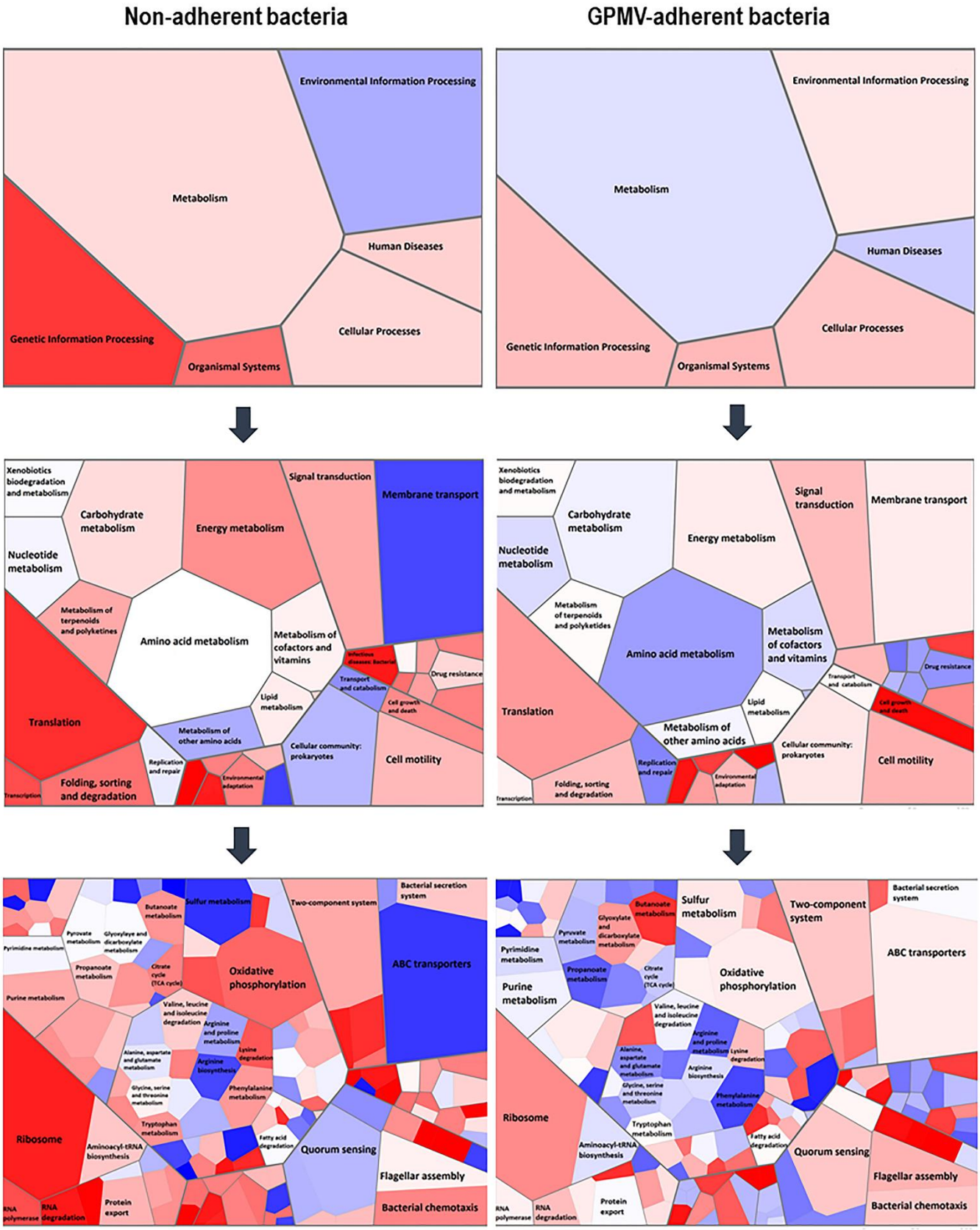

Figure V.6. Evaluation of functional roles of the differentially expressed genes (P <0.01; fold change greater or equal to 1.5 or less or equal to -1.5). A KEGG pathway analysis was performed, and statistically significant alterations are illustrated as Voronoi tessellations, created using Voronto mapper web service (Santamaría and Pierre, 2012).

V.4.6 *B. cenocepacia* K56-2 modulates adhesion and invasion factors expression upon GPMV-adhesion

Several genes that promote *B. cenocepacia* K56-2 interaction with the host cell, including the ones that encode for adhesins, outer membrane proteins, lipoproteins and proteins involved in pilus and flagella assembly and function were differentially regulated upon GPMV-adhesion (Figure V.7). The altered expression of these genes may represent a prompt response to the sensing of the host-membrane surface with the consequent increase of bacterial adhesion. Data shown numerous pilus associated genes with an enhanced expression after 30 min of GPMV-adhesion, namely flp type pilus subunit *BCAL1525* and flp type pilus assembly protein coding genes – *BCAL1526, BCAL1528*, *BCAL1529*, *BCAL1530*, *BCAL1531* and *BCAL1532*. Nearby putative lipoproteins *BCAL1533*, *BCAL1520*, *BCAL1523* and *BCAL1524* were also found to be highly induced. Apart from that, it is noteworthy that although *BCAM2461* (*cblA* - giant cable pilus) coding gene was repressed, *BCAM2143* (*adhA* - cable pilus associated adhesin) was up-regulated, indicating a possible differential role played by both proteins during the early stages of bacteria-host cell interaction. Considering flagella related genes, nine had an altered expression during *B. cenocepacia*-GPMV adhesion. Among them, flagellar biosynthesis proteins – *BCAL0141* (*flhA*), *BCAL0140* (*flhB*) and *BCAL0143* (putative), *BCAL3506* (*fliM* - flagellar motor switch) and *BCAL0567* (*flpE1* - flagellar hook protein) were found to be upregulated genes. On the other hand, *BCAL0126* (*motA* - flagellar motor protein), *BCAL0576* (*flgK* - flagellar hook-associated protein) and *BCAL0114* (*fliC* - flagellin) were found to be downregulated during adhesion.

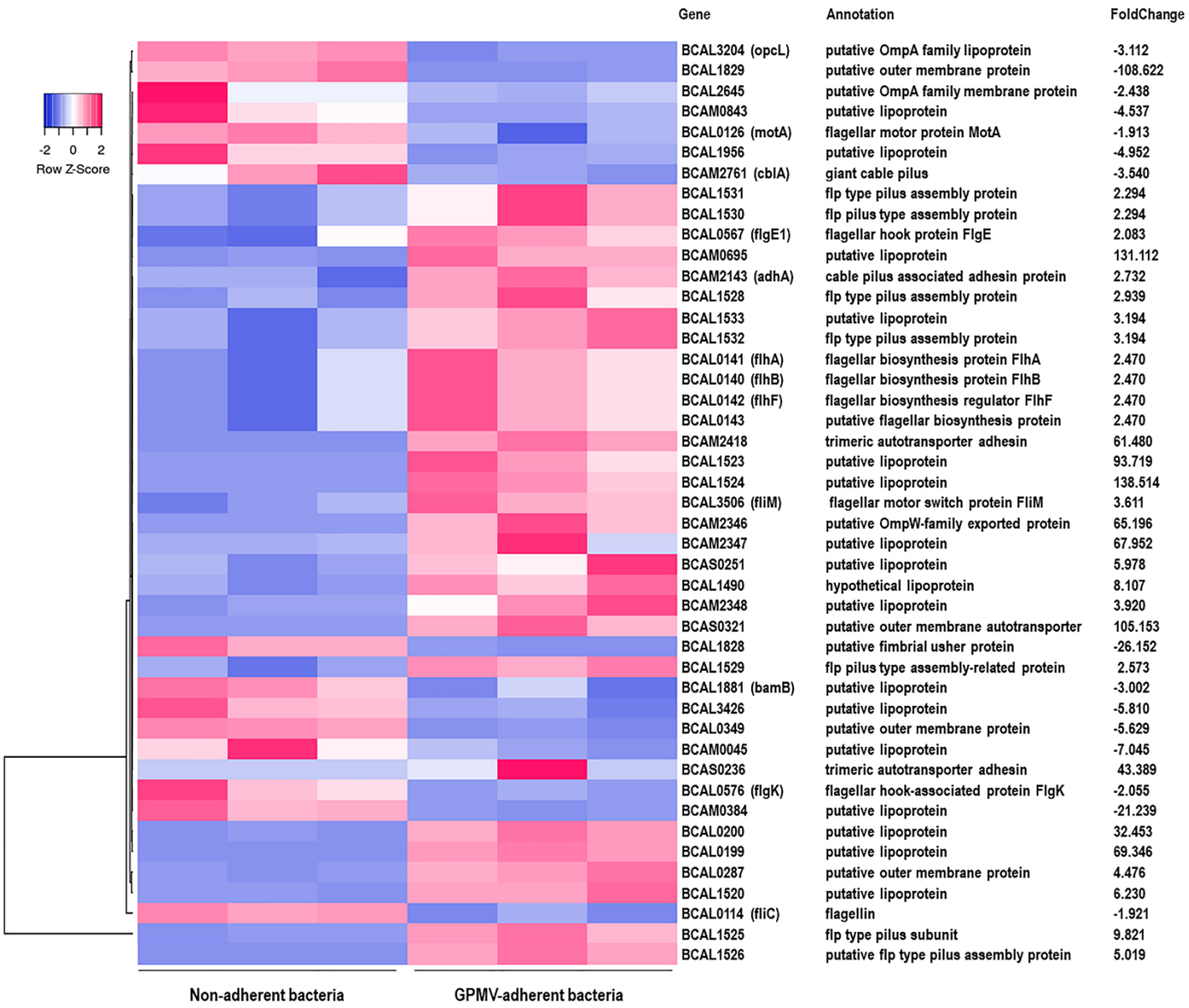

Figure V.7. Heat map of *B. cenocepacia* adhesion and invasion related genes expression during adhesion to 16HBE14o- GPMVs. Colors from white to pink indicate upregulated genes; colors from white to blue indicate downregulated genes. Heat maps were created using Heatmapper online platform (http://www.heatmapper.ca) (Babicki, et al. 2016). Several genes that promote *B. cenocepacia* K56-2 interaction with the host cell, including genes that encode for adhesins, outer membrane proteins, lipoproteins and proteins involved in pilus and flagella assembly were differentially regulated upon GPMV-adhesion.

Additionally, a set of lipoproteins (n=17), outer membrane proteins (n=6) and several adhesins coding genes were differentially expressed throughout adhesion. Aside from cable pilus associated adhesin, trimeric autotransporter adhesins – *BCAM2418* and *BCAS0236*, and *BCAS0321*, a putative outer membrane autotransporter, were highly overexpressed with foldchange values of 61.48, 43.389 and 105.153, respectively. Moreover, despite belonging to different autotransporter classes (type Vc and Va), BCAM2418, BCAS0236 and BCAS0321 share some common features like the presence of β-barrel membrane anchor domains and an elevated number of amino acid residues – 2775, 1496 and 4234, respectively. Nonetheless, *BCAM1881* that encodes for a putative BamB lipoprotein, that is known to be part of the BAM complex which is involved in the assembly and insertion of β-barrel proteins into the outer membrane, was repressed upon adhesion (Han, et al. 2016). The size of these autotransporter adhesins may suggest that the bacterial cell must endure an energetic effort to overproduce them and that a BAM alternative outer membrane protein assembly complex, like TAM, could be involved in the translocation of these proteins across the membrane (Kiessling, et al. 2020).

V.5 Discussion

The first contact between a bacterium and a host-cell surface is the crucial step for the development of an infection, leading to physiological alterations in both interacting cells (Pizarro-Cerdá and Cossart, 2006; Stones and Krachler, 2016). For bacteria, these alterations allow them to change and adapt to the new environment and cause an enhanced virulence fitness that may induce further invasion of host cells and destruction of epithelial tissue (David, et al. 2015; Stones and Krachler, 2016). The study of bacteria initial interactions with host cell-membranes is challenging. The exact contribution of the cell membrane physical contacts in the bacterial transcriptomic shift is hard to achieve since the surrounding environment of the host epithelium is a complex mixture of cell-derived molecules, cellular-trafficking structures, and other type of biological compounds. GPMVs derive from the cell plasma membrane offer a close approximation

to it, which make them a suitable model for a potential host membrane surrogate (Sezgin, et al. 2012). In this work we produced GPMVs from a bronchial epithelial cell line and used them for the first time as target for *B. cenocepacia* K56-2 adhesion. Further studies were also performed to understand the transcriptomic alterations caused by such contacts in the bacterial adaptation during the early host membrane contacts. Vesiculation of 16HBE14o- cell line was chemically induced and the resulting GPMVs proven to have a spherical structure with a rough surface and a discrete diameter range of 3-5 µm. Moreover, GPMVs shown to be constituted not only by plasmatic membrane structures but also by host transmembrane proteins. Western Blot assays demonstrated the presence of the same proteins in both native-cells and vesicles, indicating that, as shown by others, GPMVs share functional and structural similarities with the cells that they are originated from (Bauer, et al. 2009; Sezgin, et al. 2012). The use of GPMVs as a model to study bacterial interactions with the host cell membrane is a new and essential approach that is still undeveloped. In recent years, several findings have been made concerning the binding, interaction and penetration of viral proteins and bacterial toxins using GPMVs as membrane models (Nikolaus, et al. 2010; Manni, et al. 2015, Raghunathan, et al. 2016; Yang, et al. 2017). Nonetheless, till this date, the usage of giant vesicles in the study of host-membrane interactions with microorganisms as a whole was not yet performed.

B. cenocepacia is an opportunistic pathogen that can be commonly found in soil and aquatic environments. Its capacity to adapt to different environments such as the host respiratory tract, is noteworthy. Several transcriptional studies designed to examine gene expression of *B. cenocepacia* in different environments helped the identification of new genes that prove to be important in virulence (Yoder-Himes, et al. 2010; O'Grady and Sokol, 2011; Sass, et al. 2013). In this work we completed a transcriptional profiling at the whole genome level of *B. cenocepacia* K56-2 upon the early contacts with the host-cell membrane, using GPMVs as cellular surrogate, and compared to planktonic laboratory-grown bacteria.

Notably, we observed that the early interaction of *B. cenocepacia* K56-2 with the bronchial cell membrane led to an alteration of the bacterial metabolic pathways, like the downregulation of the central metabolism as a way to adapt to the new host

environment. These included oxidative phosphorylation, carbon metabolism, TCA cycle and glycolysis and gluconeogenesis. In contrast, genes involved in sulfur and nitrogen metabolism, glyoxylate metabolism, CoA biosynthesis and fatty acid catabolism were upregulated during bacterial adhesion to GPMVs. The interaction with the host initiated a modulation of key bacterial systems that indicates a progressive adaptation in order to exploit the nutrients available in the host during the infection cycle. A representation of the altered metabolic regime due to the evolving substrate availability is the induction of a large number of genes encoding for transport machineries, including those involved in the uptake of sugars, amino acids, potassium, sulfate and nitrogen. The adaptation to a different lifestyle by shifting major metabolic pathways was reported in other pathogenic bacteria (O'Grady and Sokol, 2011; Baddal, et al. 2015; Mariappan, et al. 2017). Nevertheless, the occurrence of this type of adjustment in the early stages of bacteria-host interaction is still poorly documented. It is possible that *B. cenocepacia* adaptation to the host environment occurs after the first physical contacts to the host surface rather than being a consequence of a chronical infection state (Mira, et al. 2011, O'Grady and Sokol, 2011). The induction of sulfur-metabolism is one example of *B. cenocepacia* adaptation to the host. The link between sulfur metabolism and virulence has been reported for several bacterial pathogens (Łochowska, et al. 2011) and as a long-term adaptation during *B. cenocepacia* host colonization (Mira, et al. 2011). The overexpression of sulfate starvation-induced genes involved in the cysteine biosynthesis pathway like the *cysTWA* (sulfate transporter operon), *cysI* and *cysH* (sulfate activation and reduction operon), *ssuDCB* (transport and desulfonation of aliphatic sulfonates) and three taurine deoxygenases (*tauD2a*, *tauD2b* and *tauD3*), responsible for the desulfonation of taurine, was reported in this work. The assimilation of sulfur from inorganic sulfate and other alternative sources seems to be a rapid response of *B. cenocepacia* to the early interactions with the host (Kertesz, 2000; Łochowska, et al. 2011). Interestingly, despite taurine being a non-essential amino acid commonly found in humans as source of sulfur, many sulfonates are known to be present in mucins and in the surface of epithelial lung cells, which could explain the prompt metabolic shift (Kertesz, 2000; Iwanicka-Nowicka, et al. 2007; Łochowska, et al. 2011).

Limited oxygen conditions are a typical feature of the lungs of CF patients, and it is also found to be a characteristic of the host-cells interior (McClean and Callaghan, 2009; Schaefers, et al. 2017). *B. cenocepacia* adaptation to a microaerophilic environment during chronic infection has been demonstrated in several studies (Mira, et al. 2011; Cullen, et al. 2018). The decrease in the expression of genes related to oxidative phosphorylation was registered upon bacterial adhesion to bronchial-cell membranes, indicating that *B. cenocepacia* K56-2 adaptation to low levels of oxygen could happen in the initial time frame of infection. After interaction with host-cell surface, *B. cenocepacia* decreased the transcript levels from genes encoding several complexes of the electron transport chain – NADH-dehydrogenase I (NDH-1), cytochrome O, cytochrome D, cytochrome C oxidase and ATP synthase. On the other hand, NADH dehydrogenase II (NDH-2) and cytochrome C reductase complex subunits coding genes were found to be upregulated. In *Pseudomonas aeruginosa*, NDH-1 translocates protons and oxidizes NADH to NAD+, while NDH-2 uses FAD as a cofactor to oxidize NADH without translocating protons (Williams, et al. 2007; Heikal, et al. 2014). Torres and colleagues (2019) reported that NDH-1 seems to be essential for robust *P. aeruginosa* growth under anaerobic conditions and that the overexpression of NDH-2 do not compensate the absence NDH-1 in the same conditions (Torres, et al. 2019). Our results suggested that during the first contacts with the host, in a possible adaptation to the intracellular environment, *B. cenocepacia* K56-2 NDH-1 is not essential, and that NDH-2 expression could be activated.

B. cenocepacia K56-2 cellular processes were found to be highly disturbed during bacterial adhesion to host membranes. The repression of genes encoding proteins related to transcription (RNA-polymerase subunits *rpoA*, *rpoB* and *rpoC*), translation (aminoacyl-tRNA synthetases *aspS*, *glnS*, *valS*, *pheT*, *hisS* and *trpS* and 30S and 50S ribosomal subunit genes) and protein export (sec dependent pathway *secY*, *secB*, *secF*, *secA* and *ffh*) was reported. The replication machinery shut out seems to occur as a preparation for the bacterial intracellular lifestyle. *B. cenocepacia* ability to invade and survive inside host-cells has been well documented, and several studies have indicated that engulfed bacteria undergo intracellular replication at reduced levels over 24-48h post-infection (Hamad, et al. 2010; Schmerk and Valvano, 2013; Valvano, 2015). The

obtained results reinforced the idea that the sensing and early contacts with the host-cell surface may prepare the *B. cenocepacia* for intracellular regime.

The bacteria capacity to move towards or away of a specific environmental signal is known as chemotaxis and is based on the action of several chemosensory pathways. The *che* pathway is required for flagellum-mediated chemotaxis and it is initiated through the recognition of a signal that created a *stimulus* responsible for modulating the phosphorylation of the response regulator that ultimately binds to the flagellar motor causing the flagellum rotation (Terashima, et al. 2008; Kumar, et al., 2013; Matilla and Krell, 2018). The majority of the genes encoding for proteins involved in the *che* chemotaxis signaling pathway were found to be suppressed, including *cheA* (two-component sensor kinase), *cheW* (adaptor protein), *tar* (methyl-accepting protein), *cheR* (methyltransferase), *cheD* (chemoreceptor glutamine deamidase), *cheB1* (chemotaxis-specific methylesterase) and *cheY* (response regulator). Apart from that, *fliC* (flagellin), *flgK* (flagellar hook-associated protein) *motA* that encodes for a flagellar motor protein and four different methyl-accepting chemotaxis proteins, responsible for sensing the environmental *stimuli*, were also down-regulated upon adhesion. Nevertheless, several genes encoding for flagellar biosynthesis and assembly proteins were induced in GPMV-adherent bacteria– *flhB*, *flhA*, *fliH*, *fliG*, *fliF*, *flgF*, *flgE1* and *fliM*, which may be seen as conflicting results. Flagella and motility represent important virulence features since the loss of motility caused reduced invasiveness of epithelial cells (Tomich, et al. 2002). Nevertheless, previous works indicated that expression of flagellar- and chemotaxis-associated genes and motility were reduced in *B. cenocepacia* strains isolated from CF patients (ET12 lineage) (Sass, et al. 2011). The obtained data implied that interaction with host-cell membranes in the early stages of *B. cenocepacia* infection may lead to a disruption of the bacteria movement in response to a chemical gradient (chemotaxis), but to an increase in the assembly of the hook and basal structures of the flagella. In *Salmonella*, the flagellar, motility and chemotaxis genes are organized in a regulon and they are arranged into three hierarchical classes. The early operon is constituted by *flhDC* genes that control the transcription of more than 30 middle genes (class 2) that are required for the structure and assembly of the hook and basal body, including the genes induced in this work. Finally, class 3 genes encode for proteins like flagellin, hook-

associated proteins and chemotaxis systems (*che* pathway) (Terashima, et al. 2008; Wolfe and Visick, 2008). It is possible that the contact between *B. cenocepacia* K56-2 and the surface of epithelial cells could trigger this type of targeted transcription that ultimately leads to the full expression of flagellar and chemotaxis genes. This time-dependent sequential gene expression could limit the effectiveness of a motile-flagella and target its formation when an active invasion of host-cells is required.

Despite flagella, other membrane appendages, known for their role in bacterial adherence and virulence, were found to be overexpressed during *B. cenocepacia* adhesion to 16HBE14o- derived GPMVs. Genes belonging to the genomic *locus BCAL1520-1537* that encodes components of Flp type pilus, *adhA* cable pilus associated adhesin, *BCAS0321* outer membrane autotransporter adhesin, and two trimeric autotransporter adhesins (TAAs) – *BCAM2418* and *BCAS0236* are examples. The expression of pilus structures has been extensively associated with bacterial adherence, motility, and host-cell invasion (Urban, et al. 2005; de Bentzmann, et al. 2006). Nevertheless, the lack of Flp pilus expression seems to be a predominant characteristic in outbreak isolates and during an established *B. cenocepacia* infection (Sass, et al. 2011, O'Grady and Sokol, 2011). The obtained data suggests that despite its absence during chronical infections, Flp pilus appear to be important in the early stages of bacteria-host confrontations. On the other hand, the expression of *cblA* (major subunit of giant cable pilus) was repressed during *B. cenocepacia*-GPMVs adhesion, indicating non-essential role for this type of pilus structure. Moreover, AdhA cable pilus associated adhesin encoding gene was found to be induced, revealing that both cable pilus and its associated adhesin may play different roles during *B. cenocepacia* adhesion to host cells. Several studies shown that both Cbl pili and AdhA are necessary for the optimal binding to cytokeratin 13, a receptor on the membrane of the host-cell. Nevertheless, when Cbl pili is absent *B. cenocepacia* remains able to adhere, indicating the importance of AdhA in that process. Also, adhesin-mediated binding to cytokeratin 13 seems to be absolutely necessary for subsequent invasion and transmigration across the epithelium (Tomich and Mohr, 2003; Urban, et al. 2005; Goldberg, et al. 2011). *B. cenocepacia* TAAs have been studied in detail during the past years and are known to be multifunctional proteins involved in many virulence related traits like biofilm formation, motility,

adhesion and invasion of host cells (Mil-Homens and Fialho, 2011; Mil-Homens and Fialho, 2012; Mil-Homens, et al. 2014; Mil-Homens, et al. 2017). The expression of BCAM2418 and BCAS0236 TAA encoding genes during the early stages of *B. cenocepacia* infection was demonstrated in a recent work (Pimenta, et al. 2020a). The overexpression of *BCAM2418* transcripts shown to be variable over time, reaching a maximum after 30 min of *B. cenocepacia* adhesion to bronchial epithelial cells. Also, the bacterial interaction with specific host-cell receptors, namely O-linked glycosylated proteins, was reported to be the trigger for the increased expression of BCAM2418 TAA (Pimenta, et al. 2020a). The obtained data in this work supported those observations as BCAM2418 TAA expression increased after bacterial interaction with the host-cell membranes. Those results not only suggested an important role played by this TAA in the early stages of infection, but also confirmed the experimental applicability of GPMVs as a host-cell surrogates in the study of the initial crosstalk between bacterial pathogens and their hosts.

In summary, in this work we produced GPMVs from a bronchial epithelial cell line and used them for the first time as a cell-like alternative to explore *B. cenocepacia* interaction with host-cell surface. The perceiving of the host membranes by the pathogenic bacteria led to a transcriptional shift that caused a cascade of metabolic and physiological adaptations to the host specific environment. Our results demonstrated that almost 1000 genes had their transcription changed after *B. cenocepacia* physical contact with cell membranes. Many of these genes encode proteins related with central metabolic pathways, transport systems, cellular processes, and virulence traits. The understanding of the changes in gene expression that occur in the early steps of an infection cycle could uncover the first mechanisms that a pathogenic bacterium uses to invade and subvert the host cell, providing new strategies to restrain *B. cenocepacia* lung infections. Further research including construction of mutant strains, is necessary to identify potential novel virulence-associated genes essential for the pathogenesis of *B. cenocepacia* during host cell initial crosstalk.

Data Availability

The sequencing data discussed in this publication have been deposited in NCBI's Gene Expression Omnibus (Edgar, et al. 2002) and are accessible through GEO Series accession number GSE155982(https://www.ncbi.nlm.nih.gov/geo/query/acc.cgi?acc=GSE15598). All processed data are available in this chapter and supplementary data (Tables V.S1 and V.S2).

Acknowledgments

This work was supported by the Portuguese Science and Technology Foundation (FCT) BIOTECnico PhD program grant PD/BD/116940/2016. Funding received by iBB e Institute for Bioengineering and Biosciences from FCT (UID/BIO/ 04565/2020), Centro de Química Estrutural from FCT (UIDB/00100/2020) and Programa Operacional Regional de Lisboa 2020 (Project N. 007317) is acknowledged. We thank Dieter Gruenert, Pacific Medical Center Research Institute, San Francisco, CA, for providing us with the 16HBE14o- cell line. We also acknowledge John LiPuma from the University of Michigan, who kindly provided a *Burkholderia* strain.

Conflict of interest

The authors have no conflict of interest to declare.

VI. FINAL DISCUSSION

Burkholderia cenocepacia has proven to be one of the most challenging opportunistic pathogens causing persistent, hard to treat, chronic respiratory infections in CF patients and other immunocompromised individuals. *B. cenocepacia* resistance to several classes of antibiotic and large array of virulence factors contribute to its enhanced pathogenicity, favoring colonization and persistence inside the host.

The process of bacterial infection includes a series of events that mediate the interaction with the host. The first steps of *B. cenocepacia*-host contact comprise adherence and penetration of the mucous layer and the following adhesion to the surface of epithelial cells (McClean and Callaghan, 2009). Nevertheless, albeit the identification of some of the virulence determinants and appendages that mediate *B. cenocepacia* adhesion, little is known regarding the early stages of host-bacteria crosstalk. Not many surface-exposed molecules have been described to mediate the binding of *B. cenocepacia* to host receptors (Figure I.2) (Tomich, et al. 2002; Goldberg, et al. 2011). More recently, trimeric autotransporter adhesins (TAAs) have been studied and are now considered key contributors for *B. cenocepacia* adhesion to epithelial cells (Mil-Homens and Fialho, 2011; Mil-Homens and Fialho, 2012; Mil-Homens, et al. 2014).

Although the absolute numbers of trimeric adhesin genes are variable among Bcc, some species could encode a large number of TAAs. The larger genome sizes and genomic fluidity of Bcc species may contribute for the high density of TAA coding genes, which may ultimately enhance bacteria capacity to adhere and colonize human hosts and other environments (Mil-Homens and Fialho, 2011). Seven TAA genes were previously identified in *B. cenocepacia* J2315 genome – *bcaA*, *bcaB*, *bcaC*, *BCAM2418* and *BCAM1115* located at chromosome 2; and *BCAS0236* and *BCAS0335* at chromosome 3. Despite sharing some common features, like their repetitive domain organization and TAA-defining C-terminal anchor domain, *B. cenocepacia* J2315 TAAs are variable among themselves with sizes ranging from 953 to 2953 aa residues (Mil-Homens and Fialho, 2011). Four of the seven TAAs described *in B. cenocepacia* seem to co-localize with two-component system proteins and other regulatory proteins, indicating that they may be targets of regulation under specific conditions. Untill now, only two TAAs (BcaA and BcaB) have been studied and characterized in terms of function and impact in *B. cenocepacia* pathogenesis (Mil-Homens, et al. 2010; Mil-Homens and Fialho, 2011; Mil-

Homens and Fialho, 2012; Mil-Homens, et al. 2014). *bcaA* (*BCAM0224*) and *bcaB* (*BCAM0223*) are organized into a cluster (TAA cluster) together with a third TAA, *bcaC* (*BCAM0219*), two hypothetical proteins (*BCAM0216* and *BCAM0217*), two hybrid histidine kinases (HK) (*BCAM0218* and *BCAM0227*), three response regulators (RR) (*BCAM0221*, *BCAM0222*, and *BCAM0228*), and one outer membrane protein (*BCAM0220*) (Mil-Homens, et al. 2010; Mil-Homens and Fialho, 2012) (Figure VI.1).

Throughout this work the characterization of these particular group of adhesins was aimed, as well as the identification of the features that directly and indirectly contribute for *B. cenocepacia* virulence. Even so, given their size, trimerization and repetitive nature, the molecular and genetic manipulation of TAA genes and peptides was hard to achieve, being extremely difficult to clone and complement TAA encoding genes as well as create *B. cenocepacia* TAA-mutant strains.

The first work presented in this thesis (Chapter II) aimed to get further insights concerning the function of BcaC and the neighbor HK BCAM0218 in *B. cenocepacia* virulence as an attempt to disclosure putative interconnections and regulatory pathways among the proteins encoded within the TAA cluster. *In silico* analysis of BcaC revealed a typical TAA head-stalk-anchor domain organization with signature C-terminal membrane β-barrel anchor, five head domains and 11 predicted stalk domains (Figure II.1). With 2953 aminoacidic residues, BcaC was found to be the largest TAA in *B. cenocepacia* K56-2, its passenger domain comprises several putative collagen-binding domains and Hep_Hag and HIM motifs whose presence are usually associated with bacterial hemagglutinins and invasins. Through the construction of an insertional mutation in *bcaC* gene, BcaC TAA expression was compromised (Figure II.1). Phenotypic alterations of the mutant strain were assessed, and results shown that *B. cenocepacia* hemagglutination activity was significantly reduced, and adherence to both ECM components (fibronectin, laminin, collagen type-I and -IV) and bronchial epithelial cells (CF and non-CF) decreased (Figure II.2).

B. cenocepacia hemagglutination ability appears to be directly linked to the expression of a functional BcaC. The prediction of hemagglutinin (HIM) and invasin (Hep_Hag) associated motifs through the passenger domain seems to be in concordance with the obtained experimental data. Hemagglutinins, commonly found in viral and bacterial

pathogens, are glycan-binding proteins known to mediate adherence to host cells. The binding between protein and receptor could be specific enough to determine the tropism of a pathogen to a species and target cells (Scheller and Cotter, 2015; Smrt and Lorieau, 2017). Additionally, invasins are also highly specific and effective proteins that are involved in binding of several bacterial pathogens to host-cell receptors, and further invasion (Palumbo and Wang, 2006). Interestingly, loss of Hep_Hag (invasin) motifs on the passenger domain of TAAs from uropathogenic bacteria dramatically affects their ability to bind ECM components, like collagen type-I (Alamuri, et al. 2010). The results obtained for *bcaC*-mutant strain, might disclosure a comparable role for BcaC in *B. cenocepacia* pathogenesis as adhesion assays also revealed the importance of this TAA during bacterial interaction with the host.

ECM is composed by a complex network of proteins and glycoproteins and it is located on the surface of different cell types and tissues. Interaction between bacterial pathogens and components of human ECM have been identified in past years as facilitators during adhesion (Liu, et al. 2018). Additionally, several TAAs were described as ECM-binding proteins that interact with fibronectin, laminin, and collagen. This kind of interactions were found to be important mediators of bacterial adhesion to host cells and immune system evasion, improving the pathogen lifetime inside the host (Leduc, et al. 2009; Singh, et al. 2016). Adherence to host cells seems to be a common trend among the *B. cenocepacia* clustered TAAs (Mil-Homens and Fialho, 2012; Mil-Homens, et al. 2014). Although the specific cell receptors and exact molecular entails required for TAAs-cell interaction are still poorly understood, it is feasible to assume that the presence of these proteins on the surface of *B. cenocepacia* play an important role in virulence. It is possible that different TAAs could interact with different classes of cell receptors, or could be target for fine-tuned regulation, being transcript in response to a specific *stimulus* or in a determined stage of infection. The genetic organization of the TAA cluster in which *bcaC* is located immediately upstream of *BCAM0218* HK and nearby several RR encoding genes suggests that a regulatory interaction, like a two-component system (TCS), could take place.

To uncover the relevance of the BCAM0218 HK coding gene as a putative modulator of the BcaC activity *BCAM0218*-defective mutant was created and its phenotypic variations

evaluated. The overall results demonstrated an interference of BCAM0218 in the expression of the *bcaC* gene (Figure II.3). *BCAM0218* mutation shown to be at least partly responsible for rescue the phenotypic defects caused by the *bcaC* absence, suggesting that BCAM0218 HK could be a putative negative modulator of the BcaC activity (Figure II.5 and II.6). The regulation of bacterial adherence events by different TCS have been described in the literature for several human pathogenic bacteria (Schaefers, et al. 2017; Choudhary, et al. 2018). The *stimuli* used by these systems could be diverse and involve different processes like quorum sensing or oxygen sensing. Concerning HK BCAM0218, the perceived chemical or environmental *stimulus* remains to be clarified as well as the involvement of other cluster proteins as TCS cognate RRs. Nevertheless, the work developed in Chapter II revealed for the first time the involvement of a *B. cenocepacia* HK in the regulation of a TAA gene expression.

Taken together, the results discussed in this work complete the initial characterization of all three clustered TAAs. Like BcaA and B, BcaC was found to be a multifunctional protein involved in several virulence-associated traits. It is believed that each TAA could play different roles in *B. cenocepacia*-host interaction, probably acting in response to a variety of environmental conditions aiming to maximize the pathogenicity of *B. cenocepacia*. Moreover, it is suggested that the TAA cluster composed of three multifunctional trimeric autotransporter adhesins may be linked to a TCS system (HK BCAM0218; RR BCAM0221 and BCAM0222) that could integrate and coordinate the multiples roles of TAAs during the infection process of *B. cenocepacia* (Figure VI.1).

Supporting the assumption that the expression of TAA encoding genes could be under regulation in different stages of infection, Chapter III started by analyzing the transcription profile of all *B. cenocepacia* K56-2 TAA genes in response to host cell contact. Results obtained after bacterial adhesion with 16HBE14o- bronchial epithelial cells, revealed a different expression pattern for all the TAA mRNAs (Figure III.1). Among those, *BCAM2418* was the TAA gene with the highest expression after contact with 16HBE14o- cells. Little is known about BCAM2418 function for *B. cenocepacia* pathogenicity but *in silico* analyzes revealed BCAM2418 as a protein with unique features, like its length (2775 aa residues), its structural polymorphism and its extensive serine-rich repeats motifs (Mil-Homens and Fialho, 2011). Additional work was done to

understand the specificity of *BCAM2418* response. Results indicated that *BCAM2418* transcriptional levels after adhesion are reliant on the nature of host cells. The contact with human bronchial epithelial cells, either CF (CFBE41o-) or non-CF (16HBE14o-), seems to induce a higher increase in gene expression when compared to adhesion to lung (A549) or cervix (HeLa) cell lines (Figure III.2). Moreover, the physical contact between both bacteria and host-cell seems to be a requirement for the rise in *BCAM2418* transcription once the non-adherent bacteria do not show the same transcriptional response. *BCAM2418* expression was found to vary with the time of cellular contact (from 15 min to 5 h), reaching the highest level of expression after 30 min of *B. cenocepacia*-16HBE14o- adhesion (Figure III.3). The presence of BCAM2418 TAA on the surface of the bacteria could play an important role in the initial steps of infection.

Considering the requirement of a close interaction between bacteria and the surface of bronchial host cell to prompt an over-expression of the *BCAM2418* gene, further assays were performed to disclose the cellular component that is specific recognized by *B. cenocepacia* K56-2. The obtained results showed that a physical contact with a protein/O-linked glycoprotein-component of the host cell surface was necessary to turn on *BCAM2418* expression (Figure III.4). *B. cenocepacia* has been known to interact with airway epithelial cells through several classes of receptors, namely glycolipids, proteins, and mucins (McClean and Callaghan, 2009). Mucins are secreted or membrane anchored high-molecular mass proteins that are heavily O-glycosylated. Secreted-mucins also known as gel-forming ones, are the major component of the airway mucous layer and are particularly relevant in the CF lungs environment (Ridley and Thornton, 2018). In this context, membrane-anchored O-glycosylated mucins may act as a host cell receptor for *B. cenocepacia* K56-2 and directly or indirectly cause the over-expression of the *BCAM2418* gene. Mucin- and ECM-coated plates were challenged with bacteria; the effect of mucins, but not the ECM proteins (collagen type-I and fibronectin), on bacterial adhesion and further *BCAM2418* transcription was noteworthy and increased over time of contact (Figure III.5). Moreover, additional results shown that the mucin O-glycans instead of the core protein itself play a crucial role on bacterial recognition/adhesion causing the activation of the *BCAM2418* gene expression (Figure III.6). The glycosylation

of mucins has been proven to be relevant receptors for infection of several human pathogens. In the lungs, *Pseudomonas aeruginosa* and different Bcc species use secretory mucins to mediate interaction with host epithelial cells (McClean and Callaghan, 2009). Other pathogens like *Salmonella enterica* serovars, *Staphylococcus aureus* and *Helicobacter pylori*, have been described to use transmembrane mucins and glycan-rich domains to gain entry into the host cells (Vesterlund, et al. 2006; Kato and Ishiwa, 2015; Huang, et al. 2016). More recently, Wheeler et al. (2019) also reported that the *P. aeruginosa* exposure to mucus triggers downregulation of virulence genes that are involved in quorum sensing, siderophore biosynthesis and toxin secretion, and rapidly disintegrates biofilms (Wheeler, et al. 2019). Additionally, mucus interactions with *P. aeruginosa* were found to be mediated by mucin-associated O-glycans that strongly regulate the bacterial phenotypes and seems to reduce adherence to human epithelia *in vitro* and attenuating infection (Wheeler, et al. 2019). Such results clearly demonstrate the role that lung mucins, particularly mucin O-glycans, could play during colonization and infection by opportunistic pathogens. Altogether, the results obtained in Chapter III point out to the importance of host glycans, especially the ones presented in mucins, as targets for *B. cenocepacia* interaction. Additionally, the sensing of this carbohydrate moieties by *B. cenocepacia* K56-2 during adhesion to bronchial epithelial cells, seems to induce the expression of *BCAM2418* TAA gene. *BCAM2418* transcription shows an on-off switch and a fine-tuned control in response to a time frame and a particular host cell environment (Figure VI.2).

As the interaction between host-glycans and *B. cenocepacia* K56-2 was proven, further assays were designed aiming to assess the particular action of BCAM2418 in those contacts. Given the failed efforts to construct a *BCAM2418* mutant, a neutralizing antibody against this TAA was produced allowing deeper studies. In Chapter IV, anti-BCAM2418 was obtained using a N-terminal fragment of *B. cenocepacia* K56-2 BCAM2418 as antigen (Figure IV.1). It was theorized that *B. cenocepacia* incubation with the produced antibody could inhibit the action of the TAA during infection. It was found that the influence of the antibody on bronchial epithelial cell adhesion was more effective targeting *B. cenocepacia* strains when compared to the other Bcc species (Figure IV.3). Additionally, *B. cenocepacia* K56-2 incubated with antibody exhibited a

diminished adhesion in a dose-dependent manner towards bronchial epithelial cells, mucins, and ECM proteins (fibronectin and collagen type-I) (Figure IV.2). Concerning *Galleria mellonella* killing assays, anti-BCAM2418 pre-incubation provided full protection only against *B. cenocepacia* K56-2, acting as a narrow spectrum anti-adhesive agent (Figure IV.4). The obtained results are in concordance with the low identity registered between BCAM2418 and respective Bcc homologous proteins (Figure IV.1).

Glycan-based technologies were used to uncover the mechanisms underlying the early stages of the bacteria-host crosstalk. Host glycans represent a large set of ligands for bacterial binding in several tissues, being important in host-bacteria cross-talk during infection (Taylor, et al. 2018). Using glycan-microarray platforms, the action of anti-BCAM2418 in the inhibition of *B. cenocepacia* binding to several classes of glycans was assessed. Fifty-two glycosylated molecules commonly encountered on the host cell surface, as part of mucins, and other glycoproteins or glycolipids were tested (Figure IV.5). Anti-BCAM2418 was also found to affect the binding of the *Burkholderia* species to host glycans (Figure IV.6). Pre-incubation of the tested bacteria with anti-BCAM2418 antibody caused a widespread reduction in the binding of *Burkholderia* strains to the microarray printed glycans. The most significant inhibitory effect was observed for the two strains of *B. cenocepacia* supporting the relevance of BCAM2418 TAA-mediated binding during the early stages of host interaction. *B. cenocepacia* K56-2 pre-treated with the anti-BCAM2418 antibody demonstrated reduced binding to 32 out of the 52 glycosylated molecules tested (Figure IV.6 and IV.7). Among those, histo-blood groups (A, B and H), Lewis structures (a, b, x and y) and other relevant glycoconjugates such as asialo-GM1 ganglioside are included. The obtained data suggest that the anti-BCAM2418 antibody prevents infection by blocking *B. cenocepacia* BCAM2418-mediated attachment to the host cell surface. The present results together with the proven overexpression of BCAM2418 gene in the bacterial adhesion context reveal the relevance of this protein in *B. cenocepacia* pathogenicity.

Additionally, using glycan microarrays the binding specificity profiles of the *Burkholderia* species were also determine. Both strains of *B. cenocepacia*, K56-2 and J2315, were found to interact in a similar manner with a comparable panel of glycoconjugates. Regarding *B. multivorans* VC13401 and *B. contaminans* IST408, albeit recognizing almost

the same glycans as *B. cenocepacia* strains, the intensity of interaction seemed to be lower (Figure IV.8). Such differences could be a consequence of variances in bacterial-surface composition that could alter the presentation and accessibility of adhesive molecules and might lead to a distinct interaction between a specific strain and the tested glycans (Conway, et al. 2004). In this work, *Burkholderia* species were found to bind to all three ABH blood group antigens, with a stronger interaction with group A, Lewis structures, specially Lewis b, and gangliosides GM1 and asialoGM1. Blood group antigens and Lewis structures are fucosylated oligosaccharides expressed on human cell surfaces and secretions, including mucin-rich airway mucus. Several studies have been demonstrated that in the CF-lungs, glycans on mucins, like blood group antigens and Lewis structures, as well as epithelial cell gangliosides like GM1 and asialoGM1 may act as ligands for opportunistic pathogens adhesion and colonization (Ruiz-Palacios, et al. 2003; Imberty, et al. 2004; McClean and Callaghan, 2009).

Overall, the work presented in Chapter III and IV opened new insights concerning the first stages of *B. cenocepacia* interaction with host cell. Particular importance was given to the participation of glycan structures in the host-pathogen interface and the role played by *B. cenocepacia* TAAs during infection. The differential expression of all seven TAA genes during adhesion indicated that each adhesin could be targeted to play a distinct role in different processes of *B. cenocepacia* infection. *BCAM2418* transcription was highly induced during the early interactions with bronchial cells, as a direct result of physical contacts between bacteria and the surface of host cells. These contacts were found to be mediated by host protein/O-glycoprotein components exposed on the membrane of the cell and an unknown *B. cenocepacia* receptor. Host glycans, either exposed on the surface of a cellular component or derived from mucins and ECM components, were found to be intrinsically associated to *B. cenocepacia* host-recognition and adaptation. Several Bcc bacteria interact with different sets of host-associated carbohydrates in what resembles a species-specific feature. *B. cenocepacia* binding to several classes of glycans is inhibit by the action of anti-BCAM2418 antibody. The bacterial incubation with anti-TAA antibody was also found (i) to prevent *B. cenocepacia* K56-2 adhesion to bronchial epithelial cells, mucins, and ECM components in a dose-dependent way; and (ii) to inhibit the virulent behavior of *B. cenocepacia* K56-

2 in *G. mellonella* insect infection model. The properties of anti-BCAM2418 antibody, allowed an indirect characterization of BCAM2418 TAA functions (Figure VI.1). With the work developed and presented in both Chapter III and IV it was possible to infer that BCAM2418 is a crucial mediator of *B. cenocepacia* K56-2 adhesion to host structures, in particular by interacting with specific classes of host glycans. Moreover, its overexpression during the early contacts between bacteria and epithelial cells indicate that an important role must be played by BCAM2418 in such context, revealing its purpose as a virulence factor with major implications on *B. cenocepacia* K56-2 pathogenesis.

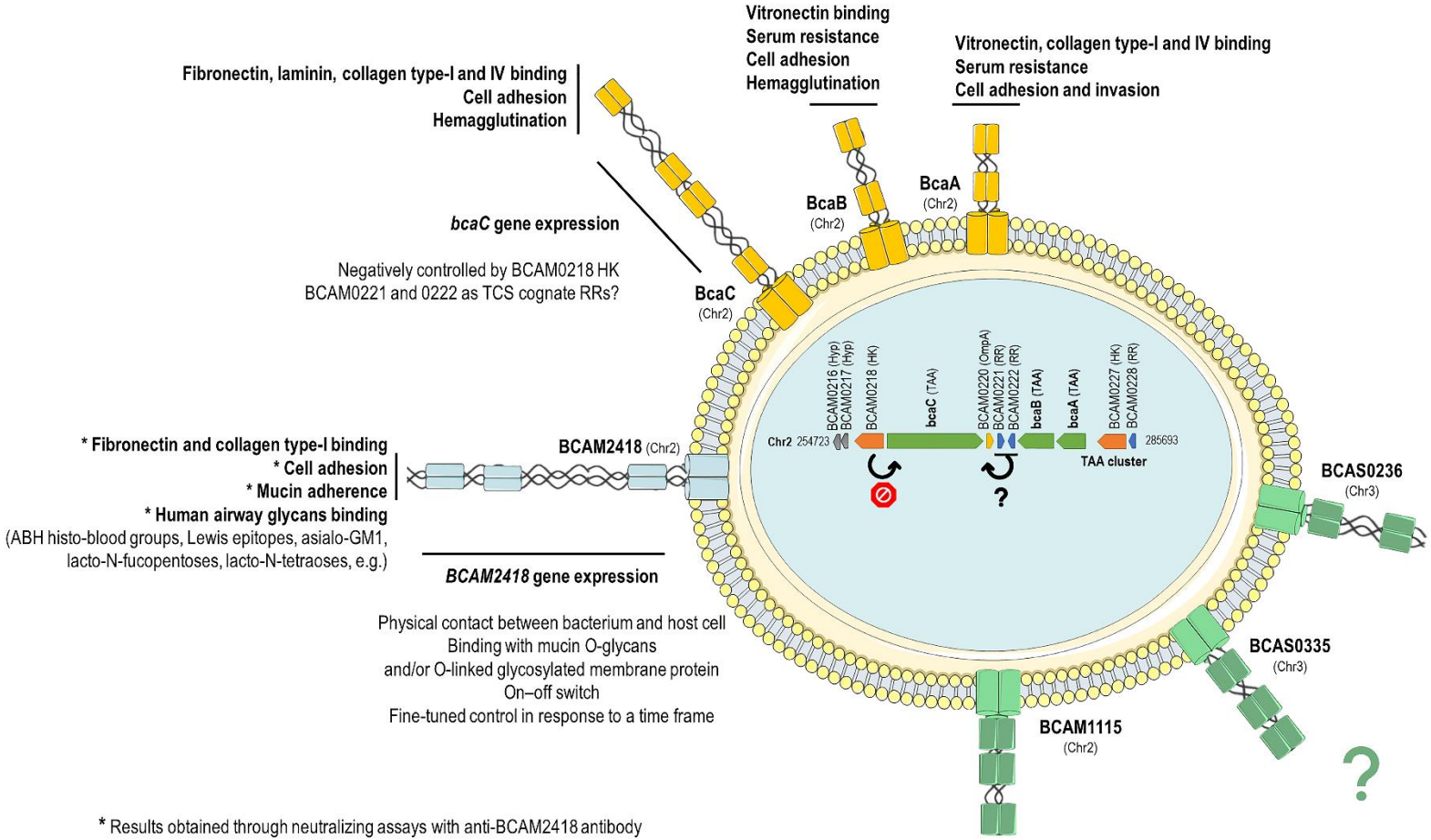

Figure VI.1. *B. cenocepacia* K56-2 TAAs – BcaA, BcaB, BcaC, BCAM2418, BCAM1115, BCAS0335 and BCAS0236. BcaC was found to be a multifunctional TAA as well as the other TAAs from the cluster. *BCAM2418* gene expression appears to be regulated in response to a physical contact between bacteria and the host cell. The presence of BCAM2418 on the surface of *B. cenocepacia* seems to be important for ECM binding, cell and mucin adhesion and to mediate interaction between the bacterium and host airway glycans.

The first contact between a bacterium and a host-cell surface is the crucial step for the development of an infection, leading to physiological alterations in both interacting cells. For bacteria, these alterations allow them to change and adapt to the new environment and increase their virulence fitness (Stones and Krachler, 2016). *B. cenocepacia* adaption to the host lungs require several strategies. The necessity to adjust to host pressures triggers alterations that may include bacterial metabolic shifts and morphological alterations (Mira, et al. 2011; Kalferstova, et al. 2015). Previous discussed results revealed that the early contacts between *B. cenocepacia* and the surface of the host cell membrane induce the expression of virulence-related genes. The main goal of Chapter V was to analyze *B. cenocepacia* K56-2 transcriptome after the first contact with the surface of host cells and assess the bacterial adaptation and virulence-associated alterations that take place in the early stages of infection. To do that, a new approach was developed to use a cell-like alternative to explore *B. cenocepacia* interaction with host-cell surface. Giant plasma membrane vesicles (GPMVs) were produced from a bronchial epithelial cell line and were used for the first time as a platform for *B. cenocepacia* K56-2 adhesion assays (Figure V.1). GPMVs share functional and structural similarities with the membrane of the cells that they are originated from (Figure V.2). Despite their biological origin GPMVs lack cytoskeletal structures and the presence of complex components from the cytosol (Sezgin, et al. 2012; Levental and Levental, 2015; Zemlji, et al. 2018). The optimizations applied for both the GPMVs production and bacterial adhesion procedures lead to a final recovery of *B. cenocepacia* RNA samples with high levels of quality and purity (Figure V.3). Further analysis was performed, and *B. cenocepacia* K56-2 transcriptional profiling was completed at whole genome level upon the early contacts with the host-cell membrane, using GPMVs as cellular surrogate (Figure V.4).

The obtained results revealed that the early interaction of *B. cenocepacia* with the bronchial cell membrane triggered major alterations of the metabolic pathways (Figure VI.2). The contact with the host seems to initiate a modulation of key bacterial systems like the downregulation of the central metabolism (oxidative phosphorylation, carbon metabolism, TCA cycle and glycolysis and gluconeogenesis) and the upregulation of genes involved in sulfur and nitrogen metabolism, glyoxylate metabolism, CoA

biosynthesis and fatty acid catabolism (Figure V.5 and V.6). The induction of genes encoding for transport machineries, including those involved in the uptake of sugars, amino acids, potassium, sulfate, and nitrogen could direct the exploitation of new sources of nutrients available in the host during infection. This type of adjustments in *B. cenocepacia* metabolic regime has been reported as a consequence of a chronical infection state (Mira, et al. 2011). Nevertheless, the data reported in this study shown that it is possible that *B. cenocepacia* adaptation to the host environment may occur soon after the first physical contact to the host membrane surface. Additionally, *B. cenocepacia* K56-2 cellular processes were found to be highly disturbed during bacterial-host adhesion with the repression of genes encoding proteins related to transcription, translation and protein export being reported (Figure VI.2). The replication machinery shut out seems to occur as a preparation for a latency regime reinforcing the idea that the sensing and early contacts with the host-cell surface may prepare *B. cenocepacia* for the microcolony environment or even intracellular lifestyle.

The expression of several genes associated with bacterial adherence, motility, and host-cell invasion were also found to be overexpressed during *B. cenocepacia* adhesion to bronchial cells-derived GPMVs (Figure V.7). Several lipoprotein and outer membrane protein (Omp) coding genes were induced upon contact with the host cell surface. Despite mainly putative and with no associated function, both classes of proteins are recognized for being required for bacterial virulence, namely for adhesion, invasion, and initiation of inflammatory processes (Kovacs-Simon, et al. 2011; McClean, 2012; McClean, et al. 2016; Dennehy, et al. 2017; Nguyen, et al. 2018). Such variation in gene expression profiles regarding surface located proteins may be a result of bacterial adaptation to the initial host cell contacts to strait the interaction of both participating cells. Likewise, the majority of the genes encoding for flagellar biosynthesis and assembly proteins were induced in GPMV-adherent bacteria, as well as components of Flp type pilus, *adhA* cable pilus associated adhesin, *BCAS0321* outer membrane autotransporter adhesin, and two TAAs – *BCAM2418* and *BCAS0236.* The lack of Flp pilus and flagellar-associated genes expression seems to be a predominant characteristic in outbreak isolates and during an established *B. cenocepacia* infection (Sass et al., 2011, O'Grady and Sokol, 2011). Nevertheless, the results from this work suggested that

despite its absence during chronical infections, Flp pilus and bacterial flagellum appear to be important in the early stages of bacteria-host confrontations. *cblA* (major subunit of giant cable pilus) transcription seems to be repressed during *B. cenocepacia*-GPMVs adhesion, indicating non-essential role for this type of pilus structure. Additionally, *adhA* cable pilus associated adhesin encoding gene was found to be induced, revealing that both structures may play different roles during *B. cenocepacia* adhesion to host cells, as other studies have previously suggested (Drevinek, et al. 2008). The overexpression registered for *BCAM2418* support the previously obtained data presented in Chapter III in which this gene transcription increased after 30 min of *B. cenocepacia* adhesion to bronchial epithelial cells. This seems to confirm the experimental applicability of GPMVs as a host-cell surrogate in the study of the initial crosstalk between bacterial pathogens and their hosts (Figure VI.2).

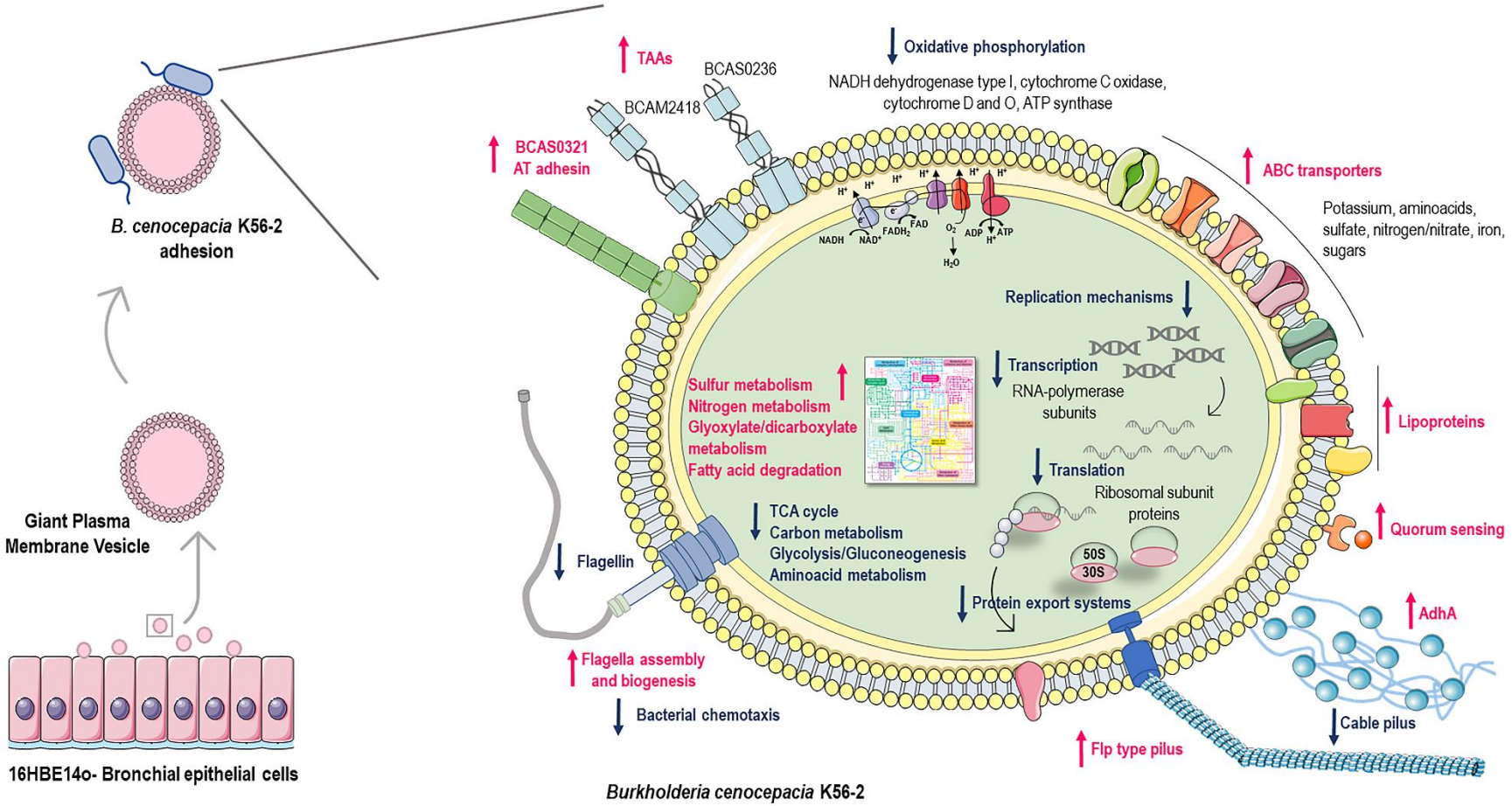

Figure VI.2. ***B. cenocepacia*** **K56-2 transcriptomic adaptation upon contact with the surface of the host cell.** 16HBE14o- bronchial epithelial cell line was used to produce Giant Plasma Membrane Vesicles (GPMVs). Adhesion between *B. cenocepacia* K56-2 and GPMVs was performed during 30 min, RNA from adherent bacteria was recovered and RNAseq was performed. Major alterations in several important pathways were registered, such as central metabolism, oxidative phosphorylation, replication, transcription, and translation; and in the expression of adhesive structures – flagella, pili, adhesins, lipoproteins and TAAs. Processes and structures upregulated are represented in pink and downregulated in blue.

The work presented in Chapter V created a new understanding of *B. cenocepacia* K56-2 adaptation during infection. The perceiving of the host membranes triggered a transcriptional shift that caused a cascade of metabolic and physiological adaptations to the host environment. The obtained results prove that *B. cenocepacia* adaptation to the host is a rapid process that occur soon after the first contacts with the surface of the cell. In past years, several studies have been pointing out to changes in *B. cenocepacia* genetic expression during long-term lung colonization. Genes involved in translation, adhesion to epithelial cells and mucins, and adaptation to nutrient- and oxygen-limited conditions on CF lungs were suggested to be central features in this transcriptional shift (O'Grady and Sokol, 2011; Mira, et al. 2011). In this chapter a gap of knowledge was fulfilled as it was demonstrated that the same pathways were altered in the early stages of *B. cenocepacia* infection. More than sensing of host cell surroundings, the bacterial physical contact with the surface of the cell showed to be a requirement to induce such transcriptional alterations. Furthermore, the results presented could imply that bacterial cells respond to their initial contact with the host membrane by triggering a coordinated expression and repression of surface adhesive molecules. This process might allow the transition from reversible to permanent bacterial attachment, soon after the first stages of host sensing (Li, et al. 2012). This mechanism may include the transition from a planktonic state to a stable association with the surface of the airway cell, thereby maximizing the adherence to the host through the expression of several Omps, lipoproteins and adhesins.

The data gathered throughout this thesis raises important questions and perspectives for future work too. Concerning Chapter II would be interesting to assess the cognate partners of BCAM0218 HK in the regulatory pathway that lead to the control of *bcaC* expression. BCAM0221 and 0222, two RR of the TAA cluster, could be preferential targets of study considering their genic location nearby BCAM0218 coding gene. Mutant strains for these two genes could be constructed and phenotypic and transcriptional analysis performed, complementing the results obtained for *BCAM0218*-defective mutant. Moreover, the production and purification of both RRs could be used for electrophoretic mobility-shift assays (EMSA) assays to demonstrate their interaction

with putative *bcaC* promoter sequences. Additionally, it would be important to try new strategies to obtain a *trans* complementation of BcaC to effectively confirm the obtained results for *bcaC*-mutant strain. Gibson assembly could be an interesting technique to explore, once it is a molecular cloning method that allows the assembly of multiple DNA fragments facilitating the production of the complete sequence of *bcaC* with ≈ 8.9 kb.

Concerning the assumption, theorized in Chapter III, that transmembrane mucins could be one of the receptors on bronchial epithelial cells responsible of the induction of *BCAM2418* expression, the elimination of those proteins on the surface of the cell may be of interest. siRNA targeting several mucin encoding genes could be used to edit cultured epithelial cells. MUC1, MUC4 and MUC16 may be significant targets as they are the most representative transmembrane mucins expressed on airway epithelial cells. Similar adhesion assays could be performed towards the edited cells and the expression of *BCAM2418* evaluated and compared to the obtained data on Chapter III. Moreover, it would be relevant to attempt new efforts in the construction of *BCAM2418*-defective strain. CRISPRi strategies, that have already been used to silence *B. cenocepacia* genes, could be interesting to test as they permit the inhibition of the expression of a target gene without the requirement to alter its sequences (Hogan, et al. 2019). This technique uses CRISPR methodologies and an inducible *cas9* to inhibit the expression of a target gene, creating alterations on the promotor region that could be reverted without the necessity of a *trans* complementation. This CRISPRi toolkit could provide a simple and rapid way to silence *BCAM2418* gene expression and produce an observable phenotype. This strategy to inhibit *BCAM2418* expression and create a *BCAM2418*-defective *B. cenocepacia* strain could also be used to add additional information to the results discussed in Chapter IV. The action of anti-BCAM2418 antibody could be also tested in another models of infection, aside from *G. mellonella*, to further determine the role of BCAM2418 in *B. cenocepacia* K56-2 virulence. Mouse models would be an interesting choice, in particular a rat chronic respiratory infection model. Moreover, glycan microarrays could be designed for the identification of a library of carbohydrates used by *B. cenocepacia* and other Bcc species to adhere and communicate with the host epithelial cells. Those glycoconjugates, suggested as ligands for bacterial receptors, could be used as decoys, inhibiting the adhesion of *B. cenocepacia* or other pathogens

towards host cells and other components and may be proposed as a starting point in the design of glycan based anti-microbial therapies (Hudak, et al. 2014).

Regarding Chapter V, and the *B. cenocepacia* K56-2 RNAseq results, it would be interesting to create a timeline of infection-related events and evaluate the respective bacterial adaptation at a whole transcriptomic level. The usage of GPMVs could be limited to the early stages of infection since the further steps of *B. cenocepacia* infection cycle might involve cellular processes such as the creation of cellular-trafficking structures. Nevertheless, the optimization of a dual-seq protocol could provide a deeper understanding on the *B. cenocepacia* adaptation through time as well as on the reprograming of host cell gene expression in response to bacterial challenge. The identification of fundamental pathways activated or repressed in *B. cenocepacia* during host cell confrontations could reveal new therapeutic targets. It would be relevant to assess if particular determinants, such as surface proteins like lipoproteins, adhesins or Omps, may also play a role in *B. cenocepacia* virulence, which in turn could became promising drug targets.

Overall, this thesis presents the functional characterization of two new *B. cenocepacia* K56-2 TAAs, BcaC and BCAM2418, which showed to play multiple virulence-associated roles. The identification of BCAM0218 HK as a negative modulator of *bcaC* expression was also achieved, demonstrating for the first time that a TAA gene expression could be under regulation and the various roles played by trimeric adhesins during infection may be coordinated in response to specific host *stimuli.* The process of *B. cenocepacia* adhesion to bronchial epithelial cells was found to work as a trigger for differential TAA genes expression. The interaction with cell membrane protein receptors with O-glycosylation arrangements proved to be crucial to prompt the expression of *B. cenocepacia* virulence associated genes, particularly *BCAM2418*. This thesis also demonstrated that Bcc bacteria could interact in different ways with distinct classes of CF-associated carbohydrate moieties, and that this binding could be mediated by TAA proteins. Finally, *B. cenocepacia* K56-2 transcriptional modulation and adaptation to the host was proven to occur in response to the initial physical contact with the membrane of airway cells. The work developed in the course of this thesis support the importance

of the early contacts between bacteria and host cell as a fundamental step for *B. cenocepacia* infection. Nevertheless, it is still a lot to yet be uncovered concerning the pathogenesis of *B. cenocepacia* and the molecular mechanisms entailed in the adhesion towards host cells. The deep understanding of the bacterial adherence requirements should be used for the development of new drugs, specifically designed to target this essential interaction.

VII. LIST OF PUBLICATIONS AND COMMUNICATIONS

Peer-reviewed scientific publications:

Pais P, Vagueiro S, Mil-Homens D, Pimenta AI, Viana R, Okamoto M, Chibana H, Fialho AM, Teixeira MC. A new regulator in the crossroads of oxidative stress resistance and virulence in *Candida glabrata*: the transcription factor CgTog1. *Virulence*. 2020 (accepted for publication). doi: 10.1080/21505594.2020.1839231

Pimenta AI, Mil-Homens D, Pinto SN, Fialho AM. Phenotypic characterization of trimeric autotransporter adhesin-defective *bcaC* mutant of *Burkholderia cenocepacia*: cross-talk towards the histidine kinase BCAM0218. *Microbes Infect*. 2020; S1286-4579(20)30096-4. doi:10.1016/j.micinf.2020.05.018

Pimenta AI, Mil-Homens D, Fialho AM. *Burkholderia cenocepacia*-host cell contact controls the transcription activity of the trimeric autotransporter adhesin BCAM2418 gene. *MicrobiologyOpen*. 2020;9(4):e998. doi:10.1002/mbo3.998

Oliveira H, Mendes A, Fraga AG, Ferreira A, Pimenta AI, Mil-Homens D, Fialho AM, Pedrosa J, Azeredo, J. K2 Capsule Depolymerase Is Highly Stable, Is Refractory to Resistance, and Protects Larvae and Mice from Acinetobacter baumannii Sepsis [published correction appears in Appl Environ Microbiol. 2020 Mar 18;86(7):]. *Appl Environ Microbiol*. 2019;85(17):e00934-19. doi:10.1128/AEM.00934-19

Submitted:

Pimenta AI, Kilcoyne M, Bernardes N, Mil-Homens D, Joshi L, Fialho AM. *Burkholderia cenocepacia* BCAM2418-induced antibody inhibits bacterial adhesion, confers protection to infection and enables identification of host glycans as adhesin targets. (Submitted to *Cellular Microbiology*, under revision).

Pimenta AI, Bernardes N, Alves, MM, Mil-Homens D, Fialho AM. *Burkholderia cenocepacia* transcriptome analysis during the early contacts with bronchial epithelial cell-derived giant plasma-membrane vesicles. (Submitted to *Scientific Reports*, under revision).

Cavalheiro M, Pereira D, Leitão C, Pais P, Ndlovu E, Pimenta AI, Santos R, Takahashi-Nakaguchi A, Okamoto M, Ola M, Chibana H, Fialho AM, Butler G, Dague E, Teixeira MC, From the first touch to biofilm establishment by the human pathogen *Candida glabrata*: a genome-wide to nanoscale view. (submitted to *Communications Biology*, under revision).

In preparation:

Pimenta AI, Fialho AM. New insights into the pathogenesis of *Burkholderia cenocepacia*: special emphasis on trimeric autotransporter adhesins as primary mediators of attachment. (in preparation).

Oral communications in national or international meetings:

Pimenta AI, Mil-Homens D, Fialho AM. Defining the role of *Burkholderia cenocepacia* Trimeric Autotransporter Adhesin BCAM2418 in the early stages of bacteria-host- cell interactions. Oral presentation at MICROBIOTEC'17, December 2017, Porto, Portugal.

Pimenta AI, Mil-Homens D, Fialho, AM. Differential gene expression of *Burkholderia cenocepacia* Trimeric Autotransporter Adhesin *BCAM2418* in the early stages of bacteria-host-cell interactions. Oral presentation at The International Burkholderia cepacia Working Group - 21st IBCWG, May 2018, Dublin, Ireland.

Poster communications in national or international meetings:

Pais P, Galocha M, Califórnia R, Pimenta AI, Mil-Homens D, Fialho AM, Butler G, Teixeira MC. Functional characterization of the transcription factor CgMrr1 suggests new players governing azole drug resistance in *Candida glabrata*. Poster presentation at the 14th ASM Conference on Candida and Candidiasis. April 2018, Providence, RI, USA.

Pedro NA, Lima C, Pimenta AI, Pinto SC, Alves M, Mira, NP. Study of the interaction between vaginal lactobacilli, *Candida albicans* and *Candida glabrata*: from physiological

aspects to transcriptomic analyses. Poster presentation at the Advanced Lecture Course on Human Fingal Pathogens. May 2019, Nice, France.

Salazar SB, Silva S, Mil-Homens D, Pimenta AI, Chibana H, Azeredo J, Fialho AM, Mira NP. The *Candida glabrata* CgHaa1-dependent system is required for biofilm formation, adhesion to epithelial cells and maximal virulence against *Galleria mellonella*. Poster presentation at the Advanced Lecture Course on Human Fingal Pathogens. May 2019, Nice, France.

Pimenta AI, Mil-Homens D, Fialho AM. Differential Gene Expression of *Burkholderia cenocepacia BCAM2418* Trimeric Autotransporter Adhesin in the initial steps of bacteria-host interaction. Poster presentation at the 8th Congress of European Microbiologists (FEMS). July 2019, Glasgow, Scotland.

Pimenta AI, Mil-Homens D, Fialho AM. A novel sensor histidine kinase controls *Burkholderia cenocepacia* trimeric autotransporter adhesin *BCAM0219* expression - role in host cell adhesion, hemagglutination and biofilm formation. Poster presentation at Gordon Conference on Microbial Adhesion and Signal Transduction. July 2019, Newport, RI, USA.

Awards:

Congress Attendance Grant given by the Federation of European Microbiological Societies (FEMS), at 2019 8th Congress of European Microbiologists, Glasgow, Scotland.

Highlighted Article - July 2020 by Microbes and Infection Journal - Phenotypic characterization of trimeric autotransporter adhesin-defective *bcaC* mutant of *Burkholderia cenocepacia*: cross-talk towards the histidine kinase BCAM0218

VIII. REFERENCES

Abisado RG, Benomar S, Klaus JR, Dandekar AA, Chandler JR. Bacterial Quorum Sensing and Microbial Community Interactions. *mBio*. 2018;9(3):e02331-17.

Alamuri P, Löwer M, Hiss JA, Himpsl SD, Schneider G, Mobley HL. Adhesion, invasion, and agglutination mediated by two trimeric autotransporters in the human uropathogen *Proteus mirabilis*. *Infect Immun*. 2010;78(11):4882-4894.

Alsharif G, Ahmad S, Islam MS, Shah R, Busby SJ, Krachler AM. Host attachment and fluid shear are integrated into a mechanical signal regulating virulence in *Escherichia coli* O157:H7. *Proc Natl Acad Sci USA*. 2015;112(17):5503-5508.

Altschul SF, Madden TL, Schäffer AA, et al. Gapped BLAST and PSI-BLAST: a new generation of protein database search programs. *Nucleic Acids Res*. 1997;25(17):3389-3402.

Alvarez BH, Gruber M, Ursinus A, Dunin-Horkawicz S, Lupas AN, Zeth K. A transition from strong right-handed to canonical left-handed supercoiling in a conserved coiled-coil segment of trimeric autotransporter adhesins. *J Struct Biol*. 2010;170(2):236-245.

Assani K, Shrestha CL, Robledo-Avila F, et al. Human Cystic Fibrosis Macrophages Have Defective Calcium-Dependent Protein Kinase C Activation of the NADPH Oxidase, an Effect Augmented by *Burkholderia cenocepacia. J Immunol*. 2017;198(5):1985-1994.

Atack JM, Winter LE, Jurcisek JA, Bakaletz LO, Barenkamp SJ, Jennings MP. Selection and Counterselection of Hia Expression Reveals a Key Role for Phase-Variable Expression of Hia in Infection Caused by Nontypeable *Haemophilus influenzae*. *J Infect Dis*. 2015;212(4):645-653.

Attia AS, Ram S, Rice PA, Hansen EJ. Binding of vitronectin by the *Moraxella catarrhalis* UspA2 protein interferes with late stages of the complement cascade. *Infect Immun*. 2006;74(3):1597-1611.

Aubert DF, Flannagan RS, Valvano MA. A novel sensor kinase-response regulator hybrid controls biofilm formation and type VI secretion system activity in *Burkholderia cenocepacia*. *Infect Immun*. 2008;76(5):1979-1991.

Aubert DF, Hu S, Valvano MA. Quantification of type VI secretion system activity in macrophages infected with *Burkholderia cenocepacia. Microbiology*. 2015;161(11):2161-2173.

Aubert DF, Xu H, Yang J, et al. A *Burkholderia* Type VI Effector Deamidates Rho GTPases to Activate the Pyrin Inflammasome and Trigger Inflammation. *Cell Host Microbe*. 2016;19(5):664-674.

Audfray A, Claudinon J, Abounit S, et al. Fucose-binding lectin from opportunistic pathogen *Burkholderia ambifaria* binds to both plant and human oligosaccharidic epitopes. *J Biol Chem*. 2012;287(6):4335-4347.

Audfray A, Varrot A, Imberty A. Bacteria love our sugars: Interaction between soluble lectins and human fucosylated glycans, structures, thermodynamics and design of competing glycocompounds. *Comptes Rendus Chimie*. 2013;16(5), 482–490.

Augusteyn RC. Alpha-crystallin: a review of its structure and function. *Clin Exp Optom*. 2004;87(6):356-366.

Babicki S, Arndt D, Marcu A, et al. Heatmapper: web-enabled heat mapping for all. *Nucleic Acids Res*. 2016;44(W1):W147-W153.

Baddal B, Muzzi A, Censini S, et al. Dual RNA-seq of Nontypeable *Haemophilus influenzae* and Host Cell Transcriptomes Reveals Novel Insights into Host-Pathogen Cross Talk. *mBio*. 2015;6(6):e01765-15.

Baker MP, Reynolds HM, Lumicisi B, Bryson CJ. Immunogenicity of protein therapeutics: The key causes, consequences and challenges. *Self Nonself*. 2010;1(4):314-322.

Balder R, Lipski S, Lazarus JJ, et al. Identification of *Burkholderia mallei* and *Burkholderia pseudomallei* adhesins for human respiratory epithelial cells. *BMC Microbiol*. 2010;10:250.

Baldwin A, Mahenthiralingam E, Drevinek P, et al. Elucidating global epidemiology of *Burkholderia multivorans* in cases of cystic fibrosis by multilocus sequence typing. *J Clin Microbiol*. 2008;46(1):290-295.

Baldwin A, Mahenthiralingam E, Drevinek P, et al. Environmental *Burkholderia cepacia* complex isolates in human infections. *Emerg Infect Dis*. 2007;13(3):458-46.

Bancerz-Kisiel A, Pieczywek M, Łada P, Szweda W. The Most Important Virulence Markers of *Yersinia enterocolitica* and Their Role during Infection. *Genes (Basel).* 2018;9(5):235.

Barnard TJ, Dautin N, Lukacik P, Bernstein HD, Buchanan SK. Autotransporter structure reveals intra-barrel cleavage followed by conformational changes. *Nat Struct Mol Biol*. 2007;14(12):1214-1220.

Bassler J, Hernandez Alvarez B, Hartmann MD, Lupas AN. A domain dictionary of trimeric autotransporter adhesins. *Int J Med Microbiol*. 2015;305(2):265-275.

Baud V, Karin M. Signal transduction by tumor necrosis factor and its relatives. *Trends Cell Biol*. 2001;11(9):372-377.

Bauer B, Davidson M, Orwar O. Proteomic analysis of plasma membrane vesicles. *Angew Chem Int Ed Engl*. 2009;48(9):1656-1659.

Bentancor LV, Routray A, Bozkurt-Guzel C, Camacho-Peiro A, Pier GB, Maira-Litrán T. Evaluation of the trimeric autotransporter Ata as a vaccine candidate against *Acinetobacter baumannii* infections. *Infect Immun*. 2012;80(10):3381-3388.

Benz I, Schmidt MA. Structures and functions of autotransporter proteins in microbial pathogens. *Int J Med Microbiol*. 2011;301(6):461-468.

Berne C, Ducret A, Hardy GG, Brun YV. Adhesins Involved in Attachment to Abiotic Surfaces by Gram-Negative Bacteria. *Microbiol Spectr*. 2015;3(4):10.1128/microbiolspec.MB-0018-2015.

Bernstein HD. Are bacterial 'autotransporters' really transporters?. *Trends Microbiol*. 2007;15(10):441-447.

Bernstein HD. Type V Secretion in Gram-Negative Bacteria. *EcoSal Plus.* 2019;8(2):10.1128/ecosalplus.ESP-0031-2018.

Bhatt S, Weingart CL. Identification of sodium chloride-regulated genes in *Burkholderia cenocepacia*. *Curr Microbiol*. 2008;56(5):418-422.

Biedzka-Sarek M, Jarva H, Hyytiäinen H, Meri S, Skurnik M. Characterization of complement factor H binding to *Yersinia enterocolitica* serotype O:3. *Infect Immun*. 2008;76(9):4100-4109.

Blom AM. Structural and functional studies of complement inhibitor C4b-binding protein. *Biochem Soc Trans*. 2002;30(Pt 6):978-982.

Bressler AM, Kaye KS, LiPuma JJ, et al. Risk factors for *Burkholderia cepacia* complex bacteremia among intensive care unit patients without cystic fibrosis: a case-control study. *Infect Control Hosp Epidemiol.* 2007;28(8):951-958.

Bruscia E, Sangiuolo F, Sinibaldi P, Goncz KK, Novelli G, Gruenert DC. Isolation of CF cell lines corrected at DeltaF508-CFTR locus by SFHR-mediated targeting. *Gene Ther*. 2002;9(11):683-685.

Burkholder, W. Sour skin, a bacterial rot of onion bulbs. *Phytopathology*. 1950;40: 115-118.

Bylund J, Burgess LA, Cescutti P, Ernst RK, Speert DP. Exopolysaccharides from *Burkholderia cenocepacia* inhibit neutrophil chemotaxis and scavenge reactive oxygen species. *J Biol Chem.* 2006;281(5):2526-2532.

Bylund J, Campsall PA, Ma RC, Conway BA, Speert DP. *Burkholderia cenocepacia* induces neutrophil necrosis in chronic granulomatous disease. *J Immunol*. 2005;174(6):3562-3569.

Campos CG, Byrd MS, Cotter PA. Functional characterization of *Burkholderia pseudomallei* trimeric autotransporters. *Infect Immun*. 2013;81(8):2788-2799.

Caraher E, Reynolds G, Murphy P, McClean S, Callaghan M. Comparison of antibiotic susceptibility of *Burkholderia cepacia* complex organisms when grown planktonically or as biofilm in vitro. *Eur J Clin Microbiol Infect Dis*. 2007;26(3):213-216.

Casasanta MA, Yoo CC, Smith HB, et al. A chemical and biological toolbox for Type Vd secretion: Characterization of the phospholipase A1 autotransporter FplA from *Fusobacterium nucleatum. J Biol Chem*. 2017;292(49):20240-20254.

Chaze T, Guillot A, Valot B, et al. O-Glycosylation of the N-terminal region of the serine-rich adhesin Srr1 of *Streptococcus agalactiae* explored by mass spectrometry. *Mol Cell Proteomics*. 2014;13(9):2168-2182.

Chessa D, Dorsey CW, Winter M, Baümler AJ. Binding specificity of *Salmonella* plasmid-encoded fimbriae assessed by glycomics. *J Biol Chem*. 2008;283(13):8118-8124.

Chiarelli LR, Scoffone VC, Trespidi G, et al. Chemical, Metabolic, and Cellular Characterization of a FtsZ Inhibitor Effective Against *Burkholderia cenocepacia. Front Microbiol*. 2020;11:562.

Chiarini L, Bevivino A, Dalmastri C, Tabacchioni S, Visca P. *Burkholderia cepacia* complex species: health hazards and biotechnological potential. *Trends Microbiol*. 2006;14(6):277-286.

Choudhary KS, Mih N, Monk J, et al. The *Staphylococcus aureus* Two-Component System AgrAC Displays Four Distinct Genomic Arrangements That Delineate Genomic Virulence Factor Signatures. *Front Microbiol*. 2018;9:1082.

Coenye T, LiPuma JJ. Multilocus restriction typing: a novel tool for studying global epidemiology of *Burkholderia cepacia* complex infection in cystic fibrosis. *J Infect Dis*. 2002;185(10):1454-1462.

Coenye T, Vandamme P, Govan JR, LiPuma JJ. Taxonomy and identification of the *Burkholderia cepacia* complex. *J Clin Microbiol*. 2001;39(10):3427-3436.

Coenye T, Vandamme P. Diversity and significance of *Burkholderia* species occupying diverse ecological niches. *Environ Microbiol*. 2003;5(9):719-729.

Colomb F, Robbe-Masselot C, Bouckaert J, Delannoy P. Epithelial mucins and bacterial adhesion. *Carbohydr Chem*. 2014;40, 596–623.

Comanducci M, Bambini S, Brunelli B, et al. NadA, a novel vaccine candidate of *Neisseria meningitidis. J Exp Med*. 2002;195(11):1445-1454.

Compant S, Nowak J, Coenye T, Clément C, Ait Barka E. Diversity and occurrence of *Burkholderia* spp. in the natural environment. *FEMS Microbiol Rev*. 2008;32(4):607-626.

Conners R, Hill DJ, Borodina E, et al. The *Moraxella* adhesin UspA1 binds to its human CEACAM1 receptor by a deformable trimeric coiled-coil. *EMBO J*. 2008;27(12):1779-1789.

Conway BA, Chu KK, Bylund J, Altman E, Speert DP. Production of exopolysaccharide by *Burkholderia cenocepacia* results in altered cell-surface interactions and altered bacterial clearance in mice. *J Infect Dis*. 2004;190(5):957-966.

Cook SR, Maiti PK, DeVinney R, Allen-Vercoe E, Bach SJ, McAllister TA. Avian- and mammalian-derived antibodies against adherence-associated proteins inhibit host cell colonization by *Escherichia coli* O157:H7. *J Appl Microbiol*. 2007;103(4):1206-1219.

Coppens F, Castaldo G, Debraekeleer A, et al. Hop-family *Helicobacter* outer membrane adhesins form a novel class of Type 5-like secretion proteins with an interrupted β-barrel domain. *Mol Microbiol.* 2018;110(1):33-46.

Cornelis GR, Biot T, Lambert de Rouvroit C, et al. The *Yersinia yop* regulon. *Mol Microbiol*. 1989;3(10):1455-1459.

Cotter SE, Surana NK, Grass S, St Geme JW 3rd. Trimeric autotransporters require trimerization of the passenger domain for stability and adhesive activity. *J Bacteriol*. 2006;188(15):5400-5407.

Cotter SE, Surana NK, St Geme JW 3rd. Trimeric autotransporters: a distinct subfamily of autotransporter proteins. *Trends Microbiol*. 2005;13(5):199-205.

Cotter SE, Yeo HJ, Juehne T, St Geme JW 3rd. Architecture and adhesive activity of the *Haemophilus influenzae* Hsf adhesin. *J Bacteriol*. 2005;187(13):4656-4664.

Coutinho CP, Barreto C, Pereira L, Lito L, Melo Cristino J, Sá-Correia I. Incidence of *Burkholderia contaminans* at a cystic fibrosis centre with an unusually high representation of *Burkholderia cepacia* during 15 years of epidemiological surveillance. *J Med Microbiol*. 2015;64(8):927-935.

Coutinho CP, de Carvalho CC, Madeira A, Pinto-de-Oliveira A, Sá-Correia I. *Burkholderia cenocepacia* phenotypic clonal variation during a 3.5-year colonization in the lungs of a cystic fibrosis patient. *Infect Immun*. 2011;79(7):2950-2960.

Cox CD, Bavi N, Martinac B. Bacterial Mechanosensors. *Annu Rev Physiol*. 2018;80:71-93.

Cozens AL, Yezzi MJ, Kunzelmann K, et al. CFTR expression and chloride secretion in polarized immortal human bronchial epithelial cells. *Am J Respir Cell Mol Biol*. 1994;10(1):38-47.

Cui C, Yang C, Song S, et al. A novel two-component system modulates quorum sensing and pathogenicity in *Burkholderia cenocepacia*. *Mol Microbiol*. 2018;108(1):32-44.

Cullen L, McClean S. Bacterial Adaptation during Chronic Respiratory Infections. *Pathogens*. 2015;4(1):66-89.

Cullen L, O'Connor A, Drevinek P, Schaffer K, McClean S. Sequential *Burkholderia cenocepacia* Isolates from Siblings with Cystic Fibrosis Show Increased Lung Cell Attachment. *Am J Respir Crit Care Med*. 2017;195(6):832-835.

Cullen L, O'Connor A, McCormack S, et al. The involvement of the low-oxygen-activated locus of *Burkholderia cenocepacia* in adaptation during cystic fibrosis infection. *Sci Rep*. 2018;8(1):13386.

Cutter D, Mason KW, Howell AP, Fink DL, Green BA, St Geme JW 3rd. Immunization with *Haemophilus influenzae* Hap adhesin protects against nasopharyngeal colonization in experimental mice. *J Infect Dis*. 2002;186(8):1115-1121.

Daigneault MC, Lo RY. Analysis of a collagen-binding trimeric autotransporter adhesin from *Mannheimia haemolytica* A1. *FEMS Microbiol Lett*. 2009;300(2):242-248.7.

Dam TK, Gabius HJ, André S, Kaltner H, Lensch M, Brewer CF. Galectins bind to the multivalent glycoprotein asialofetuin with enhanced affinities and a gradient of decreasing binding constants. *Biochemistry*. 2005;44(37):12564-12571.

Dautin N, Bernstein HD. Protein secretion in gram-negative bacteria via the autotransporter pathway. *Annu Rev Microbiol*. 2007;61:89-112.

David J, Bell RE, Clark GC. Mechanisms of Disease: Host-Pathogen Interactions between *Burkholderia* Species and Lung Epithelial Cells. *Front Cell Infect Microbiol*. 2015;5:80.

Day CJ, Tran EN, Semchenko EA, et al. Glycan:glycan interactions: High affinity biomolecular interactions that can mediate binding of pathogenic bacteria to host cells. *Proc Natl Acad Sci USA*. 2015;112(52):E7266-E7275.

de Bentzmann S, Aurouze M, Ball G, Filloux A. FppA, a novel *Pseudomonas aeruginosa* prepilin peptidase involved in assembly of type IVb pili. *J Bacteriol*. 2006;188(13):4851-4860.

de Castro E, Sigrist CJ, Gattiker A, et al. ScanProsite: detection of PROSITE signature matches and ProRule-associated functional and structural residues in proteins. *Nucleic Acids Res*. 2006;34(Web Server issue):W362-W365.

De Oliveira DM, Hartley-Tassell L, Everest-Dass A, et al. Blood Group Antigen Recognition via the Group A Streptococcal M Protein Mediates Host Colonization. *mBio*. 2017;8(1):e02237-16.

Deng L, Song J, Gao X, et al. Host adaptation of a bacterial toxin from the human pathogen *Salmonella Typhi*. *Cell*. 2014;159(6):1290-1299.

Dennehy R, Romano M, Ruggiero A, et al. The *Burkholderia cenocepacia* peptidoglycan-associated lipoprotein is involved in epithelial cell attachment and elicitation of inflammation. *Cell Microbiol*. 2017;19(5):10.1111/cmi.12691.

Depoorter E, Bull MJ, Peeters C, Coenye T, Vandamme P, Mahenthiralingam E. *Burkholderia*: an update on taxonomy and biotechnological potential as antibiotic producers. *Appl Microbiol Biotechnol*. 2016;100(12):5215-5229.

Desvaux M, Khan A, Beatson SA, Scott-Tucker A, Henderson IR. Protein secretion systems in *Fusobacterium nucleatum*: genomic identification of Type 4 piliation and complete Type V pathways brings new insight into mechanisms of pathogenesis. *Biochim Biophys Acta*. 2005;1713(2):92-112.

Deuschle E, Keller B, Siegfried A, et al. Role of β1 integrins and bacterial adhesins for Yop injection into leukocytes in *Yersinia enterocolitica* systemic mouse infection. *Int J Med Microbiol*. 2016;306(2):77-88.

Dhar P, McAuley J. The Role of the Cell Surface Mucin MUC1 as a Barrier to Infection and Regulator of Inflammation. *Front Cell Infect Microbiol*. 2019;9:117.

Dingjan T, Imberty A, Pérez S, Yuriev E, Ramsland PA. Molecular Simulations of Carbohydrates with a Fucose-Binding *Burkholderia ambifaria* Lectin Suggest Modulation by Surface Residues Outside the Fucose-Binding Pocket. *Front Pharmacol*. 2017;8:393.

Drechsler-Hake D, Alamir H, Hahn J, et al. Mononuclear phagocytes contribute to intestinal invasion and dissemination of *Yersinia enterocolitica*. *Int J Med Microbiol*. 2016;306(6):357-366.

Drevinek P, Baldwin A, Lindenburg L, et al. Oxidative stress of *Burkholderia cenocepacia* induces insertion sequence-mediated genomic rearrangements that interfere with macrorestriction-based genotyping. *J Clin Microbiol*. 2010;48(1):34-40.

Drevinek P, Holden MT, Ge Z, et al. Gene expression changes linked to antimicrobial resistance, oxidative stress, iron depletion and retained motility are observed when *Burkholderia cenocepacia* grows in cystic fibrosis sputum. *BMC Infect Dis*. 2008;8:121.

Drevinek P, Mahenthiralingam E. *Burkholderia cenocepacia* in cystic fibrosis: epidemiology and molecular mechanisms of virulence. *Clin Microbiol Infect.* 2010;16(7):821-830.

Duell BL, Su YC, Riesbeck K. Host-pathogen interactions of nontypeable *Haemophilus influenzae*: from commensal to pathogen. *FEBS Lett*. 2016;590(21):3840-3853.

Durant L, Metais A, Soulama-Mouze C, Genevard JM, Nassif X, Escaich S. Identification of candidates for a subunit vaccine against extraintestinal pathogenic *Escherichia coli. Infect Immun*. 2007;75(4):1916-1925.

Edgar R, Domrachev M, Lash AE. Gene Expression Omnibus: NCBI gene expression and hybridization array data repository. *Nucleic Acids Res*. 2002;30(1):207-210.

Edwards TE, Phan I, Abendroth J, et al. Structure of a *Burkholderia pseudomallei* trimeric autotransporter adhesin head. *PLoS One*. 2010;5(9):e12803.

El Tahir Y, Skurnik M. YadA, the multifaceted *Yersinia* adhesin. *Int J Med Microbiol*. 2001;291(3):209-218.

El-Hawiet A, Kitova EN, Klassen JS. Recognition of human milk oligosaccharides by bacterial exotoxins. *Glycobiology*. 2015;25(8):845-854.

El-Kirat-Chatel S, Mil-Homens D, Beaussart A, Fialho AM, Dufrêne YF. Single-molecule atomic force microscopy unravels the binding mechanism of a *Burkholderia cenocepacia* trimeric autotransporter adhesin. *Mol Microbiol*. 2013;89(4):649-659.

Estrada-de Los Santos P, Palmer M, Chávez-Ramírez B, et al. Whole Genome Analyses Suggests that *Burkholderia sensu lato* Contains Two Additional Novel Genera (*Mycetohabitans gen. nov*., and *Trinickia gen. nov*.): Implications for the Evolution of Diazotrophy and Nodulation in the *Burkholderiaceae. Genes (Basel).* 2018;9(8):389.

Fagnocchi L, Biolchi A, Ferlicca F, et al. Transcriptional regulation of the *nadA* gene in *Neisseria meningitidis* impacts the prediction of coverage of a multicomponent meningococcal serogroup B vaccine. *Infect Immun*. 2013;81(2):560-569.

Fan E, Chauhan N, Udatha DBRKG, Leo JC, Linke D. Type V Secretion Systems in Bacteria. *Microbiol Spectr.* 2016;4(1):10.1128/microbiolspec.VMBF-0009-2015.

Flannagan RS, Valvano MA. *Burkholderia cenocepacia* requires RpoE for growth under stress conditions and delay of phagolysosomal fusion in macrophages. *Microbiology*. 2008;154(Pt 2):643-653.

Flannery A, Gerlach JQ, Joshi L, Kilcoyne M. Assessing Bacterial Interactions Using Carbohydrate-Based Microarrays. *Microarrays (Basel)*. 2015;4(4):690-713.

Flannery A, Le Berre M, Pier GB, O'Gara JP, Kilcoyne M. Glycomics Microarrays Reveal Differential *In Situ* Presentation of the Biofilm Polysaccharide Poly-*N*-acetylglucosamine on *Acinetobacter baumannii* and *Staphylococcus aureus* Cell Surfaces. *Int J Mol Sci*. 2020;21(7):2465.

Fournier B, Hooper DC. A new two-component regulatory system involved in adhesion, autolysis, and extracellular proteolytic activity of *Staphylococcus aureus*. *J Bacteriol*. 2000;182(14):3955-3964.

Freund S, Czech B, Trülzsch K, Ackermann N, Heesemann J. Unusual, virulence plasmid-dependent growth behavior of *Yersinia enterocolitica* in three-dimensional collagen gels. *J Bacteriol*. 2008;190(12):4111-4120.

Fusco WG, Choudhary NR, Routh PA, et al. The *Haemophilus ducreyi* trimeric autotransporter adhesin DsrA protects against an experimental infection in the swine model of chancroid. *Vaccine*. 2014;32(30):3752-3758.

Galyov EE, Brett PJ, DeShazer D. Molecular insights into *Burkholderia pseudomallei* and *Burkholderia mallei* pathogenesis. *Annu Rev Microbiol*. 2010;64:495-517.

Ganesan S, Sajjan US. Host evasion by *Burkholderia cenocepacia*. *Front Cell Infect Microbiol*. 2012;1:25.

Ganesh PS, Vishnupriya S, Vadivelu J, Mariappan V, Vellasamy KM, Shankar EM. Intracellular survival and innate immune evasion of *Burkholderia cepacia*: Improved understanding of quorum sensing-controlled virulence factors, biofilm, and inhibitors. *Microbiol Immunol*. 2020;64(2):87-98.

Ge SX, Jung D, Yao R. ShinyGO: a graphical gene-set enrichment tool for animals and plants. *Bioinformatics*. 2020;36(8):2628-2629.

Geissner A, Anish C, Seeberger PH. Glycan arrays as tools for infectious disease research. *Curr Opin Chem Biol*. 2014;18:38-45.

Geissner A, Reinhardt A, Rademacher C, et al. Microbe-focused glycan array screening platform. *Proc Natl Acad Sci USA*. 2019;116(6):1958-1967.

Gibson RL, Burns JL, Ramsey BW. Pathophysiology and management of pulmonary infections in cystic fibrosis. *Am J Respir Crit Care Med*. 2003;168(8):918-951.

Gipson IK, Spurr-Michaud S, Tisdale A, Menon BB. Comparison of the transmembrane mucins MUC1 and MUC16 in epithelial barrier function. *PLoS One*. 2014;9(6):e100393.

Girard F, Batisson I, Martinez G, Breton C, Harel J, Fairbrother JM. Use of virulence factor-specific egg yolk-derived immunoglobulins as a promising alternative to antibiotics for prevention of attaching and effacing *Escherichia coli* infections. *FEMS Immunol Med Microbiol*. 2006;46(3):340-350.

Goldberg JB, Ganesan S, Comstock AT, Zhao Y, Sajjan US. Cable pili and the associated 22 kDa adhesin contribute to *Burkholderia cenocepacia* persistence *in vivo*. *PLoS One*. 2011;6(7):e22435.

Gomes MC, Tasrini Y, Subramoni S, et al. The *afc* antifungal activity cluster, which is under tight regulatory control of ShvR, is essential for transition from intracellular persistence of

Burkholderia cenocepacia to acute pro-inflammatory infection. *PLoS Pathog.* 2018;14(12):e1007473.

Green ER, Mecsas J. Bacterial Secretion Systems: An Overview. *Microbiol Spectr*. 2016;4(1):10.1128/microbiolspec.VMBF-0012-2015.

Hagan CL, Kim S, Kahne D. Reconstitution of outer membrane protein assembly from purified components. *Science*. 2010;328(5980):890-892.

Hallström T, Trajkovska E, Forsgren A, Riesbeck K. *Haemophilus influenzae* surface fibrils contribute to serum resistance by interacting with vitronectin. *J Immunol*. 2006;177(1):430-436.

Hamad MA, Skeldon AM, Valvano MA. Construction of aminoglycoside-sensitive *Burkholderia cenocepacia* strains for use in studies of intracellular bacteria with the gentamicin protection assay. *Appl Environ Microbiol*. 2010;76(10):3170-3176.

Han L, Zheng J, Wang Y, et al. Structure of the BAM complex and its implications for biogenesis of outer-membrane proteins. *Nat Struct Mol Biol*. 2016;23(3):192-196.

Hanuszkiewicz A, Pittock P, Humphries F, et al. Identification of the flagellin glycosylation system in *Burkholderia cenocepacia* and the contribution of glycosylated flagellin to evasion of human innate immune responses. *J Biol Chem*. 2014;289(27):19231-19244.

Hartmann MD, Grin I, Dunin-Horkawicz S, et al. Complete fiber structures of complex trimeric autotransporter adhesins conserved in enterobacteria. *Proc Natl Acad Sci USA*. 2012;109(51):20907-20912.

Hassan AA, Coutinho CP, Sá-Correia I. *Burkholderia cepacia* Complex Species Differ in the Frequency of Variation of the Lipopolysaccharide O-Antigen Expression During Cystic Fibrosis Chronic Respiratory Infection. *Front Cell Infect Microbiol*. 2019a;9:273.

Hassan AA, Vitorino MV, Robalo T, Rodrigues MS, Sá-Correia I. Variation of *Burkholderia cenocepacia* cell wall morphology and mechanical properties during cystic fibrosis lung infection, assessed by atomic force microscopy. *Sci Rep*. 2019b;9(1):16118.

Heikal A, Nakatani Y, Dunn E, et al. Structure of the bacterial type II NADH dehydrogenase: a monotopic membrane protein with an essential role in energy generation. *Mol Microbiol*. 2014;91(5):950-964.

Heinz E, Selkrig J, Belousoff MJ, Lithgow T. Evolution of the Translocation and Assembly Module (TAM). *Genome Biol Evol*. 2015;7(6):1628-1643.

Heise T, Dersch P. Identification of a domain in *Yersinia* virulence factor YadA that is crucial for extracellular matrix-specific cell adhesion and uptake. *Proc Natl Acad Sci USA*. 2006;103(9):3375-3380.

Henderson IR, Nataro JP. Virulence functions of autotransporter proteins. *Infect Immun*. 2001;69(3):1231-1243.

Henderson IR, Navarro-Garcia F, Desvaux M, Fernandez RC, Ala'Aldeen D. Type V protein secretion pathway: the autotransporter story. *Microbiol Mol Biol Rev*. 2004;68(4):692-744.

Herrou J, Debrie AS, Willery E, et al. Molecular evolution of the two-component system BvgAS involved in virulence regulation in *Bordetella*. *PLoS One*. 2009;4(9):e6996.

Hodak H, Jacob-Dubuisson F. Current challenges in autotransport and two-partner protein secretion pathways. *Res Microbiol*. 2007;158(8-9):631-637.

Hogan AM, Rahman ASMZ, Lightly TJ, Cardona ST. A Broad-Host-Range CRISPRi Toolkit for Silencing Gene Expression in *Burkholderia*. *ACS Synth Biol*. 2019;8(10):2372-2384.

Hoiczyk E, Roggenkamp A, Reichenbecher M, Lupas A, Heesemann J. Structure and sequence analysis of *Yersinia* YadA and *Moraxella* UspAs reveal a novel class of adhesins. *EMBO J*. 2000;19(22):5989-5999.

Holdbrook DA, Piggot TJ, Sansom MS, Khalid S. Stability and membrane interactions of an autotransport protein: MD simulations of the Hia translocator domain in a complex membrane environment. *Biochim Biophys Acta*. 2013;1828(2):715-723.

Holden MT, Seth-Smith HM, Crossman LC, et al. The genome of *Burkholderia cenocepacia* J2315, an epidemic pathogen of cystic fibrosis patients. *J Bacteriol*. 2009;191(1):261-277.

Huang Y, Wang QL, Cheng DD, Xu WT, Lu NH. Adhesion and Invasion of Gastric Mucosa Epithelial Cells by *Helicobacter pylori*. *Front Cell Infect Microbiol*. 2016;6:159.

Hudak JE, Bertozzi CR. Glycotherapy: new advances inspire a reemergence of glycans in medicine. *Chem Biol*. 2014;21(1):16-37.

Huynh KK, Plumb JD, Downey GP, Valvano MA, Grinstein S. Inactivation of macrophage Rab7 by *Burkholderia cenocepacia. J Innate Immun*. 2010;2(6):522-533.

Ieva R, Bernstein HD. Interaction of an autotransporter passenger domain with BamA during its translocation across the bacterial outer membrane. *Proc Natl Acad Sci USA*. 2009;106(45):19120-19125.

Imberty A, wimmerová M, Mitchell EP, Gilboa-Garber N. Structures of the lectins from *Pseudomonas aeruginosa*: insight into the molecular basis for host glycan recognition. *Microbes Infect*. 2004;6(2):221-228.

Inglis TJ, Sagripanti JL. Environmental factors that affect the survival and persistence of *Burkholderia pseudomallei*. *Appl Environ Microbiol*. 2006;72(11):6865-6875.

Ishijima N, Suzuki M, Ashida H, et al. BabA-mediated adherence is a potentiator of the *Helicobacter pylori* type IV secretion system activity. *J Biol Chem*. 2011;286(28):25256-25264.

Ishikawa M, Shigemori K, Hori K. Application of the adhesive bacterionanofiber AtaA to a novel microbial immobilization method for the production of indigo as a model chemical. *Biotechnol Bioeng*. 2014;111(1):16-24.

Iwanicka-Nowicka R, Zielak A, Cook AM, Thomas MS, Hryniewicz MM. Regulation of sulfur assimilation pathways in *Burkholderia cenocepacia*: identification of transcription factors CysB and SsuR and their role in control of target genes. *J Bacteriol*. 2007;189(5):1675-1688.

Iwashkiw JA, Vozza NF, Kinsella RL, Feldman MF. Pour some sugar on it: the expanding world of bacterial protein O-linked glycosylation. *Mol Microbiol*. 2013;89(1):14-28.

Jeffries JL, Jia J, Choi W, et al. *Pseudomonas aeruginosa* pyocyanin modulates mucin glycosylation with sialyl-Lewis(x) to increase binding to airway epithelial cells. *Mucosal Immunol*. 2016;9(4):1039-1050.

Jitprasutwit N, Zainal-Abidin N, Vander Broek C, et al. Identification of Candidate Host Cell Factors Required for Actin-Based Motility of *Burkholderia pseudomallei*. *J Proteome Res*. 2016;15(12):4675-4685.

Jong WS, Daleke-Schermerhorn MH, Vikström D, et al. An autotransporter display platform for the development of multivalent recombinant bacterial vector vaccines. *Microb Cell Fact*. 2014;13:162.

Jose J. Autodisplay: efficient bacterial surface display of recombinant proteins. *Appl Microbiol Biotechnol*. 2006;69(6):607-614.

Kaiser PO, Linke D, Schwarz H, Leo JC, Kempf VA. Analysis of the BadA stalk from *Bartonella henselae* reveals domain-specific and domain-overlapping functions in the host cell infection process. *Cell Microbiol*. 2012;14(2):198-209.

Kakoschke TK, Kakoschke SC, Zeuzem C, et al. The RNA Chaperone Hfq Is Essential for Virulence and Modulates the Expression of Four Adhesins in *Yersinia enterocolitica*. *Sci Rep*. 2016;6:29275.

Kalferstova L, Kolar M, Fila L, Vavrova J, Drevinek P. Gene expression profiling of *Burkholderia cenocepacia* at the time of cepacia syndrome: loss of motility as a marker of poor prognosis?. *J Clin Microbiol*. 2015;53(5):1515-1522.

Kansal R, Rasko DA, Sahl JW, et al. Transcriptional modulation of enterotoxigenic *Escherichia coli* virulence genes in response to epithelial cell interactions. *Infect Immun*. 2013;81(1):259-270.

Kato K, Ishiwa A. The role of carbohydrates in infection strategies of enteric pathogens. *Trop Med Health*. 2015;43(1):41-52.

Katsowich N, Elbaz N, Pal RR, et al. Host cell attachment elicits posttranscriptional regulation in infecting enteropathogenic bacteria. *Science*. 2017;355(6326):735-739.

Kaza SK, McClean S, Callaghan M. IL-8 released from human lung epithelial cells induced by cystic fibrosis pathogens *Burkholderia cepacia* complex affects the growth and intracellular survival of bacteria. *Int J Med Microbiol*. 2011;301(1):26-33.

Keith KE, Hynes DW, Sholdice JE, Valvano MA. Delayed association of the NADPH oxidase complex with macrophage vacuoles containing the opportunistic pathogen *Burkholderia cenocepacia. Microbiology*. 2009;155(Pt 4):1004-1015.

Keller B, Mühlenkamp M, Deuschle E, et al. *Yersinia enterocolitica* exploits different pathways to accomplish adhesion and toxin injection into host cells. *Cell Microbiol*. 2015;17(8):1179-1204.

Kelley LA, Mezulis S, Yates CM, Wass MN, Sternberg MJ. The Phyre2 web portal for protein modeling, prediction and analysis. *Nat Protoc*. 2015;10(6):845-858.

Kertesz MA. Riding the sulfur cycle-metabolism of sulfonates and sulfate esters in gram-negative bacteria. *FEMS Microbiol Rev*. 2000;24(2):135-175.

Kespichayawattana W, Intachote P, Utaisincharoen P, Sirisinha S. Virulent *Burkholderia pseudomallei* is more efficient than avirulent *Burkholderia thailandensis* in invasion of and adherence to cultured human epithelial cells. *Microb Pathog*. 2004;36(5):287-292.

Khalil HS, Øgaard J, Leo JC. Coaggregation properties of trimeric autotransporter adhesins. *Microbiologyopen*. 2020;e1109.

Kiessling AR, Malik A, Goldman A. Recent advances in the understanding of trimeric autotransporter adhesins. *Med Microbiol Immunol*. 2020;209(3):233-242.

Kilcoyne M, Twomey ME, Gerlach JQ, Kane M, Moran AP, Joshi L. *Campylobacter jejuni* strain discrimination and temperature-dependent glycome expression profiling by lectin microarray. *Carbohydr Res*. 2014;389:123-133.

Kim DS, Chao Y, Saier MH Jr. Protein-translocating trimeric autotransporters of gram-negative bacteria. *J Bacteriol*. 2006;188(16):5655-5667.

Kim KC. Role of epithelial mucins during airway infection. *Pulm Pharmacol Ther*. 2012;25(6):415-419.

Kirjavainen V, Jarva H, Biedzka-Sarek M, Blom AM, Skurnik M, Meri S. *Yersinia enterocolitica* serum resistance proteins YadA and ail bind the complement regulator C4b-binding protein. *PLoS Pathog*. 2008;4(8):e1000140.

Klimova B, Kuca K, Novotny M, Maresova P. Cystic Fibrosis Revisited - a Review Study. *Med Chem*. 2017;13(2):102-109.

Kline KA, Fälker S, Dahlberg S, Normark S, Henriques-Normark B. Bacterial adhesins in host-microbe interactions. *Cell Host Microbe*. 2009;5(6):580-592.

Köberle M, Klein-Günther A, Schütz M, et al. *Yersinia enterocolitica* targets cells of the innate and adaptive immune system by injection of Yops in a mouse infection model. *PLoS Pathog*. 2009;5(8):e1000551.

Koiwai K, Hartmann MD, Linke D, Lupas AN, Hori K. Structural Basis for Toughness and Flexibility in the C-terminal Passenger Domain of an *Acinetobacter* Trimeric Autotransporter Adhesin. *J Biol Chem*. 2016;291(8):3705-3724.

Koretke KK, Szczesny P, Gruber M, Lupas AN. Model structure of the prototypical non-fimbrial adhesin YadA of *Yersinia enterocolitica*. *J Struct Biol*. 2006;155(2):154-161.

Kostakioti M, Newman CL, Thanassi DG, Stathopoulos C. Mechanisms of protein export across the bacterial outer membrane. *J Bacteriol*. 2005;187(13):4306-4314.

Kovacs-Simon A, Titball RW, Michell SL. Lipoproteins of bacterial pathogens. *Infect Immun*. 2011;79(2):548-561.

Kreda SM, Davis CW, Rose MC. CFTR, Mucins, and Mucus Obstruction in Cystic Fibrosis. *Cold Spring Harb Perspect Med*, 2012;2(a009589), 1–32.

Krivan HC, Roberts DD, Ginsburg V. Many pulmonary pathogenic bacteria bind specifically to the carbohydrate sequence GalNAc beta 1-4Gal found in some glycolipids. *Proc Natl Acad Sci USA*. 1988;85(16):6157-6161.

Kumar B, Cardona ST. Synthetic Cystic Fibrosis Sputum Medium Regulates Flagellar Biosynthesis through the *flhF* Gene in *Burkholderia cenocepacia. Front Cell Infect Microbiol*. 2016;6:65.

Kumar S, Stecher G, Tamura K. MEGA7: Molecular Evolutionary Genetics Analysis Version 7.0 for Bigger Datasets. *Mol Biol Evol*. 2016;33(7):1870-1874.

Kumar S, Vikram S, Raghava GP. Genome annotation of *Burkholderia* sp. SJ98 with special focus on chemotaxis genes. *PLoS One*. 2013;8(8):e70624.

Laarmann S, Cutter D, Juehne T, Barenkamp SJ, St Geme JW. The *Haemophilus influenzae* Hia autotransporter harbours two adhesive pockets that reside in the passenger domain and recognize the same host cell receptor. *Mol Microbiol*. 2002;46(3):731-743.

Lambert MA, Smith SG. The PagN protein of *Salmonella enterica* serovar Typhimurium is an adhesin and invasin. *BMC Microbiol*. 2008;8:142.

Lamblin G, Degroote S, Perini J, Delmotte P, Scharfman A, Davril M, Lo-Guidice JM, Houdret N, Dumur V, Klein A, Roussel P. Human airway mucin glycosylation: A combinatory of carbohydrate determinants which vary in cystic fibrosis. *Glycoconj J,* 2001;18, 661–684.

Lambris JD, Ricklin D, Geisbrecht BV. Complement evasion by human pathogens. *Nat Rev Microbiol*. 2008;6(2):132-142.

Lamothe J, Huynh KK, Grinstein S, Valvano MA. Intracellular survival of *Burkholderia cenocepacia* in macrophages is associated with a delay in the maturation of bacteria-containing vacuoles. *Cell Microbiol.* 2007;9(1):40-53.

Lamothe J, Valvano MA. *Burkholderia cenocepacia*-induced delay of acidification and phagolysosomal fusion in cystic fibrosis transmembrane conductance regulator (CFTR)-defective macrophages. *Microbiology*. 2008;154(Pt 12):3825-3834.

Lazar Adler NR, Dean RE, Saint RJ, et al. Identification of a predicted trimeric autotransporter adhesin required for biofilm formation of *Burkholderia pseudomallei*. *PLoS One*. 2013;8(11):e79461.

Lazar Adler NR, Stevens JM, Stevens MP, Galyov EE. Autotransporters and Their Role in the Virulence of *Burkholderia pseudomallei* and *Burkholderia mallei*. *Front Microbiol*. 2011;2:151.

Lazar Adler NR, Stevens MP, Dean RE, et al. Systematic mutagenesis of genes encoding predicted autotransported proteins of *Burkholderia pseudomallei* identifies factors mediating virulence in mice, net intracellular replication and a novel protein conferring serum resistance. *PLoS One*. 2015;10(4):e0121271.

Leduc I, Olsen B, Elkins C. Localization of the domains of the *Haemophilus ducreyi* trimeric autotransporter DsrA involved in serum resistance and binding to the extracellular matrix proteins fibronectin and vitronectin. *Infect Immun*. 2009;77(2):657-666.

Lehr U, Schütz M, Oberhettinger P, et al. C-terminal amino acid residues of the trimeric autotransporter adhesin YadA of *Yersinia enterocolitica* are decisive for its recognition and assembly by BamA. *Mol Microbiol*. 2010;78(4):932-946.

Leibiger K, Schweers JM, Schütz M. Biogenesis and function of the autotransporter adhesins YadA, intimin and invasin. *Int J Med Microbiol*. 2019;309(5):331-337.

Leo JC, Elovaara H, Bihan D, et al. First analysis of a bacterial collagen-binding protein with collagen Toolkits: promiscuous binding of YadA to collagens may explain how YadA interferes with host processes. *Infect Immun*. 2010;78(7):3226-3236.

Leo JC, Grin I, Linke D. Type V secretion: mechanism(s) of autotransport through the bacterial outer membrane. *Philos Trans R Soc Lond B Biol Sci*. 2012;367(1592):1088-1101.

Leo JC, Lyskowski A, Hattula K, et al. The structure of *E. coli* IgG-binding protein D suggests a general model for bending and binding in trimeric autotransporter adhesins. *Structure*. 2011;19(7):1021-1030.

Leo JC, Oberhettinger P, Schütz M, Linke D. The inverse autotransporter family: intimin, invasin and related proteins. *Int J Med Microbiol*. 2015;305(2):276-282.

Leo JC, Skurnik M. Adhesins of human pathogens from the genus *Yersinia*. *Adv Exp Med Biol*. 2011;715:1-15.

Letunic I, Bork P. 20 years of the SMART protein domain annotation resource. *Nucleic Acids Res*. 2018;46(D1):D493-D496.

Levental KR, Levental I. Giant plasma membrane vesicles: models for understanding membrane organization. *Curr Top Membr*. 2015;75:25-57.

Lewis ER, Torres AG. The art of persistence-the secrets to *Burkholderia* chronic infections. *Pathog Dis*. 2016;74(6):ftw070.

Leyton DL, Rossiter AE, Henderson IR. From self sufficiency to dependence: mechanisms and factors important for autotransporter biogenesis. *Nat Rev Microbiol*. 2012;10(3):213-225.

Li G, Brown PJ, Tang JX, et al. Surface contact stimulates the just-in-time deployment of bacterial adhesins. *Mol Microbiol*. 2012;83(1):41-51.

Li X, Bleumink-Pluym NMC, Luijkx YMCA, Wubbolts RW, van Putten JPM, Strijbis K. MUC1 is a receptor for the *Salmonella* SiiE adhesin that enables apical invasion into enterocytes. *PLoS Pathog*. 2019;15(2):e1007566.

Lieberman TD, Flett KB, Yelin I, et al. Genetic variation of a bacterial pathogen within individuals with cystic fibrosis provides a record of selective pressures. *Nat Genet*. 2014;46(1):82-87.

Liguori A, Dello Iacono L, Maruggi G, et al. NadA3 Structures Reveal Undecad Coiled Coils and LOX1 Binding Regions Competed by Meningococcus B Vaccine-Elicited Human Antibodies. *mBio*. 2018;9(5):e01914-18.

Lillehoj EP, Guang W, Hyun SW, et al. Neuraminidase 1-mediated desialylation of the mucin 1 ectodomain releases a decoy receptor that protects against *Pseudomonas aeruginosa* lung infection. *J Biol Chem*. 2019;294(2):662-678.

Lindén SK, Sheng YH, Every AL, et al. MUC1 limits *Helicobacter pylori* infection both by steric hindrance and by acting as a releasable decoy. *PLoS Pathog*. 2009;5(10):e1000617.

Linke D, Riess T, Autenrieth IB, Lupas A, Kempf VA. Trimeric autotransporter adhesins: variable structure, common function. *Trends Microbiol*. 2006;14(6):264-270.

Lipuma JJ. The changing microbial epidemiology in cystic fibrosis. *Clin Microbiol Rev*. 2010;23(2):299-323.

Liu M, Yang S, Zheng C, Luo X, Bei W, Cai P. Binding to type I collagen is essential for the infectivity of *Vibrio parahaemolyticus* to host cells. *Cell Microbiol*. 2018;20(9):e12856.

Livak KJ, Schmittgen TD. Analysis of relative gene expression data using real-time quantitative PCR and the $2^{-\Delta\Delta CT}$ method. *Methods*.2001; 25(4):402-408.

Łochowska A, Iwanicka-Nowicka R, Zielak A, Modelewska A, Thomas MS, Hryniewicz MM. Regulation of sulfur assimilation pathways in *Burkholderia cenocepacia* through control of genes by the SsuR transcription factor. *J Bacteriol*. 2011;193(8):1843-1853.

Lu Q, Li S, Shao F. Sweet Talk: Protein Glycosylation in Bacterial Interaction with the Host. *Trends Microbiol*. 2015;23(10):630-641.

Lu YY, Franz B, Truttmann MC, et al. *Bartonella henselae* trimeric autotransporter adhesin BadA expression interferes with effector translocation by the VirB/D4 type IV secretion system. *Cell Microbiol*. 2013;15(5):759-778.

Luciani A, Villella VR, Esposito S, et al. Cystic fibrosis: a disorder with defective autophagy. *Autophagy*. 2011;7(1):104-106.

Lupas AN, Gruber M. The structure of alpha-helical coiled coils. *Adv Protein Chem*. 2005;70:37-78.

Łyskowski A, Leo JC, Goldman A. Structure and biology of trimeric autotransporter adhesins. *Adv Exp Med Biol*. 2011;715:143-158.

Madeira A, Santos PM, Coutinho CP, Pinto-de-Oliveira A, Sá-Correia I. Quantitative proteomics (2-D DIGE) reveals molecular strategies employed by *Burkholderia cenocepacia* to adapt to the airways of cystic fibrosis patients under antimicrobial therapy. *Proteomics*. 2011;11(7):1313-1328.

Mahenthiralingam E, Baldwin A, Dowson CG. *Burkholderia cepacia* complex bacteria: opportunistic pathogens with important natural biology. *J Appl Microbiol*. 2008;104(6):1539-1551.

Mahenthiralingam E, Urban TA, Goldberg JB. The multifarious, multireplicon *Burkholderia cepacia* complex. *Nat Rev Microbiol*. 2005;3(2):144-156.

Mahenthiralingam E, Vandamme P. Taxonomy and pathogenesis of the *Burkholderia cepacia* complex. *Chron Respir Dis*. 2005;2(4):209-217.

Malito E, Biancucci M, Faleri A, et al. Structure of the meningococcal vaccine antigen NadA and epitope mapping of a bactericidal antibody. *Proc Natl Acad Sci USA*. 2014;111(48):17128-17133.

Mann T, Ben-David D, Zlotkin A, et al. An outbreak of *Burkholderia cenocepacia* bacteremia in immunocompromised oncology patients*. Infection*. 2010;38(3):187-194.

Manni MM, Sot J, Goñi FM. Interaction of *Clostridium perfringens* epsilon-toxin with biological and model membranes: A putative protein receptor in cells. *Biochim Biophys Acta*. 2015;1848(3):797-804.

Mariappan V, Vellasamy KM, Vadivelu J. Host-Adaptation of *Burkholderia pseudomallei* Alters Metabolism and Virulence: a Global Proteome Analysis. *Sci Rep*. 2017;7(1):9015.

Martina P, Feliziani S, Juan C, et al. Hypermutation in *Burkholderia cepacia* complex is mediated by DNA mismatch repair inactivation and is highly prevalent in cystic fibrosis chronic respiratory infection. *Int J Med Microbiol*. 2014;304(8):1182-1191.

Martinez JER, Thomas B, Flitsch SL. Glycan Array Technology. *Adv Biochem Eng Biotechnol*. 2020;10.1007/10_2019_112.

Matilla MA, Krell T. The effect of bacterial chemotaxis on host infection and pathogenicity. *FEMS Microbiol Rev*. 2018;42(1):10.1093/femsre/fux052.

McAvoy AC, Jaiyesimi O, Threatt PH, et al. Differences in Cystic Fibrosis-Associated *Burkholderia spp.* Bacteria Metabolomes after Exposure to the Antibiotic Trimethoprim. *ACS Infect Dis.* 2020;6(5):1154-1168.

Mccarthy Y, Yang L, Twomey KB, Sass A, Tolker-Nielsen T, Mahenthiralingam E, et al. A sensor kinase recognizing the cell-cell signal BDSF (cis-2-dodecenoic acid) regulates virulence in *Burkholderia cenocepacia*. *Mol Microbiol.* 2010;77:1220e36.

McClean S, Callaghan M. *Burkholderia cepacia* complex: epithelial cell-pathogen confrontations and potential for therapeutic intervention. *J Med Microbiol*. 2009;58(Pt 1):1-12.

McClean S, Healy ME, Collins C, et al. Linocin and OmpW Are Involved in Attachment of the Cystic Fibrosis-Associated Pathogen *Burkholderia cepacia* Complex to Lung Epithelial Cells and Protect Mice against Infection. *Infect Immun*. 2016;84(5):1424-1437.

McClean S. Eight stranded β -barrel and related outer membrane proteins: role in bacterial pathogenesis. *Protein Pept Lett*. 2012;19(10):1013-1025.

McKeon SA, Nguyen DT, Viteri DF, Zlosnik JE, Sokol PA. Functional quorum sensing systems are maintained during chronic *Burkholderia cepacia* complex infections in patients with cystic fibrosis. *J Infect Dis*. 2011;203(3):383-392.

Meng G, St Geme JW 3rd, Waksman G. Repetitive architecture of the *Haemophilus influenzae* Hia trimeric autotransporter. *J Mol Biol*. 2008;384(4):824-836.

Meng G, Surana NK, St Geme JW 3rd, Waksman G. Structure of the outer membrane translocator domain of the *Haemophilus influenzae* Hia trimeric autotransporter. *EMBO J*. 2006;25(11):2297-2304.

Merry CR, Perkins M, Mu L, Peterson BK, Knackstedt RW, Weingart CL. Characterization of a novel two-component system in *Burkholderia cenocepacia*. *Curr Microbiol*. 2015;70:556e61.

Mesureur J, Feliciano JR, Wagner N, et al. Macrophages, but not neutrophils, are critical for proliferation of *Burkholderia cenocepacia* and ensuing host-damaging inflammation. *PLoS Pathog.* 2017;13(6):e1006437.

Mikula KM, Leo JC, Łyskowski A, Kedracka-Krok S, Pirog A, Goldman A. The translocation domain in trimeric autotransporter adhesins is necessary and sufficient for trimerization and autotransportation. *J Bacteriol*. 2012;194(4):827-838.

Mil-Homens D, Fialho AM. A BCAM0223 mutant of *Burkholderia cenocepacia* is deficient in hemagglutination, serum resistance, adhesion to epithelial cells and virulence. *PLoS One*. 2012;7(7):e41747.

Mil-Homens D, Fialho AM. Trimeric autotransporter adhesins in members of the *Burkholderia cepacia* complex: a multifunctional family of proteins implicated in virulence. *Front Cell Infect Microbiol*. 2011;1:13.

Mil-Homens D, Leça MI, Fernandes F, Pinto SN, Fialho AM. Characterization of BCAM0224, a multifunctional trimeric autotransporter from the human pathogen *Burkholderia cenocepacia*. *J Bacteriol.* 2014;196(11):1968-1979.

Mil-Homens D, Pinto SN, Matos RG, Arraiano C, Fialho AM. *Burkholderia cenocepacia* K56-2 trimeric autotransporter adhesin BcaA binds TNFR1 and contributes to induce airway inflammation. *Cell Microbiol*. 2017;19(4):10.1111/cmi.12677.

Mil-Homens D, Rocha EPC, Fialho AM. Genome-wide analysis of DNA repeats *in Burkholderia cenocepacia* J2315 identifies a novel adhesin-like gene unique to epidemic-associated strains of the ET-12 lineage. *Microbiology*. 2010;156(Pt 4):1084-1096.

Mira NP, Madeira A, Moreira AS, Coutinho CP, Sá-Correia I. Genomic expression analysis reveals strategies of *Burkholderia cenocepacia* to adapt to cystic fibrosis patients' airways and antimicrobial therapy. *PLoS One*. 2011;6(12):e28831.

Moonens K, Bouckaert J, Coddens A, et al. Structural insight in histo-blood group binding by the F18 fimbrial adhesin FedF. *Mol Microbiol*. 2012;86(1):82-95.

Moutevelis E, Woolfson DN. A periodic table of coiled-coil protein structures. *J Mol Biol*. 2009;385(3):726-732.

Muangsombut V, Suparak S, Pumirat P, et al. Inactivation of *Burkholderia pseudomallei bsaQ* results in decreased invasion efficiency and delayed escape of bacteria from endocytic vesicles. *Arch Microbiol*. 2008;190(6):623-631.

Mühlenkamp MC, Hallström T, Autenrieth IB, et al. Vitronectin Binds to a Specific Stretch within the Head Region of *Yersinia Adhesin* A and Thereby Modulates *Yersinia enterocolitica* Host Interaction. *J Innate Immun*. 2017;9(1):33-51.

Mullen T, Callaghan M, McClean S. Invasion of *Burkholderia cepacia* complex isolates into lung epithelial cells involves glycolipid receptors. *Microb Pathog*. 2010;49(6):381-387.

Murphy MP, Caraher E. Residence in biofilms allows *Burkholderia cepacia* complex (Bcc) bacteria to evade the antimicrobial activities of neutrophil-like dHL60 cells. *Pathog Dis*. 2015;73(8):ftv069.

Nandi T, Ong C, Singh AP, et al. A genomic survey of positive selection in *Burkholderia pseudomallei* provides insights into the evolution of accidental virulence. *PLoS Pathog*. 2010;6(4):e1000845.

Nguyen MT, Peisl L, Barletta F, Luqman A, Götz F. Toll-Like Receptor 2 and Lipoprotein-Like Lipoproteins Enhance *Staphylococcus aureus* Invasion in Epithelial. *Infect Immun*. 2018;86(8):e00343-18.

Nieckarz M, Raczkowska A, Dębski J, et al. Impact of OmpR on the membrane proteome of *Yersinia enterocolitica* in different environments: repression of major adhesin YadA and heme receptor HemR. *Environ Microbiol*. 2016;18(3):997-1021.

Nikolaus J, Scolari S, Bayraktarov E, et al. Hemagglutinin of influenza virus partitions into the non-raft domain of model membranes. *Biophys J*. 2010;99(2):489-498.

Nummelin H, Merckel MC, Leo JC, Lankinen H, Skurnik M, Goldman A. The *Yersinia adhesin* YadA collagen-binding domain structure is a novel left-handed parallel beta-roll. *EMBO J*. 2004;23(4):701-711.

Ofek I, Bayer EA, Abraham SN. Bacterial adhesion. *In*: E. Rosenberg, E. F. DeLong, S. Lory, E. Stackebrandt, & F. Thompson (Eds.), The prokaryotes (pp. 107–123). 2013. Berlin, Heidelberg: Springer.

O'Grady EP, Sokol PA. *Burkholderia cenocepacia* differential gene expression during host-pathogen interactions and adaptation to the host environment. *Front Cell Infect Microbiol*. 2011;1:15.

Ohneck EJ, Arivett BA, Fiester SE, et al. Mucin acts as a nutrient source and a signal for the differential expression of genes coding for cellular processes and virulence factors in *Acinetobacter baumannii*. *PLoS One*. 2018;13(1):e0190599.

Olland A, Falcoz PE, Kessler R, Massard G. Should cystic fibrosis patients infected with *Burkholderia cepacia* complex be listed for lung transplantation?. *Interact Cardiovasc Thorac Surg*. 2011;13(6):631-634.

Osman KL, Jefferies JM, Woelk CH, Cleary DW, Clarke SC. The adhesins of non-typeable *Haemophilus influenzae*. *Expert Rev Anti Infect Ther*. 2018;16(3):187-196.

Pacello F, D'Orazio M, Battistoni A. An ERp57-mediated disulphide exchange promotes the interaction between *Burkholderia cenocepacia* and epithelial respiratory cells. *Sci Rep*. 2016;6:21140.

Palumbo RN, Wang C. Bacterial invasin: structure, function, and implication for targeted oral gene delivery. *Curr Drug Deliv*. 2006;3(1):47-53.

Pearson MM, Laurence CA, Guinn SE, Hansen EJ. Biofilm formation by *Moraxella catarrhalis in vitro*: roles of the UspA1 adhesin and the Hag hemagglutinin. *Infect Immun*. 2006;74(3):1588-1596.

Perault AI, Chandler CE, Rasko DA, Ernst RK, Wolfgang MC, Cotter PA. Host Adaptation Predisposes *Pseudomonas aeruginosa* to Type VI Secretion System-Mediated Predation by the *Burkholderia cepacia* Complex. *Cell Host Microbe*. 2020;S1931-3128(20)30360-7.

Pimenta AI, Mil-Homens D, Fialho, AM. *Burkholderia cenocepacia*–host cell contact controls the transcription activity of the trimeric autotransporter adhesin BCAM2418 gene. *MicrobiologyOpen*. 2020a;00:e998.

Pimenta AI, Mil-Homens D, Pinto SN, Fialho AM. Phenotypic characterization of trimeric autotransporter adhesin-defective *bcaC* mutant of *Burkholderia cenocepacia*: cross-talk towards the histidine kinase BCAM0218. *Microbes Infect*. 2020b;S1286-4579(20)30096-4.

Pizarro-Cerdá J, Cossart P. Bacterial adhesion and entry into host cells. *Cell*. 2006;124(4):715-727.

Poole J, Foster E, Chaloner K, et al. Analysis of nontypeable *Haemophilus influenzae* phase-variable genes during experimental human nasopharyngeal colonization. *J Infect Dis*. 2013;208(5):720-727.

Qin W, Wang L, Lei L. New findings on the function and potential applications of the trimeric autotransporter adhesin. *Antonie Van Leeuwenhoek*. 2015;108(1):1-14.

Radin JN, Grass SA, Meng G, Cotter SE, Waksman G, St Geme JW 3rd. Structural basis for the differential binding affinities of the HsfBD1 and HsfBD2 domains in the *Haemophilus influenzae* Hsf adhesin. *J Bacteriol*. 2009;191(16):5068-5075.

Rafeeq MM, Murad HAS. Cystic fibrosis: current therapeutic targets and future approaches. *J Transl Med*. 2017;15(1):84.

Raghunathan K, Wong TH, Chinnapen DJ, Lencer WI, Jobling MG, Kenworthy AK. Glycolipid Crosslinking Is Required for Cholera Toxin to Partition Into and Stabilize Ordered Domains. *Biophys J*. 2016;111(12):2547-2550.

Rahbar MR, Zarei M, Jahangiri A, et al. Trimeric autotransporter adhesins in *Acinetobacter baumannii*, coincidental evolution at work. *Infect Genet Evol*. 2019;71:116-127.

Rhodes KA, Schweizer HP. Antibiotic resistance in *Burkholderia* species. *Drug Resist Updat*. 2016;28:82-90.

Ridley C, Thornton DJ. Mucins: the frontline defense of the lung. *Biochem Soc Trans*, 2018; 46(5), 1099–1106.

Riesbeck K. Complement evasion by the human respiratory tract pathogens *Haemophilus influenzae* and *Moraxella catarrhalis. FEBS Lett*. 2020;10.1002/1873-3468.13758.

Riess T, Andersson SG, Lupas A, et al. *Bartonella* adhesin a mediates a proangiogenic host cell response. *J Exp Med*. 2004;200(10):1267-1278.

Roggenkamp A, Ackermann N, Jacobi CA, Truelzsch K, Hoffmann H, Heesemann J. Molecular analysis of transport and oligomerization of the *Yersinia enterocolitica* adhesin YadA. *J Bacteriol*. 2003;185(13):3735-3744.

Rosales-Reyes R, Garza-Villafuerte P, Vences-Vences D, et al. Interferon-gamma-activated macrophages infected with *Burkholderia cenocepacia* process and present bacterial antigens to T-cells by class I and II major histocompatibility complex molecules. *Emerg Microbes Infect*. 2020;9(1):2000-2012.

Rosales-Reyes R, Sánchez-Gómez C, Ortiz-Navarrete V, Santos-Preciado JI. *Burkholderia cenocepacia* Induces Macropinocytosis to Enter Macrophages. *Biomed Res Int*. 2018;2018:4271560.

Roussel P, Lamblin G. The glycosylation of airway mucins in cystic fibrosis and its relationship with lung infection by *Pseudomonas aeruginosa. Adv Exp Med Biol*. 2003;535:17-32.

Ruiz-Palacios GM, Cervantes LE, Ramos P, Chavez-Munguia B, Newburg DS. *Campylobacter jejuni* binds intestinal H(O) antigen (Fuc alpha 1, 2Gal beta 1, 4GlcNAc), and fucosyloligosaccharides of human milk inhibit its binding and infection. *J Biol Chem*. 2003;278(16):14112-14120.

Ryoo D, Rydmark MO, Pang YT, Lundquist KP, Linke D, Gumbart JC. BamA is required for autotransporter secretion. *Biochim Biophys Acta Gen Subj.* 2020;1864(7):129581.

Sajjan SU, Carmody LA, Gonzalez CF, LiPuma JJ. A type IV secretion system contributes to intracellular survival and replication of *Burkholderia cenocepacia. Infect Immun.* 2008;76(12):5447-5455.

Sajjan U, Ackerley C, Forstner J. Interaction of *cblA*/adhesin-positive *Burkholderia cepacia* with squamous epithelium. *Cell Microbiol*. 2002;4(2):73-86.

Sajjan U, Corey M, Humar A, et al. Immunolocalisation of *Burkholderia cepacia* in the lungs of cystic fibrosis patients. *J Med Microbiol*. 2001;50(6):535-546.

Sajjan U, Keshavjee S, Forstner J. Responses of well-differentiated airway epithelial cell cultures from healthy donors and patients with cystic fibrosis to *Burkholderia cenocepacia* infection. *Infect Immun*. 2004;72(7):4188-4199.

Sajjan U, Liu L, Lu A, Spilker T, Forstner J, LiPuma JJ. Lack of cable pili expression by *cblA*-containing *Burkholderia cepacia* complex. *Microbiology.* 2002;148(Pt 11):3477-3484.

Sajjan U, Wu Y, Kent G, Forstner J. Preferential adherence of cable-piliated *Burkholderia cepacia* to respiratory epithelia of CF knockout mice and human cystic fibrosis lung explants. *J Med Microbiol.* 2000a;49(10):875-885.

Sajjan US, Hershenson MB, Forstner JF, LiPuma JJ. *Burkholderia cenocepacia* ET12 strain activates TNFR1 signalling in cystic fibrosis airway epithelial cells. *Cell Microbiol*. 2008;10(1):188-201.

Sajjan US, Sylvester FA, Forstner JF. Cable-piliated *Burkholderia cepacia* binds to cytokeratin 13 of epithelial cells. *Infect Immun*. 2000b;68(4):1787-1795.

Sajjan US, Yang JH, Hershenson MB, LiPuma JJ. Intracellular trafficking and replication of *Burkholderia cenocepacia* in human cystic fibrosis airway epithelial cells. *Cell Microbiol*. 2006;8(9):1456-1466.

Saldías MS, Lamothe J, Wu R, Valvano MA. *Burkholderia cenocepacia* requires the RpoN sigma factor for biofilm formation and intracellular trafficking within macrophages. *Infect Immun*. 2008;76(3):1059-1067.

Saldías MS, Ortega X, Valvano MA. *Burkholderia cenocepacia* O antigen lipopolysaccharide prevents phagocytosis by macrophages and adhesion to epithelial cells. *J Med Microbiol*. 2009;58:1542e8.

Saldías MS, Valvano MA. Interactions of *Burkholderia cenocepacia* and other *Burkholderia cepacia* complex bacteria with epithelial and phagocytic cells. *Microbiology.* 2009;155(Pt 9):2809-2817.

Santamaría R, Pierre P. Voronto: mapper for expression data to ontologies. *Bioinformatics*. 2012;28(17):2281-2282.

Sass A, Marchbank A, Tullis E, Lipuma JJ, Mahenthiralingam E. Spontaneous and evolutionary changes in the antibiotic resistance of *Burkholderia cenocepacia* observed by global gene expression analysis. *BMC Genomics*. 2011;12:373.

Sass A, Marchbank A, Tullis E, Lipuma JJ, Mahenthiralingam E. Spontaneous and evolutionary changes in the antibiotic resistance of *Burkholderia cenocepacia* observed by global gene expression analysis. *BMC Genomics*. 2011;12:373.

Sass AM, Coenye T. Low iron-induced small RNA BrrF regulates central metabolism and oxidative stress responses in *Burkholderia cenocepacia. PLoS One*. 2020;15(7):e0236405.

Sass AM, Schmerk C, Agnoli K, et al. The unexpected discovery of a novel low-oxygen-activated locus for the anoxic persistence of *Burkholderia cenocepacia*. *ISME J*. 2013;7(8):1568-1581.

Sauri A, Soprova Z, Wickström D, et al. The Bam (Omp85) complex is involved in secretion of the autotransporter haemoglobin protease. *Microbiology*. 2009;155(Pt 12):3982-3991.

Saurí A, Ten Hagen-Jongman CM, van Ulsen P, Luirink J. Estimating the size of the active translocation pore of an autotransporter. *J Mol Biol*. 2012;416(3):335-345.

Schaefers MM. Regulation of Virulence by Two-Component Systems in Pathogenic *Burkholderia. Infect Immun*. 2020;88(7):e00927-19.

Schaefers MM, Liao TL, Boisvert NM, Roux D, Yoder-Himes D, Priebe GP. An oxygen-sensing two-component system in the *Burkholderia cepacia* complex regulates biofilm, intracellular invasion, and pathogenicity. *PLoS Pathog*. 2017;13:e1006116.

Scharfman A, Delmotte P, Beau J, Lamblin G, Roussel P, Mazurier J. Sialyl-Le(x) and sulfo-sialyl-Le(x) determinants are receptors for *P. aeruginosa*. *Glycoconj J*. 2000;17(10):735-740.

Scheller EV, Cotter PA. *Bordetella* filamentous hemagglutinin and fimbriae: critical adhesins with unrealized vaccine potential. *Pathog Dis*. 2015;73(8):ftv079.

Schindler MK, Schütz MS, Mühlenkamp MC, et al. *Yersinia enterocolitica* YadA mediates complement evasion by recruitment and inactivation of C3 products. *J Immunol*. 2012;189(10):4900-4908.

Schmerk CL, Valvano MA. *Burkholderia multivorans* survival and trafficking within macrophages. *J Med Microbiol*. 2013;62(Pt 2):173-184.

Schmid N, Suppiger A, Steiner E, et al. High intracellular c-di-GMP levels antagonize quorum sensing and virulence gene expression in *Burkholderia cenocepacia* H111. *Microbiology*. 2017;163(5):754-764.

Schmid Y, Grassl GA, Bühler OT, Skurnik M, Autenrieth IB, Bohn E. *Yersinia enterocolitica* adhesin A induces production of interleukin-8 in epithelial cells. *Infect Immun*. 2004;72(12):6780-6789.

Schnetterle M, Koch L, Gorgé O, et al. Relationships Between Resistance and Virulence in *Burkholderia pseudomallei. Curr Trop Med Rep*. 2017;4,127–135.

Schulz BL, Sloane AJ, Robinson J, Prasad SS, Lindner RA, Robinson M, Bye PT, Nielson DW, Harry JL, Packer NH. Glycosylation of sputum mucins is altered in cystic fibrosis patients. *Glycobiology,* 2007;17(7), 698–712.

Schütz M, Weiss EM, Schindler M, et al. Trimer stability of YadA is critical for virulence of *Yersinia enterocolitica*. *Infect Immun*. 2010;78(6):2677-2690.

Schwab U, Leigh M, Ribeiro C, et al. Patterns of epithelial cell invasion by different species of the *Burkholderia cepacia* complex in well-differentiated human airway epithelia. *Infect Immun*. 2002;70(8):4547-4555.

Scoffone VC, Barbieri G, Buroni S, Scarselli M, Pizza M, Rappuoli R, Riccardi G. Vaccines to Overcome Antibiotic Resistance: The Challenge of *Burkholderia cenocepacia*. *Trends Microbiol.* 2020; 10. pii: S0966-842X(19)30320-8.

Scoffone VC, Chiarelli LR, Trespidi G, Mentasti M, Riccardi G, Buroni S. *Burkholderia cenocepacia* Infections in Cystic Fibrosis Patients: Drug Resistance and Therapeutic Approaches. *Front Microbiol*. 2017;8:1592.

Seed KD, Dennis JJ. Development of *Galleria mellonella* as an alternative infection model for the *Burkholderia cepacia* complex. *Infect Immun*. 2008;76(3):1267-75.

Selkrig J, Mosbahi K, Webb CT, et al. Discovery of an archetypal protein transport system in bacterial outer membranes. *Nat Struct Mol Biol*. 2012;19(5):506-S1.

Sezgin E, Kaiser HJ, Baumgart T, Schwille P, Simons K, Levental I. Elucidating membrane structure and protein behavior using giant plasma membrane vesicles. *Nat Protoc*. 2012;7(6):1042-1051.

Shahid SA, Nagaraj M, Chauhan N, et al. Solid-state NMR Study of the YadA Membrane-Anchor Domain in the Bacterial Outer Membrane. *Angew Chem Int Ed Engl*. 2015;54(43):12602-12606.

Sheets AJ, Grass SA, Miller SE, St Geme JW 3rd. Identification of a novel trimeric autotransporter adhesin in the cryptic genospecies of *Haemophilus*. *J Bacteriol*. 2008;190(12):4313-4320.

Sheets AJ, St Geme JW. Adhesive activity of the *Haemophilus* cryptic genospecies *cha* autotransporter is modulated by variation in tandem peptide repeats. *J Bacteriol*. 2011;193:329e39.

Shoulders MD, Raines RT. Collagen structure and stability. *Annu Rev Biochem*. 2009;78:929e58.

Sieira R, Bialer MG, Roset MS, Ruiz-Ranwez V, Langer T, Arocena GM, et al. Combinatorial control of adhesion of *Brucella abortus* 2308 to host cells by transcriptional rewiring of the trimeric autotransporter *btaE*. *Mol Microbiol.* 2017;103:553e65.

Sikdar R, Bernstein HD. Sequential Translocation of Polypeptides across the Bacterial Outer Membrane through the Trimeric Autotransporter Pathway. *mBio*. 2019;10(5):e01973-19.

Silva IN, Santos PM, Santos MR, et al. Long-Term Evolution of *Burkholderia multivorans* during a Chronic Cystic Fibrosis Infection Reveals Shifting Forces of Selection. *mSystems*. 2016;1(3):e00029-16.

Singh AK, Nguyen TH, Vidovszky MZ, et al. Structure and N-acetylglucosamine binding of the distal domain of mouse adenovirus 2 fibre. *J Gen Virol*. 2018;99(11):1494-1508.

Singh B, Alvarado-Kristensson M, Johansson M, et al. The Respiratory Pathogen *Moraxella catarrhalis* Targets Collagen for Maximal Adherence to Host Tissues. *mBio*. 2016;7(2):e00066.

Singh B, Jubair TA, Mörgelin M, et al. *Haemophilus influenzae* surface fibril (Hsf) is a unique twisted hairpin-like trimeric autotransporter. *Int J Med Microbiol*. 2015;305(1):27-37.

Singh B, Su Y, Riesbeck K. Vitronectin in host pathogen interactions and antimicrobial therapeutic applications. *cent.eur.j.biol.* 2011;6:973–980.

Singh B, Su YC, Al-Jubair T, et al. A fine-tuned interaction between trimeric autotransporter *Haemophilus* surface fibrils and vitronectin leads to serum resistance and adherence to respiratory epithelial cells. *Infect Immun*. 2014;82(6):2378-2389.

Sitthidet C, Korbsrisate S, Layton AN, Field TR, Stevens MP, Stevens JM. Identification of motifs of *Burkholderia pseudomallei* BimA required for intracellular motility, actin binding, and actin polymerization. *J Bacteriol*. 2011;193(8):1901-1910.

Smrt ST, Lorieau JL. Membrane Fusion and Infection of the Influenza Hemagglutinin. *Adv Exp Med Biol*. 2017;966:37-54.

Sousa SA, Feliciano JR, Pita T, Guerreiro SI, Leitão JH. *Burkholderia cepacia* complex regulation of virulence gene expression: a Review. *Genes* (Basel) 2017;8:E43.

Spahich NA, St Geme JW 3rd. Structure and function of the *Haemophilus influenzae* autotransporters. *Front Cell Infect Microbiol*. 2011;1:5.

Speert DP, Henry D, Vandamme P, Corey M, Mahenthiralingam E. Epidemiology of *Burkholderia cepacia* complex in patients with cystic fibrosis, Canada. *Emerg Infect Dis*. 2002;8(2):181-187.

Spiewak HL, Shastri S, Zhang L, et al. *Burkholderia cenocepacia* utilizes a type VI secretion system for bacterial competition. *Microbiologyopen*. 2019;8(7):e774.

St Geme JW 3rd, Cutter D. The *Haemophilus influenzae* Hia adhesin is an autotransporter protein that remains uncleaved at the C terminus and fully cell associated. *J Bacteriol*. 2000;182(21):6005-6013.

Stevens MP, Stevens JM, Jeng RL, et al. Identification of a bacterial factor required for actin-based motility of *Burkholderia pseudomallei*. *Mol Microbiol*. 2005;56(1):40-53.

Stock AM, Robinson VL, Goudreau PN. Two-component signal transduction. *Annu Rev Biochem*. 2000;69:183e215.

Stones DH, Krachler AM. Against the tide: the role of bacterial adhesion in host colonization. *Biochem Soc Trans*. 2016;44(6):1571-1580.

Stubenrauch C, Grinter R, Lithgow T. The modular nature of the β-barrel assembly machinery, illustrated in *Borrelia burgdorferi*. *Mol Microbiol*. 2016;102(5):753-756.

Subramoni S, Sokol PA. Quorum sensing systems influence *Burkholderia cenocepacia* virulence. *Future Microbiol*. 2012;7(12):1373-1387.

Sulák O, Cioci G, Delia M, et al. A TNF-like trimeric lectin domain from *Burkholderia cenocepacia* with specificity for fucosylated human histo-blood group antigens. *Structure*. 2010;18(1):59-72.

Suwannasaen D, Mahawantung J, Chaowagul W, et al. Human immune responses to *Burkholderia pseudomallei* characterized by protein microarray analysis. *J Infect Dis*. 2011;203(7):1002-1011.

Sýkorová P, Novotná J, Demo G, et al. Characterization of novel lectins from *Burkholderia pseudomallei* and *Chromobacterium violaceum* with seven-bladed β-propeller fold. *Int J Biol Macromol*. 2020; 1;152:1113-1124.

Szczesny P, Lupas A. Domain annotation of trimeric autotransporter adhesins--daTAA. *Bioinformatics*. 2008;24(10):1251-1256.

Szymanski CM, Wren BW. Protein glycosylation in bacterial mucosal pathogens. *Nat Rev Microbiol*. 2005;3(3):225-237.

Taylor SL, McGuckin MA, Wesselingh S, Rogers GB. Infection's Sweet Tooth: How Glycans Mediate Infection and Disease Susceptibility. *Trends Microbiol*. 2018;26(2):92-101.

Taylor-Cousar JL, Zariwala MA, Burch LH, et al. Histo-blood group gene polymorphisms as potential genetic modifiers of infection and cystic fibrosis lung disease severity. *PLoS One*. 2009;4(1):e4270.

Terashima H, Kojima S, Homma M. Flagellar motility in bacteria structure and function of flagellar motor. *Int Rev Cell Mol Biol*. 2008;270:39-85.

Thanassi DG. The long and the short of bacterial adhesion regulation. *J Bacteriol*. 2011;193(2):327-328.

Thibau A, Dichter AA, Vaca DJ, Linke D, Goldman A, Kempf VAJ. Immunogenicity of trimeric autotransporter adhesins and their potential as vaccine targets. *Med Microbiol Immunol*. 2020;209(3):243-263.

Thomas R, Brooks T. Common oligosaccharide moieties inhibit the adherence of typical and atypical respiratory pathogens. *J Med Microbiol*. 2004;53(Pt 9):833-840.

Tomich M, Herfst CA, Golden JW, Mohr CD. Role of flagella in host cell invasion by B*urkholderia cepacia. Infect Immun*. 2002;70(4):1799-1806.

Tomich M, Mohr CD. Adherence and autoaggregation phenotypes of a *Burkholderia cenocepacia* cable pilus mutant. *FEMS Microbiol Lett*. 2003;228(2):287-297.

Torres A, Kasturiarachi N, DuPont M, Cooper VS, Bomberger J, Zemke A. NADH Dehydrogenases in *Pseudomonas aeruginosa* Growth and Virulence. *Front Microbiol*. 2019;10:75.

Trülzsch K, Oellerich MF, Heesemann J. Invasion and dissemination of *Yersinia enterocolitica* in the mouse infection model. *Adv Exp Med Biol*. 2007;603:279-285.

Urban TA, Goldberg JB, Forstner JF, Sajjan US. Cable pili and the 22-kilodalton adhesin are required for *Burkholderia cenocepacia* binding to and transmigration across the squamous epithelium. *Infect Immun*. 2005;73(9):5426-5437.

Urban TA, Griffith A, Torok AM, Smolkin ME, Burns JL, Goldberg JB. Contribution of *Burkholderia cenocepacia* flagella to infectivity and inflammation. *Infect Immun*. 2004;72(9):5126-5134.

Valvano MA, Keith KE, Cardona ST. Survival and persistence of opportunistic *Burkholderia* species in host cells. *Curr Opin Microbiol*. 2005;8(1):99-105.

Valvano MA. Intracellular survival of *Burkholderia cepacia* complex in phagocytic cells. *Can J Microbiol*. 2015;61(9):607-615.

Van Acker H, Sass A, Bazzini S, et al. Biofilm-grown *Burkholderia cepacia* complex cells survive antibiotic treatment by avoiding production of reactive oxygen species. *PLoS One.* 2013;8(3):e58943.

Van Damme P, Leroux-Roels G, Vandermeulen C, et al. Safety and immunogenicity of non-typeable *Haemophilus influenzae-Moraxella catarrhalis* vaccine. *Vaccine*. 2019;37(23):3113-3122.

Vandamme P, Holmes B, Vancanneyt M, et al. Occurrence of multiple genomovars of *Burkholderia cepacia* in cystic fibrosis patients and proposal of *Burkholderia multivorans* sp. nov. *Int J Syst Bacteriol*. 1997;47(4):1188-1200.

Vandenbussche I, Sass A, Pinto-Carbó M, Mannweiler O, Eberl L, Coenye T. DNA Methylation Epigenetically Regulates Gene Expression in *Burkholderia cenocepacia* and Controls Biofilm Formation, Cell Aggregation, and Motility. *mSphere*. 2020;5(4):e00455-20.

Vandivier RW, Richens TR, Horstmann SA, et al. Dysfunctional cystic fibrosis transmembrane conductance regulator inhibits phagocytosis of apoptotic cells with proinflammatory consequences. *Am J Physiol Lung Cell Mol Physiol*. 2009;297(4):L677-L686.

Venkatakrishnan V, Packer N, Thaysen-Andersen M. Host mucin glycosylation plays a role in bacterial adhesion in lungs of individuals with cystic fibrosis. *Expert Rev. Respir. Med*., 2014;7(5), 553–576.

Vergunst AC, Meijer AH, Renshaw SA, O'Callaghan D. *Burkholderia cenocepacia* creates an intramacrophage replication niche in zebrafish embryos, followed by bacterial dissemination and establishment of systemic infection*. Infect Immun.* 2010;78(4):1495e508.

Verstraeten N, Braeken K, Debkumari B, et al. Living on a surface: swarming and biofilm formation. *Trends Microbiol*. 2008;16(10):496-506.

Vesterlund S, Karp M, Salminen S, Ouwehand AC. *Staphylococcus aureus* adheres to human intestinal mucus but can be displaced by certain lactic acid bacteria. *Microbiology.* 2006;152(Pt 6):1819-1826.

Vik A, Aas FE, Anonsen JH, et al. Broad spectrum O-linked protein glycosylation in the human pathogen *Neisseria gonorrhoeae*. *Proc Natl Acad Sci USA*. 2009;106(11):4447-4452.

Walpole GFW, Plumb JD, Chung D, et al. Inactivation of Rho GTPases by *Burkholderia cenocepacia* Induces a WASH-Mediated Actin Polymerization that Delays Phagosome Maturation. *Cell Rep*. 2020;31(9):107721.

Watson ME, Nelson KL, Nguyen V, et al. Adhesin genes and serum resistance in *Haemophilus influenzae* type f isolates. *J Med Microbiol*. 2013;62(Pt 4):514-524.

Wellens A, Garofalo C, Nguyen H, et al. Intervening with urinary tract infections using anti-adhesives based on the crystal structure of the FimH-oligomannose-3 complex. *PLoS One*. 2008;3(4):e2040.

Welp AL, Bomberger JM. Bacterial Community Interactions During Chronic Respiratory Disease. *Front Cell Infect Microbiol*. 2020;10:213.

West AH, Stock AM. Histidine kinases and response regulator proteins in two component signaling systems. *Trends Biochem Sci.* 2001;26:369e76.

Weynants VE, Feron CM, Goraj KK, et al. Additive and synergistic bactericidal activity of antibodies directed against minor outer membrane proteins of *Neisseria meningitidis*. *Infect Immun*. 2007;75(11):5434-5442.

Wheeler KM, Cárcamo-Oyarce G, Turner BS, et al. Mucin glycans attenuate the virulence of *Pseudomonas aeruginosa* in infection. *Nat Microbiol*. 2019;4(12):2146-2154.

Wiersinga WJ, Currie BJ, Peacock SJ. Melioidosis. *N Engl J Med*. 2012;367(11):1035-1044.

Wiersinga WJ, van der Poll T, White NJ, Day NP, Peacock SJ. Melioidosis: insights into the pathogenicity of *Burkholderia pseudomallei*. *Nat Rev Microbiol*. 2006;4(4):272-282.

Williams HD, Zlosnik JE, Ryall B. Oxygen, cyanide and energy generation in the cystic fibrosis pathogen *Pseudomonas aeruginosa*. *Adv Microb Physiol*. 2007;52:1-71.

Winsor GL, Khaira B, Van Rossum T, Lo R, Whiteside MD, Brinkman FS. The *Burkholderia* Genome Database: facilitating flexible queries and comparative analyses. *Bioinformatics*. 2008;24(23):2803-2804.

Wizemann TM, Adamou JE, Langermann S. Adhesins as targets for vaccine development. *Emerg Infect Dis*. 1999;5(3):395-403.

Wolfe AJ, Visick KL. Get the message out: cyclic-Di-GMP regulates multiple levels of flagellum-based motility. *J Bacteriol*. 2008;190(2):463-475.

Xia B, Royall JA, Damera G, Sachdev GP, Cummings RD. Altered O-glycosylation and sulfation of airway mucins associated with cystic fibrosis. *Glycobiology*. 2005;15(8):747-775.

Yabuuchi E, Kosako Y, Oyaizu H, et al. Proposal of *Burkholderia* gen. nov. and transfer of seven species of the genus *Pseudomonas* homology group II to the new genus, with the type species *Burkholderia cepacia* (Palleroni and Holmes 1981) comb. nov. *Microbiol Immunol.* 1992;36(12):1251-1275.

Yang C, Cui C, Ye Q, et al. Burkholderia cenocepacia integrates cis-2-dodecenoic acid and cyclic dimeric guanosine monophosphate signals to control virulence. Proc Natl Acad Sci USA. 2017;114(49):13006-13011.

Yang ST, Kreutzberger AJB, Kiessling V, Ganser-Pornillos BK, White JM, Tamm LK. HIV virions sense plasma membrane heterogeneity for cell entry. *Sci Adv*. 2017;3(6):e1700338.

Yeo HJ, Cotter SE, Laarmann S, Juehne T, St Geme JW 3rd, Waksman G. Structural basis for host recognition by the *Haemophilus influenzae* Hia autotransporter. *EMBO J*. 2004;23(6):1245-1256.

Yet MG, Chin CC, Wold F. The covalent structure of individual N-linked glycopeptides from ovomucoid and asialofetuin. *J Biol Chem*. 1988;263(1):111-117.

Yip CH, Ghazali AK, Nathan S. *Burkholderia pseudomallei* pathogenesis and survival in different niches. *Biochem Soc Trans*. 2020;48(2):569-579.

Yoder-Himes DR, Konstantinidis KT, Tiedje JM. Identification of potential therapeutic targets for *Burkholderia cenocepacia* by comparative transcriptomics. *PLoS One*. 2010;5(1):e8724.

Zemljič Jokhadar Š, Klančnik U, Grundner M, et al. GPMVs in variable physiological conditions: could they be used for therapy delivery?. *BMC Biophys*. 2018;11:1.

Zhang P, Chomel BB, Schau MK, et al. A family of variably expressed outer-membrane proteins (Vomp) mediates adhesion and autoaggregation in *Bartonella quintana*. *Proc Natl Acad Sci USA*. 2004;101(37):13630-13635.

Zhou J, Chen Y, Tabibi S, Alba L, Garber E, Saiman L. Antimicrobial susceptibility and synergy studies of *Burkholderia cepacia* complex isolated from patients with cystic fibrosis. *Antimicrob Agents Chemother*. 2007;51(3):1085-1088.

Zhou M, Wu H. Glycosylation and biogenesis of a family of serine-rich bacterial adhesins. *Microbiology (Reading)*. 2009;155(Pt 2):317-327.

IX. APPENDIX – SUPPLEMENTARY DATA

Table IV.S1. List of Neoglycoconjugates (NGC) used in the construction of microarrays.

Abbreviation	Neoglycoconjugate	[c] in PBS	Source	Structure
Fetuin	Fetuin	1 mg/mL	Sigma	
ASF	Asialofetuin	1 mg/mL	Sigma	
Inv	Invertase	1 mg/mL	Sigma	
Ov	Ovalbumin	1 mg/mL	Sigma	
RB	RNAse B	1 mg/mL	Sigma	
Xferrin	Transferrin	1 mg/mL	Sigma	
AGP	alpha-1-acid glycoprotein	1 mg/mL	Sigma	
α-C	α-Crystallin from bovine lens	1 mg/mL	Sigma	
M3BSA	Mana1,3(Mana1,6)Man-BSA	1 mg/mL	Dextra	Manα1,3-(Manα1,6)-Man-BSA
GlcNAcBSA	GlcNAc-BSA	1 mg/mL	Dextra	GlcNAc-Sp14-NH2(Lys)-BSA
LacNAcBSA	LacNAc-BSA	1 mg/mL	Dextra	Gal-β(1-4)-GlcNAc-Sp3-BSA
3SLNBSA	3'SialylLacNAc-BSA	1 mg/mL	Dextra	
3SLacHSA	3´-Sialyllactose-APD-HSA	1 mg/mL	IsoSep	Neu5Ac-α(2-3)-Gal-β(1-4)-Glc-APD-HSA
6SLacHSA	6´-Sialyllactose-APD-HSA	1 mg/mL	IsoSep	Neu5Ac-α(2-6)-Galβ-(1-4)-Glc-APD-HSA
2FLBSA	2'Fucosyllactose-BSA	1 mg/mL	Dextra	Fuc-α(1-2)-Gal-β-(1-4)-Glc-Sp3-BSA
3SFLBSA	3'Sialyl-3-fucosyllactose-BSA	1 mg/mL	Dextra	Neu5Ac-α(2-3)-Gal-β(1-4)[Fuc-α(1-3)]-Glc-Sp3-BSA
H2BSA	H Type II-APE-BSA	1 mg/mL	IsoSep	Fuc-α(1-2)-Gal-β(1-4)-GlcNAc-β1-APE-BSA

Table IV.S1 (continuation)

Abbreviation	Neoglycoconjugate	[c] in PBS	Source	Structure
BGABSA	Blood Group A-BSA	1 mg/mL	Dextra	GalNAc-α(1-3)-[Fuc-α(1-2)]-Gal-BSA
BGBHSA	Blood Group B-HSA	1 mg/mL	Dextra	Gal-α(1-3)-[Fuc-α(1-2)]-Gal-HSA
GGGNHSA	Galα1,3Galβ1,4GlcNAc-HSA	1 mg/mL	Dextra	Gal-α(1-3)-Gal-β(1-4)-GlcNAc-HSA
Ga3GBSA	Galα1,3Gal-BSA	1 mg/mL	Dextra	Gal-α(1-3)-Gal-Sp3-BSA
Gb4GBSA	Galβ1,4GalBSA	1 mg/mL	Dextra	Gal-β(1-4)-Gal-Sp3-BSA
Ga2GBSA	Galα1,2GalBSA	1 mg/mL	Dextra	Gal-α(1-2)-Gal-Sp3-BSA
Ovomuc	Ovomucoid	0.5 mg/mL	Sigma	
LNFPIBSA	Lacto-*N*-fucopentaose I-BSA	1 mg/mL	Dextra	Fuc-α(1,2)-Gal-β(1,3)-GlcNAc-β(1,3)-Gal-β(1,4)-Glc-BSA
LNFPIIBSA	Lacto-*N*-fucopentaose II-BSA	1 mg/mL	Dextra	Fuc-α(1,3)-Gal-β(1,3)-GlcNAc-β(1,3)-Gal-β(1,4)-Glc-BSA
LNFPIIIBSA	Lacto-*N*-fucopentaose III-BSA	1 mg/mL	Dextra	Gal-β1-[Fuc-α(1,3)]-4-GlcNAc-β(1,3)-D-Gal-β(1,4)-Glc-BSA
LNDHIBSA	Lacto-*N*-difucohexaose I-BSA	1 mg/mL	Dextra	Fuc-α(1-2)-Gal-β1-[Fuc-α(1-4)]-3-GlcNAc-β(1-3)-Gal-β(1-4)-Glc-Sp3-BSA
LebBSA	LNDI-BSA/ Lewis b-BSA	1 mg/mL	IsoSep AB	Fuc-α(1-2)-Gal-β1-[Fuc-α(1-4)]-3-GlcNAc-β(1-3)-Gal-β(1-4)-Glc-APD-BSA
LexBSA	Lewis x-BSA	1 mg/mL	Dextra	Gal-β1-[Fuc-α(1-3)]-4-GlcNAc-BSA
DiLexHSA	Di-Lewisx-APE-HSA	1 mg/mL	IsoSep	Gal-β1-[Fuc-α(1-3)]-4-GlcNAcβ-(1-3)-Gal-β1-[Fuc-α(1-3)]-4-GlcNAc-β1-O-APE-HSA
BT	Bovine thyroglobulin	1 mg/mL	Sigma	
3LexHSA	Tri-Lex-APE-HSA	1 mg/mL	IsoSep	Gal-β1-[Fuc-α(1-3)]-4-GlcNAc-β(1-3)Gal-β1-[Fuc-α(1-3)]-4-GlcNAc-β(1-3)-Gal-β1-[Fuc-α(1-3)]-4-GlcNAc-β1-O-APE-HSA
3SLexBSA3	3'Sialyl Lewis x-BSA	1 mg/mL	Dextra	Neu5Ac-α(2-3)-Gal-β1-[Fuc-α(1-3)]-4-GlcNAc-Sp3-BSA

Table IV.S1 (continuation)

Abbreviation	Neoglycoconjugate	[c] in PBS	Source	Structure
A1AT	alpha-1-antitrypsin	1 mg/mL	Sigma	
6SuLexBSA	6-Sulfo Lewis x-BSA	1 mg/mL	Dextra	(SO_4)6Gal-β1-[Fuc-α(1-3)]-4-GlcNAc-Sp3-BSA
6SuLeaBSA	6-Sulfo Lewis a-BSA	1 mg/mL	Dextra	(SO_4)6Gal-β1-[Fuc-α(1-4)]-3-GlcNAc-SP3-BSA
3SuLeaBSA	3-Sulfo Lewis a-BSA	1 mg/mL	Dextra	(SO_4)3Gal-β1-[Fuc-α(1-4)]-3-GlcNAc-BSA
3SuLexBSA	3-Sulfo Lewis x-BSA	1 mg/mL	Dextra	(SO_4)3Gal-β1-[Fuc-α(1-3)]-4-GlcNAc-BSA
DFPLNHHSA	Difucosyl-para-lacto-N-hexaose-APD-HSA (Lea/Lex)	1 mg/mL	IsoSep	Gal-β1-[Fuc-α(1-4)]-3-GlcNAc-β(1-3)-Gal-β(1-4)-[Fuc-α(1-3)]-GlcNAc-β(1-3)-Gal-β(1-4)-(Glc)-APD-HSA
LeaBSA	Lewis a-BSA	1 mg/mL	Dextra	Gal-β1-[Fuc-α(1-4)]-3-GlcNAc-Sp3-BSA
LeyHSA	Lewis y-tetrasaccharide-APE-HSA	1 mg/mL	IsoSep	Fuc-α(1-2)-Gal-β1-[Fuc-α(1-3)]-4-GlcNAc-β1-O-APE-HSA
3FLeyHSA	Tri-fucosyl-Ley-heptasaccharide-APE-HSA	1 mg/mL	IsoSep	Fuc-α(1-2)-Gal-β1-[Fuc-α(1-3)]-4-GlcNAc-β(1-3)-Gal-β(1-4)-[Fuc-α(1-3)]-GlcNAc-β1-O-APE-HSA
LNnTHSA	Lacto-N-neotetraose-APD-HSA	1 mg/mL	IsoSep	Gal-β(1-4)-GlcNAc-β(1-3)Gal-β(1-4)-(Glc)-APD-HSA
LNTHSA	Lacto-N-tetraose-APD-HSA	1 mg/mL	IsoSep	Gal-β(1-3)-GlcNAc-β(1-3)-Gal-β(1-4)-(Glc)-APD-HSA
SLNFVHSA	Sialyl-LNF V-APD-HSA	1 mg/mL	IsoSep	Fuc-α(1-2)-Gal-β1-[NeuAc-α(2-6)]-3-GlcNAc-β(1-3)-Gal-β(1-4)-(Glc)-APD-HSA
MMLNnHHSA	Monofucosyl, monosialyllacto-N-neohexaose-APD-HSA	1 mg/mL	IsoSep	Neu5Ac-α(2-3)-Gal-β(1-4)-GlcNAc-β(1-3)-[Gal-β(1-4)-Fuc-α(1-3)-GlcNAc-β(1-6)]-Gal-β(1-4)-(Glc)-APD-HSA
SLNnTHSA	Sialyl-LNnT-penta-APD-HSA	1 mg/mL	IsoSep	Neu5Ac-α(2-3)-Gal-β(1-4)-GlcNAc-β(1-3)-Gal-β(1-4)-(Glc)-APD-HSA
GM1HSA	GM1-pentasaccharide-APD-HSA	1 mg/mL	IsoSep	Gal-β(1-3)-GalNAc-β1-[Neu5Ac-α(2-3)]-4-Gal-β(1-4)-(Glc)-APD-HSA
aGM1HSA	Asialo-GM1-tetrasaccharide-APD-HSA	1 mg/mL	IsoSep	Gal-β(1-3)-GalNAc-β(1-4)-Gal-β(1-4)-(Glc)-APD-HSA

Table IV.S1 (continuation)

Abbreviation	Neoglycoconjugate	[c] in PBS	Source	Structure
GlobNTHSA	Globo-N-tetraose-APD-HSA	1 mg/mL	IsoSep	GalNAc-β(1-3)-Gal-α(1-4)-Gal-β(1-4)-(Glc)-APD-HSA
GlobTHSA	Globotriose-APD-HSA	1 mg/mL	IsoSep	Gal-α(1-4)-Gal-β(1-4)-Glc-β1-APE-HSA

Table IV.S2. Anti-BCAM2418 antibody treatment altered *Burkholderia* binding to host glycans. Bacteria, pre-incubated or not with anti-BCAM2418 antibody (0.25 mg/mL) and anti-mouse IgG (0.25mg/mL), were incubated with 52 different glycans on a carbohydrate microarray. *B. cenocepacia* (Bceno) K56-2 and *B. cenocepacia* (Bceno) J2315 were tested. Results are presented as relative fluorescence units (RFU).

	Bceno K56-2			**Bceno J2315**		
NGC	*Untreated*	*Anti-BCAM2418*	*Anti-mouse IgG*	*Untreated*	*Anti-BCAM2418*	*Anti-mouse IgG*
Fetuin	1045.62	483.96	203.25	904.52	800.08	253.25a
ASF	1273.92	470.45[a]	345.00	1288.81	761.00[b]	369.50
Inv	0	132.69	0	35.45	152.01	87.63
Ov	**635.69**	**120.66**	**1358.50[b]**	255.44	154.50	339.00
RB	97.42	1219.63[c]	168.63[a]	183.18	1258.74[d]	50.63d
Xferrin	**1711.50**	**221.09[d]**	**800.13**	890.92	388.74[b]	359.63
AGP	**599.70**	**295.91**	**355.13**	305.81	296.29	254.63
α-C	**4034.35**	**2293.61[d]**	**3417.25[a]**	4346.95	2875.77[d]	2149.75[b]
M3BSA	1158.38	4047.48[d]	533.50[d]	765.56	3974.01[d]	305.00[d]
GlcNAcBSA	1465.60	569.48[b]	499.75	1218.56	726.92[b]	356.75
LacNAcBSA	350.21	0[a]	210.13	153.95	0[b]	161.63[a]
3SLNBSA	927.73	168.50[a]	147.13	363.71	157.86	148.62
3SLacHSA	**1168.05**	**0[d]**	**767.63**	**1159.06**	**135.43[d]**	**668.12[a]**
6SLacHSA	1271.73	0d	604.62[d]	1200.27	0[d]	492.62[d]
2FLBSA	**1159.37**	**0[d]**	**574.25**	**666.16**	**119.64[b]**	**425.75**
3SFLBSA	**1366.88**	**289.26[c]**	**441.62**	847.50	567.75	381.13
H2BSA	**1092.61**	**577.64**	**1018.50**	1723.51	646.04[d]	587.00
BGABSA	**1861.91**	**329.35[d]**	**1081.38**	**1758.45**	**395.52[d]**	**595.38**
BGBHSA	1266.09	0[d]	660.50[c]	841.68	0[d]	404.50[d]
GGGNHSA	**1084.03**	**181.83[b]**	**481.38**	**636.86**	**340.37**	**441.88**
Ga3GBSA	**1453.17**	**67.86[d]**	**582.68**	**801.81**	**143.87[c]**	**335.13**
Gb4GBSA	**1223.16**	**0[d]**	**572.75**	**596.20**	**0[d]**	**398.25[a]**
Ga2GBSA	**1425.73**	**282.76[c]**	**755.38**	**704.22**	**308.83[a]**	**364.38**

Table IV.S2 (continuation)

	Bceno K56-2			Bceno J2315		
NGC	*Untreated*	*Anti-BCAM2418*	*Anti-mouse IgG*	*Untreated*	*Anti-BCAM2418*	*Anti-mouse IgG*
Ovomuc	553.23	156.49	0	331.52	190.39	125.38
LNFPIBSA	**1145.15**	**116.69^{c}**	**421.89**	**543.19**	**96.99^{a}**	**356.88**
LNFPIIBSA	**888.20**	**0^{b}**	**202.00**	**242.09**	**0**	**87.00**
LNFPIIIBSA	**378.05**	**0**	**273.25**	**282.17**	**0**	**197.25**
LNDHIBSA	**833.84**	**47.36^{a}**	**686.25**	**772.49**	**155.01^{c}**	**431.75**
LebBSA	**1320.83**	**579.48^{a}**	**1034.50**	1624.56	708.09^{d}	583.00
LexBSA	**461.46**	**33.36**	**569.50**	**478.17**	**100.59^{a}**	**370.50**
DiLexHSA	**886.40**	**98.88^{a}**	**870.13**	**671.84**	**195.54^{b}**	**424.63**
BT	1067.47	684.46	0	876.30	946.10	175.63^{b}
3LexHSA	**1020.27**	**34.51^{b}**	**634.00**	**424.14**	**36.08^{a}**	**290.50**
3SLexBSA3	**1178.21**	**136.40^{c}**	**696.13**	**451.97**	**199.83**	**498.63**
A1AT	**1251.44**	**0^{d}**	**738.13**	**486.52**	**0^{b}**	**413.13**
6SuLexBSA	**1412.63**	**108.24^{d}**	**864.50**	**664.15**	**120.03^{b}**	**402.50**
6SuLeaBSA	968.10	0^{d}	3.25	382.33	0^{c}	0
3SuLeaBSA	**990.57**	**23.32^{b}**	**182.12**	**391.10**	**2.13^{a}**	**53.62**
3SuLexBSA	769.01	0^{d}	57.63	240.46	0^{d}	163.62^{c}
DFPLNHHSA	**679.51**	**137.39**	**673.12**	**781.08**	**315.09^{b}**	**396.12**
LeaBSA	**652.25**	**89.25**	**885.75**	**562.26**	**171.94^{a}**	**500.25**
LeyHSA	**683.68**	**24.85^{a}**	**674.50**	**616.89**	**0^{c}**	**388.00**
3FLeyHSA	**1157.25**	**260.82^{b}**	**792.25**	**792.21**	**364.70^{a}**	**401.25**
LNnTHSA	**1328.08**	**349.27^{b}**	**1005.75**	1556.41	556.16^{d}	560.25
LNTHSA	**1356.22**	**767.82**	**1609.50**	**1625.15**	**835.79^{d}**	**938.50**
SLNFVHSA	**1244.13**	**285.27^{b}**	**1102.13**	**972.25**	**215.69^{d}**	**603.13**
MMLNnHHSA	**1025.38**	**129.51^{b}**	**800.63**	**570.96**	**111.68^{a}**	**501.63**
SLNnTHSA	**905.33**	**113.57^{a}**	**596.25**	**441.40**	**87.69**	**364.25**
GM1HSA	**1382.81**	**549.29^{b}**	**1102.25**	**1274.15**	**348.99^{d}**	**682.25**

Table IV.S2 (continuation)

	Bceno K56-2			Bceno J2315		
NGC	*Untreated*	*Anti-BCAM2418*	*Anti-mouse IgG*	*Untreated*	*Anti-BCAM2418*	*Anti-mouse IgG*
aGM1HSA	**1191.27**	**157.68[c]**	**869.25**	**875.95**	**21.85[d]**	**564.75[a]**
GlobNTHSA	**945.83**	**164.62[a]**	**529.25**	**523.95**	**0[c]**	**436.25**
GlobTHSA	**968.47**	**285.46[a]**	**712.13**	**644.84**	**0[d]**	**507.63[a]**

Values represent the median of six replicate features per subarray. Data were normalized to the mean for three replicate microarray slides subarray by subarray using subarray total intensity mean. Significant results are represented by letters (a – $P<0.05$; b – $P<0.01$; c – $P<0.001$; d – $P<0.001$). Bold red values indicate relevant results and were considered when [untreated/anti-BCAM2418 treated bacteria] ratio was <0.6; and [anti-mouse IgG treated bacteria/anti-BCAM2418 treated bacteria] ratio was >1.1. While statistical analysis indicates the robustness of the obtained result, ratio calculation indicates the biological relevance of the anti-BCAM2418 binding inhibition. In cases of resulting negative RFU (fluorescence intensity) after subtraction of negative controls, the result was considered as 0.

Table IV.S3. Anti-BCAM2418 antibody treatment altered *Burkholderia* binding to host glycans. Bacteria, pre-incubated or not with anti-BCAM2418 antibody (0.25 mg/mL) and anti-mouse IgG (0.25mg/mL), were incubated with 52 different glycans on a carbohydrate microarray. *B. multivorans* (Bmulti) VC13401 and *B. comtaminans* (Bcont) IST408 were tested. Results are presented as relative fluorescence units (RFU).

	Bmulti VC13401			**Bcont IST408**		
NGC	*Untreated*	*Anti-BCAM2418*	*Anti-mouse IgG*	*Untreated*	*Anti-BCAM2418*	*Anti-mouse IgG*
Fetuin	786.72	3702.75[d]	5520.25[d]	381.53	693.51[b]	113.75c
ASF	1873.02	3235.53[d]	8352.00[d]	480.42	668.68	189.50b
Inv	8.03	53.30	0	0	115.93	82.63
Ov	146.27	191.08	172.00	179.16	159.87	80.00
RB	131.56	1127.68[b]	0[b]	49.88	1251.29[d]	93.63d
Xferrin	666.09	607.59	110.63	588.91	441.89	27.63b
AGP	230.48	414.50	443.63	159.24	361.09	65.13
α-C	4166.72	2731.94[d]	3469.25	2523.79	2810.91[a]	1525.75d
M3BSA	656.05	4196.98[d]	411.00[c]	512.72	4190.69[d]	217.50d
GlcNAcBSA	1151.35	614.68	526.75	717.12	728.53	249.75b
LacNAcBSA	213.73	0	359.63	171.44	0[d]	79.62b
3SLNBSA	383.85	301.83	538.12	281.29	289.72	120.12
3SLacHSA	**1268.34**	**31.26[d]**	**688.12**	**700.32**	**206.17[d]**	**570.12[a]**
6SLacHSA	990.57	0[d]	331.62[d]	585.59	0[d]	318.62[d]
2FLBSA	468.35	328.06	441.75	**422.25**	**137.68[a]**	**199.75**
3SFLBSA	575.07	617.08	431.12	466.07	330.92	203.62
H2BSA	1215.81	243.39[b]	102.50	928.34	476.23[d]	337.00
BGABSA	**1273.37**	**375.67[b]**	**562.88**	973.58	323.00[d]	274.88
BGBHSA	731.96	0[d]	311.50[b]	552.52	0[d]	150.50[d]
GGGNHSA	418.60	333.76	664.38	406.35	282.19	182.38
Ga3GBSA	412.17	253.26	376.63	**708.78**	**162.60[d]**	**182.63**

Table IV.S3 (continuation)

	Bmulti VC13401			Bcont IST408		
NGC	*Untreated*	*Anti-BCAM2418*	*Anti-mouse IgG*	*Untreated*	*Anti-BCAM2418*	*Anti-mouse IgG*
Gb4GBSA	**381.04**	**0**	**446.25**	**502.39**	**0[d]**	**216.25**
Ga2GBSA	569.49	415.87	714.38	605.05	471.22	218.38
Ovomuc	**317.04**	**57.22**	**79.88**	145.04	128.22	184.88
LNFPIBSA	458.01	381.61	629.38	419.01	277.08	218.38
LNFPIIBSA	**254.81**	**121.73**	**340.50**	**186.41**	**24.67**	**132.00**
LNFPIIIBSA	**169.00**	**82.40**	**222.75**	**139.81**	**0**	**58.25**
LNDHIBSA	628.36	429.81	327.25	516.99	225.71[b]	204.25
LebBSA	1260.34	519.21[a]	181.00	783.97	494.90[b]	336.00
LexBSA	299.16	185.19	351.00	265.69	101.27	97.00
DiLexHSA	431.48	225.77	126.63	**420.50**	**183.30[a]**	**233.13**
BT	752.84	620.81	331.12	513.69	751.35[a]	0[d]
3LexHSA	251.20	36.49	36.50	**295.12**	**72.31**	**116.00**
3SLexBSA3	307.07	413.34	500.12	362.92	214.86	146.62
A1AT	313.47	220.52	343.13	**415.53**	**37.61[c]**	**219.62**
6SuLexBSA	438.23	476.26	755.50	539.33	299.84[a]	176.00
6SuLeaBSA	**261.04**	**14.14**	**0**	**298.13**	**0[d]**	**0[d]**
3SuLeaBSA	286.04	332.44	283.12	282.57	77.08	0
3SuLexBSA	251.94	0	914.12[a]	216.28	0	62.63
DFPLNHHSA	604.68	261.73	169.63	**464.76**	**246.28**	**281.13**
LeaBSA	**385.20**	**145.96**	**560.75**	412.58	266.60	114.25
LeyHSA	**588.54**	**5.50**	**218.50**	**380.78**	**39.75[b]**	**169.50**
3FLeyHSA	**932.96**	**321.37**	**508.25**	477.08	295.35	338.25
LNnTHSA	**1114.96**	**162.88[b]**	**291.25**	626.11	319.44[b]	331.25
LNTHSA	1298.44	531.71[a]	476.00	849.30	689.77	636.00
SLNFVHSA	**913.56**	**311.95**	**423.63**	647.37	346.69[b]	338.63
MMLNnHHSA	**619.52**	**279.44**	**291.13**	**475.97**	**152.85[b]**	**299.13**

Table IV.S3 (continuation)

	Bmulti VC13401			Bcont IST408		
NGC	*Untreated*	*Anti-BCAM2418*	*Anti-mouse IgG*	*Untreated*	*Anti-BCAM2418*	*Anti-mouse IgG*
SLNnTHSA	**439.02**	**140.29**	**247.75**	**345.26**	**91.95[a]**	**359.75**
GM1HSA	1021.08	395.26	358.25	730.45	536.34	437.25
aGM1HSA	**761.55**	**53.30[a]**	**213.25**	**635.84**	**175.05[d]**	**393.25**
GlobNTHSA	**571.28**	**138.92**	**200.75**	**378.76**	**148.50**	**375.75**
GlobTHSA	**784.29**	**271.99**	**388.13**	**483.77**	**278.26**	**500.62**

Values represent the median of six replicate features per subarray. Data were normalized to the mean for three replicate microarray slides subarray by subarray using subarray total intensity mean. Significant results are represented by letters (a – P<0.05; b – P<0.01; c – P<0.001; d – P<0.001). Bold red values indicate relevant results and were considered when [untreated/anti-BCAM2418 treated bacteria] ratio was <0.6; and [anti-mouse IgG treated bacteria/anti-BCAM2418 treated bacteria] ratio was >1.1. While statistical analysis indicates the robustness of the obtained result, ratio calculation indicates the biological relevance of the anti-BCAM2418 binding inhibition. In cases of resulting negative RFU (fluorescence intensity) after subtraction of negative controls, the result was considered as 0.

Table IV.S4. Anti-BCAM2418 antibody treatment altered *Burkholderia* binding to host glycans. Bacteria, pre-incubated or not with anti-BCAM2418 antibody (0.25 mg/mL) and anti-mouse IgG (0.25mg/mL), were incubated with 52 different glycans on a carbohydrate microarray. *E. coli* BL21-DE3 (EcoliBL21-DE3) was tested. Results are presented as relative fluorescence units (RFU).

	Ecoli BL21-DE3		
NGC	*Untreated*	*Anti-BCAM2418*	*Anti-mouse IgG*
Fetuin	327.93	1268.50[c]	140.75b
ASF	451.57	1222.59[b]	278.00a
Inv	138.64	130.38	156.12
Ov	241.73	470.94	173.00
RB	346.89	1365.83[c]	430.12a
Xferrin	1213.49	1111.85	122.12a
AGP	501.34	509.09	166.12
α-C	6467.36	5301.74[d]	2470.75d
M3BSA	1934.71	4830.92[d]	297.00d
GlcNAcBSA	2251.31	1553.85[a]	288.75b
LacNAcBSA	**749.92**	**0[b]**	**138.63**
3SLNBSA	1448.65	724.10[a]	328.63
3SLacHSA	3426.46	1465.33[d]	733.13
6SLacHSA	937.09	0[d]	449.13
2FLBSA	644.30	758.19[d]	231.25d
3SFLBSA	474.48	1058.54	276.63
H2BSA	1948.43	1570.25	499.50a
BGABSA	1201.46	1731.38	248.88d
BGBHSA	**725.40**	**0[b]**	**191.50**
GGGNHSA	610.80	773.74	206.38
Ga3GBSA	912.58	897.75	434.13
Gb4GBSA	939.80	491.35	235.75
Ga2GBSA	1101.75	1163.07	339.88
Ovomuc	566.73	207.52	268.38
LNFPIBSA	1233.09	875.49	350.38
LNFPIIBSA	691.44	467.75	602.00
LNFPIIIBSA	195.07	199.59	127.75
LNDHIBSA	616.30	773.79	349.25
LebBSA	1341.91	1478.13	558.00a
LexBSA	559.37	493.18	138.50
DiLexHSA	720.43	686.11	355.12
BT	880.32	1206.81	88.12b
3LexHSA	524.89	457.61	424.00
3SLexBSA3	447.04	571.93	290.12
A1AT	561.10	370.27	357.62
6SuLexBSA	738.40	872.67	265.50
6SuLeaBSA	437.99	159.92	0
3SuLeaBSA	398.70	403.93	189.13
3SuLexBSA	**404.12**	**0**	**1878.13d**
DFPLNHHSA	815.11	703.22	389.13

Table IV.S4 (continuation)

	Ecoli BL21-DE3		
NGC	*Untreated*	*Anti-BCAM2418*	*Anti-mouse IgG*
LeaBSA	406.16	690.52	250.75
LeyHSA	603.80	625.69	317.00
3FLeyHSA	682.980	976.73	242.75
LNnTHSA	1297.25	1200.58	529.25
LNTHSA	2428.82	1422.87[c]	1211.00
SLNFVHSA	1134.35	1056.33	529.63
MMLNnHHSA	803.34	776.94	448.13
SLNnTHSA	642.43	577.01	442.75
GM1HSA	2197.65	1354.03[b]	808.25
aGM1HSA	1118.83	983.68	530.75
GlobNTHSA	974.82	789.58	609.25
GlobTHSA	2015.91	1077.44[c]	697.13

Values represent the median of six replicate features per subarray. Data were normalized to the mean for three replicate microarray slides subarray by subarray using subarray total intensity mean. Significant results are represented by letters (a – $P<0.05$; b – $P<0.01$; c – $P<0.001$; d – $P<0.001$). Bold red values indicate relevant results and were considered when [untreated/anti-BCAM2418 treated bacteria] ratio was <0.6; and [anti-mouse IgG treated bacteria/anti-BCAM2418 treated bacteria] ratio was >1.1. While statistical analysis indicates the robustness of the obtained result, ratio calculation indicates the biological relevance of the anti-BCAM2418 binding inhibition. In cases of resulting negative RFU (fluorescence intensity) after subtraction of negative controls, the result was considered as 0.

Table V.S1. **List of genes up-regulated upon *B. cenocepacia* K56-2 adhesion (37 ˚C, 30min) to 16HBE14o- derived GPMVs.** Genes were associated in Gene Ontology of KEGG pathway database obtained in ShinyGO v0.61 software. Enrichment analysis based on hypergeometric distribution followed by FDR correction (Ge, et al. 2019).

GENE	ANNOTATION OR PREDICTED FUNTION	FOLD CHANGE
ABC TRANSPORTERS		
P-value 1.644e-64	Count 81/264	30.7%
BCAL0015	Putative branched-chain amino acid ABC transporter ATP-binding protein	9.245
BCAL0016	Putative branched-chain amino acid ABC transporter ATP-binding protein	9.245
BCAL0017	Putative branched-chain amino acid ABC transporter periplasmic protein	26.628
BCAL0018	Putative branched-chain amino acid ABC transporter permease	23.277
BCAL0019	Putative branched-chain amino acid ABC transporter permease	23.277
BCAL0151	Extracellular ligand binding protein	27.890
BCAL0334	Periplasmic solute-binding protein	5.586
BCAL0544	Putative periplasmic dipeptide transport protein	2.910
BCAL0598	Putrescine ABC transporter binding exported protein	11.197
BCAL0645	Sulfate-binding protein	8.995
BCAL0675	Extracellular solute-binding protein	1.909
BCAL1045	Periplasmic ligand binding lipoprotein	6.538
BCAL1270	*pstS* - Phosphate transport system substrate-binding exported periplasmic protein	2.983
BCAL1431	Putative ribose ABC transporter substrate-binding exported protein	34.592
BCAL1432	Putative sugar ABC transporter ATP-binding protein	17.196
BCAL1433	Putative sugar transport system permease	43.608
BCAL1620	*ssuC* - Aliphatic sulfonates transport permease	116.169
BCAL1621	*ssuB* - Aliphatic sulfonates ABC transporter ATP-binding protein	116.169
BCAL1652	Sulfate-binding protein	71.467
BCAL1653	*cysT* - Sulfate transport system permease	19.512
BCAL1654	*cysW* - Sulfate transport system permease	19.512

Table V.S1 (continuation)

GENE	ANNOTATION OR PREDICTED FUNTION	FOLD CHANGE
ABC TRANSPORTERS		
P-value 1.644e-64	Count 81/264	30.7%
BCAL1655	*cysA* - Sulfate ABC transporter ATP-binding protein	8.557
BCAL1657	Putative ribose transport system	2.021
BCAL1691	*orbC* - Putative iron transport-related ATP-binding protein	8.639
BCAL1692	*orbD* - Iron-hydroxamate transporter permease subunit	8.639
BCAL2705	ABC transporter ATP-binding protein	4.189
BCAL2706	ABC transporter ATP-binding protein	4.189
BCAL2707	Putative transport system permease	5.043
BCAL2708	Putative amino-acid transport permease	13.070
BCAL2806	Putative ABC transporter permease	17.159
BCAL2807	Putative transmembrane ABC transporter protein	17.159
BCAL3038	ABC transporter ATP-binding protein	6.378
BCAL3039	ABC transporter permease	13.731
BCAL3040	ABC transporter permease	13.731
BCAL3041	*malE* - Maltose-binding protein	10.453
BCAL3098	Putative branched-chain amino acid transporter substrate-binding protein	293.494
BCAL3099	Putative branched-chain amino acid transporter permease	21.606
BCAL3102	ABC transporter ATP-binding protein	46.045
BCAL3356	*gltK* - Glutamate/aspartate transport system permease	2.691
BCAL3357	*gltJ* - Glutamate/aspartate transport system permease	2.691
BCAL3358	Periplasmic glutamate/aspartate-binding protein	2.998
BCAM0508	Putative periplasmic binding protein	8.604
BCAM0610	Putative ligand binding protein	49.703
BCAM0611	Putative branched-chain amino acid transporter	53.972
BCAM0613	ABC transporter ATP-binding protein	12.402
BCAM0760	Histidine transport system permease	7.509

Table V.S1 (continuation)

GENE	ANNOTATION OR PREDICTED FUNTION	FOLD CHANGE
ABC TRANSPORTERS		
P-value 1.644e-64	Count 81/264	30.7%
BCAM0761	Histidine transport system permease	7.509
BCAM0766	D-ribose-binding periplasmic protein precursor	3.226
BCAM0874	Periplasmic solute-binding protein	28.680
BCAM1118	Putative periplasmic solute-binding protein	41.252
BCAM1126	Nitrate ABC transporter substrate-binding protein	134.335
BCAM1377	ABC transporter ATP-binding protein	76.572
BCAM1378	ABC transporter permease	76.572
BCAM1379	ABC transporter substrate-binding protein	38.129
BCAM1743	Periplasmic solute-binding protein	8.064
BCAM2251	Putative amino acid ABC transporter solute binding protein	2.702
BCAM2312	Putative glycine betaine transporter substrate binding protein	6.268
BCAM2317	Glycine/betaine ABC transporter substrate-binding protein	11.661
BCAM2381	Putative ABC transport exported protein	2.198
BCAM2382	Putative ABC transporter system permease	2.198
BCAM2383	ABC transporter ATP-binding protein	2.198
BCAM2384	Putative ABC transporter system permease	2.198
BCAM2407	Putative glycine betaine/L-proline ABC transporter substrate-binding protein	11.112
BCAM2409	Putative glycine-betaine ABC transporter permease	20.419
BCAM2410	Putative glycine betaine/L-proline ABC transporter ATP-binding protein	20.419
BCAM2528	Putative ABC transporter permease	63.054
BCAM2529	ABC transporter ATP-binding protein (complex MetNIQ - methionine import)	63.054
BCAM2531	Putative ABC transporter solute-binding protein	223.872
BCAM2618	Putative periplasmic lysine-arginine-ornithine-binding protein	11.084

Table V.S1 (continuation)

GENE	ANNOTATION OR PREDICTED FUNTION	FOLD CHANGE
ABC TRANSPORTERS		
P-value 1.644e-64	**Count 81/264**	**30.7%**
BCAM2620	Putative lipoprotein	26.653
BCAM2728	*oppA* - Putative periplasmic oligopeptide-binding protein precursor	22.729
BCAS0110	Periplasmic solute-binding protein	14.969
BCAS0111	Putative binding-protein-dependent transport system protein	55.369
BCAS0112	Putative binding-protein-dependent transport system protein	22.214
BCAS0113	ABC transporter ATP-binding protein	26.650
BCAS0140	Putative branched-chain amino acid ABC transporter substrate-binding protein	8.003
BCAS0141	Putative transport system protein	5.443
BCAS0142	Putative amino-acid transport system protein	5.443
BCAS0143	ABC transporter ATP-binding protein	5.443
BCAS0144	ABC transporter ATP-binding protein	5.443
BCAS0240	Periplasmic solute-binding protein	4.315
METABOLIC PATHWAYS		
P-value 8.780e-16	**Count 70/922**	**7.6%**
BCAL0010	*phhA* - Phenylalanine 4-monooxygenase	20.439
BCAL0039	*pheC* - Periplasmic cyclohexadienyl dehydratase	3.444
BCAL0059	eutB - Ethanolamine ammonia-lyase heavy chain	5.045
BCAL0060	eutC - Ethanolamine ammonia-lyase small subunit	5.045
BCAL0290	*glt2* - Glutamate synthase subunit beta	7.476
BCAL0328	*petA* - Ubiquinol-cytochrome C reductase iron-sulfur subunit	2.350
BCAL0329	*petB* - Cytochrome B; Component of the ubiquinol-cytochrome C reductase complex	2.350
BCAL0600	Putative glutamine synthetase	8.838
BCAL0603	*puuC* - Gamma-glutamyl-gamma-aminobutyraldehyde dehydrogenase	3.457
BCAL0714	Threonine peptidase, family T3	5.003

Table V.S1 (continuation)

GENE	ANNOTATION OR PREDICTED FUNTION	FOLD CHANGE
METABOLIC PATHWAYS		
P-value 8.780e-16	Count 70/922	7.6%
BCAL0795	*coaD* - Phosphopantetheine adenylyltransferase	2.068
BCAL0885	Putative 3-hydroxyacyl-CoA dehydrogenase oxidoreductase	2.019
BCAL0886	Acetyl-CoA acetyltransferase	2.365
BCAL0925	*glpK* - Glycerol kinase	10.076
BCAL1183	Aldehyde dehydrogenase family protein	2.969
BCAL1427	Myo-inositol catabolism protein	11.695
BCAL1428	Putative amine catabolism-related protein	13.589
BCAL1429	Putative TPP-binding acetolactate synthase	30.290
BCAL1435	*idh* - Inositol 2-dehydrogenase	15.127
BCAL1541	Putative acyl-CoA synthetase	7.385
BCAL1862	*phbA* - Acetyl-CoA acetyltransferase	1.852
BCAL1979	Putative fatty acid degradation protein	2.770
BCAL2118	*aceA* - Isocitrate lyase	4.940
BCAL2121	Putative dehalogenase	35.004
BCAL2122	*aceB* - Malate synthase	7.437
BCAL2198	Cysteine desulfurase	12.614
BCAL2224	*glnA* - Glutamine synthetase	29.409
BCAL2284	*acoE* - Acetyl-CoA synthetase	2.617
BCAL2304	3-hydroxybutyrate dehydrogenase	4.560
BCAL2357	*ilvC* - Ketol-acid reductoisomerase	1.814
BCAL2358	*ilvH* - Acetolactate synthase 3 regulatory subunit	2.692
BCAL2683	*cysH* - Phosphoadenosine phosphosulfate reductase	6.753
BCAL2685	*cysI* - Putative sulfite reductase	17.298
BCAL2735	Isocitrate dehydrogenase	1.996
BCAL3043	*pgl* - 6-phosphogluconolactonase	3.027
BCAL3044	*glk* - Bifunctional glucokinase/RpiR family transcriptional regulator	3.027
BCAL3104	*ureA* - Urease subunit gamma	35.232
BCAL3106	*ureC* - Urease subunit alpha	40.304
BCAL3191	Putative glutaryl-CoA dehydrogenase	3.150
BCAL3282	Phospho-2-dehydro-3-deoxyheptonate aldolase	3.730
BCAL3325	*pntB* - NAD(P) transhydrogenase subunit beta	4.404

Table V.S1 (continuation)

GENE	ANNOTATION OR PREDICTED FUNTION	FOLD CHANGE
METABOLIC PATHWAYS		
P-value 8.780e-16	Count 70/922	7.6%
BCAL3326	*pntAB* - NAD(P) transhydrogenase subunit alpha	4.404
BCAL3366	*eda* - KHG/KDPG aldolase	3.340
BCAL3474	*fadD* - Long-chain-fatty-acid--CoA ligase	3.132
BCAM0018	N-acetyl-gamma-glutamyl-phosphate reductase	60.237
BCAM0187	2-isopropylmalate synthase	8.786
BCAM0540	Putative serine acetyltransferase	79.962
BCAM0543	Putative aminotransferase	48.664
BCAM0544	Putative acetylglutamate kinase	14.310
BCAM0721	O-acetylhomoserine (thiol)-lyase	10.513
BCAM0949	*lip* - exported lipase LipA	7.761
BCAM0983	*leuC1* - Isopropylmalate isomerase large subunit	2.395
BCAM0984	*leuD1* - Isopropylmalate isomerase small subunit	3.423
BCAM1309	*ggt2* - Gamma-glutamyltransferase precursor 2	6.604
BCAM1488	Putative proline racemase	17.521
BCAM1588	Isocitrate lyase	5.194
BCAM1822	Putative NAD-dependent glutamate dehydrogenase	2.501
BCAM1833	*acnB* - Bifunctional aconitate hydratase 2/2-methylisocitrate dehydratase	2.952
BCAM1955	*ggt1* - Gamma-glutamyltransferase precursor 1	3.460
BCAM2094	*puuA* - putative gamma-glutamylputrescine synthetase	12.352
BCAM2326	Serine hydroxymethyltransferase	23.996
BCAM2368	Putative quinoprotein ethanol dehydrogenase precursor	259.175
BCAM2372	*acsA* - Acetyl-CoA synthetase	19.709
BCAM2501	Shikimate 5-dehydrogenase	11.496
BCAM2502	*aroQ* - 3-dehydroquinate dehydratase	11.496
BCAM2561	Putative 4-aminobutyrate aminotransferase	2.388
BCAS0731	*dhT* - Phenylhydantoinase	24.674
BCAS0733	Dihydropyrimidine dehydrogenase	29.277
BCAS0734	Putative oxidoreductase	28.410
BCAS0751	Putative gamma-glutamyltransferase precursor	7.275

Table V.S1 (continuation)

GENE	ANNOTATION OR PREDICTED FUNTION	FOLD CHANGE
SULFUR METABOLISM		
P-value 4.363e-12	**Count 16/56**	**28.6%**
BCAL0645	Sulfate-binding protein	8.995
BCAL1619	*ssuD* - Alkanesulfonate monooxygenase	188.767
BCAL1620	*ssuC* - Aliphatic sulfonates transport permease	116.169
BCAL1621	*ssuB* - Aliphatic sulfonates ABC transporter ATP-binding protein	116.169
BCAL1652	Sulfate-binding protein	71.467
BCAL1653	*cysT* - Sulfate transport system permease	19.512
BCAL1654	*cysW* - Sulfate transport system permease	19.512
BCAL1655	*cysA* - Sulfate ABC transporter ATP-binding protein	8.557
BCAL2683	*cysH* - Phosphoadenosine phosphosulfate reductase	6.753
BCAL2685	*cysI* - Putative sulfite reductase	17.298
BCAM0540	Putative serine acetyltransferase	79.962
BCAM1118	Putative periplasmic solute-binding protein	41.252
BCAM1121	Putative taurine dioxygenase	20.202
BCAM1122	Putative taurine dioxygenase	21.175
BCAM1126	Nitrate ABC transporter substrate-binding protein	134.335
BCAS0426	Putative taurine dioxygenase	252.922
MICROBIAL METABOLISM IN DIVERSE ENVIRONMENTS		
P-value 9.188e-12	**Count 38/393**	**9.7%**
BCAL0064	acoD - Acetaldehyde dehydrogenase	16.817
BCAL0289	glt1 - Glutamate synthase large subunit	8.139
BCAL0290	*glt2* - Glutamate synthase subunit beta	7.476
BCAL0600	Putative glutamine synthetase	8.838
BCAL0885	Putative 3-hydroxyacyl-CoA dehydrogenase oxidoreductase	2.019
BCAL0886	Acetyl-CoA acetyltransferase	2.365
BCAL1183	Aldehyde dehydrogenase family protein	2.969
BCAL1427	Myo-inositol catabolism protein	11.695
BCAL1428	Putative amine catabolism-related protein	13.589
BCAL1429	Putative TPP-binding acetolactate synthase	30.290
BCAL1435	*idh* - Inositol 2-dehydrogenase	15.127

Table V.S1 (continuation)

GENE	ANNOTATION OR PREDICTED FUNTION	FOLD CHANGE
MICROBIAL METABOLISM IN DIVERSE ENVIRONMENTS		
P-value 9.188e-12	**Count 38/393**	**9.7%**
BCAL1861	*phaC* - Acetyacetyl-CoA reductase	2.482
BCAL1862	*phbA* - Acetyl-CoA acetyltransferase	1.852
BCAL1979	Putative fatty acid degradation protein	2.770
BCAL2118	*aceA* - Isocitrate lyase	4.940
BCAL2121	Putative dehalogenase	35.004
BCAL2122	*aceB* - Malate synthase	7.437
BCAL2224	*glnA* - Glutamine synthetase	29.409
BCAL2284	*acoE* - Acetyl-CoA synthetase	2.617
BCAL2683	*cysH* - Phosphoadenosine phosphosulfate reductase	6.753
BCAL2685	*cysI* - Putative sulfite reductase	17.298
BCAL2735	Isocitrate dehydrogenase	1.996
BCAL3043	*pgl* - 6-phosphogluconolactonase	3.027
BCAL3044	*glk* - Bifunctional glucokinase/RpiR family transcriptional regulator	3.027
BCAL3104	*ureA* - Urease subunit gamma	35.232
BCAL3106	*ureC* - Urease subunit alpha	40.304
BCAL3191	Putative glutaryl-CoA dehydrogenase	3.150
BCAL3366	*eda* - KHG/KDPG aldolase	3.340
BCAM0131	*hchA* - Chaperone protein HchA	4.096
BCAM0540	Putative serine acetyltransferase	79.962
BCAM1588	Isocitrate lyase	5.194
BCAM1685	*nirB* - Putative nitrite reductase	108.386
BCAM1833	*acnB* - Bifunctional aconitate hydratase 2/2-methylisocitrate dehydratase	2.952
BCAM2094	*puuA* - putative gamma-glutamylputrescine synthetase	12.352
BCAM2326	serine hydroxymethyltransferase	23.996
BCAM2368	Putative quinoprotein ethanol dehydrogenase precursor	259.175
BCAM2372	*acsA* - Acetyl-CoA synthetase	19.709
BCAS0734	Putative oxidoreductase	28.410
BIOSYNTHESIS OF AMINO ACIDS		
P-value 1.227e-09	**Count 21/149**	**14.1%**
BCAL0010	*phhA* - Phenylalanine 4-monooxygenase	20.439
BCAL0039	*pheC* - Periplasmic cyclohexadienyl dehydratase	3.444
BCAL0290	*glt2* - Glutamate synthase subunit beta	7.476
BCAL0600	Putative glutamine synthetase	8.838

Table V.S1 (continuation)

GENE	ANNOTATION OR PREDICTED FUNTION	FOLD CHANGE
BIOSYNTHESIS OF AMINO ACIDS		
P-value 1.227e-09	**Count 21/149**	**14.1%**
BCAL2224	*glnA* - Glutamine synthetase	29.409
BCAL2357	*ilvC* - Ketol-acid reductoisomerase	1.814
BCAL2358	*ilvH* - Acetolactate synthase 3 regulatory subunit	2.692
BCAL2735	Isocitrate dehydrogenase	1.996
BCAL3282	Phospho-2-dehydro-3-deoxyheptonate aldolase	3.730
BCAM0018	N-acetyl-gamma-glutamyl-phosphate reductase	60.237
BCAM0187	2-isopropylmalate synthase	8.786
BCAM0540	Putative serine acetyltransferase	79.962
BCAM0544	Putative acetylglutamate kinase	14.310
BCAM0983	*leuC1* - Isopropylmalate isomerase large subunit	2.395
BCAM0984	*leuD1* - Isopropylmalate isomerase small subunit	3.423
BCAM1833	*acnB* - Bifunctional aconitate hydratase 2/2-methylisocitrate dehydratase	2.952
BCAM2094	*puuA* - putative gamma-glutamylputrescine synthetase	12.352
BCAM2326	serine hydroxymethyltransferase	23.996
BCAM2501	Shikimate 5-dehydrogenase	11.496
BCAM2502	*aroQ* - 3-dehydroquinate dehydratase	11.496
BCAS0734	Putative oxidoreductase	28.410
TWO-COMPONENT SYSTEM		
P-value 5.501e-09	**Count 19/132**	**14.4%**
BCAL0328	*petA* - Ubiquinol-cytochrome C reductase iron-sulfur subunit	2.350
BCAL0329	*petB* - Cytochrome B; Component of the ubiquinol-cytochrome C reductase complex	2.350
BCAL0600	Putative glutamine synthetase	8.838
BCAL1270	*pstS* - Phosphate transport system substrate-binding exported periplasmic protein	2.983
BCAL1862	*phbA* - Acetyl-CoA acetyltransferase	1.852
BCAL2222	*glnG* - nitrogen regulation protein NR(I)	13.697
BCAL2223	*glnL* - Putative nitrogen regulation protein NR(II)	20.857
BCAL2224	*glnA* - Glutamine synthetase	29.409

Table V.S1 (continuation)

GENE	ANNOTATION OR PREDICTED FUNTION	FOLD CHANGE
TWO-COMPONENT SYSTEM		
P-value 5.501e-09	**Count 19/132**	**14.4%**
BCAL2379	*kdpE* - two-component regulatory system, response regulator protein	6.253
BCAL2380	*kdpD* - two-component regulatory system, sensor kinase protein	6.253
BCAL2381	*kdpC* - Potassium-transporting ATPase subunit C	20.226
BCAL2382	*kdpB* - Potassium-transporting ATPase subunit B	9.614
BCAL2383	*kdpA* - potassium-transporting ATPase subunit A	5.524
BCAL3356	*gltK* - Glutamate/aspartate transport system permease	2.691
BCAL3357	*gltJ* - Glutamate/aspartate transport system permease	2.691
BCAL3358	Periplasmic glutamate/aspartate-binding protein	2.998
BCAM1743	Periplasmic solute-binding protein	8.064
BCAM2094	*puuA* - putative gamma-glutamylputrescine synthetase	12.352
BCAS0240	Periplasmic solute-binding protein	4.315
TAURINE AND HYPOTAURINE METABOLISM		
P-value 5.508e-09	**Count 8/15**	**53.3%**
BCAL0714	Threonine peptidase, family T3	5.003
BCAM1121	Putative taurine dioxygenase	20.202
BCAM1122	Putative taurine dioxygenase	21.175
BCAM1309	*ggt2* - gamma-glutamyltransferase precursor 2	6.604
BCAM1822	Putative NAD-dependent glutamate dehydrogenase	2.501
BCAM1955	*ggt1* - gamma-glutamyltransferase precursor 1	3.460
BCAS0426	Putative taurine dioxygenase	252.922
BCAS0751	Putative gamma-glutamyltransferase precursor	7.275
NITROGEN METABOLISM		
P-value 1.986e-08	**Count 9/24**	**37.5%**
BCAL0289	glt1 - Glutamate synthase large subunit	8.139
BCAL0290	*glt2* - Glutamate synthase subunit beta	7.476
BCAL0600	Putative glutamine synthetase	8.838
BCAL2224	*glnA* - Glutamine synthetase	29.409
BCAM1685	*nirB* - Putative nitrite reductase	108.386
BCAM1686	Putative nitrate transporter	103.320

Table V.S1 (continuation)

GENE	ANNOTATION OR PREDICTED FUNTION	FOLD CHANGE
NITROGEN METABOLISM		
P-value 1.986e-08	**Count 9/24**	**37.5%**
BCAM1822	Putative NAD-dependent glutamate dehydrogenase	2.501
BCAM2094	*puuA* - putative gamma-glutamylputrescine synthetase	12.352
BCAS0734	Putative oxidoreductase	28.410
GLYOXYLATE AND DICARBOXYLATE METABOLISM		
P-value 5.478e-07	**Count 12/68**	**17.7%**
BCAL0289	*glt1* - Glutamate synthase large subunit	8.139
BCAL0600	Putative glutamine synthetase	8.838
BCAL1861	*phaC* - Acetyacetyl-CoA reductase	2.482
BCAL1862	*phbA* - Acetyl-CoA acetyltransferase	1.852
BCAL2118	*aceA* - Isocitrate lyase	4.940
BCAL2122	*aceB* - Malate synthase	7.437
BCAL2224	*glnA* - Glutamine synthetase	29.409
BCAL3366	*eda* - KHG/KDPG aldolase	3.340
BCAM1588	Isocitrate lyase	5.194
BCAM1833	*acnB* - Bifunctional aconitate hydratase 2/2-methylisocitrate dehydratase	2.952
BCAM2094	*puuA* - putative gamma-glutamylputrescine synthetase	12.352
BCAM2326	Serine hydroxymethyltransferase	23.996
ARGININE AND PROLINE METABOLISM		
P-value 9.514e-07	**Count 12/72**	**16.7%**
BCAL0599	Putative aminotransferase	8.504
BCAL0600	Putative glutamine synthetase	8.838
BCAL0603	*puuC* - Gamma-glutamyl-gamma-aminobutyraldehyde dehydrogenase	3.457
BCAL2224	*glnA* - Glutamine synthetase	29.409
BCAL3104	*ureA* - Urease subunit gamma	35.232
BCAL3106	*ureC* - Urease subunit alpha	40.304
BCAM0018	N-acetyl-gamma-glutamyl-phosphate reductase	60.237
BCAM0544	Putative acetylglutamate kinase	14.310
BCAM1488	Putative proline racemase	17.521
BCAM1822	Putative NAD-dependent glutamate dehydrogenase	2.501
BCAM2094	*puuA* - putative gamma-glutamylputrescine synthetase	12.352
BCAM2366	Putative proline iminopeptidase	25.964

Table V.S1 (continuation)

GENE	ANNOTATION OR PREDICTED FUNTION	FOLD CHANGE
2-OXOCARBOXYLIC ACID METABOLISM		
P-value 1.685e-06	**Count 9/39**	**23.1%**
BCAL2357	*ilvC* - Ketol-acid reductoisomerase	1.814
BCAL2358	*ilvH* - Acetolactate synthase 3 regulatory subunit	2.692
BCAL2735	Isocitrate dehydrogenase	1.996
BCAM0018	N-acetyl-gamma-glutamyl-phosphate reductase	60.237
BCAM0187	2-isopropylmalate synthase	8.786
BCAM0544	Putative acetylglutamate kinase	14.310
BCAM0983	*leuC1* - Isopropylmalate isomerase large subunit	2.395
BCAM0984	*leuD1* - isopropylmalate isomerase small subunit	3.423
BCAM1833	*acnB* - Bifunctional aconitate hydratase 2/2-methylisocitrate dehydratase	2.952
BUTANOATE METABOLISM		
P-value 5.674e-06	**Count 10/58**	**17.2%**
BCAL1183	Aldehyde dehydrogenase family protein	2.969
BCAL1472	*scoA* - Succinyl-CoA:3-ketoacid-coenzyme A transferase subunit A	6.643
BCAL1473	*scoB* - Succinyl-CoA:3-ketoacid-coenzyme A transferase subunit B	7.024
BCAL1861	*phaC* - Acetyacetyl-CoA reductase	2.482
BCAL1862	*phbA* - Acetyl-CoA acetyltransferase	1.852
BCAL1863	*phbC* - Poly-beta-hydroxybutyrate polymerase	3.192
BCAL2304	3-hydroxybutyrate dehydrogenase	4.560
BCAL2358	*ilvH* - Acetolactate synthase 3 regulatory subunit	2.692
BCAL2420	Putative depolymerase/histone-like protein	1.840
BCAM2561	Putative 4-aminobutyrate aminotransferase	2.388
CARBON METABOLISM		
P-value 5.674e-06	**Count 15/136**	**11.0%**
BCAL0885	Putative 3-hydroxyacyl-CoA dehydrogenase oxidoreductase	2.019
BCAL1862	*phbA* - Acetyl-CoA acetyltransferase	1.852
BCAL1979	Putative fatty acid degradation protein	2.770
BCAL2118	*aceA* - Isocitrate lyase	4.940
BCAL2122	*aceB* - Malate synthase	7.437

Table V.S1 (continuation)

GENE	ANNOTATION OR PREDICTED FUNTION	FOLD CHANGE
CARBON METABOLISM		
P-value 5.674e-06	**Count 15/136**	**11.0%**
BCAL2284	*acoE* - Acetyl-CoA synthetase	2.617
BCAL2735	Isocitrate dehydrogenase	1.996
BCAL3043	*pgl* - 6-phosphogluconolactonase	3.027
BCAL3044	*glk* - Bifunctional glucokinase/RpiR family transcriptional regulator	3.027
BCAL3366	*eda* - KHG/KDPG aldolase	3.340
BCAM0540	Putative serine acetyltransferase	79.962
BCAM1588	Isocitrate lyase	5.194
BCAM1833	*acnB* - Bifunctional aconitate hydratase 2/2-methylisocitrate dehydratase	2.952
BCAM2326	Serine hydroxymethyltransferase	23.996
BCAM2372	*acsA* - Acetyl-CoA synthetase	19.709
FATTY ACID DEGRADATION		
P-value 6.530e-06	**Count 8/35**	**22.9%**
BCAL0885	Putative 3-hydroxyacyl-CoA dehydrogenase oxidoreductase	2.019
BCAL0886	Acetyl-CoA acetyltransferase	2.365
BCAL1541	Putative acyl-CoA synthetase	7.385
BCAL1979	Putative fatty acid degradation protein	2.770
BCAL3029	Putative alkane monooxygenase	7.469
BCAL3191	Putative glutaryl-CoA dehydrogenase	3.150
BCAL3474	*fadD* - Long-chain-fatty-acid-CoA ligase	3.132
ALANINE, ASPARTATE AND GLUTAMATE METABOLISM		
P-value 9.575e-06	**Count 8/37**	**21.6%**
BCAL0290	*glt2* - Glutamate synthase subunit beta	7.476
BCAL0600	Putative glutamine synthetase	8.838
BCAL1183	Aldehyde dehydrogenase family protein	2.969
BCAL2224	*glnA* - Glutamine synthetase	29.409
BCAM1822	Putative NAD-dependent glutamate dehydrogenase	2.501
BCAM2094	*puuA* - putative gamma-glutamylputrescine synthetase	12.352
BCAM2561	Putative 4-aminobutyrate aminotransferase	2.388
BCAS0734	Putative oxidoreductase	28.410
BIOSYNTHESIS OF SECONDARY METABOLITES		
P-value 1.150e-05	**Count 25/359**	**7.0%**
BCAL0039	*pheC* - Periplasmic cyclohexadienyl dehydratase	3.444

Table V.S1 (continuation)

GENE	ANNOTATION OR PREDICTED FUNTION	FOLD CHANGE
BIOSYNTHESIS OF SECONDARY METABOLITES		
P-value 1.150e-05	**Count 25/359**	**7.0%**
BCAL0290	*glt2* - Glutamate synthase subunit beta	7.476
BCAL0884	Putative acyl-CoA dehydrogenase oxidoreductase protein	1.704
BCAL0886	Acetyl-CoA acetyltransferase	2.365
BCAL1435	*idh* - Inositol 2-dehydrogenase	15.127
BCAL1862	*phbA* - Acetyl-CoA acetyltransferase	1.852
BCAL2284	*acoE* - Acetyl-CoA synthetase	2.617
BCAL2357	*ilvC* - Ketol-acid reductoisomerase	1.814
BCAL2358	*ilvH* - Acetolactate synthase 3 regulatory subunit	2.692
BCAL2735	Isocitrate dehydrogenase	1.996
BCAL3043	*pgl* - 6-phosphogluconolactonase	3.027
BCAL3044	*glk* - Bifunctional glucokinase/RpiR family transcriptional regulator	3.027
BCAL3282	Phospho-2-dehydro-3-deoxyheptonate aldolase	3.730
BCAM0018	N-acetyl-gamma-glutamyl-phosphate reductase	60.237
BCAM0187	2-isopropylmalate synthase	8.786
BCAM0544	Putative acetylglutamate kinase	14.310
BCAM0983	*leuC1* - Isopropylmalate isomerase large subunit	2.395
BCAM0984	*leuD1* - Isopropylmalate isomerase small subunit	3.423
BCAM1833	*acnB* - Bifunctional aconitate hydratase 2/2-methylisocitrate dehydratase	2.952
BCAM2326	Serine hydroxymethyltransferase	23.996
BCAM2368	Putative quinoprotein ethanol dehydrogenase precursor	259.175
BCAM2372	*acsA* - Acetyl-CoA synthetase	19.709
BCAM2501	Shikimate 5-dehydrogenase	11.496
BCAM2502	*aroQ* - 3-dehydroquinate dehydratase	11.496
BCAS0734	Putative oxidoreductase	28.410
ARACHIDONIC ACID METABOLISM		
P-value 1.688e-05	**Count 4/6**	**66.7%**
BCAL0714	Threonine peptidase, family T3	5.003
BCAM1309	*ggt2* - Gamma-glutamyltransferase precursor 2	6.604
BCAM1955	*ggt1* - Gamma-glutamyltransferase precursor 1	3.460

Table V.S1 (continuation)

GENE	ANNOTATION OR PREDICTED FUNTION	FOLD CHANGE
ARACHIDONIC ACID METABOLISM		
P-value 1.688e-05	**Count 4/6**	**66.7%**
BCAS0751	Putative gamma-glutamyltransferase precursor	7.275
CYANOAMINO ACID METABOLISM		
P-value 1.852e-05	**Count 5/12**	**41.7%**
BCAL0714	Threonine peptidase, family T3	5.003
BCAM1309	*ggt2* - Gamma-glutamyltransferase precursor 2	6.604
BCAM1955	*ggt1* - Gamma-glutamyltransferase precursor 1	3.460
BCAM2326	Serine hydroxymethyltransferase	23.996
BCAS0751	Putative gamma-glutamyltransferase precursor	7.275
FLAGELLAR ASSEMBLY		
P-value 0.00014	**Count 7/40**	**17.5%**
BCAL0140	*flhB* - Flagellar biosynthesis protein FlhB	2.470
BCAL0141	*flhA* - Flagellar biosynthesis protein FlhA	2.470
BCAL0523	*fliH* - Flagellar assembly protein H	2.099
BCAL0524	*fliG* - Flagellar motor switch protein G	2.099
BCAL0525	*fliF* - Flagellar MS-ring protein	2.099
BCAL0567	*flgE1* - Flagellar hook protein FlgE	2.083
BCAL3506	*fliM* - Flagellar motor switch protein FliM	3.611
VALINE, LEUCINE, AND ISOLEUCINE BIOSYNTHESIS		
P-value 0.00086	**Count 5/25**	**20.0%**
BCAL2357	*ilvC* - Ketol-acid reductoisomerase	1.814
BCAL2358	*ilvH* - Acetolactate synthase 3 regulatory subunit	2.692
BCAM0187	2-isopropylmalate synthase	8.786
BCAM0983	*leuC1* - Isopropylmalate isomerase large subunit	2.395
BCAM0984	*leuD1* - Isopropylmalate isomerase small subunit	3.423
SYNTHESIS AND DEGRADATION OF KETONE BODIES		
P-value 0.00097	**Count 4/15**	**26.7%**
BCAL1472	*scoA* - Succinyl-CoA:3-ketoacid-coenzyme A transferase subunit A	6.643
BCAL1473	*scoB* - Succinyl-CoA:3-ketoacid-coenzyme A transferase subunit B	7.024
BCAL1862	*phbA* - Acetyl-CoA acetyltransferase	1.852
BCAL2304	3-hydroxybutyrate dehydrogenase	4.560

Table V.S1 (continuation)

GENE	ANNOTATION OR PREDICTED FUNTION	FOLD CHANGE
GLUTATHIONE METABOLISM		
P-value 0.00097	**Count 6/40**	**15.0%**
BCAL0714	Threonine peptidase, family T3	5.003
BCAL2321	Putative glutathione S-transferase	2.074
BCAL2735	Isocitrate dehydrogenase	1.996
BCAM1309	*ggt2* - Gamma-glutamyltransferase precursor 2	6.604
BCAM1955	*ggt1* - Gamma-glutamyltransferase precursor 1	3.460
BCAS0751	Putative gamma-glutamyltransferase precursor	7.275
BACTERIAL CHEMOTAXIS		
P-value 0.00097	**Count 6/40**	**15.0%**
BCAL0524	*fliG* - Flagellar motor switch protein G	2.099
BCAL0544	Putative periplasmic dipeptide transport protein	2.910
BCAL0675	Extracellular solute-binding protein	1.909
BCAL1657	Putative ribose transport system	2.021
BCAL3506	*fliM* - Flagellar motor switch protein FliM	3.611
BCAM0766	D-ribose-binding periplasmic protein precursor	3.226
PHENYLALANINE, TYROSINE AND TRYPTOPHAN BIOSYNTHESIS		
P-value 0.00104	**Count 5/27**	**18.5%**
BCAL0010	*phhA* - Phenylalanine 4-monooxygenase	20.439
BCAL0039	*pheC* - Periplasmic cyclohexadienyl dehydratase	3.444
BCAL3282	Phospho-2-dehydro-3-deoxyheptonate aldolase	3.730
BCAM2501	Shikimate 5-dehydrogenase	11.496
BCAM2502	*aroQ* - 3-dehydroquinate dehydratase	11.496
PANTOTHENATE AND CoA BIOSYNTHESIS		
P-value 0.00166	**Count 5/30**	**16.7%**
BCAL0795	*coaD* - Phosphopantetheine adenylyltransferase	2.068
BCAL2357	*ilvC* - Ketol-acid reductoisomerase	1.814
BCAL2358	*ilvH* - Acetolactate synthase 3 regulatory subunit	2.692
BCAS0731	*dhT* - Phenylhydantoinase	24.674
BCAS0733	Dihydropyrimidine dehydrogenase	29.277
PROPANOATE METABOLISM		
P-value 0.00259	**Count 6/49**	**12.2%**
BCAL1862	*phbA* - Acetyl-CoA acetyltransferase	1.852

Table V.S1 (continuation)

GENE	ANNOTATION OR PREDICTED FUNTION	FOLD CHANGE
PROPANOATE METABOLISM		
P-value 0.00259	**Count 6/49**	**12.2%**
BCAL2284	*acoE* - Acetyl-CoA synthetase	2.617
BCAM1833	*acnB* - Bifunctional aconitate hydratase 2/2-methylisocitrate dehydratase	2.952
BCAM2368	Putative quinoprotein ethanol dehydrogenase precursor	259.175
BCAM2372	*acsA* - Acetyl-CoA synthetase	19.709
BCAM2561	Putative 4-aminobutyrate aminotransferase	2.388
PYRUVATE METABOLISM		
P-value 0.00283	**Count 7/68**	**10.3%**
BCAL0064	*acoD* - Acetaldehyde dehydrogenase	16.817
BCAL1862	*phbA* - Acetyl-CoA acetyltransferase	1.852
BCAL2122	*aceB* - Malate synthase	7.437
BCAL2284	*acoE* - Acetyl-CoA synthetase	2.617
BCAM0131	*hchA* - Chaperone protein HchA	4.096
BCAM0187	2-isopropylmalate synthase	8.786
BCAM2372	*acsA* - Acetyl-CoA synthetase	19.709
INOSITOL PHOSPHATE METABOLISM		
P-value 0.00294	**Count 4/21**	**19.1%**
BCAL1427	Myo-inositol catabolism protein	11.695
BCAL1428	Putative amine catabolism-related protein	13.589
BCAL1429	Putative TPP-binding acetolactate synthase	30.290
BCAL1435	*idh* - Inositol 2-dehydrogenase	15.127
FATTY ACID METABOLISM		
P-value 0.002944	**Count 6/51**	**11.8%**
BCAL0885	Putative 3-hydroxyacyl-CoA dehydrogenase oxidoreductase	2.019
BCAL0886	Acetyl-CoA acetyltransferase	2.365
BCAL1541	Putative acyl-CoA synthetase	7.385
BCAL1862	*phbA* - Acetyl-CoA acetyltransferase	1.852
BCAL1979	Putative fatty acid degradation protein	2.770
BCAL3474	*fadD* - Long-chain-fatty-acid-CoA ligase	3.132
GLYCOLYSIS / GLUCONEOGENESIS		
P-value 0.00584	**Count 5/41**	**12.2%**
BCAL0064	*acoD* - Acetaldehyde dehydrogenase	16.817
BCAL2284	*acoE* - Acetyl-CoA synthetase	2.617

Table V.S1 (continuation)

GENE	ANNOTATION OR PREDICTED FUNTION	FOLD CHANGE
GLYCOLYSIS / GLUCONEOGENESIS		
P-value 0.00584	**Count 5/41**	**12.2%**
BCAL3044	*glk* - Bifunctional glucokinase/RpiR family transcriptional regulator	3.027
BCAM2368	Putative quinoprotein ethanol dehydrogenase precursor	259.175
BCAM2372	*acsA* - Acetyl-CoA synthetase	19.709
C5-BRANCHED DIBASIC ACID METABOLISM		
P-value 0.00625	**Count 3/13**	**23.1%**
BCAL2358	*ilvH* - Acetolactate synthase 3 regulatory subunit	2.692
BCAM0983	*leuC1* - Isopropylmalate isomerase large subunit	2.395
BCAM0984	*leuD1* - Isopropylmalate isomerase small subunit	3.423
PHOSPHOTRANSFERASE SYSTEM (PTS)		
P-value 0.00988	**Count 2/5**	**40.0%**
BCAL0781	PTS system transporter subunit IIBC	3.932
BCAM0545	Putative PTS transport system	12.430
ATRAZINE DEGRADATION		
P-value 0.01413	**Count 2/6**	**33.3%**
BCAL3104	*ureA* - Urease subunit gamma	35.232
BCAL3106	*ureC* - Urease subunit alpha	40.304
BETA-ALANINE METABOLISM		
P-value 0.03684	**Count 3/25**	**12.0%**
BCAM2561	Putative 4-aminobutyrate aminotransferase	2.388
BCAS0731	*dhT* - Phenylhydantoinase	24.674
BCAS0733	Dihydropyrimidine dehydrogenase	29.277
GERANIOL DEGRADATION		
P-value 0.03747	**Count 2/10**	**20.0%**
BCAL0884	Putative acyl-CoA dehydrogenase oxidoreductase protein	1.704
BCAL0886	Acetyl-CoA acetyltransferase	2.365
VALINE, LEUCINE, AND ISOLEUCINE DEGRADATION		
P-value 0.03999	**Count 4/46**	**8.7%**
BCAL0886	Acetyl-CoA acetyltransferase	2.365
BCAL1472	*scoA* - Succinyl-CoA:3-ketoacid-coenzyme A transferase subunit A	6.643
BCAL1473	*scoB* - Succinyl-CoA:3-ketoacid-coenzyme A transferase subunit B	7.024
BCAL1862	*phbA* - Acetyl-CoA acetyltransferase	1.852
STREPTOMYCIN BIOSYNTHESIS		
P-value 0.04263	**Cont 2/11**	**18.2%**
BCAL1435	*idh* - Inositol 2-dehydrogenase	15.127

Table V.S1 (continuation)

GENE	ANNOTATION OR PREDICTED FUNTION	FOLD CHANGE
STREPTOMYCIN BIOSYNTHESIS		
P-value 0.04263	**Cont 2/11**	**18.2%**
BCAL3044	*glk* - Bifunctional glucokinase/RpiR family transcriptional regulator	3.027
GLYCEROPHOSPHOLIPID METABOLISM		
P-value 0.04874	**Count 3/29**	**10.3%**
BCAL0059	*eutB* - Ethanolamine ammonia-lyase heavy chain	5.045
BCAL0060	*eutC* - Ethanolamine ammonia-lyase small subunit	5.045
BCAL0926	*glpD* - Glycerol-3-phosphate dehydrogenase	6.127
BETA-LACTAM RESISTANCE		
P-value 0.07058	**Count 3/34**	**8.8%**
BCAM1316	Transport system outer membrane protein	6.044
BCAM2311	Putative outer membrane porin protein	8.904
BCAM2728	*oppA* - Putative periplasmic oligopeptide-binding protein precursor	22.729
GLYCEROLIPID METABOLISM		
P-value 0.07058	**Count 2/15**	**13.3%**
BCAL0925	*glpK* - Glycerol kinase	10.076
BCAM0949	*lip* - exported lipase LipA	7.761
CHLOROALKANE AND CHLOROALKENE DEGRADATION		
P-value 0.08432	**Count 2/17**	**11.8%**
BCAL2121	Putative dehalogenase	35.004
BCAM2368	Putative quinoprotein ethanol dehydrogenase precursor	259.175
RNA DEGRADATION		
P-value 0.08432	**Count 2/17**	**11.8%**
BCAL1538	Hfq protein	2.523
BCAM0548	Chaperonin GroEL	16.666
METHANE METABOLISM		
P-value 0.08473	**Count 3/38**	**7.9%**
BCAL2284	*acoE* - Acetyl-CoA synthetase	2.617
BCAM2326	Serine hydroxymethyltransferase	23.996
BCAM2372	*acsA* - Acetyl-CoA synthetase	19.709
LYSINE DEGRADATION		
P-value 0.13614	**Count 2/23**	**8.7%**
BCAL1862	*phbA* - Acetyl-CoA acetyltransferase	1.852
BCAL3191	Putative glutaryl-CoA dehydrogenase	3.150

Table V.S1 (continuation)

GENE	ANNOTATION OR PREDICTED FUNTION	FOLD CHANGE
OXIDATIVE PHOSPHORYLATION		
P-value 0.15917	**Count 3/51**	**5.9%**
BCAL0328	*petA* - Ubiquinol-cytochrome C reductase iron-sulfur subunit	2.350
BCAL0329	*petB* - Cytochrome B; Component of the ubiquinol-cytochrome C reductase complex	2.350
BCAM0166	NADH dehydrogenase	6.810
PENTOSE PHOSPHATE PATHWAY		
P-value 0.17608	**Count 2/28**	**7.1%**
BCAL3043	*pgl* - 6-phosphogluconolactonase	3.027
BCAL3366	*eda* - KHG/KDPG aldolase	3.340
NICOTINATE AND NICOTINAMIDE METABOLISM		
P-value 0.17608	**Count 2/28**	**7.1%**
BCAL3325	*pntB* - NAD(P) transhydrogenase subunit beta	4.404
BCAL3326	*pntAB* - NAD(P) transhydrogenase subunit alpha	4.404
CYSTEINE AND METHIONINE METABOLISM		
P-value 0.18232	**Count 2/29**	**6.9%**
BCAM0540	Putative serine acetyltransferase	79.962
BCAM0721	O-acetylhomoserine (thiol)-lyase	10.513
CITRATE CYCLE (TCA CYCLE)		
P-value 0.20829	**Count 2/32**	**6.3%**
BCAL2735	Isocitrate dehydrogenase	1.996
BCAM1833	*acnB* - Bifunctional aconitate hydratase 2/2-methylisocitrate dehydratase	2.952
TRYPTOPHAN METABOLISM		
P-value 0.25874	**Count 2/38**	**5.3%**
BCAL1862	*phbA* - Acetyl-CoA acetyltransferase	1.852
BCAL3191	Putative glutaryl-CoA dehydrogenase	3.150
AMINO SUGAR AND NUCLEOTIDE SUGAR METABOLISM		
P-value 0.25874	**Count 2/38**	**5.3%**
BCAL0781	PTS system transporter subunit IIBC	3.932
BCAL3044	*glk* - Bifunctional glucokinase/RpiR family transcriptional regulator	3.027
BENZOATE DEGRADATION		
P-value 0.33122	**Count 2/49**	**4.1%**
BCAL0886	Acetyl-CoA acetyltransferase	2.365
BCAL1862	*phbA* - Acetyl-CoA acetyltransferase	1.852

Table V.S1 (continuation)

GENE	ANNOTATION OR PREDICTED FUNTION	FOLD CHANGE
PYRIMIDINE METABOLISM		
P-value 0.34380	**Count 2/48**	**4.2%**
BCAS0731	*dhT* - Phenylhydantoinase	24.674
BCAS0733	Dihydropyrimidine dehydrogenase	29.277
BACTERIAL SECRETION SYSTEM		
P-value 0.36488	**Count 2/51**	**3.9%**
BCAL3527	*gspD* - Type II secretion system protein D	2.103
BCAM1316	Transport system outer membrane protein	6.044
PURINE METABOLISM		
P-value 0.60920	**Count 2/83**	**2.4%**
BCAL3104	*ureA* - Urease subunit gamma	35.232
BCAL3106	*ureC* - Urease subunit alpha	40.304

Table V.S2. List of genes down-regulated upon *B. cenocepacia* K56-2 adhesion (37 °C, 30min) to 16HBE14o- derived GPMVs. Genes were associated in Gene Ontology of KEGG pathway database obtained in ShinyGO v0.61 software. Enrichment analysis based on hypergeometric distribution followed by FDR correction (Ge, et al. 2019).

GENE	ANNOTATION OR PREDICTED FUNTION	FOLD CHANGE
METABOLIC PATHWAYS		
P-value 6.766e-59	**Count 119/922**	**12.9%**
BCAL0032	*atpF* - F0F1 ATP synthase subunit B	-3.452
BCAL0033	*atpH* - F0F1 ATP synthase subunit delta	-2.724
BCAL0034	*atpA* - F0F1 ATP synthase subunit alpha	-3.732
BCAL0035	*atpG* - F0F1 ATP synthase subunit gamma	-4.750
BCAL0036	*atpD* - F0F1 ATP synthase subunit bet	-5.251
BCAL0037	*atpC* - F0F1 ATP synthase subunit epsilon	-5.644
BCAL0073	*gcvP* - Glycine dehydrogenase	-5.789
BCAL0075	*gcvT* - Glycine cleavage system aminomethyltransferase T	-18.026
BCAL0145	*ahcY* - S-adenosyl-L-homocysteine hydrolase	-3.820
BCAL0147	*metF* - 5,10-methylenetetrahydrofolate reductase	-4.955
BCAL0226	*rpoB* - DNA-directed RNA polymerase subunit beta	-3.774
BCAL0227	*rpoC* - DNA-directed RNA polymerase subunit beta'	-8.193
BCAL0260	*rpoA* - DNA-directed RNA polymerase subunit alpha	-2.506
BCAL0264	*hemB* - Delta-aminolevulinic acid dehydratase	-2.457
BCAL0409	*paaF* - Enoyl-CoA hydratase	-2.357
BCAL0422	*dnaN* - DNA polymerase III subunit beta	-1.970
BCAL0433	*speG* - spermidine N(1)-acetyltransferase	-4.072
BCAL0611	*glmS1* - glucosamine--fructose-6-phosphate aminotransferase	-3.240
BCAL0705	Putative D-amino acid aminotransferase	-2.748
BCAL0750	*ctaD* - Cytochrome C oxidase polypeptide I	-2.084
BCAL0752	Cytochrome C oxidase assembly protein	-3.376

Table V.S2 (continuation)

GENE	ANNOTATION OR PREDICTED FUNTION	FOLD CHANGE
METABOLIC PATHWAYS		
P-value 6.766e-59	Count 119/922	12.9%
BCAL0754	Putative cytochrome C oxidase subunit III	-2.373
BCAL0784	*cydB* - Cytochrome D ubiquinol oxidase subunit II	-14.401
BCAL0785	*cydA* - Cytochrome D ubiquinol oxidase subunit I	-15.160
BCAL1059	*argM* - Bifunctional N-succinyldiaminopimelate-aminotransferase/acetylornithine transaminase protein	-9.857
BCAL1212	*bkdA1* - 2-oxoisovalerate dehydrogenase subunit alpha	-23.249
BCAL1213	*bkdA2* - 2-oxoisovalerate dehydrogenase subunit beta	-27.571
BCAL1214	*bkdB* - Branched-chain alpha-keto acid dehydrogenase subunit E2	-37.308
BCAL1215	*lpdV* - Dihydrolipoamide dehydrogenase	-20.612
BCAL1262	*carB* - Carbamoyl phosphate synthase large subunit	-2.322
BCAL1413	*glnS* - Glutaminyl-tRNA synthetase	-2.101
BCAL1467	*aroC* - chorismate synthase	-3.171
BCAL1515	*sucA* - 2-oxoglutarate dehydrogenase E1 component	-2.403
BCAL1516	*sucB* - Dihydrolipoamide succinyltransferase	-3.499
BCAL1517	*odhL* - Dihydrolipoamide dehydrogenase	-3.768
BCAL1711	*cobN* - Cobaltochelatase subunit	-9.733
BCAL1712	Putative magnesium chelatase protein	-9.733
BCAL1884	*ispG* - 4-hydroxy-3-methylbut-2-en-1-yl diphosphate synthase	-2.679
BCAL1899	*dnaX* - DNA polymerase III subunits gamma and tau	-2.607
BCAL1987	*purL* - phosphoribosylformylglycinamidine synthase	-4.133
BCAL2061	*guaA* - GMP synthase	-2.124
BCAL2063	*guaB* - inosine 5'-monophosphate dehydrogenase	-2.454
BCAL2079	*lpxA* - UDP-N-acetylglucosamine acyltransferase	-2.924
BCAL2080	*fabZ* - (3R)-hydroxymyristoyl-ACP dehydratase	-3.301

Table V.S2 (continuation)

GENE	ANNOTATION OR PREDICTED FUNTION	FOLD CHANGE
METABOLIC PATHWAYS		
P-value 6.766e-59	Count 119/922	12.9%
BCAL2141	*cyoD* - Cytochrome O ubiquinol oxidase protein	-15.188
BCAL2142	*cyoC* - cytochrome o ubiquinol oxidase subunit III	-57.917
BCAL2143	*cyoB* - ubiquinol oxidase polypeptide I	-57.917
BCAL2144	*cyoA* - ubiquinol oxidase polypeptide II	-32.937
BCAL2207	Putative dihydrolipoamide dehydrogenase	-6.063
BCAL2208	*pdhB* - Dihydrolipoamide acetyltransferase	-7.683
BCAL2209	*aceE* - Pyruvate dehydrogenase subunit E1	-4.026
BCAL2244	*hutU* - urocanate hydratase	-5.320
BCAL2303	Aromatic amino acid aminotransferase	-2.049
BCAL2331	*nuoN* - NADH dehydrogenase subunit N	-3.858
BCAL2332	*nuoM* - NADH dehydrogenase subunit M	-3.858
BCAL2333	*nuoL* - NADH dehydrogenase subunit L	-4.212
BCAL2334	*nuoK* - NADH dehydrogenase subunit K	-3.903
BCAL2335	*nuoJ* - NADH dehydrogenase subunit J	-3.648
BCAL2336	*nuoI* - NADH dehydrogenase subunit I	-6.127
BCAL2337	*nuoH* - NADH dehydrogenase subunit H	-5.679
BCAL2338	NADH dehydrogenase subunit G	-6.929
BCAL2339	*nuoF* - NADH dehydrogenase I chain F	-5.358
BCAL2340	NADH dehydrogenase subunit E	-5.358
BCAL2341	*nuoD* - NADH dehydrogenase subunit D	-4.833
BCAL2342	*nuoC* - NADH dehydrogenase subunit C	-3.220
BCAL2343	*nuoB* - NADH dehydrogenase subunit B	-4.355
BCAL2344	*nuoA* - NADH dehydrogenase subunit A	-2.184
BCAL2433	*tal* - Transaldolase B	-1.687
BCAL2638	*argH* - Argininosuccinate lyase	-3.021

Table V.S2 (continuation)

GENE	ANNOTATION OR PREDICTED FUNTION	FOLD CHANGE
METABOLIC PATHWAYS		
P-value 6.766e-59	Count 119/922	12.9%
BCAL2782	*pdxH* - Pyridoxamine 5'-phosphate oxidase	-4.034
BCAL2791	*kynU* - Putative kynureninase	-14.681
BCAL2792	*kynA* - Putative tryptophan 2,3-dioxygenase	-9.006
BCAL2908	*fumC* - Fumarate hydratase	-4.369
BCAL2952	*aroA* - 3-phosphoshikimate 1-carboxyvinyltransferase	-3.902
BCAL2955	*serC* - Phosphoserine aminotransferase	-2.204
BCAL3094	*hemN* - Coproporphyrinogen III oxidase	-36.590
BCAL3216	*cysC* - Adenylyl-sulfate kinase	-2.024
BCAL3261	*purM* - Phosphoribosylaminoimidazole synthetase	-2.290
BCAL3299	*katG* - Peroxidase/catalase KatB	-4.895
BCAL3336	purH - Bifunctional phosphoribosylaminoimidazolecarboxamide formyltransferase/IMP cyclohydrolase	-3.030
BCAL3359	Putative glutamate dehydrogenase	-9.125
BCAL3361	*purB* - Adenylosuccinate lyase	-2.545
BCAL3388	*gapA* - Glyceraldehyde 3-phosphate dehydrogenase 1	-4.547
BCAL3389	*tktA* - Transketolase	-3.302
BCAL3425	Putative sugar kinase	-3.336
BCAL3472	*coq7* - 2-nonaprenyl-3-methyl-6-methoxy-1,4-benzoquinol hydroxylase	-9.819
BCAM0286	Putative alcohol dehydrogenase	-17.616
BCAM0293	*ackA* - Putative acetate kinase	-59.243
BCAM0298	Putative phosphate acetyl/butyryl transferase	-76.193
BCAM0310	Ribonucleotide reductase-like protein	-51.056
BCAM0311	Putative 6-phosphofructokinase	-65.666
BCAM0911	*dxs* - 1-deoxy-D-xylulose-5-phosphate synthase	-1.770
BCAM0961	Aconitate hydratase	-2.465
BCAM0969	*sdhA* - Succinate dehydrogenase flavoprotein subunit	-2.639

Table V.S2 (continuation)

GENE	ANNOTATION OR PREDICTED FUNTION	FOLD CHANGE
METABOLIC PATHWAYS		
P-value 6.766e-59	**Count 119/922**	**12.9%**
BCAM0970	*sdhB* - Succinate dehydrogenase iron-sulfur subunit	-2.610
BCAM0972	*gltA* - Type II citrate synthase	-2.215
BCAM0998	*purF* - Amidophosphoribosyltransferase	-2.629
BCAM1111	*speF* - Ornithine decarboxylase	-37.980
BCAM1112	*adiA* - biodegradative arginine decarboxylase	-13.932
BCAM1204	Alanine racemase	-15.392
BCAM1243	Putative aminotransferase	-2.093
BCAM1245	Putative phosphoenolpyruvate phosphomutase/sugar nucleotidyltransferase	-2.093
BCAM1250	Putative acetyl-CoA hydrolase/transferase	-1.882
BCAM1570	Alcohol dehydrogenase	-139.172
BCAM1573	Alpha,alpha-trehalose-phosphate synthase	-2.273
BCAM1710	Putative enoyl-CoA hydratase/isomerase	-11.823
BCAM2076	*lysA* - Diaminopimelate decarboxylase	-2.864
BCAM2193	Putative 3-hydroxyisobutyrate dehydrogenase	-6.309
BCAM2194	*mmsA* - Methylmalonate-semialdehyde dehydrogenase	-4.876
BCAM2195	Putative AMP-binding protein	-3.995
BCAM2430	Putative biotin carboxylase	-15.417
BCAM2431	Enoyl-CoA hydratase	-49.561
BCAM2432	Putative biotin-dependent carboxyl transferase	-8.712
BCAM2433	Putative acyl-CoA dehydrogenase	-5.801
BCAM2817	Glycolate oxidase subunit GlcD	-9.100
BCAM2818	Glycolate oxidase FAD binding subunit	-9.100
BCAS0737	Putative acetyl-CoA acetyltransferase	-7.386
BCAS0739	Putative acetyl-CoA synthetase	-5.646
BCAS0771	Putative adenylosuccinate synthetase	-7.151
OXIDATIVE PHOSPHORYLATION		
P-value 6.705e-38	**Count 31/51**	**60.8%**
BCAL0032	*atpF* - F0F1 ATP synthase subunit B	-3.452

Table V.S2 (continuation)

GENE	ANNOTATION OR PREDICTED FUNTION	FOLD CHANGE
OXIDATIVE PHOSPHORYLATION		
P-value 6.705e-38	Count 31/51	60.8%
BCAL0033	*atpH* - F0F1 ATP synthase subunit delta	-2.724
BCAL0034	*atpA* - F0F1 ATP synthase subunit alpha	-3.732
BCAL0035	*atpG* - F0F1 ATP synthase subunit gamma	-4.750
BCAL0036	*atpD* - F0F1 ATP synthase subunit beta	-5.251
BCAL0037	*atpC* - F0F1 ATP synthase subunit epsilon	-5.644
BCAL0750	*ctaD* - Cytochrome C oxidase polypeptide I	-2.084
BCAL0752	Cytochrome C oxidase assembly protein	-3.376
BCAL0754	Putative cytochrome C oxidase subunit III	-2.373
BCAL0784	*cydB* - Cytochrome D ubiquinol oxidase subunit II	-14.401
BCAL0785	*cydA* - Cytochrome D ubiquinol oxidase subunit I	-15.160
BCAL2141	*cyoD* - Cytochrome O ubiquinol oxidase protein	-15.188
BCAL2142	*cyoC* - cytochrome O ubiquinol oxidase subunit III	-57.917
BCAL2143	*cyoB* - Ubiquinol oxidase polypeptide I	-57.917
BCAL2144	*cyoA* - Ubiquinol oxidase polypeptide II	-32.937
BCAL2331	*nuoN* - NADH dehydrogenase subunit N	-3.858
BCAL2332	*nuoM* - NADH dehydrogenase subunit M	-3.858
BCAL2333	*nuoL* - NADH dehydrogenase subunit L	-4.212
BCAL2334	*nuoK* - NADH dehydrogenase subunit K	-3.903
BCAL2335	*nuoJ* - NADH dehydrogenase subunit J	-3.648
BCAL2336	*nuoI* - NADH dehydrogenase subunit I	-6.127
BCAL2337	*nuoH* - NADH dehydrogenase subunit H	-5.679
BCAL2338	NADH dehydrogenase subunit G	-6.929
BCAL2339	*nuoF* - NADH dehydrogenase I chain F	-5.358
BCAL2340	NADH dehydrogenase subunit E	-5.358

Table V.S2 (continuation)

GENE	ANNOTATION OR PREDICTED FUNTION	FOLD CHANGE
OXIDATIVE PHOSPHORYLATION		
P-value 6.705e-38	**Count 31/51**	**60.8%**
BCAL2341	*nuoD* - NADH dehydrogenase subunit D	-4.833
BCAL2342	*nuoC* - NADH dehydrogenase subunit C	-3.220
BCAL2343	*nuoB* - NADH dehydrogenase subunit B	-4.355
BCAL2344	*nuoA* - NADH dehydrogenase subunit A	-2.184
BCAM0969	*sdhA* - Succinate dehydrogenase flavoprotein subunit	-2.639
BCAM0970	*sdhB* - Succinate dehydrogenase iron-sulfur subunit	-2.610
RIBOSOME		
P-value 9.473e-31	**Count 28/57**	**49.1%**
BCAL0222	*rplK* - 50S ribosomal protein L11	-4.197
BCAL0223	*rplA* - 50S ribosomal protein L1	-3.883
BCAL0224	*rplJ* - 50S ribosomal protein L10	-5.670
BCAL0225	*rplL* - 50S ribosomal protein L7/L12	-5.924
BCAL0233	*rpsJ* - 30S ribosomal protein S10	-3.575
BCAL0234	*rplC* - 50S ribosomal protein L3	-9.099
BCAL0236	*rplW* - 50S ribosomal protein L23	-9.099
BCAL0237	*rplB* - 50S ribosomal protein L2	-14.352
BCAL0238	*rpsS* - 30S ribosomal protein S19	-16.178
BCAL0240	*rpsC* - 30S ribosomal protein S3	-21.137
BCAL0241	*rplP* - 50S ribosomal protein L16	-16.565
BCAL0242	*rpmC* - 50S ribosomal protein L29	-19.046
BCAL0243	*rpsQ* - 30S ribosomal protein S17	-19.046
BCAL0244	*rplN* - 50S ribosomal protein L14	-2.264
BCAL0246	*rplE* - 50S ribosomal protein L5	-2.706
BCAL0247	*rpsN* - 30S ribosomal protein S14	-3.100
BCAL0248	*rpsH* - 30S ribosomal protein S8	-3.343
BCAL0249	*rplF* - 50S ribosomal protein L6	-3.773
BCAL0250	*rplR* - 50S ribosomal protein L18	-4.580
BCAL0251	*rpsE* - 30S ribosomal protein S5	-4.181
BCAL0253	*rplO* - 50S ribosomal protein L15	-5.721
BCAL0257	*rpsM* - 30S ribosomal protein S13	-2.065
BCAL0258	*rpsK* - 30S ribosomal protein S11	-2.706
BCAL0259	*rpsD* - 30S ribosomal protein S4	-2.421
BCAL0799	*rplY* - 50S ribosomal protein L25/general stress protein Ctc	-5.281
BCAL2925	*rplS* - 50S ribosomal protein L19	-4.795
BCAL2950	*rpsA* - 30S ribosomal protein S1	-1.848
BCAL3348	*rplM* - 50S ribosomal protein L13	-1.841

Table V.S2 (continuation)

GENE	ANNOTATION OR PREDICTED FUNTION	FOLD CHANGE
BIOSYNTHESIS OF SECONDARY METABOLITES		
P-value 3.326e-27	**Cout 52/359**	**14.5%**
BCAL0264	*hemB* - Delta-aminolevulinic acid dehydratase	-2.457
BCAL0409	*paaF* - Enoyl-CoA hydratase	-2.357
BCAL0611	*glmS1* - glucosamine--fructose-6-phosphate aminotransferase	-3.240
BCAL1059	*argM* - Bifunctional N-succinyldiaminopimelate-aminotransferase/acetylornithine transaminase protein	-9.857
BCAL1212	*bkdA1* - 2-oxoisovalerate dehydrogenase subunit alpha	-23.249
BCAL1213	*bkdA2* - 2-oxoisovalerate dehydrogenase subunit beta	-27.571
BCAL1214	*bkdB* - Branched-chain alpha-keto acid dehydrogenase subunit E2	-37.308
BCAL1215	*lpdV* - Dihydrolipoamide dehydrogenase	-20.612
BCAL1467	*aroC* - chorismate synthase	-3.171
BCAL1515	*sucA* - 2-oxoglutarate dehydrogenase E1 component	-2.403
BCAL1516	*sucB* - Dihydrolipoamide succinyltransferase	-3.499
BCAL1517	*odhL* - Dihydrolipoamide dehydrogenase	-3.768
BCAL1712	Putative magnesium chelatase protein	-9.733
BCAL1722	Putative exported chitinase	-9.498
BCAL1884	*ispG* - 4-hydroxy-3-methylbut-2-en-1-yl diphosphate synthase	-2.679
BCAL1987	*purL* - phosphoribosylformylglycinamidine synthase	-4.133
BCAL2063	*guaB* - inosine 5'-monophosphate dehydrogenase	-2.454
BCAL2207	Putative dihydrolipoamide dehydrogenase	-6.063
BCAL2208	*pdhB* - Dihydrolipoamide acetyltransferase	-7.683
BCAL2209	*aceE* - Pyruvate dehydrogenase subunit E1	-4.026
BCAL2303	Aromatic amino acid aminotransferase	-2.049
BCAL2433	*tal* - Transaldolase B	-1.687
BCAL2638	*argH* - Argininosuccinate lyase	-3.021
BCAL2908	*fumC* - Fumarate hydratase	-4.369

Table V.S2 (continuation)

GENE	ANNOTATION OR PREDICTED FUNTION	FOLD CHANGE
BIOSYNTHESIS OF SECONDARY METABOLITES		
P-value 3.326e-27	Cout 52/359	14.5%
BCAL2952	*aroA* - 3-phosphoshikimate 1-carboxyvinyltransferase	-3.902
BCAL3094	*hemN* - Coproporphyrinogen III oxidase	-36.590
BCAL3261	*purM* - Phosphoribosylaminoimidazole synthetase	-2.290
BCAL3336	purH - Bifunctional phosphoribosylaminoimidazolecarboxamide formyltransferase/IMP cyclohydrolase	-3.030
BCAL3361	*purB* - Adenylosuccinate lyase	-2.545
BCAL3388	*gapA* - Glyceraldehyde 3-phosphate dehydrogenase 1	-4.547
BCAL3389	*tktA* - Transketolase	-3.302
BCAL3472	*coq7* - 2-nonaprenyl-3-methyl-6-methoxy-1,4-benzoquinol hydroxylase	-9.819
BCAM0286	Putative alcohol dehydrogenase	-17.616
BCAM0311	Putative 6-phosphofructokinase	-65.666
BCAM0911	*dxs* - 1-deoxy-D-xylulose-5-phosphate synthase	-1.770
BCAM0961	Aconitate hydratase	-2.465
BCAM0969	*sdhA* - Succinate dehydrogenase flavoprotein subunit	-2.639
BCAM0970	*sdhB* - Succinate dehydrogenase iron-sulfur subunit	-2.610
BCAM0972	*gltA* - Type II citrate synthase	-2.215
BCAM0998	*purF* - Amidophosphoribosyltransferase	-2.629
BCAM1111	*speF* - Ornithine decarboxylase	-37.980
BCAM1245	Putative phosphoenolpyruvate phosphomutase/sugar nucleotidyltransferase	-2.093
BCAM1250	Putative acetyl-CoA hydrolase/transferase	-1.882
BCAM1570	Alcohol dehydrogenase	-139.172
BCAM2076	*lysA* - Diaminopimelate decarboxylase	-2.864
BCAM2195	Putative AMP-binding protein	-3.995
BCAM2196	Putative acyl-CoA dehydrogenase	-5.913
BCAM2817	Glycolate oxidase subunit GlcD	-9.100
BCAM2818	Glycolate oxidase FAD binding subunit	-9.100

Table V.S2 (continuation)

GENE	ANNOTATION OR PREDICTED FUNTION	FOLD CHANGE
BIOSYNTHESIS OF SECONDARY METABOLITES		
P-value 3.326e-27	**Cout 52/359**	**14.5%**
BCAM2831	Squlalene--hopene cyclase	-3.428
BCAS0737	Putative acetyl-CoA acetyltransferase	-7.386
BCAS0739	Putative acetyl-CoA synthetase	-5.646
MICROBIAL METABOLISM IN DIVERSE ENVIRONMENTS		
P-value 7.388e-22	**Count 48/393**	**12.2%**
BCAL0147	*metF* - 5,10-methylenetetrahydrofolate reductase	-4.955
BCAL0212	*paaE* - Putative phenylacetic acid degradation NADH oxidoreductase PaaE	-43.665
BCAL0213	*paaD* - Phenylacetic acid degradation protein PaaD	-44.213
BCAL0214	*paaC* - Phenylacetic acid degradation protein PaaC	-33.710
BCAL0215	*paaB* - Phenylacetate-CoA oxygenase subunit PaaB	-36.644
BCAL0216	*paaA* - Phenylacetate-CoA oxygenase subunit PaaA	-34.435
BCAL0406	*paaG* - Enoyl-CoA hydratase	-11.166
BCAL0409	*paaF* - Enoyl-CoA hydratase	-2.357
BCAL1059	*argM* - Bifunctional N-succinyldiaminopimelate-aminotransferase/acetylornithine transaminase protein	-9.857
BCAL1215	*lpdV* - Dihydrolipoamide dehydrogenase	-20.612
BCAL1515	*sucA* - 2-oxoglutarate dehydrogenase E1 component	-2.403
BCAL1516	*sucB* - Dihydrolipoamide succinyltransferase	-3.499
BCAL1517	*odhL* - Dihydrolipoamide dehydrogenase	-3.768
BCAL2207	Putative dihydrolipoamide dehydrogenase	-6.063
BCAL2208	*pdhB* - Dihydrolipoamide acetyltransferase	-7.683
BCAL2209	*aceE* - Pyruvate dehydrogenase subunit E1	-4.026
BCAL2433	*tal* - Transaldolase B	-1.687
BCAL2908	*fumC* - Fumarate hydratase	-4.369
BCAL2955	*serC* - Phosphoserine aminotransferase	-2.204
BCAL3179	*ldhA* - Putative D-lactate dehydrogenase	-2.995

Table V.S2 (continuation)

GENE	ANNOTATION OR PREDICTED FUNTION	FOLD CHANGE
BIOSYNTHESIS OF SECONDARY METABOLITES		
P-value 3.326e-27	**Cout 52/359**	**14.5%**
BCAL3216	*cysC* - Adenylyl-sulfate kinase	-2.024
BCAL3299	*katG* - Peroxidase/catalase KatB	-4.895
BCAL3388	*gapA* - Glyceraldehyde 3-phosphate dehydrogenase 1	-4.547
BCAL3389	*tktA* - Transketolase	-3.302
BCAM0286	Putative alcohol dehydrogenase	-17.616
BCAM0293	*ackA* - Putative acetate kinase	-59.243
BCAM0296	Acetoacetyl-CoA reductase	-76.193
BCAM0298	Putative phosphate acetyl/butyryl transferase	-76.193
BCAM0311	Putative 6-phosphofructokinase	-65.666
BCAM0810	Putative aromatic oxygenase	-10.983
BCAM0811	Putative aromatic oxygenase	-6.831
BCAM0961	Aconitate hydratase	-2.465
BCAM0969	*sdhA* - Succinate dehydrogenase flavoprotein subunit	-2.639
BCAM0970	*sdhB* - Succinate dehydrogenase iron-sulfur subunit	-2.610
BCAM0972	*gltA* - Type II citrate synthase	-2.215
BCAM1243	Putative aminotransferase	-2.093
BCAM1245	Putative phosphoenolpyruvate phosphomutase/sugar nucleotidyltransferase	-2.093
BCAM1250	Putative acetyl-CoA hydrolase/transferase	-1.882
BCAM1570	Alcohol dehydrogenase	-139.172
BCAM1711	Phenylacetate-coenzyme A ligase	-11.823
BCAM2076	*lysA* - Diaminopimelate decarboxylase	-2.864
BCAM2191	Enoyl-CoA hydratase/isomerase family	-6.309
BCAM2192	Enoyl-CoA hydratase	-6.309
BCAM2195	Putative AMP-binding protein	-3.995
BCAM2817	Glycolate oxidase subunit GlcD	-9.100
BCAM2818	Glycolate oxidase FAD binding subunit	-9.100
BCAS0737	Putative acetyl-CoA acetyltransferase	-7.386
BCAS0739	Putative acetyl-CoA synthetase	-5.646
CARBON METABOLISM		
P-value 7.871e-18	**Count 27/136**	**19.9%**
BCAL0073	*gcvP* - Glycine dehydrogenase	-5.789
BCAL0075	*gcvT* - Glycine cleavage system aminomethyltransferase T	-18.026

Table V.S2 (continuation)

GENE	ANNOTATION OR PREDICTED FUNTION	FOLD CHANGE
BIOSYNTHESIS OF SECONDARY METABOLITES		
P-value 3.326e-27	**Cout 52/359**	**14.5%**
BCAL0147	*metF* - 5,10-methylenetetrahydrofolate reductase	-4.955
BCAL1215	*lpdV* - Dihydrolipoamide dehydrogenase	-20.612
BCAL1515	*sucA* - 2-oxoglutarate dehydrogenase E1 component	-2.403
BCAL1516	*sucB* - Dihydrolipoamide succinyltransferase	-3.499
BCAL1517	*odhL* - Dihydrolipoamide dehydrogenase	-3.768
BCAL2207	Putative dihydrolipoamide dehydrogenase	-6.063
BCAL2208	*pdhB* - Dihydrolipoamide acetyltransferase	-7.683
BCAL2209	*aceE* - Pyruvate dehydrogenase subunit E1	-4.026
BCAL2433	*tal* - Transaldolase B	-1.687
BCAL2908	*fumC* - Fumarate hydratase	-4.369
BCAL2955	*serC* - Phosphoserine aminotransferase	-2.204
BCAL3388	*gapA* - Glyceraldehyde 3-phosphate dehydrogenase 1	-4.547
BCAL3389	*tktA* - Transketolase	-3.302
BCAM0293	*ackA* - Putative acetate kinase	-59.243
BCAM0298	Putative phosphate acetyl/butyryl transferase	-76.193
BCAM0311	Putative 6-phosphofructokinase	-65.666
BCAM0961	Aconitate hydratase	-2.465
BCAM0969	*sdhA* - Succinate dehydrogenase flavoprotein subunit	-2.639
BCAM0970	*sdhB* - Succinate dehydrogenase iron-sulfur subunit	-2.610
BCAM0972	*gltA* - Type II citrate synthase	-2.215
BCAM1250	Putative acetyl-CoA hydrolase/transferase	-1.882
BCAM2194	*mmsA* - Methylmalonate-semialdehyde dehydrogenase	-4.876
BCAM2195	Putative AMP-binding protein	-3.995
BCAS0737	Putative acetyl-CoA acetyltransferase	-7.386
BCAS0739	Putative acetyl-CoA synthetase	-5.646
VALINE, LEUCINE, AND ISOLEUCINE DEGRADATION		
P-value 1.500e-13	**Count 15/46**	**32.6%**
BCAL0409	*paaF* - Enoyl-CoA hydratase	-2.357

Table V.S2 (continuation)

GENE	ANNOTATION OR PREDICTED FUNTION	FOLD CHANGE
VALINE, LEUCINE, AND ISOLEUCINE DEGRADATION		
P-value 1.500e-13	**Count 15/46**	**32.6%**
BCAL1212	*bkdA1* - 2-oxoisovalerate dehydrogenase subunit alpha	-23.249
BCAL1213	*bkdA2* - 2-oxoisovalerate dehydrogenase subunit beta	-27.571
BCAL1214	*bkdB* - Branched-chain alpha-keto acid dehydrogenase subunit E2	-37.308
BCAL1215	*lpdV* - Dihydrolipoamide dehydrogenase	-20.612
BCAL1517	*odhL* - Dihydrolipoamide dehydrogenase	-3.768
BCAL2207	Putative dihydrolipoamide dehydrogenase	-6.063
BCAM1710	Putative enoyl-CoA hydratase/isomerase	-11.823
BCAM2193	Putative 3-hydroxyisobutyrate dehydrogenase	-6.309
BCAM2194	*mmsA* - Methylmalonate-semialdehyde dehydrogenase	-4.876
BCAM2430	Putative biotin carboxylase	-15.417
BCAM2431	Enoyl-CoA hydratase	-49.561
BCAM2432	Putative biotin-dependent carboxyl transferase	-8.712
BCAM2433	Putative acyl-CoA dehydrogenase	-5.801
BCAS0737	Putative acetyl-CoA acetyltransferase	-7.386
CITRATE CYCLE (TCA CYCLE)		
P-value 2.681e-13	**Count 13/32**	**40.6%**
BCAL1215	*lpdV* - Dihydrolipoamide dehydrogenase	-20.612
BCAL1515	*sucA* - 2-oxoglutarate dehydrogenase E1 component	-2.403
BCAL1516	*sucB* - Dihydrolipoamide succinyltransferase	-3.499
BCAL1517	*odhL* - Dihydrolipoamide dehydrogenase	-3.768
BCAL2207	Putative dihydrolipoamide dehydrogenase	-6.063
BCAL2208	*pdhB* - Dihydrolipoamide acetyltransferase	-7.683
BCAL2209	*aceE* - Pyruvate dehydrogenase subunit E1	-4.026
BCAL2908	*fumC* - Fumarate hydratase	-4.369
BCAM0961	Aconitate hydratase	-2.465
BCAM0969	*sdhA* - Succinate dehydrogenase flavoprotein subunit	-2.639

Table V.S2 (continuation)

GENE	ANNOTATION OR PREDICTED FUNTION	FOLD CHANGE
CITRATE CYCLE (TCA CYCLE)		
P-value 2.681e-13	**Count 13/32**	**40.6%**
BCAM0970	*sdhB* - Succinate dehydrogenase iron-sulfur subunit	-2.610
BCAM0972	*gltA* - Type II citrate synthase	-2.215
BCAM1250	Putative acetyl-CoA hydrolase/transferase	-1.882
PURINE METABOLISM		
P-value 7.431e-13	**Count 18/83**	**21.7%**
BCAL0226	*rpoB* - DNA-directed RNA polymerase subunit beta	-3.774
BCAL0227	*rpoC* - DNA-directed RNA polymerase subunit beta'	-8.193
BCAL0260	*rpoA* - DNA-directed RNA polymerase subunit alpha	-2.506
BCAL0422	*dnaN* - DNA polymerase III subunit beta	-1.970
BCAL1899	*dnaX* - DNA polymerase III subunits gamma and tau	-2.607
BCAL1987	*purL* - phosphoribosylformylglycinamidine synthase	-4.133
BCAL2061	*guaA* - GMP synthase	-2.124
BCAL2063	*guaB* - inosine 5'-monophosphate dehydrogenase	-2.454
BCAL2329	NUDIX hydrolase	-3.504
BCAL2348	*pnp* - Polynucleotide phosphorylase/polyadenylase	-1.936
BCAL3216	*cysC* - Adenylyl-sulfate kinase	-2.024
BCAL3261	*purM* - Phosphoribosylaminoimidazole synthetase	-2.290
BCAL3336	purH - Bifunctional phosphoribosylaminoimidazolecarboxamide formyltransferase/IMP cyclohydrolase	-3.030
BCAL3361	*purB* - Adenylosuccinate lyase	-2.545
BCAL3425	Putative sugar kinase	-3.336
BCAM0310	Ribonucleotide reductase-like protein	-51.056
BCAM0998	*purF* - Amidophosphoribosyltransferase	-2.629
BCAS0771	Putative adenylosuccinate synthetase	-7.151

Table V.S2 (continuation)

GENE	ANNOTATION OR PREDICTED FUNTION	FOLD CHANGE
BACTERIAL CHEMOTAXIS		
P-value 1.414e-10	**Count 13/40**	**32.5%**
BCAL0126	*motA* - Flagellar motor protein MotA	-1.913
BCAL0129	*cheA* - Chemotaxis two-component sensor kinase CheA	-2.496
BCAL0130	*cheW* - Chemotaxis protein CheW	-2.889
BCAL0131	*tar* - Methyl-accepting chemotaxis protein	-3.261
BCAL0132	*cheR* - Chemotaxis protein methyltransferase	-2.324
BCAL0133	*cheD* - Chemoreceptor glutamine deamidase CheD	-2.324
BCAL0134	*cheB1* - Chemotaxis-specific methylesterase	-2.324
BCAL0135	Chemotaxis protein CheY	-3.744
BCAL0762	Putative methyl-accepting chemotaxis protein	-5.099
BCAM1503	Putative methyl-accepting chemotaxis protein	-4.184
BCAM1572	Methyl-accepting chemotaxis protein	-2.811
BCAM1804	Methyl-accepting chemotaxis protein	-12.383
BCAM2564	*aer* - Putative aerotaxis receptor	-3.607
PYRUVATE METABOLISM		
P-value 7.225e-10	**Count 14/68**	**20.6%**
BCAL1215	*lpdV* - Dihydrolipoamide dehydrogenase	-20.612
BCAL1517	*odhL* - Dihydrolipoamide dehydrogenase	-3.768
BCAL2207	Putative dihydrolipoamide dehydrogenase	-6.063
BCAL2208	*pdhB* - Dihydrolipoamide acetyltransferase	-7.683
BCAL2209	*aceE* - Pyruvate dehydrogenase subunit E1	-4.026
BCAL2908	*fumC* - Fumarate hydratase	-4.369
BCAL3179	*ldhA* - Putative D-lactate dehydrogenase	-2.995
BCAM0293	*ackA* - Putative acetate kinase	-59.243
BCAM0298	Putative phosphate acetyl/butyryl transferase	-76.193
BCAM0387	*poxB*- Pyruvate dehydrogenase	-2.387
BCAM1250	Putative acetyl-CoA hydrolase/transferase	-1.882
BCAM2195	Putative AMP-binding protein	-3.995

Table V.S2 (continuation)

GENE	ANNOTATION OR PREDICTED FUNTION	FOLD CHANGE
PYRUVATE METABOLISM		
P-value 7.225e-10	**Count 14/68**	**20.6%**
BCAS0737	Putative acetyl-CoA acetyltransferase	-7.386
BCAS0739	Putative acetyl-CoA synthetase	-5.646
TWO-COMPONENT SYSTEM		
P-value 1.983e-09	**Count 18/132**	**13.6%**
BCAL0114	*fliC* - Flagellin	-1.921
BCAL0126	*motA* - Flagellar motor protein MotA	-1.913
BCAL0129	*cheA* - Chemotaxis two-component sensor kinase CheA	-2.496
BCAL0130	*cheW* - Chemotaxis protein CheW	-2.889
BCAL0132	*cheR* - Chemotaxis protein methyltransferase	-2.324
BCAL0134	*cheB1* - Chemotaxis-specific methylesterase	-2.324
BCAL0135	Chemotaxis protein CheY	-3.744
BCAL0499	Two-component regulatory system, response regulator protein	-4.190
BCAL0762	Putative methyl-accepting chemotaxis protein	-5.099
BCAL0784	*cydB* - Cytochrome D ubiquinol oxidase subunit II	-14.401
BCAL0785	*cydA* - Cytochrome D ubiquinol oxidase subunit I	-15.160
BCAL1674	*amrA* - Periplasmic multidrug efflux lipoprotein	-7.862
BCAL1675	*amrB* - Multidrug efflux protein	-6.194
BCAM1503	Putative methyl-accepting chemotaxis protein	-4.184
BCAM1572	Methyl-accepting chemotaxis protein	-2.811
BCAM1804	Methyl-accepting chemotaxis protein	-12.383
BCAM2564	*aer* - Putative aerotaxis receptor	-3.607
BCAS0737	Putative acetyl-CoA acetyltransferase	-7.386
GLYCOLYSIS / GLUCONEOGENESIS		
P-value 2.881e-09	**Count 11/41**	**28.8%**
BCAL1215	*lpdV* - Dihydrolipoamide dehydrogenase	-20.612
BCAL1517	*odhL* - Dihydrolipoamide dehydrogenase	-3.768
BCAL2207	Putative dihydrolipoamide dehydrogenase	-6.063

Table V.S2 (continuation)

GENE	ANNOTATION OR PREDICTED FUNTION	FOLD CHANGE
GLYCOLYSIS / GLUCONEOGENESIS		
P-value 2.881e-09	**Count 11/41**	**28.8%**
BCAL2208	*pdhB* - Dihydrolipoamide acetyltransferase	-7.683
BCAL2209	*aceE* - Pyruvate dehydrogenase subunit E1	-4.026
BCAL3388	*gapA* - Glyceraldehyde 3-phosphate dehydrogenase 1	-4.547
BCAM0286	Putative alcohol dehydrogenase	-17.616
BCAM0311	Putative 6-phosphofructokinase	-65.666
BCAM1570	Alcohol dehydrogenase	-139.172
BCAM2195	Putative AMP-binding protein	-3.995
BCAS0739	Putative acetyl-CoA synthetase	-5.646
PHENYLALANINE METABOLISM		
P-value 1.408e-08	**Count 12/59**	**20.3%**
BCAL0212	*paaE* - Putative phenylacetic acid degradation NADH oxidoreductase PaaE	-43.665
BCAL0213	*paaD* - Phenylacetic acid degradation protein PaaD	-44.213
BCAL0214	*paaC* - Phenylacetic acid degradation protein PaaC	-33.710
BCAL0215	*paaB* - Phenylacetate-CoA oxygenase subunit PaaB	-36.644
BCAL0216	*paaA* - Phenylacetate-CoA oxygenase subunit PaaA	-34.435
BCAL0406	*paaG* - Enoyl-CoA hydratase	-11.166
BCAL0409	*paaF* - Enoyl-CoA hydratase	-2.357
BCAL0705	Putative D-amino acid aminotransferase	-2.748
BCAL2303	Aromatic amino acid aminotransferase	-2.049
BCAL2933	*dada* - D-amino acid dehydrogenase small subunit	-215.050
BCAL3299	*katG* - Peroxidase/catalase KatB	-4.895
BCAM1711	Phenylacetate-coenzyme A ligase	-11.823
GLYCINE, SERINE AND THREONINE METABOLISM		
P-value 1.027e-05	**Count 9/56**	**16.1%**
BCAL0073	*gcvP* - Glycine dehydrogenase	-5.789
BCAL0075	*gcvT* - Glycine cleavage system aminomethyltransferase T	-18.026
BCAL1215	*lpdV* - Dihydrolipoamide dehydrogenase	-20.612
BCAL1517	*odhL* - Dihydrolipoamide dehydrogenase	-3.768
BCAL2207	Putative dihydrolipoamide dehydrogenase	-6.063

Table V.S2 (continuation)

GENE	ANNOTATION OR PREDICTED FUNTION	FOLD CHANGE
GLYCINE, SERINE AND THREONINE METABOLISM		
P-value 1.027e-05	**Count 9/56**	**16.1%**
BCAL2955	*serC* - Phosphoserine aminotransferase	-2.204
BCAM0010	*kbl* - 2-amino-3-ketobutyrate coenzyme A ligase	-8.746
BCAM0011	*tdh* - L-threonine 3-dehydrogenase	-6.223
BCAM0908	Putative iron-sulfur protein	-3.280
PYRIMIDINE METABOLISM		
P-value 2.654e-05	**Count 8/48**	**16.7%**
BCAL0226	*rpoB* - DNA-directed RNA polymerase subunit beta	-3.774
BCAL0227	*rpoC* - DNA-directed RNA polymerase subunit beta'	-8.193
BCAL0260	*rpoA* - DNA-directed RNA polymerase subunit alpha	-2.506
BCAL0422	*dnaN* - DNA polymerase III subunit beta	-1.970
BCAL1262	*carB* - Carbamoyl phosphate synthase large subunit	-2.322
BCAL1899	*dnaX* - DNA polymerase III subunits gamma and tau	-2.607
BCAL2348	*pnp* - Polynucleotide phosphorylase/polyadenylase	-1.936
BCAM0310	Ribonucleotide reductase-like protein	-51.056
PROPANOATE METABOLISM		
P-value 2.930e-05	**Count 8/49**	**16.3%**
BCAL0409	*paaF* - Enoyl-CoA hydratase	-2.357
BCAM0293	*ackA* - Putative acetate kinase	-59.243
BCAM0298	Putative phosphate acetyl/butyryl transferase	-76.193
BCAM0299	Putative zinc-binding alcoholdehydrogenase	-76.193
BCAM2194	*mmsA* - Methylmalonate-semialdehyde dehydrogenase	-4.876
BCAM2195	Putative AMP-binding protein	-3.995
BCAS0737	Putative acetyl-CoA acetyltransferase	-7.386
BCAS0739	Putative acetyl-CoA synthetase	-5.646
ALANINE, ASPARTATE AND GLUTAMATE METABOLISM		
P-value 3.751e-05	**Count 7/37**	**18.9%**
BCAL0611	*glmS1* - glucosamine--fructose-6-phosphate aminotransferase	-3.240
BCAL1262	*carB* - Carbamoyl phosphate synthase large subunit	-2.322

Table V.S2 (continuation)

GENE	ANNOTATION OR PREDICTED FUNTION	FOLD CHANGE
ALANINE, ASPARTATE AND GLUTAMATE METABOLISM		
P-value 3.751e-05	**Count 7/37**	**18.9%**
BCAL2638	*argH* - Argininosuccinate lyase	-3.021
BCAL3359	Putative glutamate dehydrogenase	-9.125
BCAL3361	*purB* - Adenylosuccinate lyase	-2.545
BCAM0998	*purF* - Amidophosphoribosyltransferase	-2.629
BCAS0771	Putative adenylosuccinate synthetase	-7.151
BIOSYNTHESIS OF AMINO ACIDS		
P-value 5.790e-05	**Count 13/149**	**8.7%**
BCAL1059	*argM* - Bifunctional N-succinyldiaminopimelate-aminotransferase/acetylornithine transaminase protein	-9.857
BCAL1467	*aroC* - chorismate synthase	-3.171
BCAL2303	Aromatic amino acid aminotransferase	-2.049
BCAL2433	*tal* - Transaldolase B	-1.687
BCAL2638	*argH* - Argininosuccinate lyase	-3.021
BCAL2952	*aroA* - 3-phosphoshikimate 1-carboxyvinyltransferase	-3.902
BCAL2955	*serC* - Phosphoserine aminotransferase	-2.204
BCAL3388	*gapA* - Glyceraldehyde 3-phosphate dehydrogenase 1	-4.547
BCAL3389	*tktA* - Transketolase	-3.302
BCAM0311	Putative 6-phosphofructokinase	-65.666
BCAM0961	Aconitate hydratase	-2.465
BCAM0972	*gltA* - Type II citrate synthase	-2.215
BCAM2076	*lysA* - Diaminopimelate decarboxylase	-2.864
ARGININE AND PROLINE METABOLISM		
P-value 6.220e-05	**Count 9/72**	**12.5%**
BCAL0433	*speG* - spermidine N(1)-acetyltransferase	-4.072
BCAL0705	Putative D-amino acid aminotransferase	-2.748
BCAL1059	*argM* - Bifunctional N-succinyldiaminopimelate-aminotransferase/acetylornithine transaminase protein	-9.857
BCAL1062	*astD* - Succinylglutamic semialdehyde dehydrogenase	-5.393
BCAL1063	*astB* - Succinylarginine dihydrolase	-6.067

Table V.S2 (continuation)

GENE	ANNOTATION OR PREDICTED FUNTION	FOLD CHANGE
ARGININE AND PROLINE METABOLISM		
P-value 6.220e-05	**Count 9/72**	**12.5%**
BCAL2638	*argH* - Argininosuccinate lyase	-3.021
BCAL3359	Putative glutamate dehydrogenase	-9.125
BCAM1111	*speF* - Ornithine decarboxylase	-37.980
BCAM1112	*adiA* - biodegradative arginine decarboxylase	-13.932
PROTEIN EXPORT		
P-value 6.220e-05	**Count 5/17**	**29.4%**
BCAL0254	*secY* - Preprotein translocase subunit SecY	-4.083
BCAL0742	*secB* - Preprotein translocase subunit SecB	-1.928
BCAL3307	*secF* - Preprotein translocase subunit SecF	-5.013
BCAL3433	*ffh* - Signal recognition particle protein	-2.793
BCAL3453	*secA* - Preprotein translocase subunit SecA	-2.055
RNA POLYMERASE		
P-value 0.00011	**Count 3/4**	**75.0%**
BCAL0226	*rpoB* - DNA-directed RNA polymerase subunit beta	-3.774
BCAL0227	*rpoC* - DNA-directed RNA polymerase subunit beta'	-8.193
BCAL0260	*rpoA* - DNA-directed RNA polymerase subunit alpha	-2.506
AMINOACYL-tRNA BIOSYNTHESIS		
P-value 0.00011	**Count 6/31**	**19.4%**
BCAL0880	*aspS* - Aspartyl-tRNA synthetase	-2.328
BCAL1413	*glnS* - Glutaminyl-tRNA synthetase	-2.101
BCAL1448	*valS* - Valyl-tRNA synthetase	-3.825
BCAL1486	*pheT* - Phenylalanyl-tRNA synthetase subunit beta	-2.593
BCAL1883	*hisS* - Histidyl-tRNA synthetase	-2.380
BCAL2169	*trpS* - Tryptophanyl-tRNA synthetase	-3.423
LYSINE DEGRADATION		
P-value 0.00027	**Count 5/23**	**27.7%**
BCAL0409	*paaF* - Enoyl-CoA hydratase	-2.357
BCAL0705	Putative D-amino acid aminotransferase	-2.748
BCAL1515	*sucA* - 2-oxoglutarate dehydrogenase E1 component	-2.403

Table V.S2 (continuation)

GENE	ANNOTATION OR PREDICTED FUNTION	FOLD CHANGE
LYSINE DEGRADATION		
P-value 0.00027	**Count 5/23**	**27.7%**
BCAL1516	*sucB* - Dihydrolipoamide succinyltransferase	-3.499
BCAS0737	Putative acetyl-CoA acetyltransferase	-7.386
TRYPTOPHAN METABOLISM		
P-value 0.00033	**Count 6/38**	**15.8%**
BCAL0409	*paaF* - Enoyl-CoA hydratase	-2.357
BCAL1515	*sucA* - 2-oxoglutarate dehydrogenase E1 component	-2.403
BCAL2791	*kynU* - Putative kynureninase	-14.681
BCAL2792	*kynA* - Putative tryptophan 2,3-dioxygenase	-9.006
BCAL3299	*katG* - Peroxidase/catalase KatB	-4.895
BCAS0737	Putative acetyl-CoA acetyltransferase	-7.386
METHANE METABOLISM		
P-value 0.00033	**Count 6/38**	**15.8%**
BCAL2955	*serC* - Phosphoserine aminotransferase	-2.204
BCAM0293	*ackA* - Putative acetate kinase	-59.243
BCAM0298	Putative phosphate acetyl/butyryl transferase	-76.193
BCAM0311	Putative 6-phosphofructokinase	-65.666
BCAM2195	Putative AMP-binding protein	-3.995
BCAS0739	Putative acetyl-CoA synthetase	-5.646
BUTANOATE METABOLISM		
P-value 0.00050	**Count 7/58**	**12.1%**
BCAL0409	*paaF* - Enoyl-CoA hydratase	-2.357
BCAM0296	Acetoacetyl-CoA reductase	-76.193
BCAM0297	Putative poly(3-hydroxyalkanoate) polymerase	-76.193
BCAM0969	*sdhA* - Succinate dehydrogenase flavoprotein subunit	-2.639
BCAM0970	*sdhB* - Succinate dehydrogenase iron-sulfur subunit	-2.610
BCAM1250	Putative acetyl-CoA hydrolase/transferase	-1.882
BCAS0737	Putative acetyl-CoA acetyltransferase	-7.386
RNA DEGRADATION		
P-value 0.00085	**Count 4/17**	**23.5%**
BCAL2348	*pnp* - Polynucleotide phosphorylase/polyadenylase	-1.936
BCAL3146	Chaperonin GroEL	-25.424

Table V.S2 (continuation)

GENE	ANNOTATION OR PREDICTED FUNTION	FOLD CHANGE
RNA DEGRADATION		
P-value 0.00085	**Count 4/17**	**23.5%**
BCAL3270	*dnaK* - Molecular chaperone DnaK	-9.979
BCAS0637	Chaperonin GroEL	-34.865
D-ALANINE METABOLISM		
P-value 0.00566	**Count 2/4**	**50.0%**
BCAL0705	Putative D-amino acid aminotransferase	-2.748
BCAM1204	Alanine racemase	-15.392
GLYOXYLATE AND DICARBOXYLATE METABOLISM		
P-value 0.00658	**Count 6/68**	**8.8%**
BCAM0296	Acetoacetyl-CoA reductase	-76.193
BCAM0961	Aconitate hydratase	-2.465
BCAM0972	*gltA* - Type II citrate synthase	-2.215
BCAM2817	Glycolate oxidase subunit GlcD	-9.100
BCAM2818	Glycolate oxidase FAD binding subunit	-9.100
BCAS0737	Putative acetyl-CoA acetyltransferase	-7.386
ONE CARBON POOL BY FOLATE		
P-value 0.00860	**Count 3/16**	**18.8%**
BCAL0075	*gcvT* - Glycine cleavage system aminomethyltransferase T	-18.026
BCAL0147	*metF* - 5,10-methylenetetrahydrofolate reductase	-4.955
BCAL3336	purH - Bifunctional phosphoribosylaminoimidazolecarboxamide formyltransferase/IMP cyclohydrolase	-3.030
BACTERIAL SECRETION SYSTEM		
P-value 0.00860	**Count 5/51**	**9.8%**
BCAL0254	*secY* - Preprotein translocase subunit SecY	-4.083
BCAL0742	*secB* - Preprotein translocase subunit SecB	-1.928
BCAL3307	*secF* - Preprotein translocase subunit SecF	-5.013
BCAL3433	*ffh* - Signal recognition particle protein	-2.793
BCAL3453	*secA* - Preprotein translocase subunit SecA	-2.055
FATTY ACID DEGRADATION		
P-value 0.01172	**Count 4/35**	**11.4%**
BCAL0409	*paaF* - Enoyl-CoA hydratase	-2.357

Table V.S2 (continuation)

GENE	ANNOTATION OR PREDICTED FUNTION	FOLD CHANGE
FATTY ACID DEGRADATION		
P-value 0.01172	**Count 4/35**	**11.4%**
BCAM0286	Putative alcohol dehydrogenase	-17.616
BCAM1570	Alcohol dehydrogenase	-139.172
BCAS0737	Putative acetyl-CoA acetyltransferase	-7.386
NAPHTHALENE DEGRADATION		
P-value 0.01172	**Count 2/6**	**33.3%**
BCAM0286	Putative alcohol dehydrogenase	-17.616
BCAM1570	Alcohol dehydrogenase	-139.172
TERPENOID BACKBONE BIOSYNTHESIS		
P-value 0.01475	**Count 3/20**	**15.0%**
BCAL1884	*ispG* - 4-hydroxy-3-methylbut-2-en-1-yl diphosphate synthase	-2.679
BCAM0911	*dxs* - 1-deoxy-D-xylulose-5-phosphate synthase	-1.770
BCAS0737	Putative acetyl-CoA acetyltransferase	-7.386
NUCLEOTIDE EXCISION REPAIR		
P-value 0.01529	**Count 2/7**	**28.6%**
BCAL0825	*uvrA* - excinuclease ABC subunit A	-3.135
BCAL2017	*mfd* - transcription-repair coupling factor	-2.758
VITAMIN B6 METABOLISM		
P-value 0.01955	**Count 2/8**	**25.0%**
BCAL2782	*pdxH* - Pyridoxamine 5'-phosphate oxidase	-4.034
BCAL2955	*serC* - Phosphoserine aminotransferase	-2.204
PORPHYRIN AND CHLOROPHYLL METABOLISM		
P-value 0.02107	**Count 4/43**	**9.3%**
BCAL0264	*hemB* - Delta-aminolevulinic acid dehydratase	-2.457
BCAL1711	*cobN* - Cobaltochelatase subunit	-9.733
BCAL1712	Putative magnesium chelatase protein	-9.733
BCAL3094	*hemN* - Coproporphyrinogen III oxidase	-36.590
NITROGEN METABOLISM		
P-value 0.02208	**Count 3/24**	**12.5%**
BCAL1830	Putative 2-nitropropane dioxygenase	-53.392
BCAL3359	Putative glutamate dehydrogenase	-9.125
BCAM2815	Putative 2-nitropropane dioxygenase	-11.758

Table V.S2 (continuation)

GENE	ANNOTATION OR PREDICTED FUNTION	FOLD CHANGE
AMINOBENZOATE DEGRADATION		
P-value 0.02409	**Count 3/25**	**12.0%**
BCAL0409	*paaF* - Enoyl-CoA hydratase	-2.357
BCAM0810	Putative aromatic oxygenase	-10.983
BCAM0811	Putative aromatic oxygenase	-6.831
GERANIOL DEGRADATION		
P-value 0.02758	**Count 2/10**	**20.0%**
BCAL0409	*paaF* - Enoyl-CoA hydratase	-2.357
BCAM2196	Putative acyl-CoA dehydrogenase	-5.913
PHENYLALANINE, TYROSINE AND TRYPTOPHAN BIOSYNTHESIS		
P-value 0.02829	**Count 3/27**	**11.1%**
BCAL1467	*aroC* - chorismate synthase	-3.171
BCAL2303	Aromatic amino acid aminotransferase	-2.049
BCAL2952	*aroA* - 3-phosphoshikimate 1-carboxyvinyltransferase	-3.902
PENTOSE PHOSPHATE PATHWAY		
P-value 0.03047	**Count 3/28**	**10.7%**
BCAL2433	*tal* - Transaldolase B	-1.687
BCAL3389	*tktA* - Transketolase	-3.302
BCAM0311	Putative 6-phosphofructokinase	-65.666
PHOSPHONATE AND PHOSPHINATE METABOLISM		
P-value 0.03097	**Count 2/11**	**18.2%**
BCAM1243	Putative aminotransferase	-2.093
BCAM1245	Putative phosphoenolpyruvate phosphomutase/sugar nucleotidyltransferase	-2.093
FATTY ACID METABOLISM		
P-value 0.03160	**Count 4/51**	**7.8%**
BCAL0409	*paaF* - Enoyl-CoA hydratase	-2.357
BCAL2080	*fabZ* - (3R)-hydroxymyristoyl-ACP dehydratase	-3.301
BCAL2719	Putative transmembrane fatty acid desaturase	-2.523
BCAS0737	Putative acetyl-CoA acetyltransferase	-7.386
CARBON FIXATION IN PHOTOSYNTHETIC ORGANISMS		
P-value 0.04087	**Count 2/13**	**15.4%**
BCAL3388	*gapA* - Glyceraldehyde 3-phosphate dehydrogenase 1	-4.547
BCAL3389	*tktA* - Transketolase	-3.302
BETA-LACTAM RESISTANCE		
P-value 0.04547	**Count 3/34**	**8.8%**
BCAL1674	*amrA* - Periplasmic multidrug efflux lipoprotein	-7.862
BCAL1675	*amrB* - Multidrug efflux protein	-6.194

Table V.S2 (continuation)

GENE	ANNOTATION OR PREDICTED FUNTION	FOLD CHANGE
BETA-LACTAM RESISTANCE		
P-value 0.04547	**Count 3/34**	**8.8%**
BCAL2820	*oprM* - Efflux system outer membrane protein	-4.056
BETA-LACTAM RESISTANCE		
P-value 0.04547	**Count 3/34**	**8.8%**
BCAL2303	Aromatic amino acid aminotransferase	-2.049
BCAM0286	Putative alcohol dehydrogenase	-17.616
BCAM1570	Alcohol dehydrogenase	-139.172
TAURINE AND HYPOTAURINE METABOLISM		
P-value 0.05023	**Count 2/15**	**13.3%**
BCAM0293	*ackA* - Putative acetate kinase	-59.243
BCAM0298	Putative phosphate acetyl/butyryl transferase	-76.193
DNA REPLICATION		
P-value 0.05549	**Count 2/16**	**12.5%**
BCAL0422	*dnaN* - DNA polymerase III subunit beta	-1.970
BCAL1899	*dnaX* - DNA polymerase III subunits gamma and tau	-2.607
CHLOROALKANE AND CHLOROALKENE DEGRADATION		
P-value 0.05964	**Count 2/17**	**11.8%**
BCAM0286	Putative alcohol dehydrogenase	-17.616
BCAM1570	Alcohol dehydrogenase	-139.172
2-OXOCARBOXYLIC ACID METABOLISM		
P-value 0.05964	**Count 3/39**	**7.7%**
BCAL1059	*argM* - Bifunctional N-succinyldiaminopimelate-aminotransferase/acetylornithine transaminase protein	-9.857
BCAM0961	Aconitate hydratase	-2.465
BCAM0972	*gltA* - Type II citrate synthase	-2.215
FLAGELLAR ASSEMBLY		
P-value 0.06202	**Count 3/40**	**7.5%**
BCAL0114	*fliC* - Flagellin	-1.921
BCAL0126	*motA* - Flagellar motor protein MotA	-1.913
BCAL0576	*flgK* - Flagellar hook-associated protein FlgK	-2.055
MISMATCH REPAIR		
P-value 0.06373	**Count 2/18**	**11.1%**
BCAL0422	*dnaN* - DNA polymerase III subunit beta	-1.970
BCAL1899	*dnaX* - DNA polymerase III subunits gamma and tau	-2.607

Table V.S2 (continuation)

GENE	ANNOTATION OR PREDICTED FUNTION	FOLD CHANGE
LYSINE BIOSYNTHESIS		
P-value 0.08943	**Count 2/22**	**9.1%**
BCAL1059	*argM* - Bifunctional N-succinyldiaminopimelate-aminotransferase/acetylornithine transaminase protein	-9.857
BCAM2076	*lysA* - Diaminopimelate decarboxylase	-2.864
BETA-ALANINE METABOLISM		
P-value 0.10760	**Count 2/25**	**8.0%**
BCAL0409	*paaF* - Enoyl-CoA hydratase	-2.357
BCAM2194	*mmsA* - Methylmalonate-semialdehyde dehydrogenase	-4.876
HOMOLOGOUS RECOMBINATION		
P-value 0.10760	**Count 2/25**	**8.0%**
BCAL0422	*dnaN* - DNA polymerase III subunit beta	-1.970
BCAL1899	*dnaX* - DNA polymerase III subunits gamma and tau	-2.607
CYSTEINE AND METHIONINE METABOLISM		
P-value 0.13558	**Count 2/29**	**6.9%**
BCAL0145	*ahcY* - S-adenosyl-L-homocysteine hydrolase	-3.820
BCAL2303	Aromatic amino acid aminotransferase	-2.049
AMINO SUGAR AND NUCLEOTIDE SUGAR METABOLISM		
P-value 0.20468	**Count 2/38**	**5.3%**
BCAL0611	*glmS1* - glucosamine--fructose-6-phosphate aminotransferase	-3.240
BCAL1722	Putative exported chitinase	-9.498
BENZOATE DEGRADATION		
P-value 0.26684	**Count 2/46**	**4.4%**
BCAL0409	*paaF* - Enoyl-CoA hydratase	-2.357
BCAS0737	Putative acetyl-CoA acetyltransferase	-7.386
DEGRADATION OF AROMATIC COMPOUNDS		
P-value 0.33540	**Count 2/55**	**3.6%**
BCAM0286	Putative alcohol dehydrogenase	-17.616
BCAM1570	Alcohol dehydrogenase	-139.172
SULFUR METABOLISM		
P-value 0.33788	**Count 2/56**	**3.6%**
BCAL1819	NAD(FAD)-dependent dehydrogenase	-13.704
BCAL3216	*cysC* - Adenylyl-sulfate kinase	-2.024

Table V.S2 (continuation)

GENE	ANNOTATION OR PREDICTED FUNTION	FOLD CHANGE
ABC TRANSPORTERS		
P-value 0.65953	**Count 5/264**	**1.9%**
BCAL0043	Putative extracellular ligand-binding protein	-4.156
BCAL1055	Histidine transport system permease	-3.966
BCAL1056	Histidine transport system permease	-3.966
BCAL1057	Histidine ABC transporter ATP-binding protein	-3.759
BCAL1065	Periplasmic solute-binding protein	-6.270